Physique à quelques et à N- corps dans les gaz de Rydberg froids

Paul Huillery

UNIVERSITÉ PARIS-SUD

ECOLE DOCTORALE ONDE ET MATIÈRE
LABORATOIRE AIMÉ COTTON

DISCIPLINE : PHYSIQUE

THÈSE DE DOCTORAT

Soutenue le 12 mars 2013 par

Paul Huillery

Few and Many-body Physics in cold Rydberg gases

Directeur de thèse :	M. Daniel Comparat	Chargé de recherche (Paris-Sud)
Co-directeur de thèse :	M. Ennio Arimondo	Professeur (Pise)

Composition du jury :

Président du jury :	M. Christopher Westbrook	Directeur de recherche (Paris-Sud)
Rapporteurs :	M. Immanuel Bloch	Professeur (Munich)
	M. Michael Fleischhauer	Professeur (Kaiserslautern)
Examinateurs :	Mme. Maria Allegrini	Professeur (Pise)
	M. Francesco Fuso	Professeur (Pise)
	M. Pierre Pillet	Directeur de recherche (Paris-Sud)

Contents

Introduction

The physical description of a system is often done with 2-body treatments. There are two good reasons for that. First, the 2-body Physics determines the behavior of a large range of systems. Secondly, the 2-body systems are the only ones that can be treated exactly. As soon as there is 3 body involved in a problem, it can not be solved without approximations (analytically). This is known in Physics as the N-body problem.
However, the nature does not care about analytical solution and some systems required to go beyond the 2-body treatment. This is the case of nucleus, atoms, molecules, solids, stars,... In those systems, very interesting phenomena arise from the interactions between more than two body. Describing them is a big challenge for fundamental Physics. Controlling them is a big source of technological progress.

We have two main approaches to deal with N-body problems. When we aim to describe a system in details, we are often limited to small systems (sub-systems) and we talk about few-body Physics. On the other hand, when we look out the details and we aim to extract general behaviors, this is often adapted to large systems and we talk about many-body Physics.

The systems investigated in the frame of this thesis are cold atomic gases.

The cold atoms techniques have been developed for around 50 years and represent a fantastic tool for atomic Physics. It has been recognized by a Nobel prize in 1997 awarded jointly to Steven Chu, Claude Cohen-Tannoudji and William D. Phillips "for development of methods to cool and trap atoms with laser light".
To form a cold atomic gas, the motion of the atoms is progressively reduced. As an ultimate stage, it is possible to reach the Bose-Einstein Condensation (BEC). In a BEC, all the trapped atoms have the minimum degree of motion allowed by their quantum nature, they behave identically forming a so-called giant matter wave. Observed for the first time in 1995, the obtention of a BEC has been also recognized by a Nobel Prize in 2001 awarded jointly to Eric A. Cornell, Wolfgang Ketterle and Carl E. Wieman.

In a BEC, the temperature is of the order of few nK meaning that the thermal speed of the atoms is less than 1 mm.s^{-1}.

In the experiments carried out in the frame of this thesis, starting from a cold atomic sample, we generate interatomic interactions by creating Rydberg atoms.

A Rydberg atom is an atom with one electron in a very excited state. In comparison to an atom in the ground state, a Rydberg atom has exaggerated properties. The most evident one is its size. Given the principal quantum number n of the so-called Rydberg electron, the size of the Rydberg atom scales as n^2. The size of a Rydberg atom with $n = 100$ is of the order of 1 μm. This is illustrated on the figure 1 where we have schematically represented a Rydberg atom.

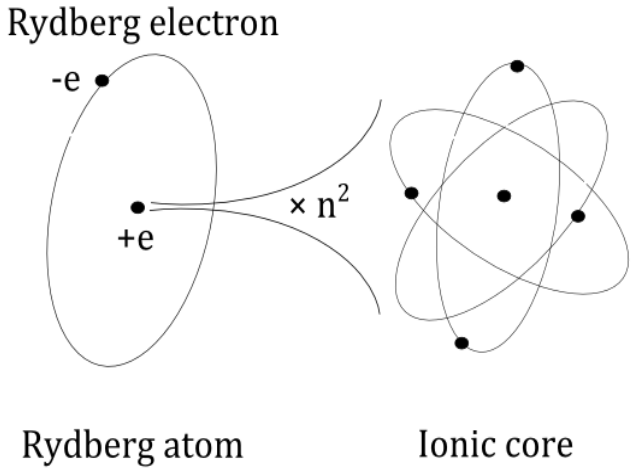

Figure 1: Schematic representation of a Rydberg atom.

The huge distance between the Rydberg electron and the ionic core confers to Rydberg atoms a fantastic property: Rydberg atoms are extremely sensitive to any electromagnetic perturbation.
A weak external electric field modifies considerably the quantum states of the Rydberg electron. This provides an efficient way to control experimentally the internal state of Rydberg atoms.
Applying an electric field is also a way to ionize Rydberg atoms. This is a very largely used method to detect them in cold atoms experiments. A Rydberg atom with $n = 100$ is ionized at an electric field of around 10V.cm^{-1}.
This sensitivity to electric fields makes of Rydberg atoms very promising systems to build high precision field sensors.
As a paradigm of their sensitivity, Rydberg atoms have been used to implement non de-

structive measurements of single photons. This experimental feat takes part of the Nobel Prize awarded jointly in 2012 to Serge Haroche and David J. Wineland "for groundbreaking experimental methods that enable measuring and manipulation of individual quantum systems".

In the frame of the realization of interacting systems, we use the fact that Rydberg atoms interact together through long-range electrostatic interactions.
A particularity of the interactions between Rydberg atoms is their modularity. They can be isotropic or not, the radial dependence can follow different scaling law and overall the interactions strength depends a lot of the Rydberg state which is involved and takes a huge value for highly excited states.
Experimentally, the choice of the Rydberg state and the application of an electric field allow to change those interaction parameters in a controllable way.

Cold Rydberg gases provide us very nice conditions to study an ensemble of interacting particles.

As a first nice feature, we can manage to perform very short experiments where the atoms almost do not move. Then the experiments consist in an almost static "picture" of the investigated systems. This provides great simplifications in theoretical treatments which is known as the frozen gas approximation.
Secondly, cold atoms techniques allow a great control on the atomic ensemble properties, starting with its shape. In this frame, the use of optical lattice offers fantastic possibilities. As illustrative examples, we show on the figure 2 three images of atomic samples prepared in different conditions.
Finally, cold atomic gases are very dilute systems and if we do not want to, the atoms do not interact. The interactions which give rise to the N-body Physics that we want to access are created in a controllable way. Also, since no similar effects are naturally present in the system, we can manage to observe the investigated process through very clean and isolated signals.

In the frame of this thesis, I have taken part to two different experimental researchs. One in Orsay, in the group of Dr. Pierre Pillet under the supervision of Dr. Daniel Comparat. The other at Pisa in the group of Prof. Ennio Arimondo. Orsay's experiments are of the few-body type, Pisa's one of the many-body type.

The interactions between Rydberg atoms appear first in presence of an external electric field. A small electric field "distorts" Rydberg atoms which acquire a permanent

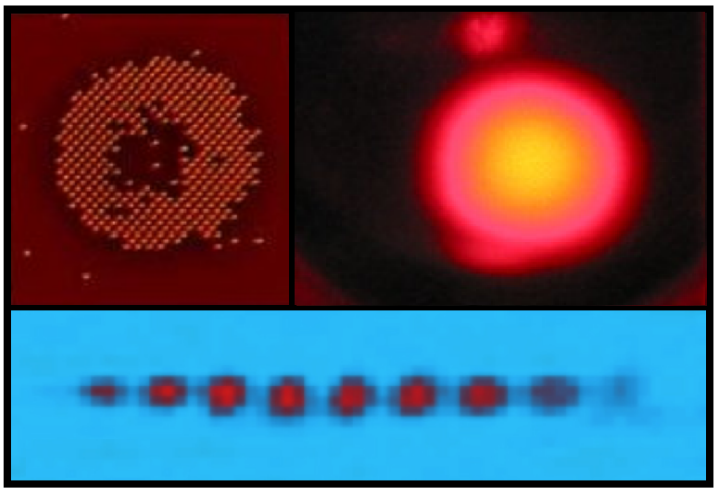

Figure 2: Cold atoms in various conditions. Top-Left, fluorescence imaging of single rubidium atoms in a 2-dimensional optical lattice in the Mott insulator regime. This image has been obtained in the group of Prof. Immanuel Bloch in Munich, taken from http://www.quantum-munich.de. Top-Right, Picture of a Magneto-Optical Trap of lithium atoms containing around 10 billions of atoms. This picture has been obtained in the group of Prof. Tilman Esslinger in Zurich, taken from http://www.quantumoptics.ethz.ch. Bottom, In-situ absorption imaging of a BEC of rubidium atoms split into packets using a 1-dimensional optical lattice, the packets contain in average 10 thousand of atoms. This image has been obtained in the group of Prof. Ennio Arimondo in Pisa, during this thesis.

electric dipole moment. In presence of electric field, Rydberg atoms interact thus like classical electric dipoles.
In absence of external electric field, Rydberg atoms still interact. We talk in this case about induced dipole interactions more known under the name of Van-der-Waals interactions.
To this regards exist very interesting situations where the induced dipole interactions between Rydberg atoms takes huge values. Those situations are called Förster resonances, they appear "accidentally" when the energy of two 2-body Rydberg states is equal. In this case, the atoms interact through a resonant exchange of excitation as represented on the figure 3.
Experimentally, we can voluntary create those situations by applying a very weak electric field which brings at resonance the energies of two particular 2-body quantum states.

One part of this thesis has consisted in the realization of such Förster resonances in a Magneto-Optical Trap of Cesium.
In addition to the realization and the optimization of 2-body Förster resonances, it has

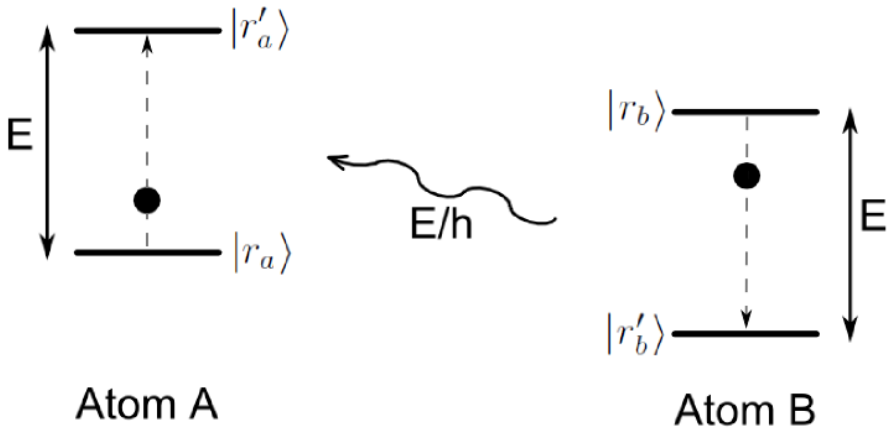

Figure 3: Schematic representation of a pair of Rydberg atoms interacting through a Förster resonance. Both atoms interact through the exchange of a "virtual" photon, the interaction is considerably enhanced by the resonant character of the process : $E_{|r_a\rangle} + E_{|r_b\rangle} = E_{|r'_a\rangle} + E_{|r'_b\rangle}$.

been possible to use the proximity (in electric field) of two 2-body Förster resonances to generate a 4-body process.
We have indeed observed the mutual interaction between 4 Rydberg atoms through the modification of their individual internal states.
This observation, reported in [Gurian et al., 2012], is an important contribution to the few-body Physics. Namely because, in addition to its observation, this coherent process between 4 Rydberg atoms can be well characterized theoretically, at a quantum level. It has been for example possible to enhance the 4-body process efficiency by changing in a controllable and deterministic way the electric field during the process.

The interactions between Rydberg atoms have also strong manifestations when considering the coupling of an ensemble of Rydberg atoms with the electromagnetic field.
When a so-called strongly interacting Rydberg gas is driven by a resonant laser field, the excitation of the atoms toward Rydberg states is reduced due to Rydberg atoms interactions. This is the so-called Dipole Blockade phenomenon.
In the limit case, only one Rydberg excitation can be present in the system. Such systems have been proposed to implement quantum gates, fundamental elements for quantum computation.
Strongly interacting Rydberg ensembles have also very interesting photon emission properties. They could be used to create single photon sources or non-classical light sources.

When involved in Electromagnetic-Induced Transparency (EIT) schemes, blockaded Rydberg ensembles have been used to demonstrate a giant Kerr effect.
Strongly interacting Rydberg gases could finally be used to mimic various quantum behaviors. In this case, we talk about quantum simulation. The modularity of Rydberg atoms interactions together with the one of cold atomic gases offer the possibility to reproduce the dynamics of other interacting systems, for example solid-state Physics systems.

In a fundamental point of view, the description of strongly interacting Rydberg gases has stimulated a big theoretical interest. Since it is a many-body problem, the associated Hamiltonian can not be solved for more than a mesoscopic number of atoms. However, due to the very attractive properties that we expect from such systems, it is very interesting to be able to describe them.
An important feature which is well demonstrated theoretically is that a strongly interacting Rydberg gas driven by a laser field gives rise to collective excitations. A large part of the blockaded Rydberg ensembles properties come from those collective excitations which have for example a characteristic enhanced dynamics.

In the frame of this thesis, the dipole blockade has been investigated theoretically using the so-called Dicke collective states. Those collective quantum states are defined in function of their symmetry relative to the laser excitation. It has been possible to use those symmetry properties to describe efficiently the collective dynamics of the system.

The dipole blockade has been also investigated experimentally during this thesis, by using an ultra-cold rubidium gas.
A first result, reported in [Viteau et al., 2011], has consisted in the first experimental demonstration of a coherent Rydberg excitation of a BEC confined in a 1-dimensional optical lattice. The collective nature of the Rydberg excitations have been observed through its characteristic enhanced dynamics. This is an important result since such a geometry should be one of the most useful to observe and use the collective properties of blockaded Rydberg ensemble.
Another important result, reported in [Viteau et al., 2012], has been the observation of a highly sub-poissonian (correlated) statistics of the Rydberg excitation. This feature is also a strong signature of the collective excitations and confirms for example the potential of strongly interacting Rydberg ensembles for non-classical light sources generation.

In chapter 1, we present the basis of the Rydberg atoms Physics. The theoretical description of the Rydberg states is presented in simple terms. We present the fundamental

interaction processes between two Rydberg atoms. We also give a non exhaustive but quite complete overview of the theoretical and experimental studies done on strongly interacting Rydberg gases. The purpose is to extract the principal features of such systems which have been the subject of a very big number of publications for the last ten years.

In chapter 2, we present the calculations done at Orsay concerning the quantum states of two interacting Rydberg atoms in presence of static, uniform, external electric and magnetic fields. A computer program has been realized to do this. My personal contribution to this work has been to write down all the formulas corresponding to the investigated effects. Those formulas were all previously existing and my task has been to unify them in a consistent system which is presented in this chapter. The code implementation has been mainly done by Dr. Patrick Cheinet. I have been involved in the manipulation of the 2-body calculations to extract the outputs that are presented at the end of this chapter. Also, a personal initiative has been to start to establish the validity conditions of such calculations and to look at other existing calculating methods as presented in the beginning of this chapter.

In chapter 3, we present the experiments done at Orsay concerning the realization of few-body interaction processes. We namely present the experimental observation of the 4-body process reported in [Gurian et al., 2012]. The experimental setup used for those experiments has been built from scratch in the frame of this thesis. During 3 months, I have worked on it with a bachelor student Matthieu Barachan and 6 months alone. During this period it has been possible to obtain the Magneto Optical Trap of cesium and to start to set up the Rydberg experiment. I then have been joined by Joshua Gurian as a post-doctoral researcher. We have together observed the first Rydberg signal and started to calibrate the detection setup before I left for Pisa. The few-body experiments have been performed by Joshua Gurian and Dr. Patrick Cheinet who joined the team soon after I left. I have personally developed the single ions imaging acquisition which should be used in future experiments.

In chapter 4, we present the experiments done at Pisa concerning the Rydberg excitation in 1-dimensional optical lattice reported in [Viteau et al., 2011] and the observation of the sub-poissonian counting statistics of the Rydberg excitation reported in [Viteau et al., 2012]. The Pisa experimental setup was already well handled by three post-doctoral researchers, Marc Bason, Nicola Malossi and Matthieu Viteau as well as Dr. Donatella Ciampini and Dr. Oliver Morsh when I arrived. I have progressively taken part to the experiments. A personal work has been to study the physical information associated to

the so-called Mandel Q factor as presented in this chapter. I have also study numerically the effect of the laser jitter on the Q factor as presented in the appendix B.

In chapter 5, we present the theoretical studies of the interacting Rydberg gases that has been done in collaboration between Orsay and Pisa using the so-called Dicke collective states. We namely present the cooperative model that we have developped in order to model strongly interacting Rydberg gases. This model is briefly touched in the reference [Viteau et al., 2012] and will be the subject of another publication. The original idea of the cooperative model comes from Dr. Pierre Pillet. My personal contribution to this subject has been to develop the visibility of the cooperative model. I have been strongly involved in the physical interpretation of the model. I have also made the calculations using the Dicke collective states in some simple situations which are presented at the end of this chapter. Those calculations show the interest of the Dicke basis for many-body modeling and allow to make some links between the model and other theoretical developments. I have also done the Mean-Field calculations presented in the appendix D.

Chapter 1

Rydberg atoms, Rydberg-Rydberg interactions and strongly interacting Rydberg gases

1.1 Historical contribution of Rydberg atoms to atomic Physics

1.1.1 Natural existence of Rydberg atoms

While the presence of Rydberg atoms is very unlikely on earth due to the fact that their ionization energies are well below thermal energy, we can find Rydberg atoms in interstellar medium as well as in plasma medium [Gallagher, 1994].
In plasma, it is the radiative recombination of low energy electrons and ions which leads to the formation of Rydberg atoms.
In interstellar medium, the very low density allows for the existence of Rydberg atoms as proved by the 2.4 GHz signal, well known by the radio-astronomers, which correspond to the transition between $n = 109$ and $n = 108$ states of hydrogen. We can find in interstellar medium Rydberg states up to $n = 800$.

1.1.2 Early atomic spectroscopy and series laws

During the second half of the 19th century, physicists accumulated numbers of spectroscopic data of different elements using astronomic or laboratory signal. As it is very nicely depicted in the book of H.E. White, Introduction to atomic spectra [White, 1934], several physicists were then trying to find arithmetic laws able to describe the observed

spectrums. This was a totally empirical task as it was well before the first relevant atomic model established by N. Bohr in 1913.
In 1885, as shown on fig 1.1, stellar observations allow to extend the observed spectrum of the hydrogen atom to 14 lines, involving thus Rydberg states. The same year, J. Balmer succeeds to write a simple formula describing perfectly the wavelengths of the observed lines. Others, still unobserved, lines predicted by the Balmer's formula were then observed proving the success of this early spectroscopic work.

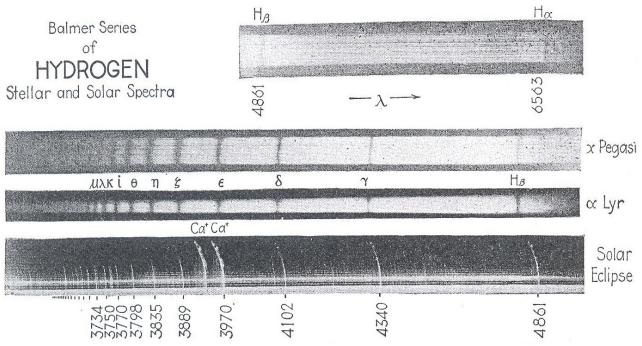

Figure 1.1: Spectroscopic data, from [White, 1934]

In 1888, J. Rydberg presented a new formula, generalization of the Balmer one, describing the wavenumber of spectral lines of Hydrogen and other alkali atoms.

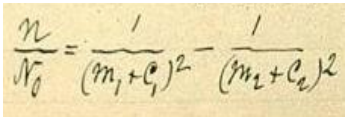

Figure 1.2: Original Rydberg formula [1], here n is the wavenumber of the lines, N_0 is a constant, m_1 and m_2 are two integers with $m_2 > m_1$, c_1 and c_2 are numbers dependent of the atomic specie and the series

This empirical formula gave in fact very interesting input for atomic Physics theory, namely the fact to express relation in term of wavenumber (proportional to the frequency, i.e., the photons energy), the use of universal constant identical for all the atomic species and the appearance of an important notion known now as the quantum defect.
This initial spectroscopic work have represented a solid experimental base and was determinant for the establishment of the quantum theory that followed. We could mention,

[1]The Rydberg formula as presented to Matematiskt-Fysiska frening, original document written November 5th, 1888 by Gustaf Daniel Heüman (1868-1934).

as an example, the notation, still used today, for the first values of the electron orbital momentum : s, p and d... coming from the names given by J. Rydberg to different kind of observed series being sharp, principal and diffuse.

1.2 General properties of Rydberg atoms

Quantum mechanics has been developed intensively during the first half of the 20^{th} century. One of the big advance was the establishment of the Schrödinger equation (1926) and concerning atomic Physics, its analytical solving for the Hydrogen atoms. We can find such development in many references, for example [Cohen-Tannoudji et al., 1986; Messiah, 1962], we assume here the reader to be familiar to the basis of atomic Physics and we focus on the main results concerning Rydberg atoms.

1.2.1 General remarks

Technicality of this section

The quantum treatment of Rydberg atoms, despite its relative simplicity compared to other systems, remains quite technical. As detailed calculations are presented in the Chapter 2 of this manuscript we stay in the present section on a non so technical level of description, allowing nevertheless to catch all the interesting features of Rydberg atoms Physics.

Basis of the Alkali Rydberg states

The description of the electronics quantum states of multi-electron atoms is a N-body problem impossible to solve exactly. the TDDFT (Time Dependent Density Functional Theory) [Runge and Gross, 1984; Marques et al., 2006] or Hartree-Fock methods with treatment of the electronic correlations (Post Hartree-Fock methods) aim to find approximated solutions [Friedrich, 1998].
A Rydberg atom is an atom with one electron in a highly excited state. We are interested, in a precise way, only to this so-called Rydberg electron because it is its behavior which determines all the electromagnetic properties of the atoms.
Since the Rydberg electron stays essentially far from all the other particles, we can reasonably separate this electron from the rest of the atom. Doing this, we have to deal with an effective 2-body problem, the dynamics of the Rydberg electron being described in considering an effective potential combining the effect of the nucleus and the other electrons.

This approximation could be done in principle, for all atomic species, even for molecules, as long as there is only one electron, in a highly excited state. Nevertheless, we consider in this thesis that we are dealing with alkali atoms, for which this approximation leads to quit accurate results. This is due to the fact that those atoms contain only one electron in the last shell. It is this electron which is excited in a Rydberg state and the other electron are forming full shells below it.
The main effect of the others electrons is to screen the nuclear charge, the effective potential seen by the Rydberg electron is then in first approximation the same than for the Hydrogen atom. In addition, despites the complexity of the Rydberg core structure, the Quantum Defect Theory (QDT) (see the review [Seaton, 1983]) allows to take in account its effects in a very convenient way. In the frame of the QDT, the description of the electronics quantum states of the Rydberg electron is formally similar to the case of Hydrogen. This theoretical simplicity is a big advantage of Rydberg atoms.
Even in the case of Hydrogen, the simple Coulomb potential, representing the electrostatics interaction between the nucleus and the electron, has to be completed by several other effects, like the spin-orbit coupling, the relativist effects and the effect of the nucleus spin. Taking into account those effects, leads in the quantum treatment to work with the most adapted basis. In the case of Rydberg states, we can very reasonably consider only the spin-orbit coupling, other effects and their corresponding energies being small enough to be neglected [1]. Consequently Rydberg states can be reasonably described using the fine-structure basis. We can write them using the Dirac's ket formalism as $|n, l, j, m_j\rangle$. Another widely used notation is the spectroscopic notation, nl_j (for example $63p_{3/2}$), where m_j is not specified.

Atomic units

In this manuscript, we will often express physical quantities in atomic units. Atomic units are defined by $\hbar = e = m_e = 4\pi\epsilon_0 = 1$. The following table gives the correspondence between atomic units and SI units of few quantities, starting from the 4 fundamental ones.

Other derived atomic units can be defined from this one, it is the case for speed, time, force, power, intensity, electric potential, electric field, electric dipole moment, magnetic field...

Obviously, dimensionless physical constant have the same value in any units system. It is the case for the fine-structure constant α

[1] Experimental measurements of hyperfine structure can be found in [Farley et al., 1977] (rubidium and cesium) and [Weber and Sansonetti, 1987; Goy et al., 1982] (cesium)

[2] The NIST Reference on Constants, Units and Uncertainty, for actualyzed values go to http://physics.nist.gov/cuu/Constants/ (http://www.nist.gov/)

Quantity	Name and symbol	value in SI units
Charge	Elementary charge, e	$1.602176565(35)10^{-19}$C
Mass	Rest electron mass, m_e	$0.910938291(40)10^{-30}$kg
Action	Reduced Planck's constant, $\hbar$	$1.054571726(47)10^{-34}$J.s
Electric constant	$1/4\pi\epsilon_0$	$8.9875517873681\ 10^{9}$kg.m^3.s^{-2}.C^{-2}
Length	Bohr's radius, a_0	$0.52917720859(36)10^{-10}$m
Energy	Hartree's energy, E_H	$4.35974417(75)10^{-18}$J

Table 1.1: Some atomic units, CODATA values [2](01/04/2012).

$$\alpha = \frac{e^2}{4\pi\epsilon_0\hbar c} \approx \frac{1}{137} \tag{1.1}$$

Where c is the speed of light. We see here that the value of c in atomic units is $c = 1/\alpha \approx 137$

1.2.2 Rydberg energies

general formula

For a given atomic specie and a given Rydberg state $|n, l, j, m_j\rangle$, in absence of external field, its energy, independent of m_j, is given by

$$E_{nlj} = -\frac{R_y}{(n - \delta_{nlj})^2} \tag{1.2}$$

Where R_y is the Rydberg's constant and δ_{nlj} is the quantum defect. Here the zero of energy is set to the ionization limit.
The Rydberg constant depend very slightly of the atomic specie through a multiplicative factor $\frac{1}{1+m_e/M}$ where M is the mass of the atomic nucleus. Looking out this factor, the Rydberg's constant can be express in function of other fundamental physical quantities

$$R_y = \frac{m_e e^4}{2(4\pi\epsilon_0\hbar)^2} \tag{1.3}$$

or again

$$R_y = \frac{1}{2}\alpha^2 m_e c^2 \tag{1.4}$$

The value of R_y is $\frac{1}{2}$ in atomic units, it corresponds to $13.60569253(30)$ eV. We also define R_∞ by $R_y = hcR_\infty$. R_∞ is the most accurately measured fundamental physical constant [Pohl et al., 2010].

Its value in SI units is $1.0973731568539(55).10^7$ m^{-1}.

It is interesting to notice that, as in the case of Hydrogen, the energy difference between two close Rydberg states scales as n^{-3}. This concerns the energy difference between two n-manifold as well as the fine-structure splitting.

quantum defect

The Rydberg energies formula is very close from the analytically determined Hydrogen energies formula. The only difference consists in the presence of the quantum defects δ_{nlj} (for Hydrogen all quantum defects are null). The physical meaning of the quantum defect is to reflect the fact that Rydberg core is not only a simple proton as it is the case for Hydrogen.
A very important point is that quantum defects and then Rydberg energies have to be determined experimentally. The values of quantum defects are indeed used as an input for many theoretical treatments of Rydberg atoms.
Nevertheless, it is possible to express the quantum defects using a simple relation involving only few parameters.

$$\delta_{nlj} = \delta_0(lj) + \frac{\delta_2(lj)}{(n-\delta_0(lj))^2} + \frac{\delta_4(lj)}{(n-\delta_0(lj))^4} + ... \tag{1.5}$$

This relation is called the Ritz's formula. The coefficients $\delta_0(lj)$ and $\delta_{2i}(lj)$ have to be determined experimentally for each atomic species.
Interestingly, the values of the quantum defects depend only very slightly of the principal quantum number, n. Besides, effects of the Rydberg core being non negligible only in the case of penetrating orbitals, the values of the quantum defects decrease very rapidly with the orbital momentum l and can be considered null for l bigger than few units.
Taking the case of cesium, we find in the reference [Goy et al., 1982] the following values of $\delta_0(lj)$ and $\delta_2(lj)$.

Such a table allows to determine the energies of all the Rydberg states of cesium. Although it depends of the Rydberg state in question, the order of magnitude of the precision obtained in such a determination is 10 MHz.
In other, more recent works, the quantum defect values of most of the alkali species have been determined up to $\delta_8(lj)$. The values of the quantum defects of lithium, sodium, potassium, rubidium and cesium atoms are reported in [Beterov et al., 2012], taken from the references therein.

$Series$	δ_0	δ_2
ns	4.049325	0.2462
$np_{1/2}$	3.591556	0.3714
$np_{3/2}$	3.559058	0.3740
$nd_{3/2}$	2.475365	0.5554
$nd_{5/2}$	2.466210	0.0670
$nf_{5/2}$	0.033392	-0.191
$nf_{7/2}$	0.033537	-0.191

Table 1.2: Cesium quantum defects, from [Goy et al., 1982]

Rydberg states in laboratory

Rydberg energies of the most commonly used alkali atoms are now very well known with a good precision via a precise determination of the quantum defects. On a technical point of view, the Rydberg states spectroscopy took a huge benefit from laser development (1960). Whereas first methods to create Rydberg atoms (electron impact or energy exchange) did not offer a very precise control on the populated Rydberg states, laser excitation of atomic sample toward Rydberg states allows to excite selectively a unique Rydberg state (for early experiment, see [Fabre et al., 1975; Harvey and Stoicheff, 1977; Lee et al., 1978] and the review [Fabre and Haroche, 1983]).
In today experiments, with the knowledge of Rydberg energies and the use of laser fields, we can excite selectively a given Rydberg states, easily up to $n = 100$, from ground states atoms. The fantastic point is that the Rydberg states binding energy is so small that we can excite a big range of Rydberg states using the same laser, if the wavelength of this latter can be tuned of only few nm.
Besides, the use of microwave fields allows to make transition between two Rydberg states close enough in energy.

1.2.3 Rydberg wave-functions

Rydberg wave-functions are known analytically in the case of Hydrogen [Bethe and Salpeter, 1957] but have to be approximatively evaluated for other atoms. The wave-functions can be decomposed, as in the case of Hydrogen, in an angular part and a radial part. Only the radial part differs from the case of Hydrogen, consequently, the selection rules coming from the angular part remains valid.
The difficulty comes from the determination of the radial wave functions. Several methods can be used to do this, all involving the knowledge of quantum defects. In the frame of the QDT, evaluation of the radial wave-functions can be done numerically us-

ing the Numerov integration method [Numerov, 1924]. An alternative way is the use of a semi-classical approach WKB [Friedrich, 1998]. Model potential can also be derived to reproduce the experimentally observed energies allowing to determine the radial wave-functions, this approach can be found in the reference [Klapisch, 1971].
In the frame of this thesis, we used the QDT approach with the Numerov integration method with the so-called Coulomb approximation. Excluding the small region containing the Rydberg core which is in a sens treated as a black-box, the QDT allows to determine quasi-exactly the electronic radial wave-functions of the Rydberg states. Although the precise form of the wave-functions inside the Rydberg core region might be required in some case, the knowledge of the wave-function outside this region, is sufficient for the determination of a large number of physical quantities. Namely, it is shown [Bates and Damgaard, 1949], that in the case of alkali atoms, we can determine accurately the transition dipole matrix using the QDT. The transition dipole matrix is a very important object allowing to calculate the coupling of an atom with a laser field, the stark effect or again the dipole-dipole interaction between two Rydberg atoms.
The numerical evaluation of Rydberg radial wave-functions via the Numerov method as well as the determination of the transition dipole matrix is presented in the Chapter 2 of this thesis. We see in the fig 1.3 a typical radial wave function calculated with this method.

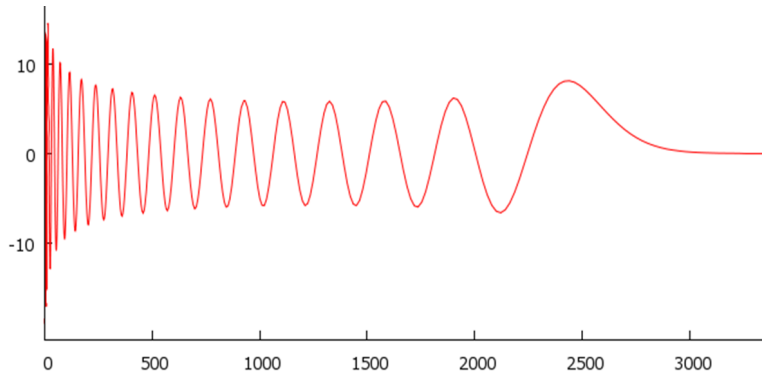

Figure 1.3: Radial wave function of the Rydberg state 40s of cesium calculated by the Numerov method under the Coulomb approximation. The distance from the core is given in atomic unit, the vertical axis has arbitrary unit.

1.2.4 Rydberg properties

From the knowledge of the Rydberg states wave-functions, physical properties of the Rydberg states can be determined. Interestingly, as the principal quantum number n

increases, the values of several physical quantities become exaggeratively huge in comparison to the ones of the fundamental states. This confers to the Rydberg atoms very unusual properties which are at the origin of the interest of the Rydberg atoms Physics. Rydberg properties have been already reported in many references, see for example [Gallagher, 1994].

Size of Rydberg atoms

First of all, the size of the Rydberg atoms, determined by the spatial expansion of the electronic wave-functions, become very rapidly huge as n increases. A good estimation of the average distance between the nucleus and the Rydberg electron, $\bar{R}$, is given in atomic units by

$$\bar{R} = 2n^2 \tag{1.6}$$

For large n, the size of Rydberg atoms is just enormous in comparison to normal atoms. Whereas heavy alkali atoms in their fundamental state have a size of the order of 1nm, the size of a Rydberg atom in the $n = 100$ state is of the order of 1μm.

Radiative lifetimes

An non very intuitive property of Rydberg atoms is that they have a very long radiative lifetime. A very simplified formula to estimate the lifetime of Rydberg states due to the vacuum radiation τ_{vac} is given by

$$\tau_{vac} \approx n^3(l + \frac{1}{2})^2 10^{-10}\text{s} \tag{1.7}$$

The accuracy of this formula is of the order of 10% and a much more accurate evaluation can be found in the reference [Horbatsch et al., 2005].
In addition, it is important for Rydberg states to take into account the effects of the blackbody radiation. A very precise study of this question is reported in [Farley and Wing, 1981] and more recently in [Beterov et al., 2009]. For a temperature T, a rough estimation of the additionnal decay rate Γ_{BBR} due to blackbody radiation is given by

$$\Gamma_{BBR} \approx 2.10^7 \frac{T(K)}{300K} n^{-2}\text{s}^{-1} \tag{1.8}$$

Even in presence of blackbody radiation, Rydberg lifetimes are very long. For $n = 100$ it is of the order of 100μs which is huge in comparison for example with the lifetime of the cesium first excited state which is around 30ns [Steck, 2003].

On the experimental point of view, this very long lifetime is one of the very nice advantage of Rydberg atoms. Indeed, in addition to the possibility to act on Rydberg atoms during this time, Rydberg states can very often be considered as infinitively long lived states in the modeling of the experiments.

Electric dipole moment

Another quantity which takes exaggerated values in the case of Rydberg states is the instantaneous electric dipole moment. Like the size of the Rydberg atoms its value in atomic units is n^2. The atomic unit for electric dipole moment being

$$ea_0 = 8.48.10^{-30} \text{ C.m} = 2.54 \text{ Debye} \tag{1.9}$$

The instantaneous electric dipole moments of Rydberg atoms can take values exceeding 10 000 Debye, to be compared with the electric dipole moment of the water molecule which is 1.83 Debye.
This notion of instantaneous electric dipole moment corresponds to a classical vision of the atom. In the quantum treatment, we have to use the transition dipole matrix whom relevant coefficient values follow the same scaling that the instantaneous electric dipole moment. It is the big value of the transition dipole matrix which is at the origin of the strong interactions between Rydberg atoms.

Sensitivity to electric field

The last property of Rydberg atoms that we will present here is their extreme sensitivity to an external electric field.
The case of the Hydrogen atom in presence of a dc electric field is well known to have analytical solution [Silverstone, 1978], the effect of the electric field is to lift linearly the l-degeneracy of the n manifold. The case of alkali atoms present a similar behavior, with particularities for the low l states for which the degeneracy is already lifted in zero-field due to the quantum defects.
The standard way to calculate the external electric field effect (Stark effect), was first presented in this reference [Zimmerman et al., 1979], it is also treated in the Chapter 2 of this thesis. We show in the fig 1.4 a typical Stark diagram, where Rydberg states energies are plotted versus the electric field.

Moreover, the presence of an electric field stronger than a certain value leads to the ionization of the Rydberg atoms. A good approximation of the field at which a non-hydrogenic Rydberg atom is ionized E_i is given by the so-called classical ionization limit [Gallagher, 1994]

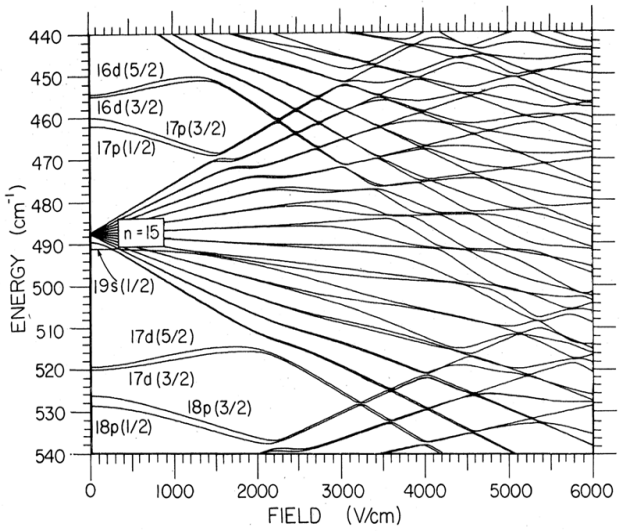

FIG. 20. Cesium, $|m_j| = \frac{1}{2}$.

Figure 1.4: Stark diagram of cesium around $n = 15$, from [Zimmerman et al., 1979]. A tiny mistake has been done in this diagram and the level above the manifold are $18d_j$ and $19p_j$

$$E_i = \frac{1}{16n^4} \tag{1.10}$$

Bellow the ionization field, the effect of the electric field is to modify the Rydberg energies as we see on the fig 1.4. The associated eigenstates are also modified, there is a mixing of the zero-field basis states in presence of electric field. One of the consequence of this mixing is to lift the selection rules relative to laser excitation. Another very interesting consequence in the frame of Rydberg-Rydberg interaction is that, in presence of electric field, Rydberg atoms acquire a permanent electric dipole moment. This can be quantified by the polarizability. In the regime of weak electric field, the polarizability of a Rydberg state scales as n^7 [Gallagher, 1994].
On the experimental point of view, the behavior of Rydberg atoms in electric field offers very nice advantages, it allows first to control the Rydberg energies by tuning the electric field applied to the atoms, secondly as we will see in the following section it allows to control the interactions between Rydberg atoms, finally it allows to ionize them. The remarkable point being the very week values (and then easily experimentally controllable) of the electric field involved in this processes, for example the required field to reach the ionization is of the order of 10V.cm^{-1} for $n = 100$.
The ability to ionize Rydberg atoms with relatively small electric field provides a very widely used way to detect them in cold atoms experiments, using the so-called field-

ionization detection. The principle of this method is to ionize the Rydberg atoms and use a charged particles detector to detect the created ions or electrons. The detection of charged particles being much more convenient than neutral one, this method allows interesting features as single particles detection or states selectivity.
The extreme sensitivity of Rydberg atoms to electric field could finally be exploited for the realization of high precision electric field sensors [Osterwalder and Merkt, 1999].

Rydberg properties and scaling law

As we can see in the precedent examples, physical quantities often follow scaling law parametrized by the principal quantum number n. We summarized them in the following table.

Quantities	scaling
Binding energy	n^{-2}
Energy difference between two n-manifold	n^{-3}
Fine-structure splitting	n^{-3}
Size	n^{2}
Geometrical cross section	n^{4}
Lifetime (for low l states)	n^{3}
Electric dipole moment	n^{2}
Polarizability	n^{7}
Classical ionization limit	n^{-4}

Table 1.3: Rydberg scaling law

1.3 Interaction between Rydberg atoms

One of the main interest of the Rydberg atoms Physics comes from the fact that Rydberg atoms can interact with each other. In a sense, Rydberg atoms are so sensitive to external perturbations that they can feel the presence of other Rydberg atoms even at large distances. Interactions between Rydberg atoms have the particularity to be very flexible, in term of strength, sign (we can have attractive or repulsive interactions), radial and angular dependencies. In addition, we can experimentally control those parameters essentially with the choice of the Rydberg state and the use of electric fields. This makes interacting Rydberg gases a very intense research field, experimentally as well as theoretically.

1.3.1 Electrostatic multipolar interactions

The nature of the interactions between Rydberg atoms is electrostatic. We can characterize the interaction between two Rydberg atoms in considering the Rydberg atoms as two electrostatic distributions.
A very useful description of an electrostatic distribution is the multipolar expansion. It consists in writing the distribution as a series of terms, the multipolar moments, for which we can calculate the radiated field. The firsts terms of the series are charge, dipole, quadrupole,... The interaction between two charge distributions can then be written as a series of multipolar interactions which are the interactions between two multipolar moments (one of each distributions). The first terms of the multipolar interactions series being, charge-charge, charge-dipole, dipole-dipole, charge-quadrupole, dipole-quadrupole,...
We see here that the hardly computable interaction between two random distributions is split into two main task, the computation of the multipolar moments of each distributions and the calculation of the interaction between multipolar moments, the interest being that the last can be done once and for all. In addition, all the power of the multipolar description comes from the fact that the different terms of the series are classified in term of strength of interaction and in practice only the few first terms are relevant in the total interaction.
A very important point is that the multipolar expansion is only valid in the case of two well spatially separated distributions.
This development was first done in the frame of classical electrostatic. However, it can be easily translated in quantum mechanics by the definition of the electrical multipolar operators (see Chapter 2).
In the case of Rydberg atoms, which are neutral particles, the most important term is the dipole-dipole term. Interaction between Rydberg atoms can be comfortably considered as dipole-dipole type, quadrupolar terms being much smaller [Singer et al., 2005].

1.3.2 Dipole-Dipole interaction between two Rydberg atoms

Classical dipole-dipole interaction

To start with dipole-dipole interaction, we present in this section results obtained by classical calculations. Those results can be transfered in quantum mechanics. In addition, it allow to introduce quite simply the so-called retardated dipole-dipole interaction.

Instantaneous dipole-dipole interaction

An electrostatic dipole, defined by its dipole moment $\vec{\mu}$, situated at the origin generates an electric field at the position $\vec{R} = R\vec{n}$ given in SI units by

$$\vec{E}(\vec{R}) = \frac{1}{4\pi\epsilon_0}\frac{3(\vec{n}.\vec{\mu})\vec{n} - \vec{\mu}}{R^3} \tag{1.11}$$

The dipole-dipole interaction, V_{dd}, between two classical dipoles a and b separated by a distance R along the direction of $\vec{n}$ is then

$$V_{dd} = -\vec{E_a}.\vec{\mu_b} = -\vec{E_b}.\vec{\mu_a} = \frac{1}{4\pi\epsilon_0}\frac{\vec{\mu_a}.\vec{\mu_b} - 3(\vec{\mu_a}.\vec{n})(\vec{\mu_b}.\vec{n})}{R^3} \tag{1.12}$$

We see that the dipole-dipole interaction presents a strong angular dependency, in function of the relative angle between each dipole moments and the axis between the dipoles, the interaction can either be attractive or repulsive (or null). In presence of an external electric field $\vec{F}$, stronger than the sum of the fields generate by the dipoles, those latter are aligned along the direction of $\vec{F}$. In this case, defining the angle θ between $\vec{n}$ and the field direction ($\cos\theta = \vec{n}.\vec{F}/\|\vec{F}\|$) we have

$$V_{dd} = \frac{\mu_a\mu_b}{4\pi\epsilon_0 R^3}(1 - 3\cos^2\theta) \tag{1.13}$$

In this formula, the radial dependence appears a bit more clearly. We have a maximally attractive interaction for the so-called head-to-tail configuration ($\leftarrow\leftarrow$) and a maximally repulsive one for the so-called side-to-side configuration ($\uparrow\uparrow$). The interaction is null for the so-called magic angle ($\theta = \arccos(\sqrt{\frac{1}{3}}) = 54.74^\circ$).

Retardated dipole-dipole interaction

Considering now an oscillating dipole with a dipole moment $\vec{\mu}\exp(-i\omega t)$ in complex representation. This dipole radiates an electromagnetic field at the position $\vec{R} = R\vec{n}$ whom electric part is $\vec{E}(t) = \vec{E}(\vec{R})\exp(-i\omega t)$ with

$$\vec{E}(\vec{R}) = \frac{exp(ikR)}{4\pi\epsilon_0}\left((k^2(\vec{n}\times\vec{\mu})\times\vec{n})\frac{1}{R} + (3(\vec{n}.\vec{\mu})\vec{n} - \vec{\mu})\left(\frac{1}{R^3} - \frac{ik}{R^2}\right)\right) \tag{1.14}$$

Where $k = \omega/c$ is the wavenumber of the emitted light.

Taking two of those oscillating dipoles a and b, having opposite oscillation frequency, separated by a distance R along the direction of $\vec{n}$. They interact via the so-called retar-

dated potential with an interaction energy $V_{Rdd} = Re[-\vec{E_a}(\vec{R}).\vec{\mu_b}] = Re[-\vec{E_b}(\vec{R}).\vec{\mu_a}]$ given by

$$V_{Rdd} = \frac{1}{4\pi\epsilon_0} \left((\vec{\mu_a}.\vec{\mu_b} - 3(\vec{\mu_a}.\vec{n})(\vec{\mu_b}.\vec{n})) \left(\frac{cos(kR)}{R^3} + \frac{ksin(kR)}{R^2} \right) + (\vec{\mu_a}.\vec{\mu_b} - (\vec{\mu_a}.\vec{n})(\vec{\mu_b}.\vec{n})) \frac{k^2 cos(kR)}{R} \right) \tag{1.15}$$

At short distances, $R < \lambda/2\pi$, λ being the wavelength of the emitted light by the dipoles, this energy is essentially the dipole-dipole interaction energy of the equation 1.12. At large distance, $R > \lambda$, only the term in $1/R$ is important.

Atomic dipole moment and transition dipole matrix

The equations 1.12 and 1.15 correspond to the case of classical dipoles, to obtain their quantum mechanical equivalents, we replace the vectorial dipole moments by operators. We define in this section the atomic dipole operator in the case of Rydberg atoms.
As already mentioned, we can consider that a Rydberg atom is formed by a core whose total electric charge is $+e$ and a Rydberg electron with an electric charge $-e$, the dipole operator, $\hat{\mu}$, of a Rydberg atom is then totally determined by the position of the Rydberg electron around the core, ie, the Rydberg wave function.
We define dipole operator of the Rydberg atom as

$$\hat{\mu} = e\hat{r} \tag{1.16}$$

Where $\hat{r}$ is the position operator of the Rydberg electron. The dipole operator is an odd operator.

It is very useful to express the dipole operator in the zero-field Rydberg states basis, this gives the so-called transition dipole matrix. The transition dipole matrix elements are

$$\vec{\mu}_{rr'} = \langle\, r \,|\hat{\mu}|\, r' \rangle \tag{1.17}$$

Where $|r\rangle = |n, l, j, m_j\rangle$ and $|r'\rangle = \left|n', l', j', m'_j\right\rangle$ are two zero-field Rydberg states. $\vec{\mu}_{rr'}$ is often called the dipole moment of the transition $|r\rangle \leftrightarrow |r'\rangle$.

A formal expression of the dipole operator using the transition matrix is

$$\hat{\mu} = \sum_{r,r'} \vec{\mu}_{rr'} \left|r\right\rangle \left\langle r'\right| \tag{1.18}$$

The classical value of the dipole moment, $\vec{\mu}_\Psi$, of a Rydberg atom in a state $|\Psi\rangle$ which is not necessarily a zero-field state, is given by the expectation value of $\hat{\mu}$ in the state $|\Psi\rangle$.

$$\vec{\mu}_\Psi = \left\langle \hat{\mu} \right\rangle_\Psi = \left\langle \Psi \left| \hat{\mu} \right| \Psi \right\rangle \tag{1.19}$$

Due to the selection rules on the angular part of the zero-field Rydberg wave functions, many terms of the transition matrix are null. In particular, they are null on the diagonal, $\vec{\mu}_{rr} = \vec{0}$, meaning that all the zero-field Rydberg states have no permanent electric dipole. In fact, only the transition dipole matrix elements between two Rydberg states for which we have $l' = \pm l$ and $m'_j = m_j$ or $m'_j = m_j \pm 1$ are non null.

The calculation of the transition dipole matrix is presented in the Chapter 2 of this manuscript.

Hamiltonian of the dipole-dipole interaction

The Hamiltonian representing the dipole-dipole interaction between two atoms a and b separated by a distance R along the direction of $\vec{n}$ is given by the classical expression of the dipole-dipole interaction given by the equation 1.12 replacing the classical dipole moments by the dipole operator of each atoms.

$$\hat{H}_{dd} = \frac{1}{4\pi\epsilon_0} \frac{\hat{\mu}_a.\hat{\mu}_b - 3(\hat{\mu}_a.\vec{n})(\hat{\mu}_b.\vec{n})}{R^3} \tag{1.20}$$

An important point is that we consider here that the two Rydberg atoms are well spatially separated, i.e., there is no spatial overlap between the wave functions. Indeed, we do not consider electronic exchange interaction. We can here do the link with the validity condition of the multipolar expansion where the two distributions have to be well spatially separated. Typically, The two Rydberg atoms have to be separated by more than $\approx 4n^2 a_0$ which is known as the LeRoy radius.

Interestingly, this Hamiltonian, obtained here by analogy with the classical case can be found starting directly from the electrostatic interaction Hamiltonian between two atoms, with the already mentioned approximation for Rydberg atoms, i.e., the Rydberg core is consider as a punctual charge $+e$. Considering two atoms a (core A, electron 1) and b (core B, electron 2) separated by $\vec{R}_{AB} = R\vec{n}$, the interaction Hamiltonian is in SI units

$$\hat{H}_{ab} = \frac{1}{4\pi\epsilon_0}\left(\frac{e^2}{R} - \frac{e^2}{\hat{r}_{A2}} - \frac{e^2}{\hat{r}_{B1}} + \frac{e^2}{\hat{r}_{12}}\right) \tag{1.21}$$

Here we write this Hamiltonian in the Born approximation leading to consider that the distance R between the two atoms is a parameter of the problem.
In writing $\hat{r}_{A2} = \vec{R}_{AB} + \hat{r}_{B2}$ and similar forms for $\hat{r}_{B1}$ and $\hat{r}_{12}$, with the use of the vectorial expansion $(\|\vec{R} + \vec{r}\|^2)^{-1/2} = \frac{1}{R}\left(1 - \frac{\vec{r}.\vec{n}}{R} + \frac{3(\vec{r}.\vec{n})^2 - r^2}{2R^2}\right)$, the leading term for large R of the Hamiltonian is given by

$$\hat{H}_{ab} = \frac{e^2}{4\pi\epsilon_0}\frac{\hat{r}_{A1}.\hat{r}_{B2} - 3(\hat{r}_{A1}.\vec{n})(\hat{r}_{B2}.\vec{n})}{R^3} = \frac{1}{4\pi\epsilon_0}\frac{\hat{\mu}_a.\hat{\mu}_b - 3(\hat{\mu}_a.\vec{n})(\hat{\mu}_b.\vec{n})}{R^3} = \hat{H}_{dd} \tag{1.22}$$

An expression of $\hat{H}_{dd}$ is often given in the particular case where $\vec{n}$ is along the quantification axis, called (Oz)

$$\hat{H}_{dd} = \frac{1}{4\pi\epsilon_0 R^3}(\hat{\mu_a}.\hat{\mu_b} - 3\hat{\mu_{z}}_a.\hat{\mu_{z}}_b) \tag{1.23}$$

Where $\hat{\mu_z}$ is the dipole operator along (Oz).

The Hamiltonian $\hat{H}_{dd}$ acts in the two-atoms space. In the most general case, considering a pair of two-atoms states $|r_a, r'_b\rangle$ and $|r''_a, r'''_b\rangle$, a and b being the two atoms separated by $R\vec{n}$ and $|r\rangle$, $|r'\rangle$, $|r''\rangle$ and $|r''\rangle$ 4 Rydberg states. The dipole-dipole coupling between those two states is

$$\langle r_a, r'_b|\, \hat{H}_{dd}\, |r''_a, r'''_b\rangle = \frac{1}{4\pi\epsilon_0}\frac{\vec{\mu}_{rr''}.\vec{\mu}_{r'r'''} - 3(\vec{\mu}_{rr''}.\vec{n})(\vec{\mu}_{r'r'''}.\vec{n})}{R^3} \tag{1.24}$$

Where $\vec{\mu}_{rr''} = \langle\, r\,|\hat{\mu}|\, r''\rangle$ and $\vec{\mu}_{r'r'''} = \langle\, r'\,|\hat{\mu}|\, r'''\rangle$

Stark Hamiltonian

As mentioned in the section 1.2.4, Rydberg atoms are very sensitive to the presence of an external electric field. Especially, the presence of an electric field gives them a permanent electric dipole moment.
The effect of an external electric field or Stark effect is given by the following Hamiltonian, we consider here a classical field, $\vec{F}$

$$\hat{H}_F = -\hat{\mu}.\vec{F} \tag{1.25}$$

Here again we see the analogy between the classical energy of an electric dipole $\vec{\mu}$

in an electric field $\vec{F}$ given by $-\vec{\mu}.\vec{F}$.

The dipole coupling due to the Stark effect between two Rydberg states $|r\rangle$ and $|r'\rangle$ is given by

$$\langle\, r|\hat{H}_F|r'\rangle = -\vec{\mu}_{rr'}.\vec{F} \tag{1.26}$$

The Stark effect being also determined by the transition dipole matrix, we have here again the selection rules imposed by the angular part of the Rydberg wave functions. Consequently, a Rydberg state is not shift by himself by the Stark effect but through the coupling with the other Rydberg states.
The diagonalization of the Stark Hamiltonian for a given electric field gives new eigenstates with new energies. To get an idea of the Stark effect on Rydberg atoms, it is interesting to represent the Rydberg energies in function of the strength of the electric field, this is what we call a Stark diagram as the one shown in the fig 1.4.

Full calculation vs model cases of Rydberg-Rydberg interaction

In principle, the calculation of interactions between two Rydberg atoms (as well as the Stark effect) with their associated potential curves where energies are plotted in function of the distance between the two Rydberg atoms, necessitates to take into account the full basis of the two-atoms Rydberg states (one atom basis for the Stark effect). This is what is done in calculations presented in the Chapter 2 of this manuscript.
However, it is often possible to consider two-level models as simplified treatments. Those model cases, presented in the next sections, allow to get the main physical ideas of Rydberg-Rydberg interactions and fully take part to the Rydberg atoms literature. The effects of the long-range dipole-dipole interactions between Rydberg atoms have been reviewed in [Gallagher and Pillet, 2008].

Dipole-Dipole interaction in electric field

The most simple case of interaction is when Rydberg atoms have a permanent dipole moment, so, in presence of electric field. Indeed, in electric field, the mixing of the zero-field Rydberg states by the Stark effect leads to new eigenstates which possess a permanent dipole moment.

In the case of Rydberg states with non-null quantum defect ($l = s, p, d$), which are the states concretely excited in experiments, and for a relatively small electric field, $\vec{F}$, we can often consider that a given state $|r\rangle$ is coupled under the effect of the electric field with only one other state $|r'\rangle$ being the closest state in energy with allowed dipole

transition. As illustrative example, in the cesium, the states $|r\rangle = |n, p\rangle$ are mainly coupled with the states $|r'\rangle = |n-1, d\rangle$.

In this case, the total Hamiltonian, including the Stark one is represented in the two states basis $|r\rangle, |r'\rangle$ by the following matrix

$$\begin{pmatrix} E_r & -\mu_{rr'}F \\ -\mu_{rr'}F & E_{r'} \end{pmatrix} \tag{1.27}$$

Where E_r and $E_{r'} = E_r + \delta_{rr'}$ are the energies of $|r\rangle$ and $|r'\rangle$ in absence of electric field and $\mu_{rr'}$ the transition dipole matrix element $\langle\, r\,|\hat{\mu}|\, r'\rangle$.
When diagonalizing this Hamiltonian, we obtain new eigenstates $|r(\vec{F})\rangle$ and $|r'(\vec{F})\rangle$. Looking at the state $|r(\vec{F})\rangle$, we have

$$|r(\vec{F})\rangle = cos(\frac{\Theta}{2})\,|r\rangle - sin(\frac{\Theta}{2})\,|r'\rangle \tag{1.28}$$

Where Θ is a scale parameter defined by $tan\Theta = \frac{\mu_{rr'}F}{\delta_{rr'}/2}$.

In addition to have a slightly different energy in comparison to $|r\rangle$, $E_{r(\vec{F})} = E_r + \frac{\delta_{rr'}}{2}(1 - \sqrt{1 + tan(\Theta)^2})$, $|r(\vec{F})\rangle$ possesses a classical permanent dipole moment, $\vec{\mu}_r(\vec{F})$ aligned along the direction of $\vec{F}$ with the value

$$\mu_r(F) = \mu_{rr'}sin\Theta \tag{1.29}$$

Consequently, two Rydberg atoms separated by $R\vec{n}$ excited in electric field in the state $|r(\vec{F})\rangle$ interact as classical dipoles with a dipole-dipole interaction energy given by the equation 1.13 where $\mu_a = \mu_b = \mu_r(F) = \mu_{rr'}sin\Theta$

$$V_{dd} = \frac{\mu_{rr'}^2 sin^2\Theta}{4\pi\epsilon_0 R^3}(1 - 3cos^2\theta) \tag{1.30}$$

Experimentally, the application of a small electric field is a very simple way to control the interaction strength between Rydberg atoms. The other one being to change the principal quantum number n, with a scaling as n^4, coming from the n^2 scaling of the transition dipole matrix.

Migration reaction and Förster resonance

In absence of electric field, Rydberg atoms have no permanent dipole moments. Considering two atoms a and b separated by $R\vec{n}$ in the two-atoms state $|r_a, r'_b\rangle$, this state does not possess by itself an interaction energy due to the dipole-dipole Hamiltonian

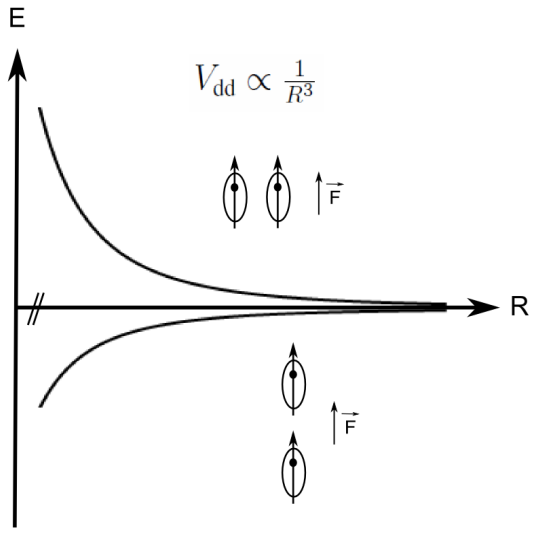

Figure 1.5: dipole-dipole interaction in presence of an external electric field

$\hat{H}_{dd}$ given in the equation 1.20. We have to consider the dipole-dipole coupling with other two-atoms states to calculate the Rydberg-Rydberg interaction between the two atoms.
For another given two-atoms state $|r''_a, r'''_b\rangle$, this coupling is $\langle r_a, r'_b| \hat{H}_{dd} |r''_a, r'''_b\rangle$ whose expression is given by equation 1.24.

A very interesting situation is when there is a state $|r''_a, r'''_b\rangle$ coupled via $\hat{H}_{dd}$ to $|r_a, r'_b\rangle$ and having the same energy, i.e., $E_r + E_{r'} = E_{r''} + E_{r'''} = E_{R(\infty)}$.
In this case, we have a mutual exchange of excitation between the two atoms due to dipole-dipole coupling which can be viewed as a resonant reaction $r + r' \leftrightarrow r'' + r'''$.
The total Hamiltonian, including $\hat{H}_{dd}$, is written in the two states basis $(|r_a, r'_b\rangle, |r''_a, r'''_b\rangle)$ as

$$\begin{pmatrix} E_{R(\infty)} & V \\ V^\dagger & E_{R(\infty)} \end{pmatrix} \tag{1.31}$$

Where $V = \langle r_a, r'_b| \hat{H}_{dd} |r''_a, r'''_b\rangle$.

Before calculating the new eigenstates and their shift in energy in comparison to the non interacting case, we will use this case of two interacting resonant dipoles to introduce "semi-classically" the retardated potential.
Due to the dipole-dipole coupling V, the two-atoms system is doing Rabi oscillations between the states $|r_a, r'_b\rangle$ and $|r''_a, r'''_b\rangle$ with a frequency $2\pi\frac{V}{\hbar}$. Looking at each atoms

separately, at every time, they are both doing a transition between two quantum states, $|r\rangle \rightarrow |r''\rangle$ for the atom a and $|r'\rangle \rightarrow |r'''\rangle$ for the atom b. Consequently, they can be considered as classical oscillating electric dipoles $\vec{\mu} exp(-i\omega t)$ where $\vec{\mu}$ is the transition dipole matrix element of the transition and $\hbar\omega$ the energy of the transition. For instance $\vec{\mu}_a = \vec{\mu}_{rr''} = \langle\, r\,|\hat{\mu}|\, r''\rangle$ and $\hbar\omega_a = E_r - E_{r''}$ for the atom a and $\vec{\mu}_b = \vec{\mu}_{r'r'''} = \langle\, r'\,|\hat{\mu}|\, r'''\rangle$ and $\hbar\omega_b = -\hbar\omega_a = E_{r'} - E_{r'''}$. This situation is exactly the one leading to the retardated potential presented in the section 1.3.2.
In such a situation, the two Rydberg atoms a and b have an interaction energy V_{Rdd}, given by the equation 1.15 where we have to replace the classical dipole moments by the appropriated transition dipole matrix elements and k by $\frac{\omega_a}{c}$.

We see with this ideal case of two atoms with a perfectly resonant coupling that the dipole-dipole Hamiltonian $\hat{H}_{dd}$ should be replaced by the retardated dipole-dipole Hamiltonian (equivalent to the equation 1.15 replacing vectors by operators) when dipole-dipole interaction comes from the coupling between different two-atoms states. This corresponds to the fact that the dipole moment of a transition is not a permanent dipole given by $\vec{\mu}_{rr'} = \langle\, r\,|\hat{\mu}|\, r'\rangle$ but an oscillating dipole given by $\vec{\mu}_{rr'} exp(-i\omega_{rr'}t)$.
However, the interaction energy V_{Rdd} given in the equation 1.15 is valid only in the case of two resonant dipoles with exactly opposite oscillation frequencies. A derivation of the retardated Hamiltonian in the general case would necessitate tedious quantum electrodynamic calculations (a derivation of the retardated dipole-dipole quantum Hamiltonian for the resonant case is for example given in the appendix of the reference [Comparat and Pillet, 2010]).
Interestingly, for interatomic distances R shorter than $\frac{\omega}{c}$ where ω is the frequency of the atomic transition, the equation 1.15 is equivalent to the classical dipole-dipole interation 1.12. For transition between close Rydberg states, $\frac{\omega}{c}$ is a very large distance, consequently, we use in all the following $\hat{H}_{dd}$ as the Hamiltonian of the dipole-dipole interaction and neglect the retardation effects.

The diagonalization of the matrix 1.31 leads to two new eigenstates $\frac{1}{\sqrt{2}}(|r_a, r'_b\rangle + |r''_a, r'''_b\rangle)$ and $\frac{1}{\sqrt{2}}(|r_a, r'_b\rangle - |r''_a, r'''_b\rangle)$. Their energies are given by

$$E_{\pm} = E_{R(\infty)} \pm E_{dd} \tag{1.32}$$

Where $E_{dd} = V = \langle r_a, r'_b|\, \hat{H}_{dd}\, |r''_a, r'''_b\rangle$. We see here that, in the case of resonant exchange of excitation, the two-atoms states are shifted in comparison with the non interacting case by the quantity E_{dd} with a characteristic radial dependency in $\frac{1}{R^3}$. We say that the energy shift due to the dipole-dipole interaction in the case of resonant

reaction is of the form $\frac{C_3}{R^3}$ where the C_3 coefficient is given by

$$C_3 = \vec{\mu}_{rr''}.\vec{\mu}_{r'r'''} \tag{1.33}$$

The scaling in n^2 of the transition dipole matrix gives a scaling of C_3 in n^4.
The resonant exchange of excitation is finally a very nice way to create entanglement between two Rydberg atoms.

Migration reaction

One excitation exchange reaction between Rydberg atoms is always exactly resonant. It is the reaction $|r_a, r'_b\rangle \leftrightarrow |r'_a, r_b\rangle$ where the two atoms simply exchange their Rydberg states, this reaction will appears if $|r\rangle \rightarrow |r'\rangle$ has a non null transition dipole matrix element $\vec{\mu}_{rr'}$. It is the case, for example of the reaction $|ns, np\rangle \leftrightarrow |np, ns\rangle$.
Although this reaction is always resonant, it necessitates nevertheless to prepare experimentally the atoms in two different Rydberg states.
An interesting situation would be to have one atom in a state $|r\rangle$ surrounded by atoms in another state $|r'\rangle$, this would lead to a diffusion of the $|r\rangle$ excitation [Mourachko et al., 2004] with possible analogy with diffusion of excitons [Tokihiro et al., 1995; Mülken et al., 2007] or spin glasses systems [Castellani and Cavagna, 2005]. It could be also a way to implement experimentally a quantum random walk [Côté et al., 2006].
In this case, the dynamics of the diffusion plays a very important role and the use of the retardated Hamiltonian is desirable.

Förster resonance

We are especially interested in the reaction of the form $|r_a, r_b\rangle \leftrightarrow |r'_a, r''_b\rangle$. The initial state being formed by two atoms in the same Rydberg state, this situation has a stronger link than the Migration reaction to most of the Rydberg experiments.
A priori, the energy conservation condition, $2E_r = E_{r'} + E_{r''}$ is hardly filled. However, it is possible to bring this reaction exactly at resonance if an experimental parameter allows to tune the Rydberg state energies. It is the case with the application of a very small electric field. We are not interested here in the creation of permanent dipole moment due to the Stark effect but only at the shift in energy of the Rydberg states. As an example, in cesium, by stark effect, the $|n, p\rangle$ energy level can be put midway between the energy of the $|n, s\rangle$ and $|n + 1, s\rangle$ states.
Interest of Förster resonance is first that it generates strong interactions between Rydberg atoms of the form $\frac{C_3}{R^3}$. Secondly, starting from a gas where we excite one Rydberg state, new Rydberg states will be created by exchange of excitation due to the Förster

resonance. This last point is a very useful way to find and optimize Förster resonances experimentally, we have to use in this case a state-selective detection. The two atoms of the pair are finally entangled when they interact trough a Förster resonance, the eigenstates being $\frac{1}{\sqrt{2}}(|r_a, r_b\rangle + |r'_a, r''_b\rangle)$ and $\frac{1}{\sqrt{2}}(|r_a, r_b\rangle - |r'_a, r''_b\rangle)$.
The name of Förster resonance has been given by Thad Walker and Mark Saffman in [Walker and Saffman, 2005] by analogy with the FRET (Förster Resonant Energy Transfer). The FRET is a process present in biology [Förtser, 1948] and occurs when the dipolar interaction between two molecules allows an energy transfer from one molecule to the other, becoming then fluorescent.

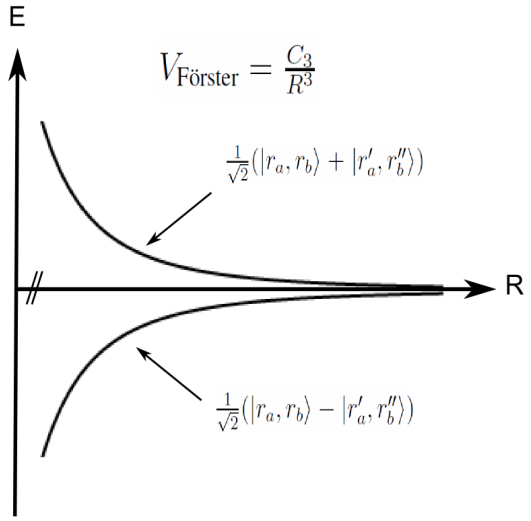

Figure 1.6: Rydberg-Rydberg interaction in the case of Förster resonance

Van-der-Waals interaction

The Van-der-Waals interaction corresponds to the case where there is no external electric field and no resonant reaction. As in the case of Förster resonance, we are interested to calculate the interaction energy of a pair of atoms a and b separated by $R\vec{n}$ in the same Rydberg state, i.e., $|r_a, r_b\rangle$. The interaction energy of the pair of atoms is determined by the coupling with all the other two-atoms states, however, in order to treat the problem with a two level description, we will consider the coupling with only one other state $|r''_a, r'''_b\rangle)$ being the closest state in energy with allowed dipole transition.
In this case, the total Hamiltonian is written in the two states basis $(|r_a, r_b\rangle, |r'_a, r''_b\rangle)$ as

$$\begin{pmatrix} E_{R(\infty)} & V \\ V^\dagger & E_{R(\infty)} + \delta_E \end{pmatrix} \tag{1.34}$$

Where $V = \langle r_a, r_b | \hat{H}_{dd} | r'_a, r''_b \rangle$, $E_{R(\infty)} = 2E_r$ and δ_E is the so-called Förster energy mismatch between the two states, $\delta_E = E_{r'} + E_{r''} - 2E_r$.
The diagonalization of this Hamiltonian leads to two new eigenstates $\widetilde{|r_a, r_b\rangle}$ and $\widetilde{|r'_a, r''_b\rangle}$. Looking at $\widetilde{|r_a, r_b\rangle}$, its energy is given by $E_{R(\infty)} + E_{VdW}$ with

$$E_{VdW} = \frac{\delta_E}{2} + \sqrt{\left(\frac{\delta_E}{2}\right)^2 + VV^\dagger} \tag{1.35}$$

and its component on the states $|r_a, r_b\rangle$ and $|r'_a, r''_b\rangle$ are in the ratio $\frac{V}{E_{VdW} - \delta_E}$.

In the limit of large distance, i.e., when V is much smaller than δ_E, we obtain

$$E_{VdW} = \frac{VV^\dagger}{\delta_E} \tag{1.36}$$

This result at large distance is exactly the one obtained by the second order perturbation theory.

As V has a characteristic radial dependency scaling as $\frac{1}{R^3}$, the energy shift E_{VdW} scales as $\frac{1}{R^6}$. We say that the energy shift due to the dipole-dipole interaction in absence of resonant reaction and for large distance is of the form $\frac{C_6}{R^6}$ where the C_6 coefficient or Van-der-Waals coefficient is given by

$$C_6 = \frac{(\vec{\mu}_{rr'}.\vec{\mu}_{rr''})^2}{\delta_E} = \frac{C_3^2}{\delta_E} \tag{1.37}$$

The scaling in n^2 of the transition dipole matrix together with the scaling in n^{-3} of energy difference between close Rydberg states give a scaling of the C_6 coefficient in n^{11}

Limitation of those two-levels models

This treatment of the dipole-dipole interaction using two-levels models is very interesting to extract the main physical ideas of the dipole-dipole interaction with namely the radial dependencies and the scaling laws in function of n. However, several reasons impose to go beyond those two-levels models.

In the case of Van-der-Waals interaction, we can first consider that there is not only one other state coupled with the initial one. A possible treatment is to use the second order perturbation theory, the total Van-der-Waals shift of one state is then given by the sum of the two-levels Van-der-Waals shifts relative to all the other states. This is what is done in reference [Singer et al., 2005].

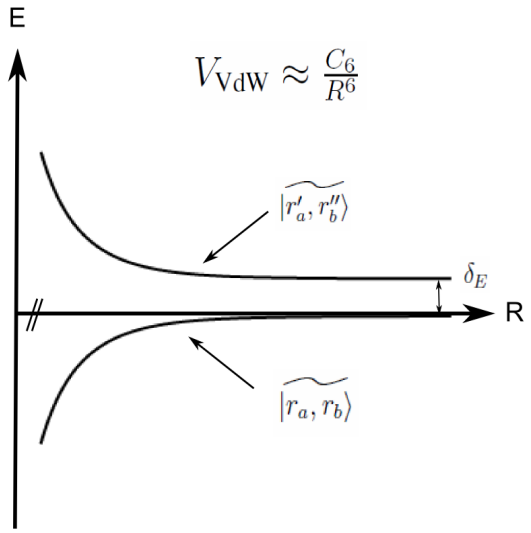

Figure 1.7: Rydberg-Rydberg interaction in the Van-der-Waals case

Another limitation of this two-levels models is due to the zero-field Rydberg states degeneracy relative to the quantum number m_j, called Zeeman degeneracy. The calculation of dipole-dipole interaction should be done, at least, inside each subspace of states of the form $|r_a, r_b\rangle = |(n,l,j)_a,(n,l,j)_b\rangle$ coupled with $|r'_a, r''_b\rangle = |(n',l',j')_a,(n'',l'',j'')_b\rangle$. This was done in the reference [Walker and Saffman, 2008]. It appears that dipole-dipole interaction can take a very wide spectrum of values in function of the different possible combinations of the m_j of the two atoms. The new eigenstates are, after diagonalization, superpositions of natural $\left|(n,l,j,m_j)_a,(n,l,j,m'_j)_b\right\rangle$ states (see chapter 2), this explains why results obtained in [Singer et al., 2005] are not completely sufficient to describe the Rydberg-Rydberg interaction.

Another interesting feature of Rydberg-Rydberg interaction which is non visible with the two-levels models is the existence of molecular potential well. It appears that a particular two-atoms Rydberg state can be attractive at long distance and becomes repulsive at shorter one due to the successive interactions with two other states. This can lead to the formation of Rydberg-ground state molecules as predicted in [Greene et al., 2000] and observed in [Bendkowsky et al., 2009] as well as Rydberg-Rydberg molecules as predicted in [Boisseau et al., 2002; Farooqi et al., 2003] and observed in [Overstreet et al., 2009].

Finally, a strong effect of the dense Rydberg spectrum appears for very small inter-

atomic distance (few μm). At such distances the interactions are so strong that a huge number of pair states are coupled together. The eigenstates of a pair of interacting Rydberg atoms are superpositions of many non-interacting ones and their energies are almost chaotic. The associated potential, the so-called Spaghetti curves, can be determined only numerically.

All those interesting features of the Rydberg-Rydberg interaction are presented in the chapter 2 of this manuscript.

1.3.3 Few-body effects

We have, up to know, considered the Rydberg-Rydberg interaction between only two atoms. The treatment of N atoms possessing each one N_R Rydberg states has a complexity growing in $(N_R)^N$. If very interesting phenomenon can arise from the interactions between few Rydberg atoms, general calculations of already the 3-body interactions, has not been performed yet. In addition to the huge number of states involved in the problem, one obvious complication which nevertheless is quite problematic comes from the fact that we need 3 coordinates to define the relative position between 3 Rydberg atoms (for example 2 distances and 1 angle) whereas only 1 distance is required in the case of two atoms. Potential curves of the 2-body problem are replaced by potential hyper-surfaces at 3 dimensions.
Nevertheless, theoretical analysis of 3-body Rydberg interactions has been performed in some specific situations as reported for example in [Pohl and Berman, 2009; Cano and Fortágh, 2012]. In [Han, 2010] 3-body interactions calculations and successfull comparison with experimental observations are reported. In [Younge et al., 2009] an experimental observation is reported together with theoretical analysis showing that taking into account several-body interactions is needed (the precise number is not reported).
In the frame of this thesis, a demonstration of a coherent 4-body process has been realized [Gurian et al., 2012], this is the subject of the chapter 3 of this manuscript.

1.3.4 Many-body effects

The case of an ensemble of many interacting Rydberg atoms is even more complex. Nevertheless, the presence of many-body atomic correlation, the possible analogies with solid state Physics and the possible application in quantum information makes this topic very attractive.
Theoretically, a possibility is to treat the problem with statistical Physics approaches. However, since quantum correlations play a central role in such many-body interacting

system, the development of sophisticated theoretical models including the full dynamics and the description of quantum correlations is currently an intense field of research.
On the experimental side, many-body effects in Rydberg gases has been observed now for more than ten years [Anderson et al., 1998; Mourachko et al., 1998]. Because the main (if not the only) tool of modern atomic Physic experiment is the use of electromagnetic field, many-body Rydberg interactions effects are largely studied via the coupling of an atomic ensemble with the electromagnetic field. In this frame, one central phenomena focused the attention of experimental and theoretical studies, the dipole blockade. The Dipole blockade is the subject of the next section.

1.4 Dipole blockade

The dipole blockade phenomenon [Jaksch et al., 2000; Lukin et al., 2001] and its numerous exciting applications is the subject of several articles, see for example the reviews [Comparat and Pillet, 2010; Saffman et al., 2010], most of the applications are in the context of quantum computation and quantum simulation. We will present the main discoveries of this last ten years on dipole blockade Physics all along this section as well as in the section 1.5 which is focused on the possible applications.

1.4.1 Principle of the dipole blockade

The Dipole blockade phenomenon is directly linked to the presence of interactions between Rydberg atoms. For simplicity reasons, we first present the dipole blockade phenomenon without paying too much attention to the detail of the Rydberg-Rydberg interaction, we just assume that two Rydberg atoms in a state $|r\rangle$ separated by a distance R has an interaction energy $V_r(R)$. Doing this we assume that the Rydberg-Rydberg interaction is isotropic, the strong angular dependency of the dipole-dipole interaction is then forgotten, although it has obviously an effect when we consider 3 dimensional ensemble.
The dipole blockade phenomena appears in the situation where, in an atomic sample, atoms in the ground state $|g\rangle$ are coupled with a laser field resonant with the transition $|g\rangle \rightarrow |r\rangle$ to a Rydberg state. The laser field has thus a frequency ω_L equal to the frequency ω_{gr} of the transition between the ground state and the Rydberg state for an isolated atom in zero-field. The effect of the laser field on a isolated atoms is described via the Rabi frequency, $\Omega = \langle g| - \vec{\mu}.\vec{E}|r\rangle$.
The principle of the dipole blockade is that, due to the shift in energy $V_r(R)$ induced by the interaction between Rydberg atoms, the firstly created Rydberg excitations bring the

laser out of resonance for further ones which are then blockaded. The dipole blockade mainly appears as a self-limitation of the Rydberg excitations.
We will first present the situation where Rydberg-Rydberg interactions allow the presence of only one Rydberg excitation. We call this situation a fully blockaded ensemble. In this frame, we are going to treat two different cases, the conditional excitation and the collective excitation. Whereas all the atoms of the atomic ensemble are excited together by the same laser field in the case of collective excitations, the atoms are excited individually (selectively) in the case of conditional excitations.

Conditional excitation

For a conditional excitation, we consider that an atom i is initially excited in the Rydberg state, the state of the full ensemble of N atoms being then

$$|r_i\rangle = |g_1, ..., g_{i-1}, r_i, g_{i+1}, ..., g_N\rangle \tag{1.38}$$

Considering the effect of the Rydberg-Rydberg interaction, every atom j of the sample have their Rydberg state shifted due to the presence of the Rydberg excitation of the atom i. The shift on the atom j being $V_{ij} = V(R_{ij})$ where R_{ij} is the distance between atom i and atom j. A relevant quantity of the problem is the so-called blockade radius, R_b defined as

$$\hbar\Delta\omega_{eff} = V(R_b) \tag{1.39}$$

Where $\Delta\omega_{eff}$ is the effective linewidth of the laser given by the combined effect of the natural linewidth and all the possible sources of broadening (intensity broadening, Fourier broadening, ...)

The blockade radius corresponds physically to the minimum distance from the atom i at which an atom j can be excited in the Rydberg state. Indeed, below R_b, the Rydberg shift $V(R)$ being bigger than the effective linewidth of the laser it prevents other Rydberg excitations (see fig 1.8).
We can imagine, as a useful vision, that the Rydberg excited atom i is surrounded by a so-called blockade-sphere whose radius is R_b inside which no other Rydberg excitations are possible.
For a sample whose size is smaller than R_b , i.e. a fully blockaded ensemble, the presence of a the Rydberg atom i prevents totally the possibility to excite other Rydberg atoms. In this case, the Rydberg excitation of all the other atoms is conditioned by the excitation of the atom i.

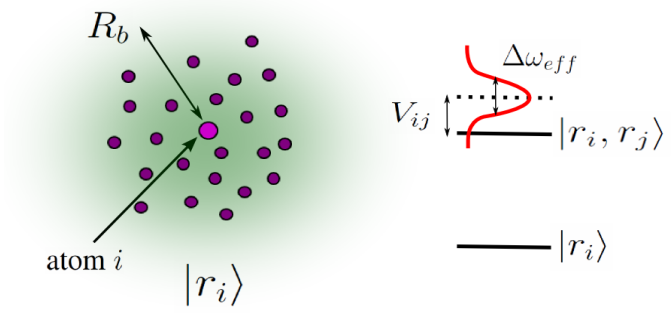

Figure 1.8: Schematic vision of the conditional dipole blockade. On the left, a fully blockaded ensemble is represented, the atom i is in the Rydberg state and prevents other Rydberg excitation within a blockade sphere. On the right, the energy level of any doubly excited state is schematically represented, in comparison to the non interacting (dashed level) the level are shifted by V_{ij}, the laser whom the spectrum is represented by the red curve is out of resonance.

Collective excitation

In the case of collective excitation, we shine all the atoms together with the same laser field. The atoms being indistinguishable relatively to the laser excitation, Rydberg excitations are shared collectively by all the atoms.
The state, $|\Psi_1\rangle$, describing the presence of 1 Rydberg excitation is in this case the symmetrical superposition of the states $|r_i\rangle$ of the equation 1.38 where we take into account the relative phase of the laser field (wave vector $\vec{k}$) in the position $\vec{R}_i$ of each atoms.

$$|\Psi_1\rangle = \frac{1}{\sqrt{N}}\sum_{i=1}^{N} e^{-i\vec{R}_i.\vec{k}}\,|r_i\rangle \tag{1.40}$$

This phase factor is relevant when considering cooperative emission of the Rydberg excitation but not for the blockade phenomenon itself. In the following we will thus systematically forget the phase factor $e^{-i\vec{R}_i.\vec{k}}$. In the fig 1.9 we represent schematically the construction of the state $|\Psi_1\rangle$

In the case of a fully blockaded ensemble, the state $|\Psi_1\rangle$ is the only state containing Rydberg excitation which can be populated, all the states with two Rydberg excitations being shifted out of resonance of the laser field due to the Rydberg-Rydberg interaction. So, $|\Psi_1\rangle$ together with the collective ground state $|G\rangle = |g_1, ..., g_N\rangle$ where all the atoms are in the ground state, form the full basis of the system. Interestingly, the Rabi frequency, Ω_N, associated to the excitation of the state $|\Psi_1\rangle$ from the ground state $|\,G\rangle$, differs from the case of a single isolated atom by a factor $\sqrt{N}$ where N is the number of atoms in the sample.

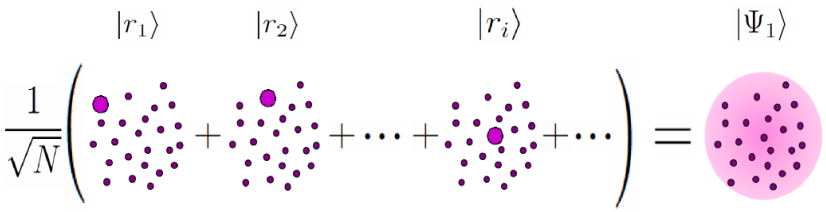

Figure 1.9: Schematic vision of the symmetrical state $|\Psi_1\rangle$

$$\Omega_N = \sqrt{N}\Omega \tag{1.41}$$

A fully blockaded ensemble, can be considered as a two-level system, characterized by an enhanced coupling with the laser field. It became common to call it a Super-atom in the Rydberg literature.

1.4.2 Non fully blockaded ensemble

Whereas the laser excitation of a fully blockaded ensemble takes formally a very simple form, the case of an ensemble where several Rydberg excitations can be present at the same time is much more problematic. If the corresponding equations are not very hard to formulate, the problem is linked to the big number of quantum states that we have to consider (2^N in considering N two-level atoms) which rapidly makes the system uncomputable.
We present here the theoretical frame relative to the laser excitation of a non fully blockaded ensemble, namely, the several approximations commonly done to express the corresponding Hamiltonian.

Atomic gas in the frozen approximation

We consider an atomic gas composed by N atoms. Atoms are considered to be two-level atoms, levels being the ground state $|g\rangle$ and a Rydberg state $|r\rangle$. We note $\hbar\omega_{gr} = E_r - E_g$ the transition energy between the ground state and the Rydberg state.
As already mentioned, the Rydberg-Rydberg interaction is first considered to be isotropic and we define $V(R)$ as the interaction energy of two atoms in the Rydberg state $|r\rangle$ separated by the distance R.
We consider that the Rydberg state $|r\rangle$ has an infinite lifetime since the typical duration of a dipole blockade experiment ($\approx 1\mu s$) is much shorter than Rydberg lifetime ($\approx 100\mu s$).
Finally, we use the so-called frozen gas approximation, which consists in neglecting all

the atomic motion. This is justifies in most of the cold Rydberg experiments due to the ultra low temperature and the short duration of the experiments. In fact, in addition to the thermal motion, the possible motion due to the force generated by the Rydberg-Rydberg interaction should also be considered carefully to justify the frozen approximation. Also, the "thermal speed" of the atoms can play a role through the Doppler effect.

Laser field

We consider the effect of the laser field with a semi-classical treatment. As suggested by the introduction of the Rabi frequency $\Omega = \langle g| - \vec{\mu}.\vec{E}|r\rangle$, we treat the atom-laser interaction with the electric dipole approximation and we use the rotative waves approximation.
The laser is supposed to be perfectly monochromatic.
We finally define the detuning of the laser relatively to the atomic resonance $\delta = \omega_L - \omega_{gr}$, with this convention, a red detuned laser has a negative detuning.

Hamiltonian of the system

The Hamiltonian of the system that we just describe, with the mentioned approximations can be written as follows

$$H = -\hbar\delta\sum_{i=1}^{N}\hat{\sigma}_{rr}^{i} + \frac{\hbar\Omega}{2}\sum_{i=1}^{N}\left[\hat{\sigma}_{gr}^{i} + \hat{\sigma}_{rg}^{i}\right] + \sum_{i=1,j<i}^{N} V_{ij}\hat{\sigma}_{rr}^{i}\hat{\sigma}_{rr}^{j}$$

Where we define transition and projection operators $\hat{\sigma}_{\alpha\beta}^{i} = |\alpha_i\rangle\langle\beta_i|\,(\alpha,\beta = g,r)$. Here $V_{ij} = V(R_{ij})$ where R_{ij} is the distance between atoms i and j.

In the frame of the dipole blockade, this Hamiltonian is the most simple that we can write. Nevertheless, a lot of physical effects could be add, we mention here some of them. To deal more properly with the large variety of Rydberg-Rydberg interaction, we should add an angular dependency to the interaction potential R_{ij} becoming $\vec{R}_{ij}$. This Hamiltonian could be completed by non-Hamiltonian operators allowing to deal with decoherence effects like finite life time of the Rydberg state and laser linewidth. Finally, it would be very interesting to consider three-levels atoms in order to deal with two-photon excitation or EIT effect.
All those effects appears still in the frozen gas approximation, the inclusion of the spatial motion of the atoms could allow to consider for example dynamical collisions.
Some of the theoretical references mentioned in the following deals with this additional effects.

1.4.3 Theoretical treatments of the dipole blockade

The difficulty to solve the Schrödinger equation (Von Neumann if needed) associated to the Hamiltonian 1.42 (or improved one) is the number of states involved in the system. Brute calculations are in fact uncomputable for more than few tens of atoms and approximations have to be done. Several theoretical approaches have been developed and implemented in the last few years. In function of the type and the level of the approximations, the different approaches offer different clues for the understanding of the dipole blockade Physics. We give here only the essence of those methods, details can be found in the references mentioned in the text.

Mean-Field approaches

Mean-Field theory is a very convenient way to deal with many-body systems. Mean-Field treatments are largely used in solid-state Physics, we find also a famous example in atomic Physics, the Gross-Pitaevskii equation which describes Bose-Einstein Condensates.
The spirit of a Mean-Field theory consists in one hypothesis : all the particles behave identically. Consequently, the goal is to describe the behavior of one particle, the effects of the interaction between particles being taken into account via an effective potential, a bath, in which each single particle evolves.
Formally, for an assembly of N identical particles evolving under the effect of an Hamiltonian H, the equation of evolution of the density operator $\hat{\sigma}^i$ of a particular particle i is given by

$$i\hbar\frac{d}{dt}\left[\hat{\sigma}^i(t)\right] = \underset{j\neq i}{Tr}\left[H, \hat{\sigma}(t)\right] \tag{1.42}$$

Where $\hat{\sigma}$ is the density operator of the full system.
The Mean-Field hypothesis consists in writting

$$\hat{\sigma}^j = \hat{\sigma}^i, \forall j \neq i \tag{1.43}$$

By this way, we obtain a self consistent equation of evolution of $\hat{\sigma}^i$. We see here that the enormous advantage of a mean-field treatment is that the equation of evolution of the full system is reduced to a single particle equation, independently of the size of the system. However, in a pure Mean-Field theory (zero-order Mean-Field theory) quantum correlation between particles are totally neglected. Consequently, Mean-Field theory fails to describe accurately strongly interacting systems where quantum correlations play a central role.
Nevertheless, it is possible to partially consider quantum correlations in the frame of

Mean-Field theory. Those improvements use the same spirit than the Bogoliubov hierarchy in kinetic theory, the purpose is to evaluate or calculate quantum correlations at the level of few particles. For example as a first improvement, we can evaluate the two-body correlation function and include it in the Mean-Field equation (first-order Mean-Field theory). To go beyond, we can evaluate the three-body correlation function allowing to calculate the two-body one (second-order Mean-Field theory), etc...

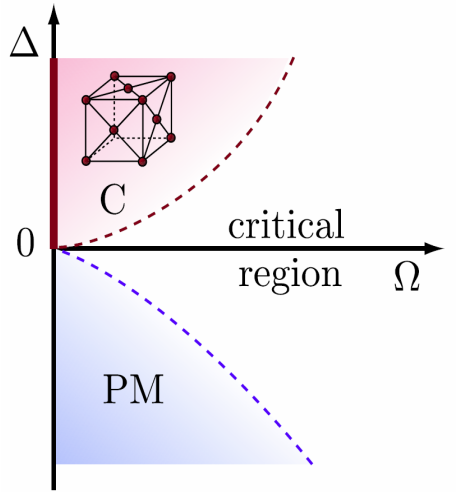

Figure 1.10: Phase diagram in the blockade regime, from [Weimer et al., 2008], Δ is the detuning of the laser, Ω the Rabi frequency. On the $\Omega = 0$ line, a second order phase transition appears between a paramagnetic phase (PM) and a crystalline phase (C).

In the frame of blockaded Rydberg ensembles, the implementation of first-order Mean-Field theory has been reported several times, for example in [Tong et al., 2004; Weimer et al., 2008]. In those references, the two-body correlation function is evaluated from the fact that we can not excite two Rydberg atoms closer than the blockade radius R_b (see Eq (1.39)). Thus, its value is 1 for $R > R_b$ and 0 for $R < R_b$.
From this Mean-Field model, the ground state of the system has been investigated at the thermodynamical equilibrium, in function of the "laser parameters" δ and Ω which are experimentally easily tunable. A phase diagram of the ground state at zero temperature is reported in the reference [Weimer et al., 2008] in the case of repulsive interactions, it exhibits a very interesting crystalline phase as we can see in the fig 1.10.
The phase transition toward the crystalline phase is found to be a second order quantum phase transition. Phase transition Physics has been intensively studied [Huang, 1963] and provides very interesting results. Namely, it appears that the behavior of a macroscopic system close to the critical point of a second order phase transition does not depend of the microscopic details of the interaction between particles (in our case the

critical point is for $\Omega = 0$ and $\delta = 0$). This means that the physical observables of the system follow universal scaling laws.
In the case of blockaded Rydberg ensemble, universal scaling have been reported in the reference [Weimer et al., 2008]. It is shown that for an atomic cloud with a dimensionality d and a density n, considering a resonant excitation ($\delta = 0$) and a Rydberg-Rydberg interaction of the form $V(R) = C_p/R^p$, the system is fully characterize by a dimensionless parameter $\alpha = \frac{\hbar\Omega}{C_p n^{p/d}}$. In the limit of $\alpha \ll 1$, the fraction of atom excited in the Rydberg state f_R follow an universal scaling law given by

$$f_R \propto \alpha^{\frac{2d}{2p+d}} \tag{1.44}$$

Despites this very interesting results, the first-order Mean-Field theory for Rydberg blockaded ensemble is still an approximated treatment and several experimental observations are not reproduced. Particularly, one problem appears when we look at the scan of a Rydberg line, i.e., when the number of Rydberg excitation is studied in function of the detuning of the laser δ. Whereas experimentally, the maximum number of Rydberg excitation is found for $\delta = 0$, the first order Mean-Field theory predict a shift of the line proportional to the strength of the interactions between Rydberg atoms.
A second-order Mean-Field theory has been developed in the reference [Schempp et al., 2010]. Interestingly, authors show that theoretical results give this time the right features concerning the scan of the Rydberg line, the line being not shifted in comparison to the non interacting case.

Rate equations

Rate equations methods consist in, starting from the full Hamiltonian, adiabatically eliminate the coherence between quantum states. The obtained equations allow to calculate the populations of the different quantum states in a very efficient way, using for example Monte-Carlo methods. The main advantage of the rate equations is that there are quite easy, i.e., fast, to solve numerically, providing the possibility to simulate large systems. In addition, rate equations are very convenient for dealing with multi-level particle and to include non-Hamiltonian effects.
In the frame of Rydberg blockaded ensemble, implementation of rate equations have been for example reported in the following references [Ates et al., 2006, 2007b,a; Chotia et al., 2008]. In [Ates et al., 2007a], the case of a three-level atom is treated with a 2-photon resonant excitation. Very interestingly, authors emphasis on the possible existence of an antiblockade effect due to the Autler-Townes splitting of the intermediate state of the 2-photon excitation. This phenomenon appears when the Autler-Townes splitting is of the same range of value than the Rydberg-Rydberg interaction. This is

also the subject of [Ates et al., 2007b]. In [Chotia et al., 2008], in addition to the Rydberg excitation, authors have also implement the spatial dynamics of the atoms under the effect of the forces resulting from the Rydberg-Rydberg interaction. This forces lead to possible collisions between Rydberg atoms when interactions are attractive and can induce ionization.

The main drawback of the rate equations is that there are a priori blind to all the effects of quantum interferences which comes from the relative phase between the quantum states. This can be problematic in the frame of Rydberg blockaded ensembles as interatomic quantum correlations are expected to play a role.

Full resolution of the Hamiltonian

A general, tedious but exact method consists in the resolution of the Schrödinger (Von Neumann) equation associated to the full system.
Once again, this method becomes quickly uncomputable when the number of atom increases. However, there is several way to be "smart" in the implementation of the equations.
In the frame of Rydberg blockaded ensemble, one consideration is very convenient, the fact that the number of Rydberg excitation is limited means that there is plenty of states which will be not populated and that we can remove from the Hilbert space. Indeed, all the states which contain more than a certain number of Rydberg excitation can be forgotten, it is also the same for all the state containing two Rydberg atoms separated by less than the blockade radius R_b. By this way, the number of states involved in the resolution is hardly reduce.
An other way to simplify the resolution is to consider that the atoms are spatially regularly positioned. This makes that a lot of interaction terms are equal and provides great simplifications for the numerical resolution. Very interestingly, this situation corresponds experimentally to the use of optical lattices, which is more and more current in today experiments.
The following reference report for example the results of the implementation of such a full resolution, [Schauß et al., 2012].

Perfect blockade methods

The most sophisticated methods to model the blockaded Rydberg ensembles are developed in the frame of lattice configurations (1- or 2-dimensional).
As in the case of a complete resolution, working with spatially ordered samples allow first to use the corresponding symmetries to simplify the problem. In regards to this

question, ring lattices give rise to a very high degree of symmetry and are the most investigated systems. In addition to those symmetries, we can use the so-called perfect blockade approximation. This approximation, studied in detail in [Sun and Robicheaux, 2008b], consists in model the Rydberg-Rydberg interaction potential with a step function. At large distance, the interaction is considered to be null. At short distance, the interaction is considered to be infinite. If this approximation seems to be very rude, it is in fact very reasonably accurate when applying to atomic ensemble trapped in optical lattices. This lies in the fact that the Rydberg-Rydberg interaction decreases very quickly with the interatomic distance, especially in the case of Van-der-Waals interaction ($1/R^6$).
Under the perfect blockade approximations, all the configurations which can be excited have the same interaction energy (0). The energy of those configurations is then entirely determined by the number of Rydberg excitations that they contain, once dressed by a laser field, it is possible to consider all the different configurations as the microcanonical states of a statistical ensemble. In this frame, it is possible to describe the long term evolution of the system as a thermalization [Olmos et al., 2010; Olmos and Lesanovsky, 2011; Ates et al., 2012] (revivals are considered as the "very-long term" which will anyway not occure due to decoherence effects). As highlighted in those references, this is linked to the very interesting question : How the fully quantum and coherent evolution of a close system leads to thermalization.
With the techniques developed in those references and before in [Olmos et al., 2009a,b; Olmos et al., 2010] It has been possible to reach very rich descriptions of the excitation dynamics of Rydberg atoms confined in optical lattice as well as to study the attractive emission properties of the created many-body quantum states [Olmos and Lesanovsky, 2010; Laycock et al., 2011].

For a given geometry, it is also possible to describe the Rydberg excitations as quantum "hard-object", hard-rod in 1D [Ates and Lesanovsky, 2012], hard-square in 2D [Ji and Lesanovsky, 2011] whom the size is related to the number of lattice sites which are blockaded due to the presence of a single Rydberg excitation. Those treatments allow to describe the interacting Rydberg gas confined in lattice configurations as a so-called Tonk's gas. Another slightly different approach is reported in [Lesanovsky, 2011].

Very interestingly, in the reference [Ates et al., 2012] the possibility to describe such systems using Fokker-Planck equations is investigated. It is shown that this method, which has the advantage to be much less computation demanding, leads to accurate results in a large range of situations. Unfortunately, Starting with all the atoms in the ground states takes part of the less well described situations.

The methods using the perfect blockade approximation have the advantage to be applicable to every kind of interacting spin (2-levels) systems.

Super-Atom model

If the four first methods are quite general for the treatment of many-body systems, the Super-Atom model has been developed specifically for Rydberg blockaded ensemble. The Super-Atom model was first reported in the reference [Robicheaux and Hernández, 2005] and is the subject of several other ones as [Hernández and Robicheaux, 2006, 2008a; Sun and Robicheaux, 2008a; Stanojevic and Côté, 2009].
The main idea of the Super-Atom model is to insert in the description of a non-fully blockaded ensemble the results obtained for a fully blockaded ensemble.
As described in the section 1.4.1, in the case where only one Rydberg excitation can be present in an ensemble, the full ensemble behaves formally as a two-level atom coupled to the laser field with a collective Rabi frequency $\sqrt{N}\Omega$, where N is the number of atoms of the ensemble called in this case a Super-Atom.

In the Super-Atom model, starting from a random ensemble of atoms, the Super-Atoms are build "manually" by grouping together closest atoms. The ensemble is then decomposed in a certain number of Super-atoms, each one containing a certain number of atoms defining its Rabi frequency.
Once this building step done, it is possible to write and solve the Hamiltonian corresponding to this assembly of Super-Atoms, similar to 1.42 except that the Rabi frequency is different for each Super-Atom and depend of the number of atoms that they contain. If compare to the initial situation, the number of particles is now reduced, the numerical complexity also.
A Typical result of the Super-Atom model calculation is shown on the Fig.1.11.

An important point in this development is the number of Super-Atoms which are buildup. In practice, the number of Super-Atoms is set to the maximum number allowing to compute the equations, for instance few tens. Since the atomic correlations are slightly modified, the number of atoms that the Super-Atoms contain has also to be limited to stay reasonably close to the initial Hamiltonian. In a sense, atomic correlations are loosed at the scale of real atoms and transfered to the scale of Super-Atoms.

In addition to simplified the numerical resolution, the Super-Atom model gives a very interesting picture of the Rydberg excitation of a blockaded Rydberg gas where spatial correlations and fast collective Rabi frequencies are naturally present. However, the

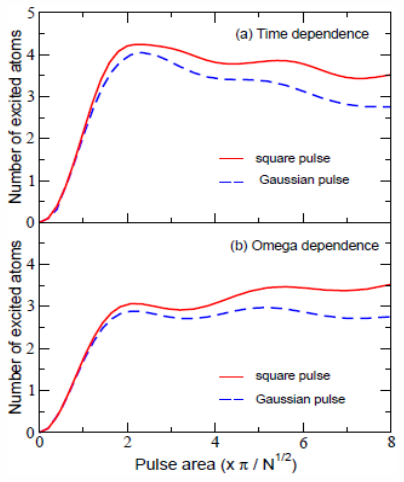

Figure 1.11: Results of the Super Atom Model from [Stanojevic and Côté, 2009]. We see here a time evolution of the Rydberg excitation of 5S rubidium atom to the state $70P_{\frac{3}{2}}$ with $N = 70$ and $d = 10^{11}$ at.cm^{-3}, those results correspond to the average over several spatial distributions, "single shot" results exhibit more visible oscillations.

Super-Atoms picture need to be manipulate carefully when applicate to large atomic ensemble. To be safe, Super-Atom model has to be restricted, as it is done in the associated theoretical references, to mesoscopic atomic ensembles.

Nevertheless, the Super-Atoms picture has been largely used in the Rydberg literature to describes excitation of large sample. In the case of large ensemble, to give an intuitive vision to the system, we can imagine that the number of Super-Atoms is the number of Rydberg excitations which can be present in the system (see fig 1.12).
In this case the system is composed by several Super-atoms interacting slightly together and each super atom is doing quasi complete Rabi oscillations under the effect of the laser. The frequency of the oscillations differs for each Super-Atom, depending the local intensity of the laser as well as the number of atom which contains, i.e., the local density at the position of the Super-Atom.
For a large atomic sample and inhomogeneous atomic density or laser intensity, we get a smooth curve resulting of the averaging of the Super-Atoms Rabi oscillations. This is represented on the fig 1.12.

In the case of very homogeneous sample, the oscillations of the Super-Atoms should be roughly in phase and visible in the total number of Rydberg excitations. The fact is that such simultaneous oscillations of several Super-Atoms had never been observed experimentally.

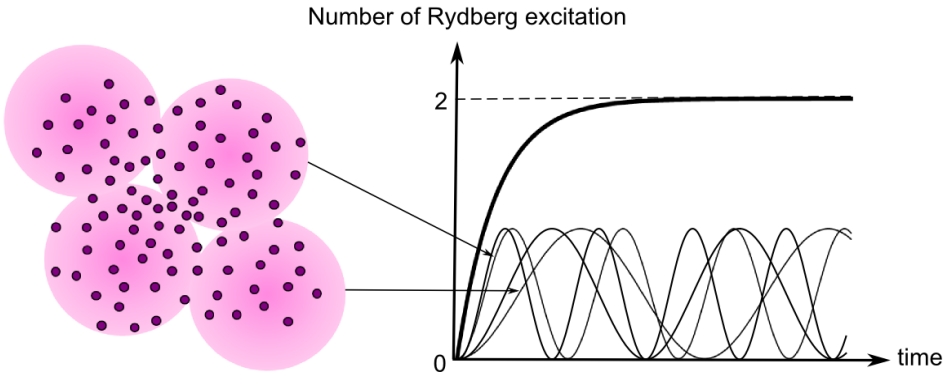

Figure 1.12: Schematic vision of the Super-Atom picture in the case of large atomic ensemble. On the left, we see a schematic vision of an atomic ensemble divided in 4 Super-Atoms. On the right, the total number of Rydberg excitations is represented in function of the time (thick curve), we also show the excitation carried by each Super-Atom (thin curves), the sum of the Rydberg excitations carried by the 4 Super-Atoms gives the total number of Rydberg excitations. All those curves are only illustrative and do not correspond to real calculations.

Collective Dicke basis and cooperative model

When looking at the properties of symmetry of the laser excitation of an assembly of indistinguishable two-level atoms, it exists a basis which contains naturally those properties. This is the so-called Dicke basis, developed by R. Dicke and reported in the reference [Dicke, 1954]. The Dicke basis appears to be very useful to deal with the coupling between an electromagnetic field and a many-atoms system, it has been first developed to describe the phenomenon of collective spontaneous emission, the so-called Superradiance (see for example the review [Lin and Yelin, 2012]).

In the frame of this thesis, we have studied the Rydberg excitation of an atomic ensemble using the Dicke basis, this is the subject the chapter 5 of this manuscript. In this section, we present briefly the Dicke basis in the case of interacting particles and we show how the collective states symmetry properties, caught by the Dicke basis, can influence the dynamics of the system.

The natural basis to describe a two-level atoms sample (levels being the ground state $|g\rangle$ and a Rydberg state $|r\rangle$), contains states of the form

$$|\Psi\rangle = |g_1, r_2, ..., r_{i-1}, g_i, g_{i+1}, r_{i+2}, ..., g_N\rangle \tag{1.45}$$

Where the state of the N individual atoms is specified. We call this state an atomic

state, atomic states forming the atomic basis.
The Dicke basis is completely equivalent to the atomic basis. However, the Dicke states are defined to be the eigenstates of collective operators (see chapter 5) and they are superposition of several atomic states.

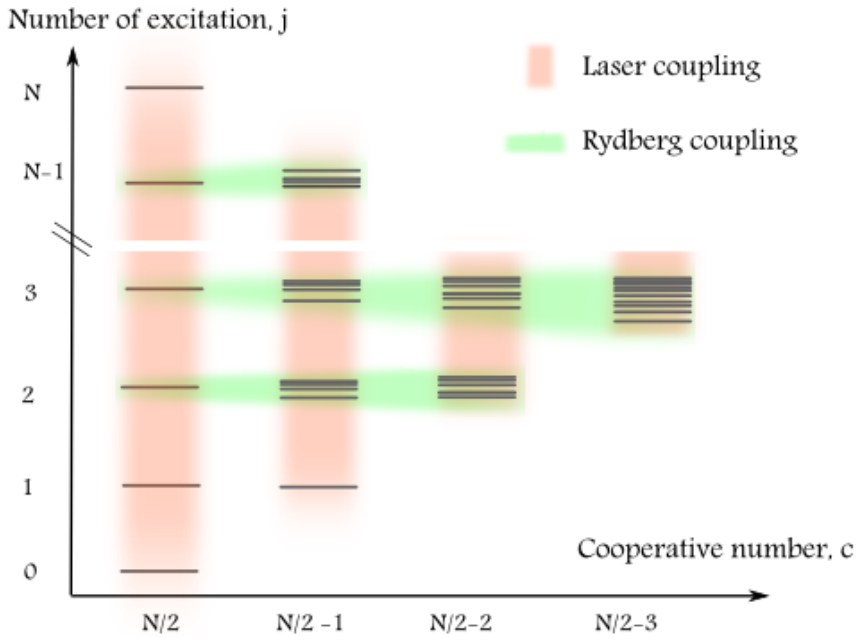

Figure 1.13: Dicke states in the case of interacting particles. An electromagnetic field acts independently in each subset of states with the same symmetry (vertically) with $\Delta j = \pm 1$, the Rydberg-Rydberg interaction couples the states with the same number of excitation (horizontally). States with same j and c are not degenerated in energy due to the Rydberg-Rydberg interaction, their number is given in the text

A Dicke state is characterized by three numbers, the number of excitation that the state contains, $j \in [\![0; N]\!]$ and a cooperative number $c \in [\![|\frac{N}{2} - j|; \frac{N}{2}]\!]$ representing the symmetry of the state, a third "white" number allows to define a complete basis where several states have the same j and c.
A Dicke state $|j, c\rangle$ is a superposition of atomic states containing j excitations and c reflects how this superposition is symmetric or not relatively to the exchanges of atoms. The number of states with the same j and c is given by $\binom{N}{N/2-c} - \binom{N}{N/2-(c+1)}$. It is important to note that, for a given j, the states with the minimum cooperative number are much more numerous than the other states. On the other hand, there is only one state with the maximum degree of symmetry, the so-called fully-symmetrical Dicke state.

The great feature of the Dicke states is that only the states with the same cooperative

number c are coupled together under the effect of an electromagnetic field (to be rigorous we have in this case to introduce the relative phase of the laser at the position of the atoms in the collective operators). On the other hand, considering interacting particles, the states having the same number of excitations j are coupled together due to the interactions.

The resolution of the full Hamiltonian using the Dicke basis is a-priori as heavy as in the case of the atomic basis. However, we can qualitatively investigate the behavior of a large atomic ensemble in the frame of the Dicke basis.

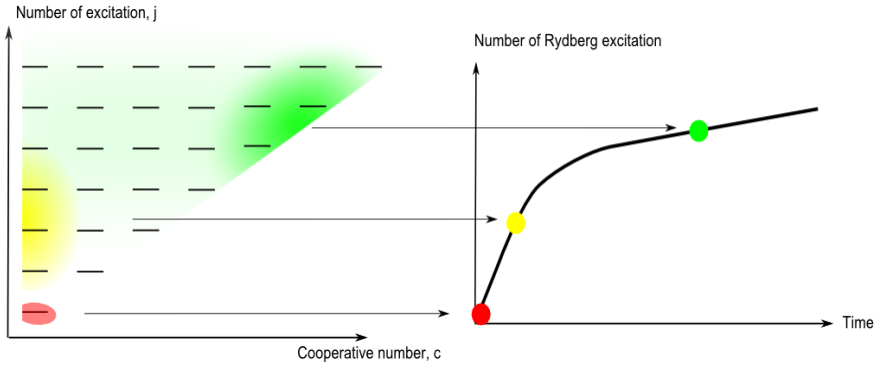

Figure 1.14: Schematic vision of the collective vision in the case of large atomic ensemble. The degeneracy in energy of the different states with same j and s is not represented. The colored areas give an idea of the population of the Dicke states at different time

The following behavior, represented schematically in the fig 5.10 can be proposed. For a small number of Rydberg excitation, the interactions between Rydberg atoms are quite small and the excitations should be mainly present trough the fully-symmetrical Dicke states. However, when the number of Rydberg excitation becomes important, the different configurations for the Rydberg excitations leads to important interaction energies, for example a lot of them would be not populated (blockaded). The interactions induce in this case a strong coupling toward non symmetrical states. The Dicke states with the minimum of symmetry being the most numerous, a big part of the Rydberg excitations should be concentrated on those states. The fact that those states are non coupled to states containing less excitations should then have an effect on the excitation dynamics, the Rydberg excitation being partially maintained to high values.
Within this description, the system is quickly "lost" in the multitude of non-symmetrical states, as in the case of the perfect blockade methods, revivals should occurs well after decoherence and we refine here the notion of thermalisation.

The description of the Rydberg excitation presented here leads to a behavior quite different of the one obtained in pushing the Super-Atom picture to the case of large atomic ensemble. Within this collective description, the Rydberg excitations are delocalyzed over the wall sample and the system does not contain Rabi oscillations of several subsystems.
As we will see in the section 1.4.4 and latter in the chapter 5, the non-shifted position of the Rydberg line becomes in this frame quite intuitive.

1.4.4 Experimental studies of the dipole blockade

Since the numerical complexity of the Rydberg excitation of atomic gas in the blockade regime makes the theoretical treatments impossible to implement for large ensemble, experimental studies on this subject constitutes an indispensable source of information. Since ten years, a big number of dipole blockade experiments have been performed by several groups, providing very interesting results. In this section, we report some of the main obtained results.

Multi-photon excitation and coherence of the excitation

Before to present experiments dealing directly with the dipole blockade phenomenon, we present briefly in this section the experimental procedure to excite Rydberg state from the the ground states with a particular focus on the coherence of the excitation. In almost all the experimental setups, the Rydberg state is reached via a 2-photon excitation, i.e., the excitation scheme is $|g\rangle \rightarrow |e\rangle \rightarrow |r\rangle$ where $|e\rangle$ is an intermediate state. In most of the case the transition $|g\rangle \rightarrow |e\rangle$ is the transition used to cool the atomic sample. If 2-photon excitation is the most current, direct excitation has been reported in [Thoumany et al., 2009b], 3-photon excitations in [Vogt et al., 2006; Thoumany et al., 2009a; Ryabtsev et al., 2011].
The main reason to work with 2-photon excitation is technological. Considering that the transition $|g\rangle \rightarrow |e\rangle$ is the cooling transition for which the corresponding laser system is already present in the lab, the laser sources corresponding to the second step of the 2-photon excitation are much more developed than those allowing to excite directly the Rydberg state from the ground state. This is due to the corresponding wavelengths which are in the UV range for the direct excitation and in the visible range for the second step of the 2-photon excitation (at least for rubidium and cesium atoms). So, 2-photon excitation allows to get much higher power (or much lower price). Nevertheless, another advantage of the 2-photon excitation is the possibility to excite, in zero-field, s

and d states whereas direct excitation allows only the excitation of p states.
Using a 2-photon excitation, it is nevertheless desirable to have a coherent excitation of the Rydberg state from the ground state to study properly the quantum dynamics of the system. This means that the population of the intermediate state $|e\rangle$ has to be avoided as this state has generally a very short life time and suffers from spontaneous emission. This can be done in detuning the first step of the excitation from the transition $|g\rangle \rightarrow |e\rangle$ (the second step has then to be detuned by the opposite quantity to have a resonant excitation of the Rydberg state). As reported in the reference [Brion et al., 2007] (here the case of a lambda system is treated), for a sufficiently large detuning, we can "forgot" the intermediate state and consider that we have a coherent excitation $|g\rangle \rightarrow |r\rangle$, the associated Rabi frequency is then given by $\frac{\Omega_{ge}\Omega_{er}}{2\Delta}$ where Ω_{ge} and Ω_{er} are the Rabi frequencies of the two transitions and Δ the detuning from the intermediate state.
Using this technique, the coherent excitation of a Rydberg state has been demonstrated in the case of a single atom, first in [Johnson et al., 2008] and later in other experiments with different Rydberg level [Urban et al., 2009; Gaëtan et al., 2009; Isenhower et al., 2010; Zuo et al., 2009]. Despites the numerous possible source of dephasing, slightly visible Rabi oscillation between the ground state and a non-interacting Rydberg state has been reported in [Reetz-Lamour et al., 2008] in an assembly of around 100 atoms.
Although the spontaneous emission from the intermediate level induces decoherence in the system, some experiments use a 2-photon excitation resonant with the intermediate level. As mentioned in the section 1.4.3, in this case, an antiblockade effect can arise due to the Autler-Townes splitting of the intermediate state, this has been observed in [Amthor et al., 2010].
Interestingly, coherent population of a Rydberg level have also been performed using stimulating induced Raman adiabatic passage (STIRAP) as reported in the references [Kritsun et al., 2004; Cubel et al., 2005].

Experiments with 2 atoms

Although experiments with two atoms was not the first ones which have been reported on the dipole blockade, they provides a so clear evidence of the dipole blockade phenomenon and its collective dynamics that it is quite natural to start with this results.
The first result of a collective excitation of two atoms in the blockade regime has been reported in the reference [Gaëtan et al., 2009] and almost simultaneously in [Urban et al., 2009].
In the experiment performed in [Gaëtan et al., 2009], two ground states rubidium atoms are confined in two independent optical dipole traps. The two atoms, separated by a distance of 3.6 μm set to be smaller than the blockade radius, are simultaneously il-

luminated by the Rydberg excitation laser beams (it is a two-photon excitation). This situation is then exactly the one presented in the section 1.4.1 with $N = 2$.

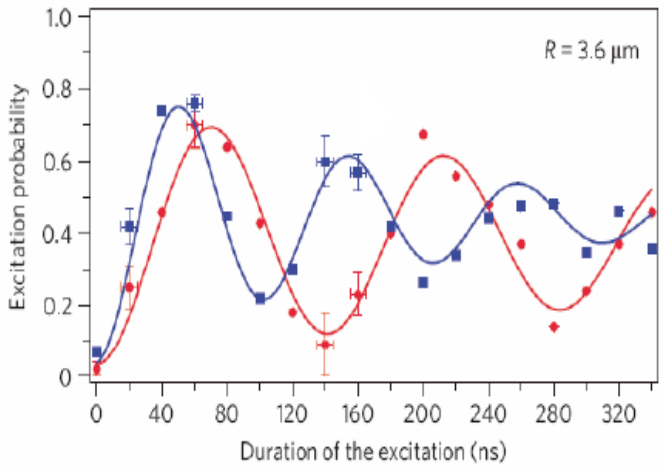

Figure 1.15: Collective excitation of two atoms in the blockade regime, from [Gaëtan et al., 2009]. Blue squares fitted by the blue curve represent the probability to have one Rydberg excitation present in the two-atoms system, for comparison, red circles fitted by the red curve correspond to the single atom case.

On the fig 1.15, we clearly see the two-atoms system doing Rabi oscillations between the state $|g, g\rangle$ and the state $\frac{1}{\sqrt{2}}(|r, g\rangle + |g, r\rangle)$. The collective Rabi frequency had been measured to be 1.38 ± 0.03 faster than the single atom case which is very close to the theoretical factor $\sqrt{2}$.

In addition to wonderfully illustrate the dipole blockade phenomenon in the case of two atoms, this experiment show also the possibility to entangled two atoms using the dipole blockade. We will come back on this last point in the section 1.5.

Quenching of the Rydberg excitation

The most obvious effect of the dipole blockade is to limit the number of Rydberg excitation present in an atomic gas. This effect have been the first one to be studied.
The first demonstration of such a quenching of the Rydberg excitation was reported in [Tong et al., 2004]. In this experiment, Rydberg state are excited with a narrow-band pulsed dye laser. We see in the fig 1.16) that the number of Rydberg excitation is

strongly limited when dealing with strongly interacting Rydberg states (high n). Here, interaction between Rydberg atoms is of the type Van-der-Waals.

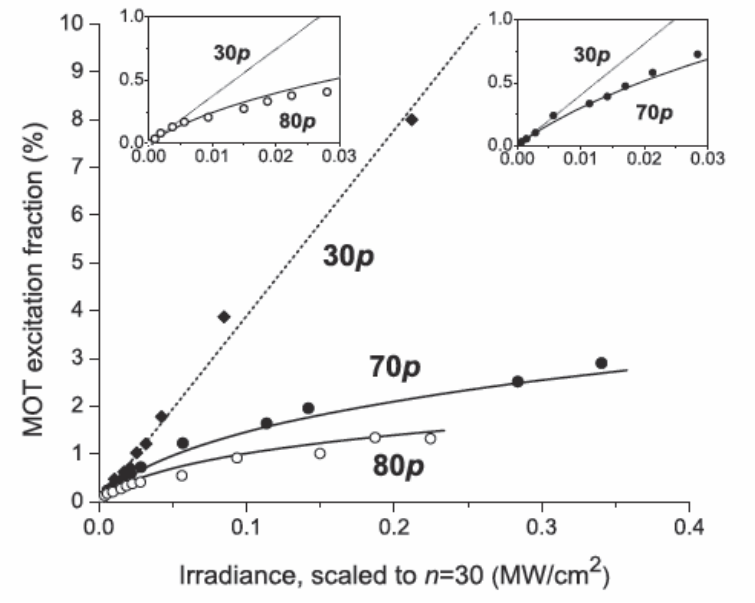

Figure 1.16: Quenching of the Rydberg excitation, from [Tong et al., 2004]. We see here the dependence of the Rydberg excitation fraction in function of the laser power exciting Rydberg states. Data are shown for three different n, in the case $n = 30$ interactions are almost negligible

If this pioneer experiment used pulsed dye laser, most of the blockade experiments are using continuous wave (cw) laser. Using cw laser, the observation of the quenching of the Rydberg excitation due to the dipole blockade has been reported, in the case of Förster resonance [Vogt et al., 2006] and in the case of interaction between permanent dipoles in presence of electric field [Vogt et al., 2007].

Using quantitative measurements of the limitation of the Rydberg excitation, it have been possible to check the radial and angular dependences of the dipole-dipole interaction. The dependence in $1/R^3$ in the case of Förster resonance has been demonstrated in [van Ditzhuijzen et al., 2008] using two spatially separated atomic sample. The angular dependence of the dipole-dipole interaction in the case of permanent dipoles created by the presence of an external electric field has been demonstrated in [Carroll et al., 2004] using a quasi one dimensional cylindrical atomic sample which could be rotated with respect to the external electric field.

In the experiments of dipole blockade, a particular attention has to be payed to the

presence of ions. Indeed, the electric field generated by an ion (much stronger that the one generated by a Rydberg atom) has also the effect to block the Rydberg excitation. As an example, it is shown in [Ates et al., 2007a] (rate equations calculations) that the presence of ions could explain the experimental results reported in [Singer et al., 2004] and that the blockade effect due to Van-der-Waals interactions might be enhanced by ions creation.
The creation of ions during the experiments can be avoided in working as much as possible with low intensities and short laser pulses.

Shape and position of the Rydberg line

In this section we are interested in the shape and the position of the Rydberg line in the regime of blockade. Experimentally, it can be studied in performing a scan of the Rydberg line where the number of Rydberg excitation is measured in function of the detuning of the laser.
As already discuss in the section 1.4.3, basic Mean-Field models predict a shift and an asymmetric broadening of the Rydberg line due to the Rydberg-Rydberg interactions. Those results are in fact quite intuitive since we could think that the Rydberg excitation is more efficient when the detuning of the laser compensates the energy shift created by the Rydberg interactions.
However, it appears experimentally that the Rydberg line is not shifted even in the case of strong interactions, at least at the level of the laser linewidth. There is nevertheless an effective broadening of the line which is simply due to the quenching of the Rydberg excitation. In the fig 1.17, we see a scan of a Rydberg line in two situations, one with small Van-der-Waals interactions, the other with stronger interactions induced by the application of an external electric field.

The fact that the Rydberg line in the blockade regime is not shifted match theoretical predictions of second-order Mean-Field treatment [Schempp et al., 2010]. In this treatment we can find additional shifted resonances due to multi-photon absorption processes but they have in the general case a quite small probability to be excited.

To give a physical interpretation of the absence of shift in the case of large ensembles, we can look at the beginning of the Rydberg excitation in considering collective excitations. For small numbers of Rydberg excitations, only few configurations leads to significant interaction energies (the first excitation contains rigorously no interaction energy), a large majority of the configurations are almost non shifted. Consequently, since it allows the excitation of the largest number of configurations, the Rydberg excitation is more favorable with a laser field resonant with the non-interacting Rydberg

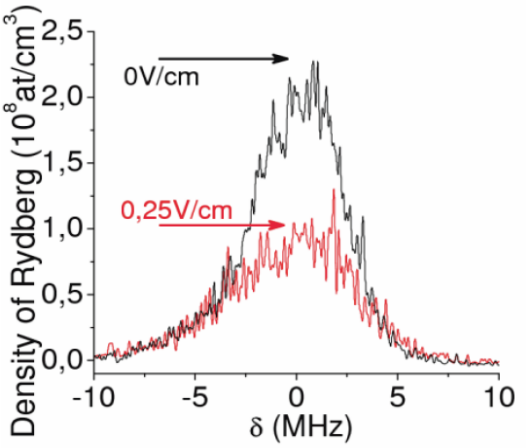

Figure 1.17: Scan of the $75p_{3/2}$ Rydberg line, from [Vogt et al., 2007]. Black curve is obtained in absence of electric field, red one in presence of a small electric field. Here, the lines has been voluntary set to the same position but the measured difference in position has been found to correspond to the Stark effect on the Rydberg level $75p_{3/2}$

transition. If a detuning from resonance should be favorable for a system closer to the saturation, interacting Rydberg gases remind us that slow and steady wins the race.

Nevertheless, this feature concerns the use of a single laser excitation with fixed frequency. Very interesting behavior can be explored when dealing with a chirped laser pulse [Pohl et al., 2009] or sequential excitations with variable frequency. For example, the observation of the Rydberg-Rydberg interaction spectrum (both for Van-der-Waals and pure dipole-dipole interaction) has been reported in [Reinhard et al., 2008]. To do this, the authors use several independently tunable laser pulses to spectroscopically probe the spectrum in a double-resonance excitation scheme. Finally, it is also possible to apply micro-wave field once the Rydberg excitation done in order to induce transition between close Rydberg states. Those transitions being strongly affected by Rydberg-Rydberg interaction, this constitutes a nice way to study them [Afrousheh et al., 2004]. This latter point is also a way to enhance the interactions, indeed, in dressing a Rydberg level by micro-wave field, the corresponding ac Stark shift can generate another kind of Förster resonances [Bohlouli-Zanjani et al., 2007; Tauschinsky et al., 2008].

Dynamics of the Rydberg excitation

The study of the dynamics of the Rydberg excitation in a blockaded ensemble is of primarily interest due to the characteristic dynamics associated to the collective nature of the excitations.

To study such a dynamics, a simple way is to measure the number of Rydberg excitation created by a laser pulse whom we vary the duration or the intensity. First report of such an experiment is found in the reference [Heidemann et al., 2007] where the interactions between the Rydberg atoms are of the type Van-der-Waals.

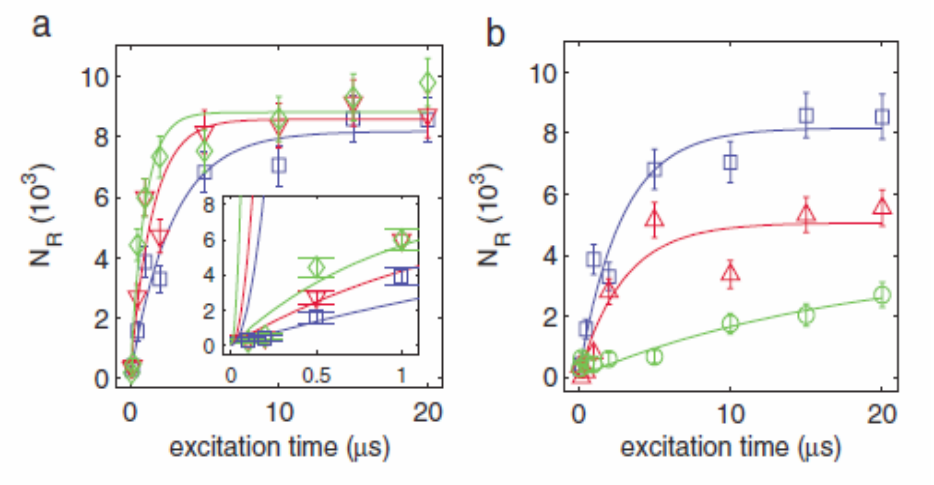

Figure 1.18: Dynamics of the Rydberg excitation, from [Heidemann et al., 2007]. a, the number of Rydberg excitation versus the excitation time for different densities. b, the number of Rydberg excitation versus the excitation time for different laser intensities. Solid lines are fits of the experimental data with exponential saturation function

The dynamics of the Rydberg excitation in a blockaded ensemble is found to have a characteristic behavior composed by a fast increase of the Rydberg excitation follows by a saturation regime, as we can see on the fig 1.18.
As reported in [Heidemann et al., 2008], this behavior have been also observed for the Rydberg excitation of a Bose-Einstein condensate.
In [Löw et al., 2009], it is shown that the saturation value of the Rydberg excitation follows the scaling law obtained by the Mean-Field theory (see section 1.4.3, eq.1.44).
Concerning the initial raise of the Rydberg excitation, it is found to be linked to the ratio between the number of Rydberg excitation and the total number of atom present in the system, i.e., the number of atoms per blockade sphere. This reflects the collective dynamics of the Rydberg excitation.

"Echo" experiments

The dynamics of the Rydberg excitation has been also studied in so-called echo experiments. The technique of rotary echo was first developed in the frame of Magnetic

Nuclear Resonance (RMN). It consists to let evolve a system under the effect of a perturbation for a time T and suddenly change the sign of the perturbation. If the evolution of the system is fully coherent and determined by the sole perturbation, we expect that the system come back in its initial state after a total time $2T$.
In the case of the laser excitation of an atomic gas, it is possible to excite the system for a time T and suddenly change the phase of the laser by the quantity π. This corresponds to change the Rabi frequency of the laser from Ω to $-\Omega$. In the case where the system does not suffer from any decoherence process and for a completely coherent laser excitation, the system will come back exactly to its initial state after the total time $2T$. However, in the case of a Rydberg excitation, the evolution of the system is not only determined by the laser excitation but also by the Rydberg-Rydberg interactions. The fact to change the sign of the laser excitation does not affect the Rydberg-Rydberg interactions and consequently, the system will not come back to its initial state after the time $2T$. In this case, the difference between the initial and the final states reflects the effect of the Rydberg-Rydberg interactions.
Such experiment of echo has been reported in the reference [Raitzsch et al., 2008; Younge and Raithel, 2009]. We find also a theoretical study of this subject in [Hernández and Robicheaux, 2008b; Raitzsch et al., 2009; Wüster et al., 2010]. In the experiments, the atoms are initially in the ground state, the echo sequence is performed and the fraction of atoms in the Rydberg state after the sequence is measured. Neglecting all sources of decoherence, this fraction is only linked to the Rydberg-Rydberg interactions. By changing the total time of the echo sequence, it is possible to extract a dephasing rate, i.e., the dephasing of the Rydberg excitations due to the Rydberg-Rydberg interactions. The experiment of [Raitzsch et al., 2008] is performed within a timescale which correspond to the "beginning" of the Rydberg excitation, i.e., the Rabi frequency of the laser excitation is reversed well before the saturation of the Rydberg excitations. If, for this excitation time, there is already a quenching of the Rydberg excitation in comparison to the non-interacting case, the dephasing time is found to be relatively long (for instance few 100 ns, meaning dephasing rate of the order of few MHz), proving that Rydberg excitations are organized in such a manner that interaction energies stay quite small.
Such a measure of the dephasing rate due to the Rydberg-Rydberg excitation can also be done in performing EIT experiments. In the reference [Raitzsch et al., 2009], authors present the investigation of dephasing rates using both methods (echo and EIT) as well as numerical calculations. The dephasing rate is found from the calculations to follow a scaling law with the number of excited Rydberg atom in the "middle" of the sequence, the reported exponent is 2.16 ± 12, and agree well with the experimental measurements.

Statistics of the Rydberg excitation

A way to study the Rydberg excitation in the blockade regime is the statistics of the Rydberg excitation. We are here interested not only to the specific number of Rydberg excitation that are present in a given situation but also at the statistical distribution of the number of Rydberg excitation when the same situation is repeated several times.
In addition to the average number of Rydberg excitation n, we can experimentally measure the variance σ_n. A convenient dimensionless quantity linked to the variance is the Mandel Q factor [Mandel, 1979] (a very close quantity is the Fano factor which differs from the Q factor by 1 unity)

$$Q = \frac{\sigma_n}{n} - 1 \tag{1.46}$$

If the value of the Q factor is 0 for a poissonian statistics, i.e., for an uncorrelated process, the Q factor takes negative value for sub-poissonian statistics, i.e., correlated process. In a quantum system, the value of the Q factor depend a lot of the basis in which we project the system in the measurement process. The Q factor is in this case link to the quantum projection noise. The value of the Q factor gives in fact crucial informations on the quantum states which are populated and detected, this question is studied in the chapters 4 of this manuscript.
In the frame of the dipole blockade, we expect to get negative value of the Q factor due to the collective nature of the Rydberg excitation.

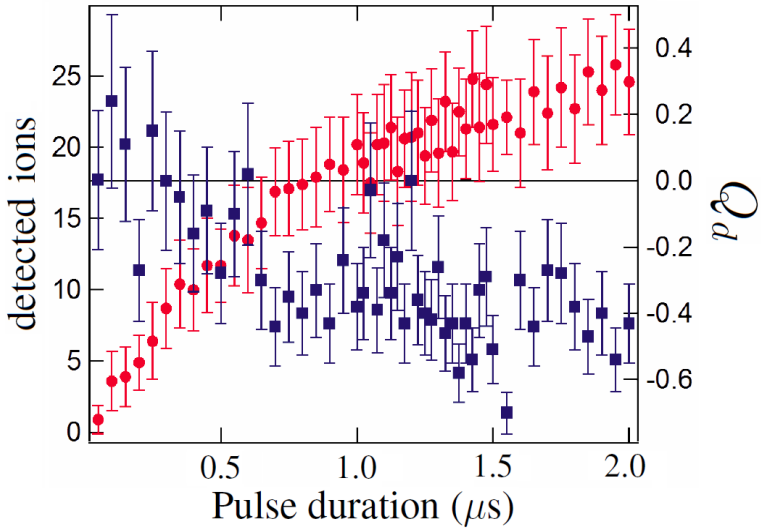

Figure 1.19: Counting statistics of the Rydberg excitation, from [Viteau et al., 2012]. Red circles represent the number of detected ions, blue squares represent the detected Q factor

Observation of sub-poissonian statistics in blockaded Rydberg ensemble has been reported in the following references [Liebisch et al., 2005, 2007; Reinhard et al., 2008; Ryabtsev et al., 2010; Viteau et al., 2012; Hofmann et al., 2012]. The effect of a finite detection efficiency has been study in [Ryabtsev et al., 2007a,b]. Theoretical study about sub-poissonian statistics is for example reported in [Ates et al., 2006] using rate equations and in [Robicheaux and Hernández, 2005] using Super-Atom model. We show in the fig 1.19 experimental data obtained in the frame of this thesis, reported in [Viteau et al., 2012] where both average number of Rydberg excitation, n, and Mandel Q factor, are measured in function of the excitation laser pulse duration. In this experiment, Rydberg excitations are detected using field-ionization method, measured quantity is then the number of ions arriving on the detector. Taking in account the detection efficiency, evaluated to be $\eta = 35 \pm 10\%$, the value of the Q factor of the Rydberg excitation itself has to be divided by η. It is thus found to be very close to -1, the lowest possible value that the Q factor can take. As we will see in the chapter 4, this observation indicates first that the system is projected onto collective states but also that the collective states which are simultaneously populated contain a quite similar number of Rydberg excitations .

Spatial correlations

Another very interesting feature of the Rydberg excitation in the blockade regime is the spatial distribution of the Rydberg excitations. As described by the blockade sphere picture, the fact that the presence of two Rydberg excitation closer than the blockade radius is forbidden leads to a crystal-type spatial distribution of the Rydberg excitation. The observation of the spatial distribution involves a detection scheme allowing to image the atomic cloud. In the case of a field-ionization detection, this can be done using a spatially resolved charge detector, for example, micro-channel plate detector (MCP) followed by a phosphor screen, we get in this case a 2D imaging. Observation of spatial correlation of the Rydberg excitation using this method has been reported in the reference [Schwarzkopf et al., 2011].
Another way to image the spatial distribution of the Rydberg excitations is to use optical detection. A theoretical proposal using EIT scheme involving a "probe" Rydberg state which interact slightly with the excited one can be found in the reference [Günter et al., 2012]. However this method have not been implemented yet.
An experimental observation of the spatial distribution of Rydberg excitations using optical detection have been reported in the reference [Schauß et al., 2012]. In this experiment, the atomic sample consists in a mesoscopic 2D atomic array obtained in loading an ultra-cold atomic cloud in square optical lattices in the Mott-insulator regime. After the Rydberg excitation laser pulse, the created Rydberg excitations are detected by the

following way : The atoms in the ground state are putted out of the sample by a resonant laser beam, the Rydberg atoms are then deexcited to the ground state via stimulated emission and finally detected using fluorescence imaging.

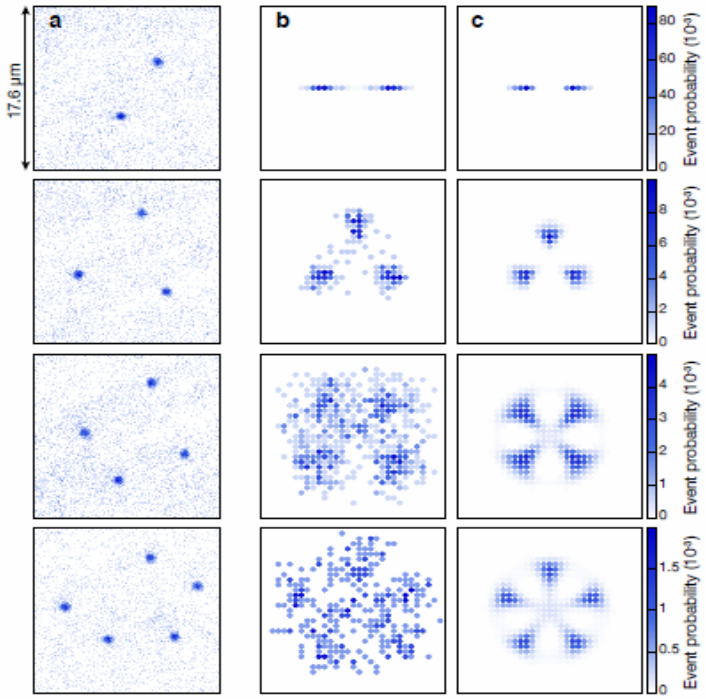

Figure 1.20: Spatial distribution of few Rydberg excitations in the regime of blockade, from [Schauß et al., 2012]. a), single shot images. b), average over several images, each image is centered and rotated to get the best superposition. c), numerical simulation

In the fig 1.20 we clearly see the presence of spatial correlations between few Rydberg excitations within a mesoscopic atomic sample. Together with numerical simulation obtained by the full resolution of the Hamiltonian solvable in this case due to the mesoscopic number of atoms spatially ordered and the small number of Rydberg excitations (see section 1.4.3), this result clearly indicates the crystal-type spatial distribution of the Rydberg excitations in the blockade regime.

EIT experiments

A very interesting type of experiment is when Rydberg states are involved in Electromagnetically Induced Transparency (EIT [Boller et al., 1991]) schemes [Mohapatra et al., 2007; Weatherill et al., 2008; Bason et al., 2008; Zhao et al., 2009; Pritchard et al., 2010]. We found theoretical support on this subject in [Ates et al., 2011; Petrosyan et al., 2011]. For an overview of this subject, we can refer to the recent review [Pritchard et al.,

2012].
As demonstrated in [Pritchard et al., 2010], in the case of strongly interacting Rydberg states, the strong Rydberg-Rydberg interactions are mapped onto the probing optical field and they mainly appear as optical nonlinearities when looking at the transmission of the resonant probe beam in function of its intensity.

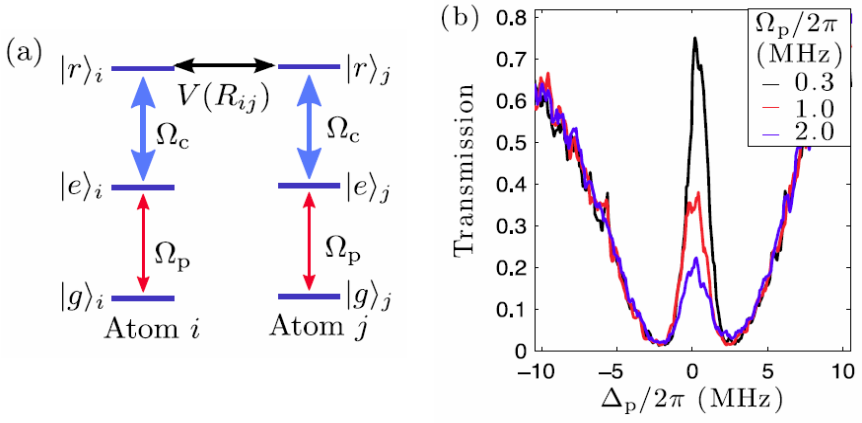

Figure 1.21: EIT experiment with Rydberg states, from [Pritchard et al., 2010]. a), EIT scheme in presence of Rydberg-Rydberg interactions. b), transmission signal of the probe beam for three different intensities. This experiment was made with rubidium atoms, level being $|g\rangle = 5s$, $|e\rangle = 5p_{3/2}$ and $|r\rangle = 60s$

On the fig 1.21, we see that as a consequence of the dipole blockade, the transmission of the probe beam is reduced when its intensity is increased. Indeed, Rydberg-Rydberg interactions modify the energy of the collective excited Rydberg states and "break" the EIT mechanism.
To look at the width of the transparency window is a way to measure the dephasing rate of the Rydberg excitation due to the Rydberg-Rydberg interaction like in an echo sequence. In [Pritchard et al., 2010] since no additional broadening have been seen, the dephasing rate has been found to be at least lower than 110kHz.

The non linearity of the probe beam transmission in the transparency window due to the dipole-dipole interactions has been used to demonstrate a giant dc Kerr effect [Mohapatra et al., 2008]. EIT technique with Rydberg atoms has also been used to measure electric field close to surfaces [Tauschinsky et al., 2010; Abel et al., 2011].

Finally, as a nice tool for Rydberg atoms experiments, the EIT scheme provides a very

efficient way to lock the frequency of a laser on a Rydberg transition [Abel et al., 2009].

From the photons side

Recently, dipole blockade has been investigated in a new type of experiments where Rydberg excitations are not detected directly but trough the photons emitted by the atomic ensemble.
Such an experiment has been reported in the reference [Dudin et al., 2012]. In this experiment, dipole blockade is investigated in the regime where ideally, only one excitation can be present (fully-blockaded ensemble). Once the Rydberg excitation done, a read-out pulse induced the deexcitation of the Rydberg excitation in an intermediate state and the photon emitted by the atomic ensemble by spontaneous emission from this intermediate state is detected.
A very important point of such an experiment concerns the state of the electromagnetic field in which the photons are emitted. Indeed, due to the collective nature of the Rydberg excitation, the relative phase of the Rydberg excitation between all the individual atoms determines strongly the direction of the emitted photon trough a phase matching condition. This effect has been study experimentally in [Boisseau et al., 2002] and theoretically for example in [Miroshnychenko et al., 2012]. In the experiment, the conservation of the light wave vectors allows to determine the direction of the photon emitted from the intermediate state when the initial Rydberg excitation is present trough a fully symmetrical state. Indeed, for such a state, the relative phase of the Rydberg excitation between the atoms is simply given by the excitation pulse. For a Rydberg excitation present trough a non-fully symmetrical state, the relative phase of the Rydberg excitation between the atoms has been modified by the Rydberg-Rydberg interactions and does not correspond to the one of the excitation pulse, in this case the emitted photon has a different direction. Consequently, the photons detected in the experiment are only those coming from the fully symmetrical state with one Rydberg excitation (due to the quasi fully blockade regime, excitation of the fully symmetrical state with two Rydberg excitations is very unlikely).

On the fig 1.22 we see that in function of the intensity of the Rydberg excitation pulse, the detected field exhibits Rabi oscillations. This indicates that the atomic system is doing Rabi oscillations between the ground state and the state with one fully symmetrical Rydberg excitation.
This result is the first experimental evidence of many-body Rabi oscillations involving a mesoscopic number of atoms, here few hundreds. The fact is that it seems very hard to prepare an atomic sample in the fully-blockaded regime. For some reasons (few body effect, decoherence processes) it appears that there is always more than one Rydberg

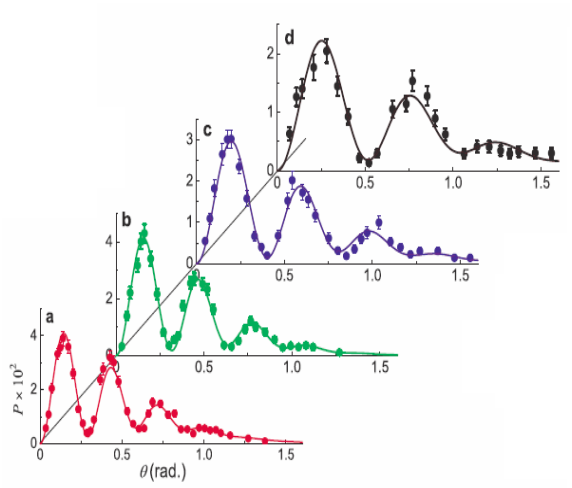

Figure 1.22: Measurement of the light emitted by the atomic sample after the Rydberg excitation, from [Dudin et al., 2012]. The probability of photoelectric detection is represented in function of the excitation pulse area (normalized by the single atom Rabi frequency), the different curves correspond to different density of the atomic sample. The solid lines are fit of the data. In this experiment, the Rydberg level is $|r\rangle = 102s_{1/2}$

excitation present in a mesoscopic atomic ensemble. However, looking at the photons, we extract the dynamics of the fully symmetrical states and the presence of multi excitations acts only as a leak of the system that we observe. This explain why collective Rabi oscillations can be observed trough photon measurements even if the number of Rydberg excitation is not strictly restricted to 1.

1.5 Rydberg atoms and quantum engineering

The study of cold Rydberg gases offers very nice perspectives for fundamental research about interacting system as we have seen trough the dipole blockade phenomenon. In addition to this fundamental interest, research on Rydberg atoms involves a so fine control, at a quantum level, of the atomic systems that it becomes possible to conceive quantum devices based on the Rydberg atoms Physics. Most of the application are in the field of quantum computation, atom-light conversion devices and high precision measurement.

Interestingly, the level of control of the cold atoms experiments allows to created very clean systems where a specific quantum behavior can be highlighted, preserved and used. Together with the versatility of the Rydberg properties themselves, the cold atom technology offer a fantastic modularity to the cold Rydberg systems. This opens many

perspectives concerning the use of Rydberg systems to mimic various physical situations exhibiting particular quantum behavior. This is called the quantum simulation.

1.5.1 Quantum entanglement

Interaction between Rydberg atoms makes them very attractive for the generation of entangled atomic states. Indeed, there is various simple situations where two or more Rydberg atoms are naturally excited in strongly entangled states due to their mutual interaction, this is the subject of the review [Walker and Saffman, 2012].
For example, we have seen in the section 1.4.4 that two Rydberg atoms in the blockade regime collectively excited by a laser pulse are entangled in the state $\frac{1}{\sqrt{2}}(|r,g\rangle + |g,r\rangle)$.
Another situation of entanglement is the resonant exchange of excitation in the case of Förster resonance or migration reaction where eigenstates of the two-atoms system are on the form $\frac{1}{\sqrt{2}}(|r_a, r'_b\rangle \pm |r''_a, r'''_b\rangle)$.
In those processes, we have to consider the precise dynamics of the quantum states. The system can be either brought in an entangled states trough adiabatic process, nor coherently evolved toward entangled states under the effect of a perturbation for example when the system is suddenly shine by a laser pulse. The initial preparation of the quantum state before the entanglement process is crucial.
In addition to the intrinsic efficient mechanisms of entanglement between Rydberg atoms, the manipulation of few atoms in optical lattices or individual dipole trap allows a precise control of the system at the level of individual atoms. This is then ideal for the study and the engineering of efficient and scalable entanglement processes.
In the reference [Gaëtan et al., 2009], dipole blockade between two atoms has been used to create an entangled state between two hyperfine ground states by laser inducing the decay of the Rydberg state. By applying global Raman rotations on both atoms, the fidelity reaches has been measured to be 0.75. This value is very relevant since it is the minimum one from which we can certified that there is quantum entanglement and from which quantum protocols including states correction can be applied.
The experimental observation of a 4-body Förster resonance, presented in the chapter 3 of this manuscript and reported in [Gurian et al., 2012] is an original example of the generation of a (non demonstrated) 4-body entangled state.

1.5.2 Quantum gates

The very exciting field of quantum computation has been introduced by R. Feynmann in 1982. The principle of a quantum computer is to perform operations on data which are encoding on quantum states of a physical system, bits of a classical computer be-

coming then qubits (quantum bits). The interest of quantum computation is to use the fascinating properties of quantum states such as superposition and entanglement to fast up the calculations.
In the middle of the 90's, two quantum algorithms has been reported, the Shor's algorithm (1994) which concerns the factorization of integer numbers and the Grover's search algorithm (1996). This algorithms clearly show that quantum computers are able to solve a problem much more faster than classical ones. For example, whereas the factorization of an integer of D digits has a complexity scaling exponentially with D in the best classical algorithms, the complexity scales as D^3 in the shor's algorithm.
Several physical systems with very different nature are currently studying in the frame of quantum computation. If quantum computation is still at its infancy, rudimentary quantum computers have been already build in laboratory, qubits taking the form of josephson junctions, quantum dots, trapped ions or again photons. For example, using photons, the successful factorization of 21 using Shor's algorithm has been reported [Martín-López et al., 2012]. To give a bit of visibility to this very effervescent field, the so-called DiVincenzo criteria [Divincenzo, 1998] established 5 mains criteria which have to be fulfill by a physical system to be potentially applicable to a scalable quantum computer.
It seems that Rydberg atoms, although there are not the best (for a question of fidelity of the operations), are good candidates for the realization of quantum computer. Quantum computation with Rydberg atoms is the subject of the revue [Saffman et al., 2010]. We will just mention here the experimental realization of quantum logical gates using neutral atoms.
One of the criteria for the realization of a quantum computer is the ability to perform logical operations on qubits. Interestingly, it has been shown that any logical operation can be done using a small set of elementary operations. One of this set is for example composed by the Hadamar gate which consists in the rotation of a single qubits and the CNOT gate acting in the two-qubits space. The matricial representation of the CNOT gate is

$$\text{CNOT} = \begin{pmatrix} 1 & 0 & 0 & 0 \\ 0 & 1 & 0 & 0 \\ 0 & 0 & 0 & 1 \\ 0 & 0 & 1 & 0 \end{pmatrix} \tag{1.47}$$

The implementation of such quantum gates is then a first, indispensable, step toward quantum computation. In the reference [Isenhower et al., 2010], authors report the first realization of the CNOT gate using neutral atoms. Here, a qubit is formed by two hyperfine levels of the ground state of a rubidium atom and the CNOT gate is

implemented on two atoms using a sequence of laser pulses resonant with a Rydberg transition. The dipole blockade is the key mechanism to implement the CNOT gate.

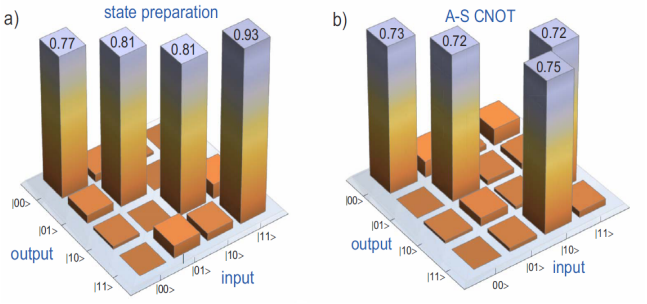

Figure 1.23: Report of the experimental realization of a CNOT gates, from [Isenhower et al., 2010]. a), measurement of the states preparation. b), measurement of the states after the laser pulses sequence.

On the fig 1.23, we see the measurement of the quantum state of the two qubits associated to the CNOT gate. In this experiment, the fidelity has been measured to be 0.73.

1.5.3 Quantum simulation

It exists two big way to compute a problem, we can use digital computer or analog computer. Today's computer are digital ones where logical and arithmetic operations are performed on several Central Processing Units (CPU). A digital computer can be used in principle to solve every kind of problem once corresponding equations are written. The implementation of quantum gates acting on qubits aims to built the quantum equivalent of a digital computer.
Analog computers work completely differently, the general principle of an analog computer is to match a problem into a physical system which exhibits the same behavior than the problem being solve. The result of a computation is then read in measuring the value of the physical quantities present in the analog computer. In contrast with digital computers, an analog computer is specifically build to solve one kind of problem.
Historically, analog computers has been largely used before digital computers becomes sufficiently powerful to solve accurately all kind of problem. As some illustrative examples, mechanical analog computers have been used during the World War II for gun fire control. Analog computers based on oil bath heated by electrical current have also been developed, in this case, informations are obtained via the measured temperature of the bath, such calculators have been used to define the flight controls of Concorde.

In the frame of quantum computation, cold atoms systems offers the possibility to build quantum analog computer. It exists namely several possible analogies between solid state systems and cold atoms systems, the latest having the advantage to be fully controllable and exempt of several complications like the presence of phonons. One major example is the study of the Bose-Hubbard model using cold atoms in optical lattices where it has been possible to observe and characterize the Superfluid-Mott insulator transition [Greiner et al., 2002]. The possibilies to form many-body systems (and then many-body quantum simulator) with cold atoms have been review in [Bloch et al., 2008].
Using Rydberg atoms, the presence of strong and variable interactions open many perspectives in the modeling of interacting many-body systems [Weimer et al., 2010, 2011]. In this frame, the study of cold Rydberg gases goes together with the study of cold polar molecules [Pupillo et al., 2008; Carr et al., 2009; Dulieu and Gabbanini, 2009] and magnetic dipolar gases [Stuhler et al., 2005; Koch et al., 2008], all those systems are review in [Lahaye et al., 2009]. Interacting Rydberg systems allow to study the asymptotic case where interaction energy is much stronger than kinetic energy.

As a first example, the Hamiltonian of the dipole blockade (see equation 1.42) is formally equivalent to the one of a spin glass [Castellani and Cavagna, 2005] in a permanent magnetic field. Here the laser detuning and the Rabi frequency play respectively the role of the longitudinal and the transverse magnetic field, the Rydberg-Rydberg interaction corresponds to the spin-spin interaction (only spin-up particles interact).

As mention in the section 1.3.2 the diffusion of a Rydberg excitation in a bath of Rydberg atoms trough exchange of excitation has a formal analogy with diffusion of excitons [Tokihiro et al., 1995]. It is also possible to implement a quantum random walk with such a system [Côté et al., 2006], in this case, Rydberg atoms have to be trap in optical lattices to make the walk totally random. The implementation of a quantum random walk [Kempe, 2003] could have very big impact on quantum computation as it allows to built a quantum generator of random numbers, which is, at least in classical computation, a central peace of several algorithms.

A very interesting way to use the properties of interaction of Rydberg atoms in cold atom systems is to weakly dressed ground state atoms with a Rydberg level. By this way, we namely preserve the very long life time of the ground state atoms allowing to let the system evolves for a very long time toward its thermodynamical equilibrium. It has been shown theoretically that such systems allow to create new kind of interaction potential between the atoms and to reach exotic quantum phases [Henkel et al., 2010].

Such systems, called dressed Rydberg gases, has been studied (up to now theoretically) for example in [Mayle et al., 2009; Pupillo et al., 2010; Honer et al., 2010; Wüster et al., 2011].

1.5.4 Quantum light sources

A very promizing application of the Rydberg gases is the generation of non-classical states of light. It could possible, using the dipole blockade phenomenon to engineer light sources generating a deterministic number of photons.
Classical light sources and standard laser sources generate an electromagnetic field with a poissonian number of photons. In the frame of high precision measurements using a light field, the statistical distribution in the number of photon can be a limiting factor known as the shot noise limit. One field of research in quantum optic is the generation of so-called squeezed light, where the uncertainty on the number of photons emitted by a source is reduced (in this case, there is more uncertainty on the photons phase).
Blockaded Rydberg ensembles could be very efficient sources of squeezed light. First due to the sub-poissonian statistics of Rydberg excitations (see section 1.4.4). Secondly due the directionality of the emitted photon linked to the collective nature of the Rydberg excitations. This last point offers fantastic perspective in the way to use the emitted field. Perfect Fock's states could be obtained at different angle of emission, the excitation statistics becoming in this case the efficiency of the process.

A simple case, which is already very interesting, is the implementation of single photon sources using fully blockaded Rydberg ensembles. This idea was proposed in the first article dealing with many-body dipole blockade [Lukin et al., 2001] and developed later in many works (for example [Saffman and Walker, 2002]). Here the fact that only one single Rydberg excitation can be present in an atomic sample leads to the emission of a single photon when the Rydberg excitation is deexcited. In the reference [Dudin et al., 2012] where the Rydberg excitation of an atomic sample is done in the quasi fully-blockaded regime (see section 1.4.4), the measurement of the second order intensity correlation function at zero delay of the light emitted by the atomic sample after the Rydberg excitation is reported. The value of the second order intensity correlation function, which is a measure of the fact that single photons are emitted, is found to be $0.006(6)$, authors claims that, to their knowledge, it is the lowest value obtained for any previously reported light source.

The generation non-classical states of light using Rydberg ensembles or more generally correlated atomic ensemble is very largely studied theoretically, we mention here

only few references, [Porras and Cirac, 2008; Olmos and Lesanovsky, 2010] more recent works are [Stanojevic et al., 2012] for Rydberg ensembles or [Miroshnychenko et al., 2012] for the photons directionnality. Other references can be found therein.

In [Honer et al., 2011], The possibility to use Rydberg ensembles to implement high fidelity photons counting device or to create non classical states of light by removing a deterministic number of photons is studied.

1.6 Rydberg atoms : frontier between neutral matter and charged matter

The last aspect of Rydberg atoms Physics that we present in this chapter concerns the fact that Rydberg atoms are very easily ionized under the effect of an electric field due to their very low binding energy.
Whereas coulomb interaction makes very difficult the spatial control of a charged particles ensemble, we can use Rydberg atoms to get a very precise control on the initial state of a charged particles distribution.

1.6.1 Charged particles beams

The use of Rydberg atoms is currently study to build new kind of charged particles beam sources. Starting from an atomic beam, we can excite the atoms in a Rydberg state and ionized them with an electric field. The spatial properties of the atomic beam is then transfered to the charged particles beam. An interesting situation is when the properties of the atomic beam is controlled by cold atoms techniques, in this case, it is possible to create charged particles beams with very low velocity dispersion.
A possible application is the realization of Focused Ions Beam (FIB), here we are interested to get a small radial velocity dispersion and then a precise focusing of the beam. FIB are used in lithography to realize nanometric structure.
An other application concerns the production of electron beams (EB) for electronic microscopy, in this case we are interesting in the small longitudinal velocity dispersion of the electrons to get a beam as monocinetic as possible and then a better imaging resolution.
For those applications, the direct ionization of cold atoms leads already to nice perspective. Nevertheless, excite Rydberg atoms can be an efficient intermediate step to reach an even better control. This have been for example studied in [Oomori et al., 1987].
The following references are related to the general topic of charged particle beams from

cold atomic sources [Freinkman et al., 2003; Hanssen et al., 2008; Debernardi et al., 2012].

1.6.2 Ultra-cold plasmas

An interesting field of research is the possible evolution of a Rydberg sample in plasma. The ionization of Rydberg atoms can appears trough several process : electric field, collision with hot background atoms, blackbody ionization (see [Beterov et al., 2007] for this last point). However, a Rydberg gas can even spontaneously evolves into a plasma trough the Penning ionization process [Walz-Flannigan et al., 2004; Robicheaux, 2005; Viteau et al., 2008]. The principle of the Penning ionization is that two atoms excited in a Rydberg state with attractive interaction collide, one atom is then ionized and the other driven in a lower electronic state. In [Amthor et al., 2007b,a; Tanner et al., 2008; Amthor et al., 2009] the possibilty of auto-ionization without collision but trough long-range dipole coupling is also studied.
Evolution of an atomic gas toward plasma has been studied in several references, for example [Killian et al., 2003; Li et al., 2004; Li et al., 2005, 2006; Killian et al., 2007]. The interest of such experiments is for example to study the dynamics of ultra-cold plasma. It has been also shown that Rydberg atoms in the plasma has a profound analogy with binary stars in star cluster [Comparat et al., 2005]. Finally, in the case where the initial atomic gas is excited in the blockade regime, we could have the formation of correlated plasma [Pohl et al., 2004b,a].

1.7 Conclusion

We have seen all along this introductory chapter to Rydberg atoms Physics the wonderful properties of Rydberg atoms and interacting Rydberg gases.
The key of those properties is the exaggerated sensitivity of Rydberg atoms to their electromagnetic environment.
Rydberg atoms benefits in addition of a particular convenience in regard to their theoretical description. Using the QDT, the Rydberg states of all alkaline species look like hydrogen ones with the very nice advantage to single the states with low angular momentum.

Rydberg atoms can be used as electric field sensors, this at the photon scale!

The Electro"static" interactions between Rydberg atoms have huge values. We have

seen that they can have various form; angular-dependent dipole-dipole, isotropic Van-der-Waals or resonant Förster ones. Overall, we can experimentally tune those interactions.

When excited in a cold atomic gas, Rydberg atoms give rise to many-body Physics. Namely, the many-body behavior of cold Rydberg ensembles have been studied through the dipole blockade phenomenon.
The collective character of the Rydberg excitations in the regime of blockade allows the study of very interesting coupling properties between such ensembles and the electromagnetic field.

Cold Rydberg gases could be used as universal quantum simulators, namely with the development of Rydberg dressing techniques. Rydberg atoms could be also used to build photonic devices.
Concerning technological issue, a point which has not been mentioned in this chapter is that the interesting properties of Rydberg atoms can also be exploited in some case without be "cold" allowing to be free of heavy experimental apparatus [Kübler et al., 2010; Sedlacek et al., 2012].

Chapter 2

Calculation of the quantum states of two interacting Rydberg atoms in presence of electric and magnetic field

In this chapter, we present a way to calculate the electronic quantum states of a system of 2 interacting alcalin Rydberg atoms in presence of static, uniform, external electric and magnetic fields. In the frame of this thesis, we have implemented an program in C++, to do it. In this chapter, we present the physical formalism linked to those calculations and we give explicitly all the formula necessary to implement the code. Finally we present some results of the calculations.

2.1 General working of the programm

We will not, in this manuscript, deal with the programming part of the calculations, but just give the main ideas of the program working. For information, the code, in its actual version, is composed by around 50 header files with more than 6500 lines in total. This code might be diffuse but need to be made more user friendly before that.

As mentioned in the section 1.2.2, an indispensable input for the quantum calculations on Rydberg atoms is the knowledge of the quantum defects. So, in our program, in addition to the physical constants usally required for atomic physic calculation, we need to set the experimentally obtained values of the quantum defects, we did it for cesium, rubidium and lithium atoms (and hydrogen!).

From the knowledge of the quantum defect, we calculate the Rydberg electronic wave

functions and energies of one Rydberg atom in absence of external fields. We do it in the frame of the QDT with Numerov integration method in the so-called Coulomb approximation for the radial part of the wave function. This allows to fully characterize a quantum basis $\{|r\rangle\} = \{|n, l, j, m_j\rangle\}_{nljm_j}$, the zero-field basis, from which all the calculations are effectuated. Any state $|r\rangle = |n, l, j, m_j\rangle$ of this basis is an eigenstate of the zero-field Hamiltonian H_0 with the eigenenergy E_{nlj}.
In this basis, for a Rydberg atom a, we can write the Hamiltonians relative to the presence of a static electric field $\vec{F}$ and a static magnetic field $\vec{B}$, we note them respectively H_S and H_Z for Stark and Zeeman Hamiltonian. In diagonalyzing the total Hamiltonian $H_a = H_0 + H_S + H_Z$, we obtain the energies of the Rydberg states of an atom in presence of the external fields and we can express them in the zero-field basis.
Working in the zero-field two-atoms basis (tensorial product of two zero-field basis) we can write the Hamiltonian of the electrostatic interaction $H_{ab}(\vec{R}_{ab})$ between two Rydberg atoms a and b, separated by $\vec{R}_{ab} = \vec{R}_a + \vec{R}_b$. In diagonalyzing the total Hamiltonian $H_{tot} = H_a \otimes \mathbb{1} + \mathbb{1} \otimes H_b + H_{ab}$ we obtain the energy of the two interacting Rydberg atoms in presence of a static, uniform, electric and magnetic fields and we can express the new eigenstate in the zero-field two-atoms basis.

To extract the results of those calculations, it is often useful to plot the eigenenergies in function of one parameter ($\|\vec{F}\|$, $\|\vec{R}_{ab}\|$) in keeping constant the other ones. In our program we use GNUplot which allows to ask for the desired graphics directly from the C++ code. We use also in the program different existing libraries from GSL (GNU Scientific Library), namely gsl_eigen.h for diagonalization routines and gsl_sf_coupling.h for angular momentum coupling.

2.2 Alternative, approximation und uncertainty

In this section we discuss the different choices that we made to implement the calculations when alternative methods exist. We discuss also the approximations which are done and give order of magnitude for the associated uncertainties. We try also to highlight in this section the conditions for which the calculations that we have implemented are the most accurate.

2.2.1 Quantum defects and Rydberg states basis

The experimental determination of the quantum defects is an indispensable input for Rydberg calculations, this for all the theoretical treatments. For one given atomic specie, the values of the quantum defects are determined in measuring the energy of transition

between the different Rydberg states and the ground state using high-precision spectroscopy, the obtained precision is of the order of few MHz. Interestingly, for Rydberg states with not so high principal quantum numbers n, it is even possible to resolve experimentally the hyperfine structure of the energy spectrum. In the case of cesium, from the data reported in [Goy et al., 1982] we can interpolate that the hyperfine splitting is below 1MHz only for $n > 28$ for $np_{1/2}$(F=3-F=4), $n > 23$ for $np_{3/2}$(F=2-F=5) and $n > 40$ for $ns_{1/2}$(F=3-F=4). We see here that the description of the Rydberg states using the fine structure basis is well adapted only for Rydberg states with a relatively high principal quantum number. For now, in our calculations, we do not deal at all with the hyperfine structure and we can then consider that the accuracy of the calculations are fully valid at the scale of few MHz for $n > 40$. Nevertheless, the accuracy of the treatment with the fine structure basis of the lower Rydberg states remains quite good as the energy scale of the hyperfine splittings is very small in comparison with the energy scale between the different Rydberg states of the fine structure basis, for example, still in cesium, if the hyperfine splitting between the states $24s_{1/2}$F=3 and $24s_{1/2}$F=4 is around 7 MHz, the fine structure basis Rydberg state the closest in energy from $24s_{1/2}$ is $20f_{7/2}$ and the difference in energy between those two states is around 14GHz.

2.2.2 Radial matrix elements

To calculate the coupling terms between the zero-field Rydberg states due to the electric and/or magnetic "perturbation", we need to determine the so-called radial matrix elements (see section 2.4). Those elements depend of the radial wave functions of the Rydberg states.
To calculate the radial wave functions of a Rydberg state, we use the knowledge of its energy. Consequently, the uncertainty on the Rydberg states energy, i.e., on the quantum defects, induces an uncertainty on the radial matrix elements.

In addition to the uncertainty on the energy of the Rydberg states, the non exact knowledge of the radial potential view by the Rydberg electron induces also an uncertainty on the determination of the radial wave functions.
In our program, we use the so-called Coulomb approximation to calculate the radial wave functions of the zero-field Rydberg states. The Coulomb approximation consists in approximating the potential created by the nucleus and the core-electrons by the simple Coulomb potential of a punctual charge. This approximation is very accurate at large distances, i.e., when the Rydberg electron is far from the core. However, this approximation leads to less accurate evaluation of the Rydberg wave functions in the core

region.
An important point concerning the calculations that we present in this chapter is that we are interested in the matrix elements between two Rydberg states. Because the Rydberg wave functions have a huge spatial expansion, the radial matrix elements between two Rydberg states is very weakly dependent of the value of the wave functions close from the core. Consequently, the use of the coulomb approximation leads to a very accurate determination of the radial matrix elements between two Rydberg states.

The calculation of the radial matrix element between the ground state and a Rydberg state are involved in the determination of the Rabi frequency of such a transition. It is then very important to calculate it precisely. In addition to the "near core" region which has to be carefully checked, the angular selection rules depends the hyperfine structure of the ground state. Consequently, in the present state of the program, those radial matrix elements are not accessible, concerning the selection rules, we can find in [Löw et al., 2012] the corresponding formula.

Interestingly, it exists alternative methods to the Coulomb approximation (NCA) to calculate the radial wave functions of Rydberg states. As proposed in [Klapisch, 1971], we can determine models potentials (MMP) describing the potential seen by the Rydberg electron such that the eigenvalues of the model potentials corresponds to the real one. In this method, the model potentials are adjusted in order to reproduce the experimental energies of the Rydberg states and depend then of the quantum defect values.
Also, methods have been proposed aiming to evaluate directly the radial matrix elements, in this case, the Rydberg wave function itself is not investigated. In [Klarsfeld, 1989], analytical formula are derived as interpolation of case of hydrogen for non integer principal quantum number (MCA). Another method of this type has been proposed in [D'yachkov and Pankratov, 1994] (DP) where analytical formula are derive following quasi-classical calculations. Very interestingly, formula are proposed for the matrix elements between two bound states but also between a bound and a continuum states as well as between two continuum states. A big advantage of the methods which use analytical formulas is to avoid completely the eventual derives of the numerical methods.

The methods DP has been used for example in [Beterov et al., 2012] to determine Cooper minima in the transition probability from ground to Rydberg states. In this reference, the results are compared with the ones given by the Coulomb approximation showing in a general way a good agreement. However, additional Cooper minima are fond using the DP method.

In the reference [Piotrowicz et al., 2011], authors report experimental measurements of the reduced dipole matrix elements (strongly linked to the radial matrix elements) between ground and Rydberg states of Rubidium 87. Very interestingly they have done a comparison of their experimental results with the different theoretical calculations that we have mentioned. In the fig2.1 we show a graphic extracted from this article.

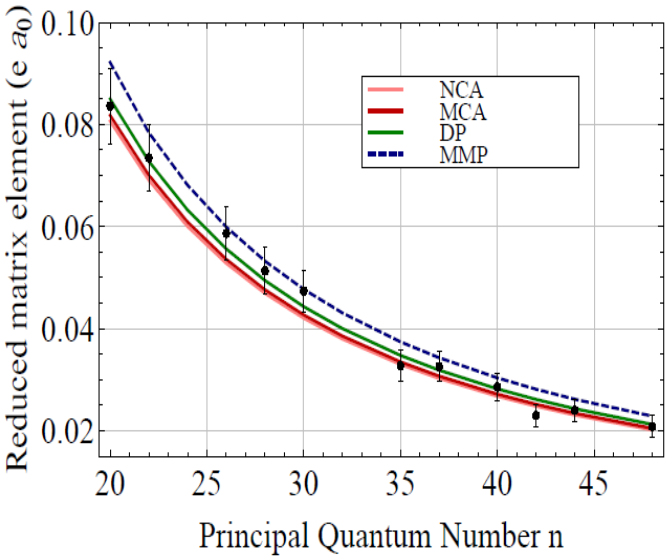

Figure 2.1: Reduced dipole matrix elements in function of the principal quantum number, from [Piotrowicz et al., 2011]. In this graph, experimental results (markers with error bars) are compared with different theoretical calculations (lines)

On the fig2.1, we see that in a general way, the different calculations leads to similar results.

2.2.3 Basis set for the calculations

In principle, we should work every time with the full basis and even include the continuum states. In practice, the presence of external fields as well as Rydberg-Rydberg interactions do not coupled all the states together. Because we are often interested in a particular energy region and not to the full Rydberg spectrum, we can limit the calculation to a subset of states close in energy. Nevertheless, the zero-field Rydberg states are still strongly mixed by external fields or by the Rydberg-Rydberg interaction and the number of states to take in account to get accurate results can be quite important. For example, to get accurate calculation of the Stark effect on one Rydberg state induced by a field whom the strength is the half of the ionization field, we need to take in account at least 5 multiplicities around the Rydberg state in question.

In our program, we do not deal at all with continuum states. Consequently, the calculation of the Stark effect near the ionization limit is not accurately treated.

2.2.4 Axis of quantification

Each of the Hamiltonian that we want to treat (Stark, Zeeman and interaction ones) taken separately, could be calculated in choosing the most convenient axis of quantification of the atoms (often noted Oz). For fields Hamiltonian it correspond to take the axis of quantification along the field direction, i.e., the quantum number m_j is in the case the projection of the total angular momentum j along the field direction. For the interaction Hamiltonian, it correspond to the internuclear axis.
Such a good choice of the axis of quantification, for each Hamiltonian taken separately, leads to quite simple expressions of the corresponding matrix elements and the formula usually found in the literature are always given with this convention.
However, in our case, as we want to treat all the effects in the same time, we have to define a unique quantification axis (a unique basis). We can note that those considerations concern only the angular part of the physical problem.
One possibility could be to use the Wigner rotation matrix. Those matrix allows to calculate the matrix elements of an Hamiltonian in a given coordinate system (for a given axis of quantification) in function of the matrix elements in an other coordinate system which differs from the first one by a given 3-dimensional rotation. It could be then possible to calculate for each Hamiltonian the matrix elements with the most simple (given the simplest formula) axis of quantification and, from this, calculate the matrix elements in the common basis using the appropriated Wigner rotation matrix.
In our treatment, we choose to calculate directly the matrix elements of the different Hamiltonians in a previously defined basis. This means, for example, that the Stark Hamiltonian has to be express for an electric field which is not along the quantification axis but along a "random" direction in comparison to the axis of quantification. This gives more complicated expression of the matrix elements since $H_S = -\hat{\mu}.\vec{F}$ is not simply $-\hat{\mu}_z F_z$ but $-(\hat{\mu}_x F_x + \hat{\mu} y F_y + \hat{\mu}_z F_z)$. In this manuscript, we present the formula associated to this treatment.

The use of Wigner rotation matrix leads formally to a slightly simpler treatment since it corresponds to a deeper use of angular momentum theory results. From a programing point of view, the implementation of both methods are roughly similar. However, the fact to determine directly the matrix elements in a random basis leads to more explicit formula where the selection rules are slightly more visible.

2.3 Zero-field Rydberg states

2.3.1 Zero-field Rydberg energies

In absence of external field, the energy E_{nlj} of a Rydberg state $|n, l, j, m_j\rangle$ is given by the equation 1.2 of the section 1.2.2 that we record here

$$E_{nlj} = -\frac{R_y}{(n - \delta_{nlj})^2} \tag{2.1}$$

The values of the quantum defect δ_{nlj} can be, for each alcalin specie, evaluated from the knowledge of few parameters via the Ritz's formula (equation 1.5 section 1.2.2)

$$\delta_{nlj} = \delta_0(lj) + \frac{\delta_2(lj)}{(n - \delta_0(lj))^2} + ... \tag{2.2}$$

We already give in the section 1.2.2 (Tab.1.2) the values of the quantum defects for cesium atom. We give here the value for rubidium atoms.

$Series$	δ_0	δ_2
ns	3.1311804	0.1784
$np_{1/2}$	2.6548849	0.2900
$np_{3/2}$	2.6416737	0.2950
$nd_{3/2}$	1.34809171	−0.60286
$nd_{5/2}$	1.34646572	−0.59600

Table 2.1: Rubidium quantum defects, from [Li et al., 2003] and [Han et al., 2006]

2.3.2 Zero-field Rydberg wave functions

In absence of external fields, one Rydberg atom possesses a very useful symmetry : it is invariant by any three-dimensional rotations of the coordinates system. A very convenient consequence is that the angular part of the problem can be completely analytically determined.
In defining the position vector of the Rydberg electron as $\vec{r} = \{r, \theta, \phi\}$, i.e., using spherical coordinates (see section 2.5.2), the wave function $\Psi_{nlmj_m}(\vec{r})$ of a Rydberg state $|n, l, j, m_j\rangle$ can be formally decomposed in a radial part and an angular part

$$\Psi_{nljm_j}(\vec{r}) = R_{nlj}(r)\Theta_{ljm_j}(\theta, \phi) \tag{2.3}$$

The radial part not depend of m_j and the angular part not depend of n.
The angular part of the wave function is the same than in the case of hydrogen and can

be determined in function of the spherical harmonics (see section 2.5). Also we will focus in this section on the radial part. The radial part of the wave function $R_{nlj}(r)$ satisfies the following equation

$$\left[-\frac{\hbar^2\nabla^2_{\vec{r}}}{2\mu_e} - V_{eff}(r)\right] R_{nlj} = E_{nlj}R_{nlj} \tag{2.4}$$

Where $\mu_e = \frac{m_e m_{core}}{m_e+m_{core}}$ is the reduced mass of the problem (m_e and m_{core} are respectively the electron mass and the mass of the ionic core). V_{eff} is the potential view by the Rydberg electron due to the presence of the ionic core.
The point is that V_{eff} is not exactly known and will be approximately determined. By contrast E_{nlj} is known, or more precisely, measured experimentally.

As a simple but in fact quite accurate approximation, we can consider that V_{eff} is the simple Coulomb potential. We give in the apendix appendix A more accurate form of V_{eff}.

$$V_{eff}(r) = -\frac{e^2}{r} \tag{2.5}$$

By introducing the function $u(r) = rR(r)$ we can write the equation 2.4 as

$$\left[\frac{d^2}{dr^2} - \frac{l(l+1)}{r^2} + \frac{2\mu_e}{\hbar^2}(E_{nlj} - V_{eff}(r))\right] u(r) = 0 \tag{2.6}$$

This differential equation can be solved by the Numerov's method. The Numerov's method is a general method to solve numerically second order differential equation of the form

$$\left[\frac{d^2}{dr^2} + f(r)\right] u(r) = 0 \tag{2.7}$$

Where $f(r)$ is a known function of r.
By identifying $f(r) = \frac{l(l+1)}{r^2} - \frac{2\mu_e}{\hbar^2}(E_{nlj} - V_{eff}(r))$ we see that the Numerov's method is well adapted to solve the equation 2.6.
The Numerov's method is presented in the appendix A, we give here only the principle. The continuous variable r is discretized, giving a list of adjacent coordinates $\{r_i\}$ at witch we will find the value of $u(r)$. The core of the Numerov's method consists in an iterative technique, it allows to calculate the value of $u(r_i)$ knowing $u(r_{i-1})$ and $u(r_{i-2})$. We need thus to initiating the calculation in setting the value of u at two adjacent positions, for example $u(r_{i_0})$ and $u(r_{i_0-1})$, the function is then calculated from one coordinate to the next and the obtained radial wave function is normalized.

In our case the initialization is straightforward as we know that the value of the radial wave function of any Rydberg states goes to zero at large distance. So we will use the Numerov's method to calculate the Rydberg wave function starting at large r and progressively going toward the ionic core.
We see here that the numerov's method is particularly adapted to the calculation of the radial Rydberg wave function. Indeed, if the effective potential V_{eff} is not known exactly, the real potential differs from the approximated potential only at short distance. Since the Rydberg electron has a very big spatial expansion, the calculation of the wave function is very accurate for a large range of distance.

We have represented in the fig 1.3 of chapter 1 a typical radial wave function calculated by the Numerov's method and the Coulomb approximation.

2.4 Radial matrix elements

The knowledge of the radial wave functions is needed to calculate the coupling terms between the Rydberg states in regard to the electromagnetic interaction of the atom and its environment. For the electrostatic couplings, if the angular part mostly determines the selection rules, the radial part gives the overall strength of the couplings. The spread of the spatial overlap between 2 Rydberg states, proportional to n^2 is then a relevant quantity.

The radial matrix elements $R_{nlj}^{n'l'j'}$ are the radial part of the elements of the position operator $\hat{r}$ between two zero-field Rydberg states.

$$R_{nlj}^{n'l'j'} = \int R_{n'l'j'}(r) R_{nlj}(r) r r^2 dr \tag{2.8}$$

Using the radial matrix elements, we can formally write the elements of the position operator $\hat{r}$ between two zero-field Rydberg states $\left\langle n, l, j, m_j \left| \hat{r} \right| n', l', j', m'_j \right\rangle$ as

$$\left\langle n, l, j, m_j \left| \hat{r} \right| n', l', j', m'_j \right\rangle = R_{nlj}^{n'l'j'} \left\langle l, j, m_j \left| \hat{n} \right| l', j', m'_j \right\rangle \tag{2.9}$$

Where $\hat{n}$ is the "unity position operator", in a sens it could be write as $\left(\hat{\theta,\phi}\right)_{r=1}$ [1].

[1]To push a bit the notation we could right $\hat{r} = \hat{r}_{\int d\theta d\phi} \otimes \left(\hat{\theta,\phi}\right)_{r=1}$, this gives with the rank of the operators $\hat{r}^{(1)} = \hat{r}^{(0)}_{\int d\theta d\phi} \otimes \left(\hat{\theta,\phi}\right)^{(1)}_{r=1}$. $\hat{r}^{(0)}_{\int d\theta d\phi}$ noted r in the text is a scalar operator. $\left(\hat{\theta,\phi}\right)^{(1)}_{r=1}$ noted $\hat{n}$ in the text is an irreducible tensorial operator of rank 1 (see section2.5.2). It could seem strange that a vectorial operator acting on the 3-dimensional space depends only of two coordinates. What is underlying here is the homomorphism of the group of the 3-dimensional pure rotations SO(3) onto the so-called 2-

The values of $\left\langle l, j, m_j \left| \hat{n} \right| l', j', m'_j \right\rangle$ depend only of the angular part of the wave functions.

The same treatment can be done in considering all the operators $\hat{r}^\sigma$, where σ is a positive integer. In this case we have to consider for the radial part the quantities $R_{nlj}^{n'l'j'(\sigma)}$

$$R_{nlj}^{n'l'j'(\sigma)} = \int R_{n'l'j'}(r) R_{nlj}(r) r^\sigma r^2 dr \tag{2.10}$$

In the case $\sigma = 0$, the orthogonalization of the zero-field Rydberg wave function impose to have

$$R_{nlj}^{n'lj(0)} = \delta_{nn'} \tag{2.11}$$

2.5 Resolution of the angular problem

We see in the last section that, in the treatment of a Rydberg atoms in zero-field, we can separate the problem in a radial part and an angular part. Very interestingly, due to the symmetry of the system under rotation of the spatial coordinates, the treatment of the angular part can be almost completely determined by group theory considerations. In this section, we present briefly the results of such considerations which are involved in the treatment of a Rydberg atom. For a more complete description, we can refer to the references [Wigner and Griffin, 1959; Tinkham, 1964; Varshalovich et al., 1987], the convention used in this manuscript are the ones of [Varshalovich et al., 1987].

2.5.1 Angular part of the zero-field Rydberg wave functions

In the equation 2.3, we wrote a formal expression of the zero-field wave functions of a Rydberg atom in separating the radial part and the angular part. However, this expression does not deal properly with the spin of the electron which appears only inside the quantum number j.
In addition to the spatial coordinates, the total wave functions of a Rydberg atoms depend also of spin coordinates. We note in the following the spin coordinates by ϵ. The quite tricky dependence of the wave function according to the spin coordinates can be entirely treated with the angular part of the wave function since the spin corresponds to an intrinsic angular momentum. For the radial part, the presence of the spin trough the quantum number j is sufficient, this is true since the spin itself (not its orientation) has

dimensional unitary group SU(2)

a invariant value, $\frac{1}{2}$.
Taking in account the spin coordinates, the "angular momenta" wave function can be write as

$$\Theta_{lsjm_j}(\theta, \phi, \epsilon) \tag{2.12}$$

Here, we have added explicitly the spin quantum number s to make the following development clearer. Also in all the following, we systematically forget the principal quantum number n. Formally, we consider only the angular problem and work with angular basis.

The coupling between two angular momentum is a well known problem in quantum mechanics. We assume here the reader familiar with this problem and we focus on the points interesting for our main purpose.
Due to the spin-orbit coupling, the coupled basis $|l, s, j, m_j\rangle$ is the good basis for the treatment of a Rydberg atom. Indeed, the zero-field Hamiltonian is diagonal in this basis. However, it will be required to work also with the uncoupled basis $|l, m_l, s, m_s\rangle$ as, only in this basis, the orbital and the spin angular momentum are well decoupled.
For example, in the uncoupled basis, the "spin-angular" wave functions are well separated in orbital and spin parts

$$\Theta_{lm_lsm_s}(\theta, \phi, \epsilon) = Y_{lm_l}(\theta, \phi)\Xi_{sm_s}(\epsilon) \tag{2.13}$$

Here, the functions $Y_{lm_l}(\theta, \phi)$ are the so-called spherical harmonics.

The matrix allowing to do the link between the coupled basis $|l, s, j, m_j\rangle$ and the uncoupled basis $|l, m_l, s, m_s\rangle$ can be totally determined. Its elements are the so-called Clebsh-Gordan coefficients noted $C^{jm_j}_{lm_lsm_s}$ and we have

$$|l, s, j, m_j\rangle = \sum_{m_l m_s} C^{jm_j}_{lm_lsm_s} |l, m_l, s, m_s\rangle \tag{2.14}$$

We can find direct analytical expression for all the Clebsh-Gordan coefficients in [Tinkham, 1964]. They can also be determined using recursive formulas.

In combining equations 2.13 and 2.14, we obtain a formal expression of the spin-angular part of the zero-field wave functions of the coupled basis states $|l, s, j, m_j\rangle$

$$\Theta_{lsjm_j}(\theta, \phi, \epsilon) = \sum_{m_l m_s} C^{jm_j}_{lm_lsm_s} Y_{lm_l}(\theta, \phi)\Xi_{sm_s}(\epsilon) \tag{2.15}$$

It is usefull to introduce quantities equivalent to the Clebsh-Gordan coefficients, the so-called 3j-symbols defined by

$$\begin{pmatrix} l & s & j \\ m_l & m_s & m_j \end{pmatrix} = (-1)^{j+m_j+2l} \frac{1}{\sqrt{2j+1}} C^{jm_j}_{l-m_l s-m_s} \tag{2.16}$$

2.5.2 Spherical coordinates, spherical harmonics and irreducible tensors

Spherical coordinates

Due to the spherical symmetry of a Rydberg atom, it is very convenient to use spherical coordinates. There is several way to define spherical coordinates in function of Cartesian ones (x, y, z), in quantum mechanics, we usually give a particular role to the z-axis and we define the spherical coordinates (r, θ, ϕ) as

$$\begin{aligned} r &= \sqrt{x^2+y^2+z^2} \\ \theta &= \arccos \tfrac{z}{r} \\ \phi &= \arcsin \tfrac{y}{\sqrt{x^2+y^2}} \end{aligned} \tag{2.17}$$

Spherical harmonics

A spherical harmonic $Y_{lm}(\theta, \phi)$ is a complex function defined for $\theta \in [0, \pi]$ and $\phi \in [0, 2\pi]$.

The way to define them mathematically is the following.
Considering the equation $\nabla^2 f = 0$ in spherical coordinates, in injecting functions of the form $f(r, \theta, \phi) = r^l y(\theta, \phi)$ in the equation, we get a set of differential equations where r drop out and l is a parameter. For each l, the corresponding equation possesses $2l + 1$ linearly independent solutions, we define the spherical harmonics $Y_{lm}(\theta, \phi)$ being those solutions.
The spherical harmonics $Y_{lm}(\theta, \phi)$ have the form

$$Y_{lm}(\theta, \phi) = \Phi_m(\phi)\Theta_{lm}(\theta) \tag{2.18}$$

Where we have

$$
\begin{aligned}
&\Phi_m(\phi) = \tfrac{1}{\sqrt{2\pi}} \mathrm{e}^{im\phi} \\
&\Theta_{lm}(\theta) = (-1)^m \left[\tfrac{2l+1}{2}\tfrac{(l-m)!}{(l+m)!}\right]^{\frac{1}{2}} \sin^m\theta \tfrac{d^m}{d(\cos\theta)^m} P_l(\cos\theta) \text{ for } m \geq 0 \\
&\Theta_{l-m}(\theta) = \left[\tfrac{2l+1}{2}\tfrac{(l-m)!}{(l+m)!}\right]^{\frac{1}{2}} \sin^m\theta \tfrac{d^m}{d(\cos\theta)^m} P_l(\cos\theta)
\end{aligned}
\tag{2.19}
$$

Where $P_l(\cos\theta)$ are the Legendre polynomials given by

$$
P_l(\cos\theta) = \frac{1}{2^l l!} \frac{d^l}{d(\cos\theta)^l} (\cos^2\theta - 1)^l \tag{2.20}
$$

In quantum mechanics, the spherical harmonics play a very important role as they are the eigenfunctions of the angular momentum operators $\hat{L}^2$ and $\hat{L}_z$.

$$
\hat{L}^2 Y_{lm} = l(l+1) Y_{lm} \tag{2.21}
$$

$$
\hat{L}_z Y_{lm} = m Y_{lm} \tag{2.22}
$$

The angular momentum operator $\hat{L}$ being the generator of the rotations.
Physically, the spherical harmonics describes the way that a particle move in a central potential.

Irreducible tensors

Taking a tensor of rank l, $T^{(l)}$, this tensor is said irreducible if its $2l+1$ components, $T^{(l)}_m$ are transformed like the spherical harmonics Y_{lm} under rotation of the spatial coordinates. This quite abstract definition is in fact linked to mathematical considerations which concern the commutation rules that the components has to follow (the same than angular momentum). We will focus here on the practical consequences

Every scalar is an irreducible tensor of rank 0.

Every vector or vectorial operator $\vec{r}$ is an irreducible tensor of rank 1 if we define its components as

$$r_{+1} = -\frac{1}{\sqrt{2}}(x+iy) = -\frac{1}{\sqrt{2}} r \sin\theta \mathrm{e}^{i\phi} \quad (2.23)$$

$$r_0 = z = r\cos\theta \quad (2.24)$$

$$r_{-1} = \frac{1}{\sqrt{2}}(x-iy) = \frac{1}{\sqrt{2}} r \sin\theta \mathrm{e}^{-i\phi} \quad (2.25)$$

Where the components are given respectively in Cartesian and spherical coordinates.

The use of irreducible tensors simplify a lot the expression in quantum mechanics calculation. It allows namely to use the Wigner-Eckart theorem.
A large variety of mathematical operations involving irreducible tensors can be performed. We give here only the one concerning the scalar product of two irreducible tensors of rank 1 (2 vectors), $A^{(1)}$ and $B^{(1)}$. Such a scalar product is given by

$$A^{(1)}.B^{(1)} = A_0 B_0 - A_{-1}B_{+1} - A_{+1}B_{-1} \quad (2.26)$$

2.5.3 The Wigner-Eckart theorem

The Wigner Eckart theorem is a powerful theorem allowing to deal in a very simple way with the dependence on the orientation of the system coordinates of the values of a tensorial operator matrix elements.

The Wigner Eckart theorem states that for an irreducible tensorial operator of rank k, $\hat{T}^{(k)}$. The matrix elements of the components $\hat{T}^{(k)}_q$ of this irreducible tensor in the basis $|l, s, j, m_j\rangle$ can be express as

$$\langle l, s, j, m_j | \hat{T}^{(k)}_q | l', s', j', m'_j \rangle = (-1)^{j-m_j} \begin{pmatrix} j & 1 & j' \\ -m_j & q & m'_j \end{pmatrix} \langle l, s, j || \hat{T}^{(k)} || l', s', j' \rangle \quad (2.27)$$

Where $\langle l, s, j || \hat{T}^{(k)} || l', s', j' \rangle$ is a so-called reduced matrix element which does not depend of m_j, m'_j and q. It can be view as the non-oriented value of the matrix element of the irreducible tensor.
The evaluation of the reduced matrix elements of some specific operators is given in the section 2.5.4. Nevertheless, we see here that, for a given irreducible tensor and two set of quantum states having the same "non-oriented" quantum numbers, the Wigner-Eckart theorem allows to find the ratio between all the possible matrix elements, whatever the components of the tensor and the orientation of the quantum states are.

Using Clebsh-Gordan coefficients instead of 3j-symbols, the Wigner-Eckart theorem is

$$\langle l,s,j,m_j|\hat{T}^{(k)}_q|l',s',j',m'_j\rangle = \frac{(-1)^{2k}}{\sqrt{2j+1}} C^{jm_j}_{j'm'_j kq}\langle l,s,j||\hat{T}^{(k)}||l',s',j'\rangle \tag{2.28}$$

2.5.4 Reduced matrix elements

First of all, it exist a usefull relation between the reduced matrix elements of an irreducible tensorial operator of rank k, $\hat{T}^{(k)}$, express in the coupled basis, i.e., $\langle l,s,j||\hat{T}^{(k)}||l',s',j'\rangle$ and its equivalent in the uncoupled basis, $\langle l,s||\hat{T}^{(k)}||l',s'\rangle$. This relation depends if the irreducible tensorial operator $\hat{T}^{(k)}$ acts on the spatial coordinates (it is the case of $\hat{r}$ or $\hat{L}$) or on the spin coordinates (it is the case of $\hat{S}$).
For an operator acting on the spatial coordinates we have

$$\langle l,s,j||\hat{T}^{(k)}||l',s',j'\rangle = \delta_{ss'}(-1)^{j'+l+s+k}\sqrt{(2j+1)(2j'+1)}\begin{Bmatrix} l' & s & j' \\ j & k & l \end{Bmatrix}\langle l||\hat{T}^{(k)}||l'\rangle \tag{2.29}$$

and for an operator acting on the spin coordinates

$$\langle l,s,j||\hat{T}^{(k)}||l',s',j'\rangle = \delta_{ll'}(-1)^{j+l+s+k}\sqrt{(2j+1)(2j'+1)}\begin{Bmatrix} s' & l & j' \\ j & k & s \end{Bmatrix}\langle s||\hat{T}^{(k)}||s'\rangle \tag{2.30}$$

In those relations, we have used the so-called 6j-symbols defined for example in [Varshalovich et al., 1987]. The 6j-symbols are combinaison of 3j-symbols and their are largely use in angular momentum theory as they simplified a lot the calculations. If the 3j-symbols appear when we deal with the coupling of two angular momentum, 6j-symbols appear directly when we deal with the coupling of three angular momentum. 6j-symbols are proportional to the so-called Racah coefficients.

With the convention used here, the reduced matrix elements are not fully normalized. This appears clearly with the value of the reduced element of the identity operator

$$\langle l||\hat{I}||l'\rangle = \delta_{ll'}\sqrt{2l+1} \tag{2.31}$$

We give now the values of the reduced matrix elements of $\hat{n}$ (unity position operator), $\hat{L}$ and $\hat{S}$ in the uncoupled basis. All are vectorial operator so irreducible operator

of rank 1 in choosing the good expression of their components.

$$\langle l, s \,||\hat{n}||\, l', s' \rangle = \delta_{ss'} \sqrt{2l'+1} C^{l0}_{l'010} \tag{2.32}$$

$$\langle l, s||\hat{L}||l', s' \rangle = \delta_{ss'} \delta_{ll'} \sqrt{2l+1} \sqrt{l(l+1)} \tag{2.33}$$

$$\langle l, s||\hat{S}||l', s' \rangle = \delta_{ss'} \delta_{ll'} \sqrt{2s+1} \sqrt{s(s+1)} \tag{2.34}$$

Finally we give the value of the reduced matrix elements in the uncoupled basis of the spherical harmonic operator $\hat{Y}_k$ which is a tensorial operator of rank k acting only on the spatial coordinates.

$$\langle l, s||\hat{Y}_k||l', s' \rangle = \delta_{ss'} \sqrt{2l'+1} \sqrt{\frac{2k+1}{4\pi}} C^{l0}_{l'0k0} \tag{2.35}$$

2.6 Matrix elements in the zero-field Rydberg basis

In this section, we give the general method to calculate the matrix elements of a component of an irreducible tensorial operator, $\hat{T}$, in the zero-field Rydberg basis $|n, l, j, m_j\rangle$. This method uses the different relations given in the preceding section.
The first step is to separate the problem in a radial part and an angular part. For all the angular operators, the radial does not play a role. For operators like the position operator, $\hat{r}$, this can be done in writing $\hat{r} = r\hat{n}$. In this expression r becomes a scalar quantity and is taking in account in the radial part trough the radial matrix elements (equation 2.9). $\hat{n}$ is then taking in account in the angular part of the problem. The same idea can be applied for all the operators whom the radial dependence can be separated from the angular one.
In the treatment of the angular part, the first operation consists in applied the Wigner-Eckart theorem (equation 2.27) allowing to be free of the orientation of the system. The relevant quantities which have to be calculated are then the reduced matrix elements. Up to now, the problem is still treated in the coupled basis. To evaluate the reduced matrix elements, it is possibly required to move in the uncoupled basis, in this case we can use the equations 2.29 or 2.30. Finally the reduced matrix elements are evaluated and the full matrix element can be reconstructed.

It is interesting to notice that an other possible treatment of the angular problem could be to move directly in the uncoupled basis using the equation 2.14 and then use the Wigner-Eckart theorem in this basis. Those two treatments should be completely equivalent,

however, the first one imply lighter formula. This is due to the use of the 6j-coefficients which combine several 3j-coefficients.
We could also think that it could be possible to work directly with the uncoupled basis, i.e., to express the different matrix elements of the system in the uncoupled basis. However, because the states of the uncoupled basis are not eigenstates of the zero-field Hamiltonian due to the spin-orbit coupling, the energies of those states are not accessible experimentally. We see here that the determination of the radial wave functions of the uncoupled basis states with the Numerov method is more problematic. It is sometimes proposed in order to work directly in the uncoupled basis to take the energies of the uncoupled states as the average energies of the coupled states.

2.7 Rydberg states in presence of static, uniform, external fields

In this section we present the way to determine the quantum eigenstates of a Rydberg atom in presence of static, uniform, electric and magnetic fields. In both case we give the explicit way to calculate all the matrix elements between two states of the zero-field Rydberg basis.

2.7.1 electric field

The effect of an electric field $\vec{F}$ is take in account by the Stark Hamiltonian H_S given in the equation 1.25 of the chapter 1.

$$H_S = -\hat{\mu}.\vec{F} = -e\hat{r}.\vec{F} \tag{2.36}$$

In writing the vectors and vectorial operators as irreducible tensor of rank 1, the matrix elements of the Stark Hamiltonian in the zero field basis are given by

$$\left\langle n,l,j,m_j \left| H_S \right| n',l',j',m'_j \right\rangle = -eR_{nlj}^{n'l'j'} \sum_{q=-1}^{1} F_{-q}(-1)^q \left\langle l,j,m_j \left| n_q \right| l',j',m'_j \right\rangle \tag{2.37}$$

Where $R_{nlj}^{n'l'j'}$ is the radial matrix element given in the equation 2.8 and n_q the component q of the unity position operator $\hat{n}$.
According to the Wigner-Eckart theorem we have

$$\langle l, j, m_j \,|n_q|\, l', j', m'_j \rangle = (-1)^{j-m_j} \begin{pmatrix} j & 1 & j' \\ -m_j & q & m'_j \end{pmatrix} \langle l, j \,||\hat{n}||\, l', j' \rangle \tag{2.38}$$

As $\hat{n}$ depends of the spatial coordinates of the electron and not of the spin ones, we have, using the equation 2.29

$$\langle l, j \,||\hat{n}||\, l', j' \rangle = (-1)^{j'+l+s+1} \sqrt{(2j+1)(2j'+1)} \begin{Bmatrix} l' & s & j' \\ j & 1 & l \end{Bmatrix} \langle l \,||\hat{n}||\, l' \rangle \tag{2.39}$$

and we have

$$\langle l \,||\hat{n}||\, l' \rangle = (-1)^l \sqrt{(2l+1)(2l'+1)} \begin{pmatrix} l & 1 & l' \\ 0 & 0 & 0 \end{pmatrix} \tag{2.40}$$

Combining equation 2.37, 2.38, 2.39, 2.40 we get an explicit expression of the matrix elements of the Stark Hamiltonian in the zero-field basis.
Due to the selection rules hidden in the 3j and 6j symbols, only few elements are non null, namely $\langle n, l, j, m_j \,|H_S|\, n', l', j', m'_j \rangle \neq 0$ if $\left|m_j - m'_j\right| \leq 1$, $|j - j'| \leq 1$ and $|l - l'| = 1$. From this last equality, we see that the Hamiltonian Stark is null on the diagonal in the zero-field basis.

2.7.2 magnetic field

The effect of an magnetic field $\vec{B}$ is take in account by the Zeeman Hamiltonian H_Z given by

$$H_Z = \frac{\mu_B}{\hbar}(g_l \hat{L} + g_s \hat{S}).\vec{B} + \frac{e^2}{8m_e}(\vec{B} \wedge \hat{r})^2 \tag{2.41}$$

Where μ_B is the Bohr's magneton, g_s and g_l the electron spin and the electron orbital "$g-$factors" or Lande's factor (their respective value are ≈ 1 and ≈ 2). The second term is sometimes called the quadratic or diamagnetic Zeeman effect, it can be rewrite as

$$\frac{e^2}{8m_e}(\vec{B} \wedge \hat{r})^2 = \frac{e^2}{8m_e}(B^2 \hat{r}^2 - (\vec{B}.\hat{r})^2) \tag{2.42}$$

We see that the Zeeman Hamiltonian can be separated in 4 terms that we will treat separately. To simplify the notations we do not write in the following the scalar factors of each terms which appears in the equation 2.41.

term in $\vec{\mathbf{L}}.\vec{\mathbf{B}}$

This term does not present any radial dependence so we remove the n quantum number, however, we do not add now the selection rule $n = n'$ imposed by the radial part as it would be wrong (as long as other quantum number can be different in the two states) but wait for the proper moment. By the same time we express the vector $\vec{B}$ and the vectorial operator $\hat{L}$ as irreducible tensors of rank 1.

$$\langle n, l, j, m_j | \hat{L}.\vec{B} | n', l', j', m'_j \rangle = \sum_{q=-1}^{1} B_{-q} (-1)^q \langle l, j, m_j | L_q | l', j', m'_j \rangle \tag{2.43}$$

According to the Wigner-Eckart theorem

$$\left\langle l, j, m_j \left| L_q \right| l', j', m'_j \right\rangle = (-1)^{j-m_j} \begin{pmatrix} j & 1 & j' \\ -m_j & q & m'_j \end{pmatrix} \langle l, j || \hat{L} || l', j' \rangle \tag{2.44}$$

According to the equation 2.29

$$\langle l, j || \hat{L} || l', j' \rangle = (-1)^{j'+l+s+1} \sqrt{(2j+1)(2j'+1)} \begin{Bmatrix} l' & s & j' \\ j & 1 & l \end{Bmatrix} \langle l || \hat{L} || l' \rangle \tag{2.45}$$

We can then use the equation 2.33 and we add the "radial" dependence.

$$\langle l || \hat{L} || l' \rangle = \delta_{nn'} \delta_{ll'} \sqrt{2l+1} \sqrt{l(l+1)} \tag{2.46}$$

In the last equation, the factor $\sqrt{2l+1}$ is a normalization factor and $\sqrt{l(l+1)}$ is the expectation value of the operator $\hat{L}$.
Combining all those equation leads to the matrix elements corresponding to the term in $\vec{L}.\vec{B}$.

term in $\vec{\mathbf{S}}.\vec{\mathbf{B}}$

In this section we add the quantum number $s = 1/2$ in the notation. The treatment of the radial dependence is the same than for the term in $\vec{L}.\vec{B}$.

$$\langle n, l, s, j, m_j | \hat{S}.\vec{B} | n', l', s, j', m'_j \rangle = \sum_{q=-1}^{1} B_{-q} (-1)^q \left\langle l, s, j, m_j \left| S_q \right| l', s, j', m'_j \right\rangle \tag{2.47}$$

According to the Wigner-Eckart theorem

$$\left\langle l, s, j, m_j \left| S_q \right| l', s, j', m'_j \right\rangle = (-1)^{j-m_j} \begin{pmatrix} j & 1 & j' \\ -m_j & q & m'_j \end{pmatrix} \langle l, s, j || \hat{S} || l', s, j' \rangle \tag{2.48}$$

According to the equation 2.30

$$\langle l,s,j||\hat{S}||l',s,j'\rangle = \delta_{ll'}(-1)^{j+l+s+1}\sqrt{(2j+1)(2j'+1)}\begin{Bmatrix} s & l & j' \\ j & 1 & s \end{Bmatrix}\langle l,s||\hat{S}^1||l',s\rangle \tag{2.49}$$

Using the equation 2.34

$$\langle l,s||\hat{S}||l',s\rangle = \delta_{nn'}\delta_{ll'}\sqrt{2s+1}\sqrt{s(s+1)} = \delta_{nn'}\delta_{ll'}\sqrt{2s+1}\frac{\sqrt{3}}{2} \tag{2.50}$$

In the last equation, the factor $\sqrt{2s+1}$ is a normalization factor and $\sqrt{s(s+1)}$ is the expectation value of the operator $\hat{S}$.
Combining all those equation leads to the matrix elements corresponding to the term in $\vec{S}.\vec{B}$.

Together with the term in $\vec{L}.\vec{B}$, it gives the most important effect of a relatively small magnetic field since the quadratic Zeeman effect is important only for strong field (of the order of 1 Tesla).
The matrix elements of both term $\vec{L}.\vec{B}$ and $\vec{S}.\vec{B}$ are non null on the diagonal, this means that each zero-field Rydberg states is shifted by himself under the effect of a magnetic field. Also the magnetic field induces a coupling between some of the zero-field Rydberg states. The selection rules are given by $\left|m_j - m'_j\right| \leq 1$ and $|j-j'| \leq 1$ and $l = l'$

term in $\mathbf{B^2r^2}$

Both terms of the quadratic Zeeman effect can not be, a priori, expressed in term of irreducible tensorial operators. Consequently, in the treatment of the angular part we can not use the Wigner-Eckart theorem.
The radial part can still be treated independently and we have

$$\langle n,l,j,m_j|B^2\hat{r}^2|n',l',j',m'_j\rangle = B^2 R_{nlj}^{n'l'j'(2)}\left\langle l,j,m_j\left|\hat{n}^2\right|l',j',m'_j\right\rangle \tag{2.51}$$

Where $R_{nlj}^{n'l'j'(2)}$ is given by the equation 2.10.

For the treatment of the angular part, we need to switch directly in the uncoupled basis

$|l, m_l, s, m_s\rangle$ through the equation 2.14.
In the uncoupled basis, the operator $\hat{n}^2$ is diagonal and we have simply

$$\left\langle l, m_l, s, m_s \left| \hat{n}^2 \right| l', m'_l, s', m'_s \right\rangle = \delta_{ll'}\delta_{m_l m'_l}\delta_{ss'}\delta_{m_s m'_s} \tag{2.52}$$

term in $(\vec{\mathbf{B}}.\vec{\mathbf{r}})^2$

We first treat the radial part

$$\langle n, l, j, m_j|(\vec{B}.\hat{r})^2|n', l', j', m'_j\rangle = R_{nlj}^{n'l'j'(2)}\langle l, j, m_j|(\vec{B}.\hat{n})^2|l', j', m'_j\rangle \tag{2.53}$$

Where $R_{nlj}^{n'l'j'(2)}$ is given by the equation 2.10.

For the treatment of the angular part, we switch in the uncoupled basis $|l, m_l, s, m_s\rangle$ through the equation 2.14. We then have to calculate terms of the form

$$\langle l, m_l, s, m_s|(\vec{B}.\hat{n})^2|l', m'_l, s', m'_s\rangle \tag{2.54}$$

In writing $\vec{B}$ and $\hat{n}$ in terms of irreducible tensor of rank 1, we have

$$\begin{aligned}(\vec{B}.\hat{n})^2 &= n_0^2B_0^2 + n_{-1}^2B_1^2 + n_1^2B_{-1}^2 \\ &\quad -2n_0n_{-1}B_0B_1 \\ &\quad -2n_0n_1B_0B_{-1} \\ &\quad +2n_1n_{-1}B_{-1}B_1\end{aligned} \tag{2.55}$$

We see here that we have 9 terms to calculate all of the form

$$B_uB_v\left\langle l, m_l, s, m_s \left| n_\mu n_\nu \right| l', m'_l, s', m'_s\right\rangle = B_uB_v\delta_{ss'}\delta_{m_s m'_s}\left\langle l, m_l \left| n_\mu n_\nu \right| l', m'_l\right\rangle \tag{2.56}$$

We can then use the following equation to calculate those terms

$$\left\langle l, m_l \left| n_\mu n_\nu \right| l', m'_l\right\rangle = \frac{(-1)^\mu}{3}\delta_{ll'}\delta_{m_l m'_l}\delta_{\mu(-\nu)} + \sqrt{\frac{2}{3}\frac{2l'+1}{2l+1}}C_{l'020}^{l0}\sum_{k=-2}^{2}C_{1\mu1\nu}^{2k}C_{l'm'_l2k}^{lm_l} \tag{2.57}$$

We see that the quadratic Zeeman effect coupled states with $|l - l'| = 0$ or $|l - l'| =$

2. It is proportional to B^2 and to $R_{nlj}^{n'l'j'(2)}$.
In the frame of this thesis, we have only consider the effect of relatively small magnetic field for which the effect of this diamagnetic term is almost negligible. However, a very interesting Physic arise from the effect of a strong magnetic field on Rydberg atoms with namely the appearance of chao. The fact is that, under the effect of a strong magnetic field, the classical motion of the Rydberg electron does not follow cycling orbital but can potentially explore the full space around the core. This chaotic behavior leads namely to a characteristic distribution of the eigenenergy of the Rydberg states. This has been quite intensively studied during the nineties and we can refer for example to the following reference [Bouloufa et al., 1992] for an experimental demonstration.

2.8 Multipolar electrostatic interaction between two Rydberg atoms

In this section, we present the way to calculate the electrostatic multipolar interactions between two Rydberg atoms. As there is two atoms, we have to work in the two atoms basis. We will express all the matrix elements of the multipolar interaction in the two atoms zero-field basis, i.e., for states of the form $\Psi_{ab} = |n, l, j, m_j\rangle_a \otimes |n, l, j, m_j\rangle_b$.

2.8.1 Multipolar electrostatic interactions

In the very general case, for two charge distributions a and b whom the center of mass is separated by a distance R_{ab}. Considering that the two distributions are spatially well separated. The electrostatic interaction Hamiltonian H_{int} between a and b is given by

$$H_{int} = \sum_{i,j=0}^{\infty} \frac{V_{ij}(a,b)}{R_{ab}^{i+j+1}} \tag{2.58}$$

Here we have decomposed the total electrostatic interaction in a sum of multipolar electrostatic interactions $V_{ij}(a,b)$. They are given by

$$V_{ij}(a,b) = \frac{1}{4\pi\epsilon_0} \sum_{m=-inf(i,j)}^{+inf(i,j)} \frac{(_1)^j (i+j)!}{\sqrt{(i+m)!(i-m)!(j+m)!(j-m)!}} Q_i^m(a) Q_j^{-m}(b) \tag{2.59}$$

Where $Q_i^m(a)$ is a component of a multipolar moment of the distribution a. It is given by

$$Q_i^m(a) = \sqrt{\frac{4\pi}{2j+1}} \sum_{k \in a} q_k r_{k,a}^j Y_{jm}(\theta_{k,a} \phi_{k,a}) \tag{2.60}$$

Here, k denotes the k^{th} particle of the distribution a. q_k is the electric charge of k and $r_{k,a}$, $\theta_{k,a}$ and $\phi_{k,a}$ are the spherical coordinates of k taking the center of mass of a as the origin. The Y_{jm} are the spherical harmonics.

2.8.2 Case of a Rydberg atom

In the case of a Rydberg atom, we consider that the system is composed by two particles, the Rydberg electron and an other effective particle representing the nucleus and the other electrons. This effective particle is considered to be situated at the center of mass of the atom and to have an electric charge $+e$.
Consequently, the components of the multipolar moments of a Rydberg atom are given by

$$Q_0^0 = 0 \tag{2.61}$$

Meaning that the Rydberg atom has no total electric charge.

$$Q_{j\neq 0}^m = \sqrt{\frac{4\pi}{2j+1}} (-e) r^j Y_{jm}(\theta\phi) \tag{2.62}$$

Where r, θ and ϕ are the spherical coordinates of the Rydberg electron of the atom taking the nucleus as the origin.
We see that under this form, a component of a multipolar moments Q_j^m is a component of an irreductible tensorials operators of rank j, it is then possible to use the Wigner-Eckart theorem.
In order to extract easily the radial dependence, we define the angular multipolar moments $\widetilde{Q}_j^m$ as

$$Q_j^m = -e r^j \widetilde{Q}_j^m \tag{2.63}$$

2.8.3 Matrix elements of the multipolar electrostatic interactions

Considering two Rydberg atoms a and b, we note $\Psi_{ab} = \Psi_a \otimes \Psi_b = |n, l, j, m_j\rangle_a \otimes |n, l, j, m_j\rangle_b$ a state of the zero-field two-atom basis.

The quantities that we have to calculate are of the form

$$\left\langle \Psi_{ab} \left| Q_i^m(a) Q_j^{-m}(b) \right| \Psi'_{ab} \right\rangle \tag{2.64}$$

The total electrostatic interaction will be given by a sum of several of those terms according to the equations 2.58 and 2.59.

The multipolar operators of the atom a act only on the atom a and identically the multipolar operators of the atom b act only on the atom b. Consequently, we can write the multipolar interactions as

$$\left\langle \Psi_{ab} = \Psi_a \otimes \Psi_b \left| Q_i^m(a) Q_j^{-m}(b) \right| \Psi'_{ab} = \Psi'_a \otimes \Psi'_b \right\rangle = \left\langle \Psi_a \left| Q_i^m(a) \right| \Psi'_a \right\rangle \left\langle \Psi_b \left| Q_j^{-m}(b) \right| \Psi'_b \right\rangle \tag{2.65}$$

We have then to calculate terms of the form

$$\left\langle \Psi_a \left| Q_k^q(a) \right| \Psi'_a \right\rangle = \left\langle n, l, j, m_j \left| Q_k^q \right| n', l', j', m'_j \right\rangle \tag{2.66}$$

We see here that the problem is now treated in the one-atom zero-field Rydberg basis.
We can first treat the radial part

$$\left\langle n, l, j, m_j \left| Q_k^q \right| n', l', j', m'_j \right\rangle = -eR_{nlj}^{n'l'j'(k)} \langle l, j, m_j | \widetilde{Q}_k^q | l', j', m'_j \rangle \tag{2.67}$$

Where $R_{nlj}^{n'l'j'(k)}$ is given by the equation 2.10 and $\widetilde{Q}_k^q$ defined by the equation 2.63. According to the Wigner-Eckart theorem, we have

$$\langle l, j, m_j | \widetilde{Q}_k^q | l', j', m'_j \rangle = (-1)^{j-m_j} \begin{pmatrix} j & k & j' \\ -m_j & q & m'_j \end{pmatrix} \langle l, j || \widetilde{Q}_k || l', j' \rangle \tag{2.68}$$

As $\widetilde{Q}_k$ depends of the spatial coordinates, we have, using the equation 2.29

$$\langle l, j || \widetilde{Q}_k || l', l' \rangle = (-1)^{j'+l+s+1} \sqrt{(2j+1)(2j'+1)} \begin{Bmatrix} l' & s & j' \\ j & k & l \end{Bmatrix} \langle l || \widetilde{Q}_k || l' \rangle \tag{2.69}$$

Finally using the equation 2.35

$$\langle l || \widetilde{Q}_k || l' \rangle = \sqrt{\frac{4\pi}{2k+1}} \langle l || \hat{Y}_k || l' \rangle = \sqrt{2l'+1} C_{l'0k0}^{l0} \tag{2.70}$$

Conbining the equations 2.70, 2.69, 2.68, 2.67, 2.65, 2.59 and 2.58 we obtain the matrix elements of the total electrostatic interaction H_{int} in the zero-field two-atoms Rydberg basis.
The equation 2.58 contains in fact an infinite sum, however, we can limit the sum to te first terms as their values decrease strongly when i and j increase. Taking only the first term, i.e., $i = j = 1$, we obtain the dipole-dipole interaction between the two Rydberg atoms, all the results presented in the following are limited to this case.

2.9 Results of the calculations

The calculations presented in the sections 2.7 and 2.8 have been implemented, in the frame of this thesis, in an informatic program. Several types of outputs can be asked to the program, allowing to get the results of the calculations. We present in this section the different outputs that we have look at.

2.9.1 Stark diagram

One of the most simple task that we can ask to the program is to calculate the energies of the Rydberg states in presence of a static, uniform, electric field. When we plot those energies in function of the magnitude of the electric field, we obtain a so-called Stark diagram.
Such calculations have been done for a long time and we have already shown a typical result in the fig 1.4 of the chapter 1, which is extracted from the reference [Zimmerman et al., 1979]. In order to check the validity of our calculations (overall the fidelity of their implementation) we have reproduced the same Stark diagram, shown on the fig 2.2.

The agreement with the results of [Zimmerman et al., 1979] is very good.

2.9.2 Förster resonances

From the knowledge of the Rydberg energies in presence of an electric field, it is possible to calculate the field at which Förster resonances appears (see section 1.3.2 in the chapter 1). In a first time, we can calculate the sum of the energies of two Rydberg states in function of the electric field.
A F"orster resonance is potentially present at the electric field where the energy of two 2-body states are equal. We say potentially as the two pairs of Rydberg states has to effectively interact via Rydberg-Rydberg interaction to have a Förster resonance. This

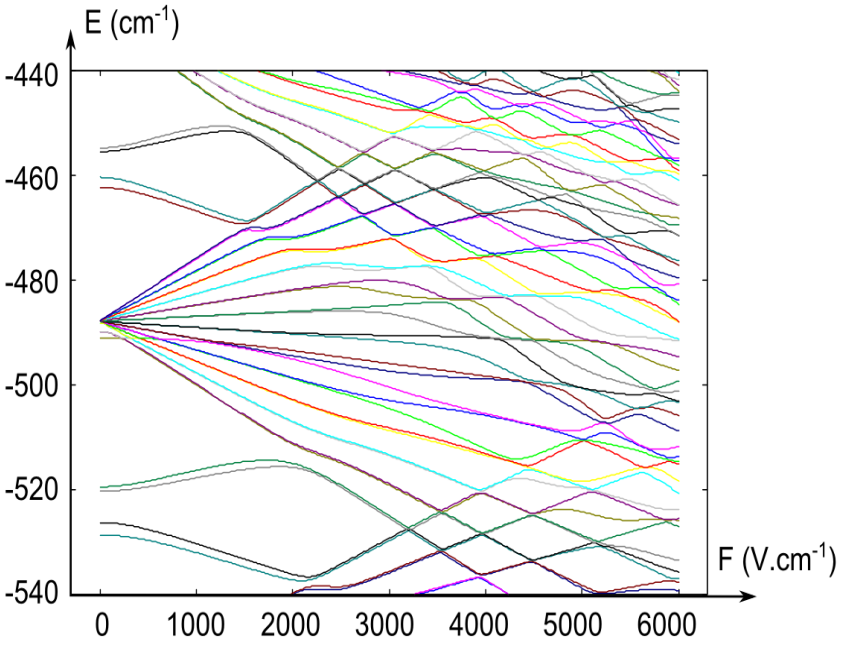

Figure 2.2: Calculation of the diagram Stark of the cesium for n around 15 and $|m_j|$=1. In the calculations, all the Rydberg states with $|m_j|$=1 and n between 13 and 20 have been taken into account

can be checked and quantified by the program.
If we can characterize the Stark tuned dipole-dipole Förster resonances using the program, it could be also possible to look for other types of Förster resonance, for example magnetic Förster resonances or Förster resonances where quadrupolar interactions are involved.

2.9.3 Spaghetti curves

An other interesting task that we can ask to the program is to plot the eigenenergies of a pair of Rydberg atoms in function of their distance. Due to the very large number of two-atoms quantum states we obtained an ensemble of so-called spaghetti curves as we can see on the fig 2.3. To build the 2-body basis in which the calculations are done, we first define the 1-body basis. The 1-body basis includes several multiplicities with eventually a restriction on the orbital and magnetic quantum numbers. Then the 2-body quantum states are chosen within all the possible pairs. We have implemented several way to choose the 2-body states. We can for example ask explicitly for predefined states. As we are often interested in the potential curve of one particular 2-body state. We can take all the states in a given range of energy around this state, eventually with

condition on the coupling strengths. For example, we can take a given number of state being the most coupled to the state of interest, then a given number of states being the most coupled to the most coupled, etc... The purpose of this selection is to get the most accurate result in limiting the basis of the calculations (the calculation time).

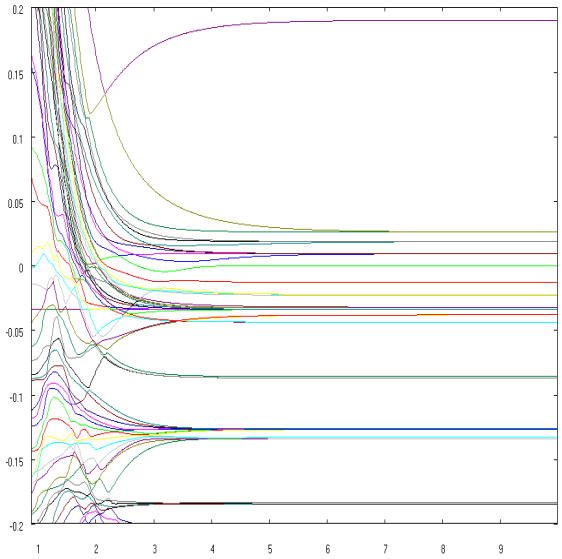

Figure 2.3: Calculation of the 2-body eigenenergies in function of the interatomic distance. Energies are given in cm^{-1}, the distances in μm. The zero of energy corresponds to the non-interacting energy of two Rydberg atoms in the state $70p_{3/2}$. We took for the calculations the 10 2-body states the most coupled to $70p_{3/2}(m_j = -1/2) + 70p_{3/2}(m_j = -1/2)$ the 4 states the most coupled to each of those states and the 2 states the most coupled to each of all the states already chosen. All of the 2-body states are chosen to be composed by Rydberg state with n between 62 and 75 and $l < 6$ (up to g states) with all the possible j and m_j

In an energy diagram like the one of the fig 2.3, we can obtain the dependence of the Rydberg-Rydberg interaction of a particular 2-atoms state in function of the distance between the two Rydberg atoms. By doing a fit of such a curve, we could obtain the C_3 or C_6 coefficients of a Rydberg state.
However, we see in the fig2.3 that the interaction between two Rydberg atoms presents in fact a much more complicated behavior than the one obtained in the two-levels approximation presented in the chapter 1. Namely, at short distance, the interaction between the Rydberg atoms becomes very important and the number of quantum states which are mixed together is huge.
It is important to recall here the limit of validity of the dipole-dipole Hamiltonian. The two Rydberg atoms of the pair have to be well spatially separated. On the fig2.3, the

size of each atom is around 0.5μm and the calculations are then valid only for a radius larger than 1 μm.
It is quite interesting to determine, in addition to the eigenenergies, the eigenstates of the pair of interacting atoms. In expressing those new eigenstates in the basis of the non-interacting ones, we get an idea of how the states are mixed together under the effect of the Rydberg-Rydberg interaction. In the fig2.4 we have (tried to) represented the fraction of one non-interacting two-atoms Rydberg state present in each of the new eigenstates.

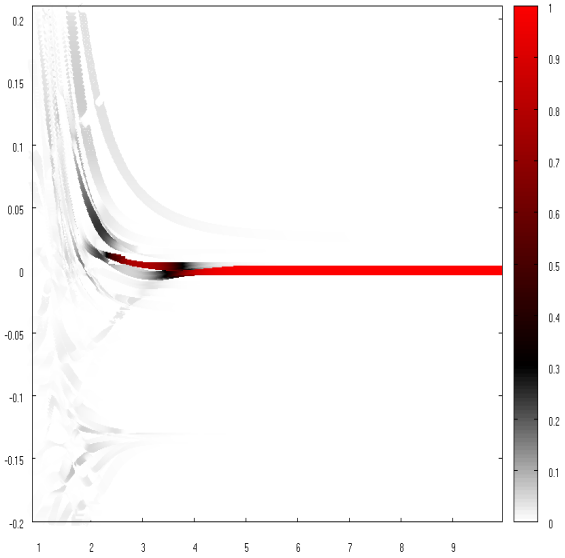

Figure 2.4: Fraction of the non-interacting state $70p_{3/2}(m_j$=-1/2) + $70p_{3/2}(m_j$=-1/2) present in the interacting states. The calculation are the same than the one of the fig 2.3

We see that, for two close atoms, an initial non-interacting 2-body Rydberg state is highly diluted in many interacting states. At small interatomic distances, there is almost no meaning to speak of two atoms excited in a well defined Rydberg state. For example, say that we have two atoms separated by 1.5μm in the $70p_{3/2}$ Rydberg state is quite ambiguous.

2.9.4 Zeeman degeneracy

The fact that a Rydberg state with a total angular quantum number j possesses $2j+1$ different magnetic quantum number m_j (that we call here the Zeeman degeneracy) has very strong consequences on the Rydberg-Rydberg interaction. This has been studied in details in the reference [Walker and Saffman, 2008], we can also look at this feature using our program.

On the figZeemanDeg, we have plotted the 2-body eigenenergies in function of the distance between the two atoms in taking into account the $43d_{5/2}+43d_{5/2}$ states and the $45p_{3/2}+41f$ states which is the 2-body "state" the most coupled with the first one. For f states both $j=5/2$ and $j=7/2$ are taken into account and for all the states all the possible m_j are considered.

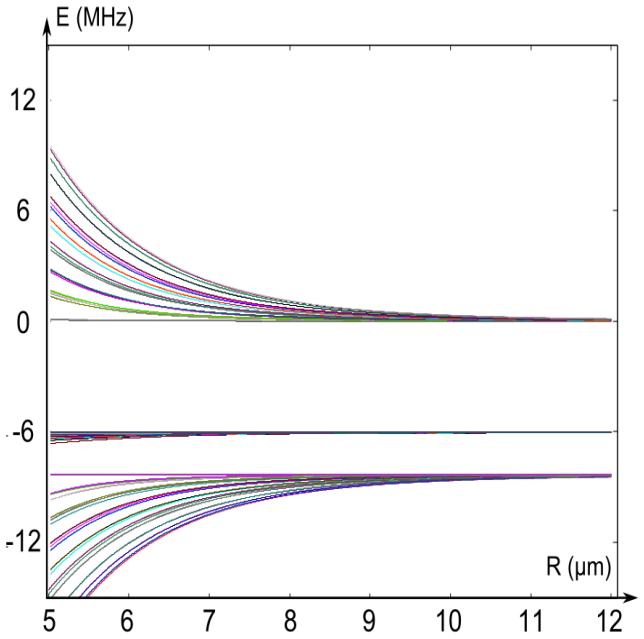

Figure 2.5: Potential curves resulting from the different "Zeeman configurations" of the channel $d_{5/2}+d_{5/2}\rightarrow p_{3/2}+f$. The diagram obtain here has been previously reported in the reference [Saffman et al., 2010]. This has been used to check the validity of our program for 2-body calculations.

We see on the fig 2.5 that the Rydberg-Rydberg interaction has very different strength for the different combinaison of the magnetic quantum numbers of the two atoms. In terms of C_6 coefficients, in the fig 2.5, the ratio between the biggest and the smallest one exceds 300.

It is important to figure out that the eigenstates which correspond to those interaction energies are not of the form (we consider now only $f=7/2$ for simplicity)

$$\alpha\left(|43,d,5/2,m_j\rangle\otimes|43,d,5/2,m'_j\rangle\right)+\beta\left(|45,p,3/2,m''_j\rangle\otimes|41,f,7/2,m'''_j\rangle\right) \tag{2.71}$$

but of the form

$$\sum_{m_j,m'_j} \alpha_{m_j m'_j} \left(|43, d, 5/2, m_j\rangle \otimes |43, d, 5/2, m'_j\rangle \right) + \sum_{m_j,m'_j} \beta_{m_j m'_j} \left(|45, p, 3/2, m''_j\rangle \otimes |41, f, 7/2, m'''_j\rangle \right) \tag{2.72}$$

This can be explained as following. In writing only the m_j, the dipole-dipole interaction coupled a state $\left(|m_j\rangle \otimes \left|m'_j\right\rangle\right)$ with a state $\left(\left|m''_j\right\rangle \otimes \left|m'''_j\right\rangle\right)$ if we have $m_j + m'_j = m''_j + m'''_j$, however, looking at one of the atom, we can have $m_j = m''_j \pm 1$. So, starting with a state $\left(43d_{5/2} \otimes 43d_{5/2}\right) \left(|m_j\rangle \otimes \left|m'_j\right\rangle\right)$, this state is coupled for example with $\left(45p_{3/2} \otimes 41f_{7/2}\right) \left(|m_j - 1\rangle \otimes \left|m'_j + 1\right\rangle\right)$ which is also coupled with $\left(43d_{5/2} \otimes 43d_{5/2}\right) \left(|m_j - 2\rangle \otimes \left|m'_j + 2\right\rangle\right)$.
We understand here why the eigenstates are superpositions of several states with different combination of m_j.

This indicates that to get the true eigenstates of the dipole-dipole interaction, we need to diagonalize the Hamiltonian by using, at least, the full Zeeman multiplets of the interacting two-atoms states, here $\left(43d_{5/2} + 43d_{5/2}\right)$ and $\left(45p_{3/2} + 41f_{7/2}\right)$. In the reference [Singer et al., 2005], the determination of the C_6 coefficients of the Rydberg states is done using second order perturbation theory and thus it does not take fully in account the effect of the Zeeman degeneracy.
The decomposition of the eigenstates on the natural two-atom basis (as well as the ratio between the different eigenenergies) depends only on the angular quantum numbers and can be fully determined for each "channel of interaction" (in our example, $d_{5/2} + d_{5/2} \rightarrow p_{3/2} + f_{7/2}$) taking the interatomic axis as quantification axis. This is what is done in the reference [Walker and Saffman, 2008] and the authors give a link to a web page where the eigenvectors are explicitly given.

The effect of the Zeeman degeneracy plays a big role in the dipole blockade experiments due to the existence of combination of m_j which lead to very small interactions and thus limit the blockade efficiency. Also, since the coupling associated to the different configurations depend of the laser(s) polarization and its relative orientation with the interatomic axis, the Rydberg-Rydberg interaction in zero-field is no more isotropic due to the Zemman degeneracy.

2.9.5 Effective two-levels atoms

The results presented in the sections 2.9.3 and 2.5 underline an important difficulty for the theoretical treatment of the interacting Rydberg gases. This concerns the use of two-

levels atoms.
In the Hamiltonian of the dipole blockade (see section 1.4.1 of the chapter 1), the atoms are considered to be two-levels systems, the levels are the ground state and one Rydberg state. Those two levels are coupled by a laser field with a given Rabi frequency and two atoms in the Rydberg state interact via a given potential corresponding to the Rydberg-Rydberg interactions.
However, if we first look out the Zeeman degeneracy, we should consider that a particular doubly excited Rydberg state does not have the same decomposition on the non-interacting Rydberg states for all the interatomic distances. Consequently, due to the laser excitation selection rules, the Rabi frequency associated to the excitation of a doubly excited Rydberg state should be considered to be dependent of the interatomic distance.
At large interatomic distances, we can consider that each doubly excited Rydberg state is composed by two non-interacting states. The ratio between the componentt of the doubly excited Rydberg state on the non-interacting states is given in the section 1.3.2 of the chapter 1. This ratio tends toward 1 when the dipole-dipole coupling becomes much larger than the initial Förster defect. The Rabi frequency associated to the laser coupling of the doubly excited state is in this case reduced by a factor $\sqrt{2}$.
At small interatomic distance, each doubly excited state is a composed by many non-interacting states. The fraction of a doubly excited state compatible with the laser excitation selection rules is hardly reduced. A precise study of the composition of the doubly excited states would allow to quantify this effect.

To resume, the excitation of a doubly excited state should be associated a Rabi frequency having a quite complex dependence with the distance between the two Rydberg atoms. In a general way the Rabi frequency decrease with the interatomic distance.

We propose here a very rudimentary way to take in account the variation in function of the interatomic distance of the Rabi frequency associated to the excitation of a doubly excited Rydberg state. It consists in introducing a cutting distance R_c. For $R > R_c$, the Rabi frequency can be considered to be constant and equal to the one of the non-interacting case (of a single atom). For $R < R_c$, we can consider that the Rabi frequency is zero. The cutting distance R_c can be evaluated by defining a cutting ratio (few percent) corresponding to the coupled part of the doubly excited state for a given laser excitation, it would correspond to $R_c \approx 1.5\mu$m on the fig 2.4 (and thus 2.3).
The introduction of the cutting distance is a very rough modeling of the underlying effect. However, due to its "step shape" it can be very easily include in different kind of equations.

The effect of the Zeeman degeneracy is even more problematic for the modeling of an interacting Rydberg gas with two-levels atoms. Indeed, the different doubly excited Rydberg states corresponding to different combination of magnetic quantum numbers are only slightly degenerated for a large range of interatomic distances. Consequently they can be all populated in the same time by the laser excitation, each one having its own Rabi frequency and its own interaction energy shift.
The Rabi frequency associated to each of those states depends of the polarization of the excitation laser(s) via the selection rules on the magnetic quantum number. We have also to take in account the relative orientation between the interatomic axis and the polarization axis. The decomposition of each "Zeeman" eigenstate on the natural two-atoms basis allows to calculate the associated Rabi frequency.
For a correct treatment of the laser excitation of a pair of interacting Rydberg atoms, we should consider this multi-levels structure of the doubly excited state.
As it has been highlighted by the authors of [Walker and Saffman, 2008], the simplest way to maintain the contact between experiments and theoretical model which use two-levels atoms (up to know, all the theoretical models) is to excite s-states. Indeed, if the s-states have 2 Zeeman sub-levels, it is shown in [Walker and Saffman, 2008] that all the Zeeman configurations corresponding to the channel ns+ns$\rightarrow$n$'$p+n$''$p are associated to the same interaction curve. This channel is the only one directly coupled by dipole-dipole interaction. In other words, in the case of s-state, the dipole-dipole interaction does not leave the degeneracy associated to the magnetic quantum numbers.
For the other interaction channels, we have to define an effective doubly excited Rydberg level.
One possibility could be to consider only the less interacting Zeeman configuration since this configuration will be the most populated by an excitation resonant with the non-interacting case. However, this has to be considered with care as the laser selection rules can lead to a very inefficient coupling of this configuration.
Interestingly, in [Walker and Saffman, 2008], an effective interaction shift is proposed in order to take in account the effect of all the configurations and their relative Rabi frequencies. From this we can obtain the effective angular dependence of the Rydberg-Rydberg interaction for a given polarization of the excitation laser.

2.9.6 Molecular potential wells

In the ensemble of spaghetti curves as the ones shown in the fig2.3, we can find very interesting curves which correspond to molecular potential wells. As mentioned in the section 1.3.2 of the chapter 1, the existence of those potential wells indicates the possi-

bility to form giant molecules composed by two Rydberg atoms. Such molecules have been indeed observed experimentally as it is reported in [Overstreet et al., 2009]. In such molecules, sometimes called "Macro-dimers", the two Rydberg atoms are not sharing a valence electron as it is the case in a classical covalent link but the electrostatic interactions are such that it is energetically more favorable for the two Rydberg atoms to stay at a particular distance.
In the fig 2.6 we present such a potential well.

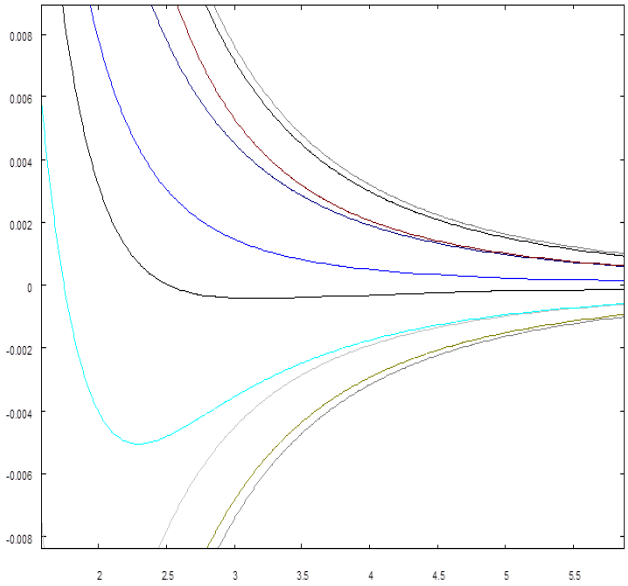

Figure 2.6: Molecular potential well resulting from the interaction of two Rydberg atoms in the channel $60s + 59p$. We see here the channel $60s + 59p_{3/2}$, the channel $60s + 59p_{1/2}$ situated below leads to the underlining molecular potential well. All the m_j are taken into account in the calculations.

The states involved in the potential well of the fig 2.6 are the same than the ones used in the photoassociation process, however, instead of being the first excited levels, the levels are Rydberg ones.
We can see on the fig 2.6 the huge distance at which the two Rydberg atoms are bounded, in the order of few μm. We also see that the depth of the potential well is of the order of 150 MHz. Those characteristics would make possible to observe experimentally this type of macro-dimers. However, 2-colors excitation have to be performed since two different Rydberg states are involved.

2.10 Conclusion and outlooks

The calculations presented in this chapter and overall their implementation represent a very nice theoretical support for the Rydberg atoms Physics.
If the theoretical knowledges involved in those calculations are known for a long time, the possibility to numerically determine the interacting 2-body Rydberg states in presence of external fields is more recent. This task would not have been envisagable even twenty years ago and those calculations are a nice illustration of the possibilities offer by the today computer for Physics calculations.

In the frame of the Rydberg-Rydberg interactions, those calculations allow to go well beyond the two-levels approximations presented in the chapter 1. Concerning the long-range behavior of the interactions it allows to obtaine a better precision. However, the short-range behavior of the interacting 2-body Rydberg states exhibits very complex features. A precise study of the spaghetti curves in the μm range should be done with care since the excitation of very close pairs might have an effect for very dense ultra-cold atomic samples.

An interesting feature of those calculations is also the possibility to study the "magnetic quantum number effects". We have seen that the Zeeman degeneracy play a big role in the interaction between $l \neq 0$ Rydberg atoms. Similar effects could also be studied concerning the Förster resonances. To this regards, the possibility to include the Zeeman effect in the calculations pave the way toward a very precise experimental control of those features.

As mentionned in the begining of this chapter, the calculations presented here are well adapted and accurate for highly excited Rydberg states and not close to the ionization limit (in electric field). Further developments will consist in the inclusion of both first excited states (hyper-fine structure) and continuum states. This would allow to access accurately to relevent physical quantities like the oscillator strengths between ground and Rydberg states or photoionization rates. More generally, it should be very interesting to check the general accuracy, efficency and possibilities of different calculation methods. A comparison of the codes developed by different groups could be also very benefic. We have mentionned in the chapter 1 the potential of Rydberg atoms for several technologic perspectives (high precision field sensor, quantum simulation, atom-light quantum devices), the effective realization of such technologies will be for sure linked to the existence of reliable data base on Rydberg atoms properties.

Chapter 3

Few-body experiments

In this chapter, we present the experiments done in the "Laboratoire Aime Cotton" at Orsay in the frame of this thesis.
The main purpose of those experiments has been to study phenomena, present in a cold Rydberg gase, resulting from the interactions between few-body. We paid a special attention to the phenomenon of Stark tuned Förster resonance. In this process, a resonant coupling between two 2-body quantum states is revealed through an exchange of excitations between the atoms, leading by the way to particularly non trivial cases of entanglement.
The 2-body Förster resonances can be quite well characterized theoretically as we have seen in the chapter 1 and 2. The interest to observe or implement such 2-body phenomena is to confirm their conditions of appearance, or to progress in their effective realization. We have for example obtained experimentally a complete saturation of a 2-body Förster resonance. In [Nipper et al., 2012a], Förster resonance are studied using Ramsay interferometry allowing to characteryze the interactions with a very high precision.
The experimental study of few-body processes has a quite different interest. First, the theoretical modeling of such processes is much more tedious and there predictions more singular. Studying them experimentally allow to determine a way to go. Also, few-body effects can lead to very interesting features. The most relevant example is the Efimov Physics [Efimov, 1970] which have been obsered in cold atomic gases [Kraemer et al., 2006]. For Rydberg atoms, few-body effects are less spectacular but they give rise to interesting cases of interactions. For example, an anti-blockade effect resulting from the interaction of three Rydberg atoms is reported in [Pohl and Berman, 2009]. In a general way, the interaction potentials between several Rydberg atoms should be always different than the sum of 2-body ones. Particular cases of "non-additive" potentials between 3 Rydberg atoms have been reported in [Cano and Fortágh, 2012].

In the frame of this thesis, the main obtained result, reported in [Gurian et al., 2012], is the observation of a 4-body process resulting from a coherent combination of two 2-body Förster resonances. Up to our knowledge, it has been the first observation of a 4-body process associated to an almost complete description of the underlying quantum states.
The beginning of this chapter is devolved to the description of the experimental setup used for those experiments. This setup has been build from scratch in the frame of this thesis. Since the cold atoms techniques are now well known, we mainly focus in this manuscript, on the aspects of the experimental setup relative to the study of Rydberg atoms gases.

3.1 A cold atomic sample

In this section, we present very briefly the experimental setup required for the realization of a Magneto-Optical Trap (MOT) of cesium atoms
The general principle of a MOT, and more generally of the cooling and trapping of neutral atoms can be found for example in the following reviews [Phillips et al., 1985; Cohen-Tannoudji, 1992; Metcalf and van der Straten, 1994; Adams, 1997] as well as in the book [Metcalf and van der Straten, 1999].

3.1.1 Vacuum chamber

The heart of every cold atoms experiment takes place in a vacuum chamber.
The main room of our chamber has 18 windows in order to have a good optical access. Inside the chamber there is a peace of cesium (few grams) from which cesium atoms can be evaporated, there is also 3 cesium dispensers, this two complementary systems allows to control the vapor pressure of cesium inside the chamber. We have disposed in the vacuum chamber a pressure gauge and an ionic pump (Varian 40l/s). 10 electrodes are placed inside the chamber to control the electric field environment. Two charged particles detectors used to the detection of the Rydberg atoms are finally present inside the chamber.

Reaching a high level of vacuum is not done without the appropriated equipment but vacuum technology is very well developed and this equipment exists even for almost perfect vacuum. As a paradigm, in the so-called regime of very-high vacuum (below 10^{-11} mbar) the limiting factor for the pressure can be nothing less than hydrogen or helium atoms passing trough the vacuum chamber (helium pass through the glass and

hydrogen pass even through the stainless steel). We can find in the reference [Chambers et al., 1998] a quite complete introduction to vacuum technology. We mention here few practical considerations.
First, an extreme care has to be payed to the property of the vacuum elements. We use for example several ultrasonic bath with water, ethanol, acetone,... to wash the elements. A simple fingerprint can "kill" a vacuum for billions years!.
To start to lower the pressure from atmosphere one, we have to use a primary pump and a turbo molecular pump. Ionic pump can be typically turn on at a pressure lower than 10^{-6} mbar.
To reach this level of vacuum, we have to steam the wole chamber in order that a maximum of chemical elements present in the materials be outgassed and pump. The best is to heat as most as possible for the longest time, in reality the temperature is limited as some elements (pump, windows) do not support very high temperature. The documentations has to be check with care to avoid complications. Also the raise and fall of the temperature have to be done slowly to avoid mechanicals deformations during the variation of temperature. The steaming duration can be typically one or two weeks.
The outgassing of different materials is extensively studied in the frame of spacecraft and a very large choice of " vacuum friendly" glues or ceramics is now available[1].

To realize a MOT, the pressure inside the chamber have to be lower than 10^{-7} mbar. At this pressure, we are in the so-called high vacuum regime.
In our experiments we typically work with a pressure around 10^{-8} mbar.

3.1.2 Magnetic field

In our setup, the magnetic field required for the MOT of cesium is created by two coils in anti-Helmotz configuration. The magnetic field gradient at the position of the MOT in the direction of the coils axis is around 15 G.cm^{-1}. The gradient is two times smaller in the other directions (thanks to div$\vec{B} = 0$).
In order to compensate the earth magnetic field (around 0.5G) as well as the magnetic field created by the ionic pump (which is first surrounded by μ-metal) there is 3 pairs of coils in Helmholtz configuration, one along each spatial direction.

[1] see for example outgassing.nasa.gouv

3.1.3 Laser fields

On the fig 3.1, we have represented the energy diagram of the cesium first atomic levels including the so-called D2 line which contains the atomic transitions involved in a MOT. we have highlighted on this scheme the transitions driven by the so-called cooling and repumping lasers.
The cooling transition is $6s_{1/2}(F = 4) \rightarrow 6p_{3/2}(F = 5)$, the repumping one is $6s_{1/2}(F = 3) \rightarrow 6p_{3/2}(F = 4)$.

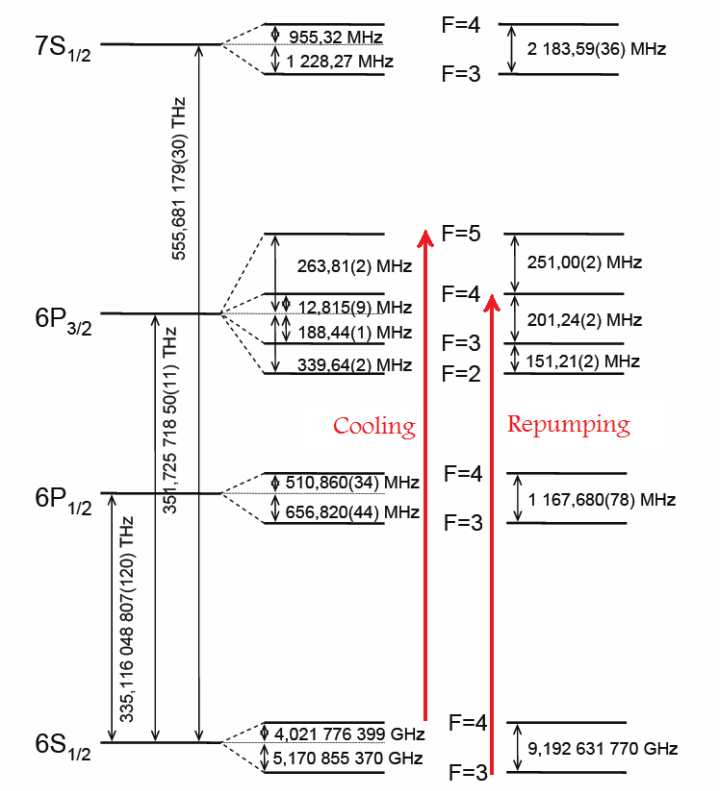

Figure 3.1: Energy diagram of the cesium first levels

In the reference [Steck, 2003] we find the characteristic of the D2 line whom we record here the ones useful for a MOT. Namely, the wavelength in the air λ_{air}, the intensity saturation of the cooling transition I_{sat} and the natural linewidth of the excited state Γ.

$$\lambda_{air} = 852.120532(26)\text{nm} \tag{3.1}$$
$$I_{sat} = 1.1049(20)\text{mW.cm}^{-2} \tag{3.2}$$
$$\Gamma = 2\pi \times 5.234(13)\text{MHz} \tag{3.3}$$

In our experimental setup, both laser are stabilized using the well known saturated absorption technique. This very nice technique consists in using directly cesium atoms as a reference to stabilize the lasers on the cesium transitions. The linewidth of those stabilized lasers are around 200 kHz. As it is typically required for a MOT, the cooling laser is detuned from the exact resonance of a quantity of $15\text{MHz} \approx 3\Gamma$ toward the red. The cooling laser is a DBR diode with an output power of around 60mW (as well as the repumping laser). The cooling laser is separated in 5 beams (we use a retro-reflecting beam along the vertical axis) and send toward the MOT position. There, each beam has a spatial size of around 2 cm^2 and a power around $3mW$ which corresponds to an intensity slightly larger than I_{sat}.

3.1.4 Characteristics of the MOT

As it was not required for the need of our experiments, we have not implemented a systematic measurement of the characteristics of the MOT. Indeed, the experiments that we carried out and that we will present in the following are dealing directly with Rydberg atoms, so the total number or the density of the ground state atoms are not relevant quantities. For example, the Rydberg excitation volume in our experiment is much smaller than the MOT itself.
Also the characteristics of a MOT in a standard configuration, since the Physics which is behind corresponds to well known processes, can be derived according to quite simple formula.

For example, we know that the temperature is in the order of the so-called Doppler temperature. The temperature is in fact generally lower due to a sub-Doppler cooling mechanism, the so-called Sisiphus effect [Dalibard and Cohen-Tannoudji, 1989]. The Doppler temperature T_D is given by (from [Steck, 2003] for the numerical value given here in the case of cesium)

$$T_D = \frac{\hbar\Gamma}{2k_B} = 125.26\mu K \tag{3.4}$$

As another illustrative example, we find in the reference [Grego et al., 1996] the following formula for the temperature T of a MOT of cesium.

$$T(\mu K) \approx 30 + 0.56\frac{N^{\frac{1}{3}} I^{\frac{1}{2}}}{|\delta_L|} \tag{3.5}$$

Where N is the number of atoms in the MOT, I the laser beams intensity and δ_L the detuning of the cooling laser.

Typically, for a MOT of cesium the atomic density is of the order of few 10^{10}at.cm^{-3} and the temperature of the order of 100μK.

On the fig3.2 we show a picture of our MOT.

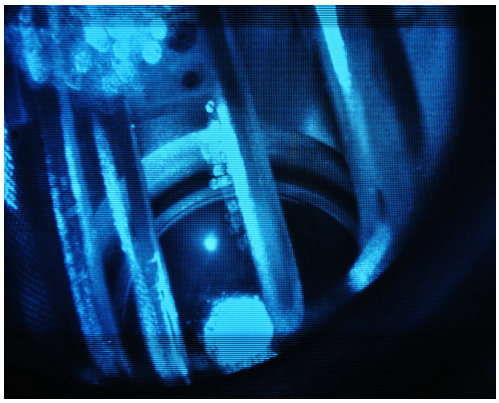

Figure 3.2: Picture of our MOT of cesium, taken through an infrared viewer

Once the MOT is formed, the principle of our experiments is to laser excite the trapped atoms toward Rydberg states. This is done in presence of electric field. Then we detect the Rydberg atoms using field ionization. On the fig 3.3, the main elements of the setup are represented. They will be described in the following sections. We recognize on the fig 3.3 the 6 beams of the MOT.

3.2 Laser excitation of Rydberg states

In this section, we present the experimental setup that we have implemented in order to excite the atoms of the MOT toward Rydberg states. In a very general way, this is done by sending laser beams with the appropriated frequencies through the MOT.
In our setup, we are able to excite Rydberg atoms using two different paths of excitation. One path consists in a 2-photons excitation, the other in a 3-photons excitation.
This two different paths allow first to excite simultaneously two different Rydberg states. As mention in the section 1.3.2 of the chapter 1, this can lead to very interesting phenomena of diffusion of excitation which should be investigated in the future of this experimental setup. Also, exciting two different Rydberg states can be very useful for the study of few-body phenomena.
Secondly, using one or the other of those two excitation paths, we can excite, even in zero field, s, p and d states.

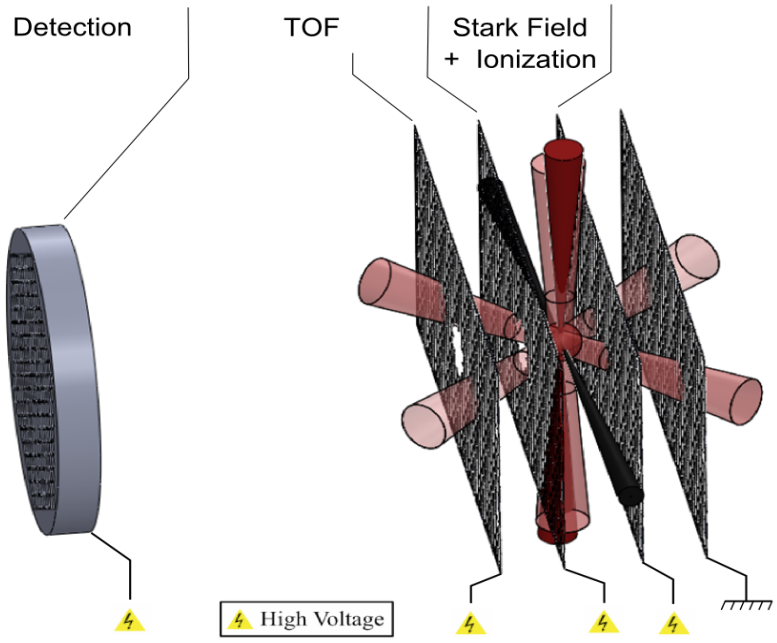

Figure 3.3: Schematic drawing of our setup. The description of the elements is given in the text. A second charged particles detector is in fact present in our setup in the opposite direction than the one represented here. The purpose is to detect simultaneously ions and electrons, however we didn't use this feature from now on. The grid the most on the right is present also for this purpose. Both will be not mentioned in the text.

For both paths, we present in the following the lasers that we use, their characteristics and the way to stabilize them. In addition to the atoms themselves, the principal tool use to characterize the different lasers is a wavemeter WS8 from Angström.

3.2.1 General remarks

In this section, we will, in a very brief and rough way, give an idea of the laser characteristics required to excite Rydberg atoms.
The optical power that we need to excite Rydberg atoms are not huge. Although it depends a lot of the size of the excitation volume (A typical length is of the order of few 100 μm), power of the order of 100 mW are largely enough to excite efficiently atoms toward Rydberg states. It is even needed in some case to reduce the available laser power. Particularly because we want to avoid as most as possible the creation of ions during the Rydberg excitation. Indeed, ions can lead to undesirable effects (local electric field, "ions blockade effect", parasite detection signal). Working with reasonable optical power and short excitation pulses is the best way to limit the number of ions.

Concerning the linewidth of the excitation, the fact is that the natural linewidths of the first excited states (which are the intermediate levels of the multi-photon excitation) are of the order of several MHz. Also, when pulsed excitation is used, the typical duration of the pulse is of the order of 1μs giving a Fourier broadening of the order of 1 MHz. Consequently, the typical linewidth that we have to aim to excite properly Rydberg states is of the order of 1 MHz.

3.2.2 2-photons excitation

We present in this section the laser excitation of a Rydberg state from the ground state using a 2-photons excitation.
Starting with cesium atoms in the ground state $6s$ we first excite them in the state $6p_{3/2}$ and then in a Rydberg state nl_j, here l can be either s or d and n range from 20 to 100. In the fig3.4, we have represented the energy diagram corresponding to this 2-photons excitation.

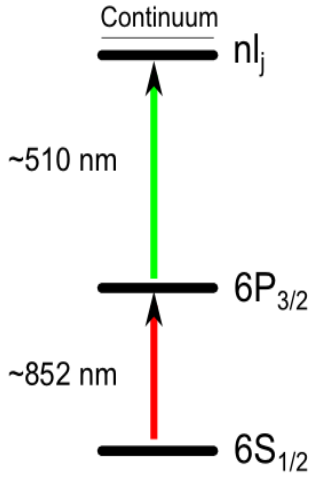

Figure 3.4: Energy diagram of the 2-photons Rydberg excitation

First photon

The first step of the excitation $6s \rightarrow 6p_{3/2}$ correspond to the cooling transition of the cesium MOT. To drive this transition, we use then the cooling laser of the MOT. We see here that in fact, we have nothing to do, indeed, inside the MOT there is permanently many atoms (a bit less than the half of the total number of atoms) excited in the state $6p_{3/2}$.

The quite low intensity of the cooling beam at the position of the atoms (see section()) does not lead to any Autler-Townes splitting or even significant intensity broadening of the level $6p_{3/2}$.
As mention in the section 1.4.4, the fact that this first step is almost resonant with the transition $6s \rightarrow 6p_{3/2}$ (the detuning is 3Γ) makes impossible that the full 2-photons excitation being coherent.
However, in the frame of the experiments that we perform, a coherent excitation is not required and the excitation by the MOT beams of the state $6p_{3/2}$ can perfectly plays the role of the first step of the 2-photons excitation.

To achieve a coherent excitation of the Rydberg state from the ground state, we could turn off the cooling beams and use another laser to do the first step of the Rydberg excitation with this time a sufficiently large detuning to avoid the population of the state $6p_{3/2}$. An other possibility could be still to use a part of the cooling beam and change its frequency with an Acousto-Optic Modulator (AOM), the frequency could be detuned up to 500 MHz with a double pass configuration which is largely enough to avoid population in the state $6p_{3/2}$.

Second photon

The second step of the Rydberg excitation correspond to the transition $6p_{3/2} \rightarrow nl_j$, for $n \in [\![20; 100]\!]$ the corresponding wavelengths range from 513 to 505 nm.
The laser that we used is a commercial one from Sacher. This laser is composed by a diode laser in external cavity lasing in the range $[\![1010; 1050]\!]$ nm. The light emitted by the diode is amplified by a MOPA and doubled in a resonant doubling cavity.
The output power that we obtain is around 150 mW. The natural linewidth of the laser is around 300 kHz. I would like to mention that the quality of this laser (stability, facility to use) is disputable.

In our setup, the frequency of the laser is stabilized and controlled using a home made "sigmameter" built in the Laboratoire Aime Cotton. The principle of this sigmameter is similar to the one of the module "i-scan" currently selling by Toptica. We describe here briefly those quite smart and useful systems which can be used in many kind of situation. On the fig 3.5 we found a scheme of the system.

The laser beam of which we want to control the frequency have first to be prepare with a well defined linear polarization α. The laser beam is then send through a Michelson's

interferometer. A polarization beam splitter whom the axis form an angle ± 45 with α is placed at the output of the interferometer. Finally, two photodiodes are placed right in the paths of the two separated beams in such a way that they both measure only the intensities contained in the center of each interference patterns.
If we note Δ_L the difference of optical path length between the two arms of the interferometer and I the intensity measured by the photodiodes, we can show that

$$I \propto 1 + \cos\left(\frac{2\pi\Delta_L}{\mathrm{c}}\nu\right) \tag{3.6}$$

where c is the speed of light and ν the frequency of the laser beam.
The trick is that we place an optical element, in one arm of the interferometer, which induces an additional dephasing of $\pi/2$ only on one of the two polarizations.
The photodiode which measure this polarization see then an intensity I' with

$$I' \propto 1 + \sin\left(\frac{2\pi\Delta_L}{\mathrm{c}}\nu\right) \tag{3.7}$$

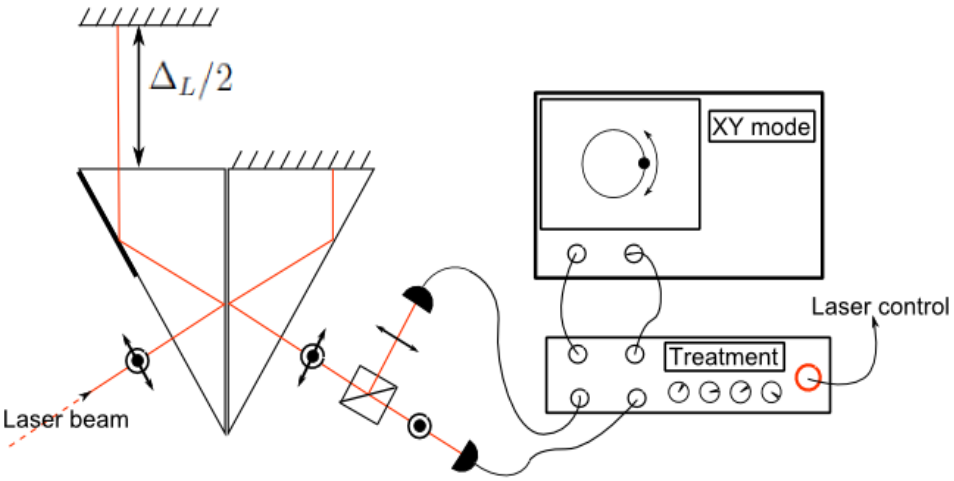

Figure 3.5: Schematic representation of the sigmameter. See text for explanations. The dephasing element is represented by the thick part on the left of the prism.

By looking with an oscilloscope in XY mode at the signal coming from the two photodiodes, we obtain a point. When the frequency ν of the laser beam varied, this point describes a circle.
This type of "angular" signal, which is directly linked to the frequency of the laser, is very interesting to control it. Indeed, with the appropriated electronics devices, (which first imply a proper modification of the offset and the amplitude of each photodiode signal to get a nice "electronically coded" circle), we can generate an error signal propor-

tional to the angular position of the point on the circle relative to an angle of reference. We can then either use the system to stabilize the laser frequency on a fixed reference but also to make a controlled scan of the laser frequency in changing continuously the reference.
One full circle represents a frequency range of $\frac{c}{\Delta_L}$ in our case, it corresponds to 300 MHz. We see here that we can reasonably obtain a precision of 1 MHz (which represents more than 1 on the circle) and, in the same time, easily scan the laser over its full mode-jump free ranges (in doing as many circles as we want with the angle of reference). Obviously, the stabilization efficiency depend of the precision of the electronic as well as the laser itself.
A big advantage of such a system, is that we can in principle send several laser beams in the same sigmameter and control them independently with several electronic boxes. Another nice feature is that this system does not depend of any modulation (of the laser(s) being locked or of the system itself).
An important point to obtain a good stabilization of the laser(s) is that the difference of optical path length between the two arms of the interferometer has to be as stable as possible. In our setup, we send in the sigmameter a part of the repumping MOT beam, which is locked on an atomic reference. We then lock the full system on it, a piezo electric allowing to act on the length of one interferometer arm. This allow for example to be free of all temperature variation effect on the length of the interferometer and reduce also the mechanical noises.

Using this system we achieve to stabilize our second step Rydberg excitation laser within 2MHz (for the green light) on an infinite time scale (since the over all system is locked with an atomic reference), with the possibility to scan the frequency on demand. The only physical parameter that we use to act on the laser is the voltage send to the controller of the piezo which controls itself the position of the grating of the extended cavity of the laser diode, this voltage being directly proportional to the error signal provided by the electronic box associated to the sigmameter.

The laser system that we use for the second step of the 2-photon excitation is enough stabilized (2 MHz) and powerful (150 mW) to efficiently excite toward Rydberg states the atoms in the state $6p_{3/2}$ present in the MOT. This laser is send through the MOT with an almost collimated shape with a typical size of 500 μm. The excitation region is then a cylindric tube with a volume of the order of 0.5mm^3. An AOM placed at the output of the laser allows to switch the laser on and off with a controlled way.

3.2.3 3-photons excitation

We present in this section the laser excitation of a Rydberg state from the ground state using a 3-photons excitation.
Starting with cesium atoms in the ground state $6s$ we first excite them in the state $6p_{3/2}$, then in the state $7s$ then in a Rydberg state np_j, here n range from 20 to 100. In the fig3.6, we have represented the energy diagram corresponding to this 3-photons excitation.

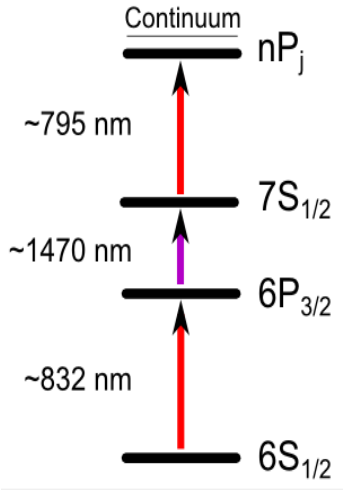

Figure 3.6: Energy diagram of the 3-photons Rydberg excitation

First photon

Exactly like in the case of the 2-photon excitation, the first step of the 3-photon excitation, driving the transition $6s \rightarrow 6p_{3/2}$ is done with the cooling beams of the MOT (see section 3.2.2).

Second photon

The second step of the 3-photons excitation corresponds to the transition $6p_{3/2} \rightarrow 7s$, the associated wavelength is around 1470nm.
The laser that we use to drive this transition is a diode laser in external cavity DL100 From Toptica having an output power around 15 mW and a natural linewidth around 100 kHz.
In our setup, this laser is stabilized using a two-colors, Doppler free, absorption measurement.

The principle of this method is to send in a cesium cell a laser already stabilized on the cooling transition by the saturated absorption technique (using a first cesium cell). This first laser has then the effect to "pump" the atoms in the state $6p_{3/2}$. The 1470 nm laser beam is then send in the same cell with a non null spatial overlap with the first laser. This laser acts thus like a probe for the transition $6p_{3/2} \rightarrow 7s$ and it can be stabilized using the corresponding absorption signal. This technique is a Doppler free absorption measurement as the first laser excites, in the cell, only the zero axial velocity atoms.
The linewidth obtained after stabilization is smaller than 1 MHz.

The 1470nm laser beam passes through an AOM before to reach the MOT where the beam is focused. At the position of the MOT, the waist of the laser is around 400 μm for a power around 3 mW, this does not generate significant intensity broadening. As the first step of the Rydberg excitation, the second step is resonant and the level $7s$ is effectively populated. This resonant excitation in the continuous case is largely sufficient to push almost all the $6p_{3/2}$ atoms out of the MOT and destroy it. This visible effect is quite useful to both align this beam on the MOT as well as find the resonance every mornings looking directly at the MOT.
The 1470nm laser beam represented on the fig 3.3 by the black beam.

Third photon

The third step of the 3-photons Rydberg correspond to the transition $7s \rightarrow np_j$ with n ranging from 20 to 100. The corresponding wavelength is around 795nm.
With use in our setup a Ti:sapphire ring laser from Sirah, working in cw mode (Ti:sapphire lasers are also largely used to generate ultra-short impulsions). The output power of the laser is around 2W.
We use an external fiber coupled Fabry-Perot cavity (sell with the laser) to stabilize the laser frequency. This cavity is regulated in temperature but not locked on an atomic reference, also the frequency of the laser is stabilized below 1 MHz but only on the "10 minutes" time scale and has to be check and if needed slightly adjusted quite often. The laser and namely its stabilization is entirely controlled with a quite well conceived software.
The Ti:sapphire laser beam passes through an AOM before to be focused on the MOT. The waist at the position of the atoms is around 300 μm. The direction of the beam is perpendicular with the one of the 1470 nm beam (second step of the Rydberg excita-

tion) as we can see on the fig 3.3 where the Ti:sapphire laser beam is represented by the dark red laser beam. The Rydberg excitation region corresponding to the 3-photons excitation is an almost spherical volume of the order 0.02 mm^3.

3.3 Control of the electric field

As it has been already mentioned several times in this manuscript, the Rydberg atoms as well as the Rydberg-Rydberg interactions are very sensitive to the presence of an electric field. Since, in our setup, we want to excite Rydberg atoms in presence of electric field, it is very important to achieve a precise control of the electric field that we applied in the Rydberg excitation region.
In this section, we present the system that we have implemented to do it and how we have characterized the created electric field.

3.3.1 General remarks

The behavior of the Rydberg atoms is, under several aspects, strongly dependent of the precise value of the electric field.
Although the electric field acts differently for each Rydberg state (here both n and l play a role), as an introduction to this section, we will give some general orders of magnitude concerning those effects.
First, the electric field modify the Rydberg states energy. The electric field has thus an effect on the condition of resonance of a Rydberg state with a given electromagnetic field. A modification of the electric field of 0.01 $V.cm^{-1}$ can easily modify the energy of a Rydberg state of 1MHz.
Secondly the presence of electric field leads to a strong modification of the Rydberg-Rydberg interactions. This appears first because the interaction between Rydberg atoms moves from Van-der-Waals to permanent dipoles types without and with electric field. However, if this first effect has a quite smooth dependence with the electric field, there is a very sharp and strong modification of the Rydberg-Rydberg interactions with the electric field when Förster resonances appear. A typical order of magnitude of the electric field width of a Förster resonance is 0.01 $V.cm^{-1}$.
Finally the presence of an electric field can lead to the ionization of the Rydberg atoms, here, a typical order of magnitude is 1000 $V.cm^{-1}$ (for $n = 20$ it is 5 $kV.cm^{-1}$).

The two values mentioned here, 0.01 $V.cm^{-1}$ and 1000 $V.cm^{-1}$, are in a sense an order of magnitude for the precision and the strength of the electric field that we should

manage to apply to have a full control on the Rydberg atoms from zero-field conditions until their ionization.

3.3.2 Electrodes around the Rydberg excitation region

To control the electric field in the Rydberg excitation region we mainly use two electrodes. Those electrodes are two parallel, large, rectangular, wire mesh grids, placed symmetrically from one side and the other of the MOT (see fig 3.3). The purpose of those electrodes is to create an electric field as uniform as possible in the Rydberg excitation region.
The size of each grid is 60×130 mm^2, they are made with wires of 80 μm thickness and the grid spacing is 1mm, the corresponding transparency is around 85%. The distance between the two grids is around 18.5 mm.
For the purpose of the Rydberg atoms detection (see section 3.4) one of those grids has a hole to make free the path of the particles toward the detector. This hole clearly induces electric field inhomogeneity, nevertheless, by applying the proper potential on a third grid present also for the need of the Rydberg detection and having also a hole (see fig 3.3), we can reduce this inhomogeneity. In our conditions, we need a ratio of around 1.6 between the potentials applied to the two holed grids to have the best "compensation" of the hole effect.
In our setup, we have placed also six other electrodes which are not represented on the fig 3.3. They are small rectangular sticks of around $5 \times 50 \times 1$ mm^3. There are placed right on the sides of the space defined by the two main grids. 2 on each lateral side, 1 on each vertical side.
Those electrodes was not present when we start the Rydberg experiments and in fact, once they had been added, the simple fact to ground them lead already to an improvement of the field homogeneity. So, in the general case, we just ground them. However, those additional electrodes could be used, if needed, to cancel the stray fields in the Rydberg excitation region as well as to generate gradients or quadrupole fields.

3.3.3 Characterization of the electric field in the Rydberg excitation region

Due to the mechanical uncertainty on position and the geometry of the electrodes, the calculation of the electric field created for given values of the applied potentials would be not very precise. However, using directly the Rydberg atoms we can obtain quite precise information on the electric field effectively present in the Rydberg excitation region.

In our setup, the electric field F, in the Rydberg excitation region, is mainly determined by the difference of potentials applied on the two main grids. In grounded one of the grid, the electric field is thus determined by the potential V of the other grid and we have $F = V/D$ where D is the distance between the two grids.
To determined the mean value of the electric field present in the Rydberg excitation region, in an absolute way, we used Stark shifted excitation measurements. The principle of this method is to reproduce experimentally a Stark diagram and to compare it with theoretical calculations.
For a given V, we record the wavelength at which a given Rydberg state is excited. Doing this for different V and different Rydberg states we end up with an experimental Stark diagram composed by several points where the energies of the Rydberg states is given in function of V.
By comparing this diagram with theoretical calculations, where the energies of the Rydberg states is given in function of F, we can determine the distance between the two grids D leading to the best correspondence between the experimental and theoretical Stark diagrams.

In our setup, we have done such measurements for the $23p_{3/2}$ and $22d_{5/2}$ states for voltages up to 200V (electric field up to 100 V.cm^{-1}) and we have evaluated that the mean value of the electric field created in the Rydberg excitation region is known in an absolute way with a relative uncertainty of the order of 5 10^{-3}.

The uncertainties on the experimental diagram are linked to the measurement of the excitation wavelenghts, which is, in our case, of the order of 5 MHz and is mainly limited by the natural width of the intermediate state of the laser excitation. The uncertainty on the applied potential V is considered to be negligible (the precision of the laboratory voltage supply is of the order of 1 mV). The uncertainty on the theoretical diagram should be evaluated from the discussion of the section2.2.1 of the chapter 2, we made only a rough evaluation of it.

In addition to the mean value of the applied electric field, it is important to characterize the inhomogeneity of the field within the Rydberg excitation region.
In our setup, it appears that this inhomogeneity is not negligible in regards to the "precision" of the Rydberg atoms. This can be observed by two different ways.
At a given mean value of the electric field, in setting our laser at a wavelength resonant with a stark shifted Rydberg transition, it can appear that we excite only a fraction of the atoms of the Rydberg excitation region since all those atoms do not see the same elec-

tric field. In other words, the inhomogeneity of the electric field can leads to a partial excitation of the atoms in the Rydberg excitation region.
Also, if now we scan a bit the wavelength of the excitation laser, we possibly excite Rydberg atoms for different wavelengths since the atoms of the Rydberg excitation region have not all the same Stark shift. In other words, the inhomogeneity of the electric field can lead to a visible broadening of the Rydberg excitation lines.

The "amplitudes" of those two effects depend obviously of the absolute inhomogeneity of the electric field within the Rydberg excitation region. However, it depends also of the slope of the Stark shift of the Rydberg states at the considered electric field as well as the effective linewidth of the laser excitation.
In our setup, in looking at the broadening of the $23p_{3/2}$ excitation line for different electric fields, we have evaluated that the relative inhomogeneity of the field within the Rydberg excitation region of the 3-photon excitation (around 0.02 mm^3) is of the order of 2 10^{-3}.

3.3.4 Possible improvements

For a given value of the applied potentials on the different electrodes, the full map of the electric field inside the chamber could be calculated using, for example, the software Simion. So, it could be very interesting to make a big effort in the mechanical conception of the electrodes and overall its realization to be able to simulate very precisely the created electric field.
In addition to a potentially better precision, this would also allow to really check the accuracy of the theoretical calculations about Rydberg atoms, what is not possible when we use them to characterize the electric field.
Interestingly, this software allows in addition to simulate the trajectories of charged particles within the calculated electric field. This could be very useful in the frame of field ionization detection. However, Simion do not take in account the mutual interactions between the particles, to calculate those effects we can use the software General Particles Tracor (GPT).

One undesirable effect in regards to the electric field could come from the presence of glass elements in the chamber (like all the view port). Indeed, glass is not conducting and can suffer from, non controllable, charging effects. This could explain why the simple fact to ground the "compensation" electrodes leads, in our setup, to an improvement of the field homogeneity.
In this frame, the use of Transparent Conducting Oxide (CTO) layers or even more

recently engineered organic conducting transparent materials offers very nice perspectives. It could allow for example to properly ground the full chamber. This would allow also to overcome the compromise optical access/ electric field control which often has to be made in the Rydberg experiments. However, up to now, any of those materials is not ideal and we might wait a bit for a practical and general use in atomic Physics experiment. For example, the most used CTO, the indium tin oxide (ITO), is transparent in the visible range but not at all in the infrared (in addition to use elements hard to find on earth, to be expensive an not environment friendly in its fabrication). Nevertheless, those materials exists, some are compatible with anti-reflecting coating and might be useful for the electric field control in Rydberg experiments.

3.4 Detection of the Rydberg atoms

In our setup, the detection of the Rydberg atoms is done using the field ionization method.
Once the Rydberg atoms are excited, this method consists in applying a pulsed electric field to ionize the Rydberg atoms. The created ions or electrons can be then accelerated toward a charged particles detector.
The detection of the Rydberg atoms is, by this way, transfered to the detection of charged particles. Due to the existing technology for charged particles detection, several interesting regime of detection can be achieved.
In our setup, we use a MicroChannel Plates (MCP) detector surrounded with a Phosphor screen. This system is schematized on the fig 3.3 by the gray cylinder.
With such a detector, it is possible to detect single particles. The detection can be also made state selective in applying a temporally shaped ionization pulse. Finally, the spatially resolved 2-dimensional detection provided by the phosphor screen allows to get a 2-dimensional spatial information on the initial Rydberg distribution. Interestingly, since the third spatial direction is mapped into the temporal one, we can get in a sense a 3-dimensional spatial information.

3.4.1 The charged particles detector

The MCP that we use in our setup is a commercial one, the F2222-21PGF from Hamamatsu, the effective surface of the MCP is 20 mm, its detection efficiency is around 30% (for the phosphor screen feature, see section 3.4.4).

The general working of a MCP is to convert an incoming flux of charged particles into

an amplified electron flux. This electron flux is then collected on an anode. The current going out from the anode, proportional to the incoming flux of particles, is finally convert in a tension signal which can be acquired an oscilloscope. The oscilloscope that we use in our setup is a Waverunner 1 GHz from LeCroy

Our MCP is composed by 2 plates, corresponding to different steps of amplification. The amplification of each step is controlled by the electric potential applied to each plates, typically of the order of 1 kV. For given applied potentials, we can define the relative gain of the MCP.

A MCP can either works in the regime of single particles detection or in the regime where a lot of particles arrive "in the same time" on the MCP, we need for that to adjust the relative gain of the MCP. The border between those two regimes is linked to the time resolution of a MCP, which is of the order of 1 ns.
For single particles detection, we have to work with high gain. In this case, the amplification is big and a single particle generates an output signal which can be detected.
If a lot of particles arrive in the same time, the gain has to be lower to not saturate the signal (or even break the MCP!). The output signal is in this case a burst (for a pulsed incoming signal), whom the area is proportional to the number of particles arriving on the MCP.

To be able to do quantitative measurements of the number of particles arriving on the MCP, we need to calibrate them.

In our setup, we used for that the signal coming from the ionization of the Rydberg atoms.
In a first step, the method that we used to calibrate the MCP consists in moving continuously from single particle regime to higher flux in changing physically the number of incoming particles. In our case, we have changed the power of the laser excitation to create different flux of particles. Starting in the single particle regime where the number of detected particles is easily known, in changing smoothly enough the flux of incoming particle, we can evaluate with a quite good precision the area corresponding to a single particle when the detected signal is a smooth packet. This first step is done with a relatively high gain as we have to be initially able to detect single particles. Also, the incoming flux of particles has to be relatively small to not saturate the MCP.
In a second step, we can, in keeping constant the flux of incoming particles, move from the initial gain to a lower one and determine the area corresponding to one particle for this lower gain.

This second step is then repeated several time to progressively calibrate the MCP for higher flux and lower gain.

The relative gain of the MCP depends of the applied potentials on the different step of amplification and it is not equivalent to change one potential or another. To do the calibration we change only one of the potential and the other has to be fixed for ever. In principle, the total gain depends also of the kinetic energy of the incoming particles but this effect is negligible in our case since the incoming particles have a quite low energy. To calibrate the MCP, we have changed only the potential applied to the external plate of the MCP. The gain of the MCP is then adjusted with this voltage. Doing this, we can have a bit of control on the TOF of the particles in keeping a fully valid calibration.

The calibration of the MCP presented in this section allows to evaluate with a quite good accuracy (the uncertainty is below 5%) the number of particles detected by the MCP.
However, the absolute value of the number of Rydberg atoms created in the experiments depends first of the fraction of the corresponding ions or electrons reaching the MCP. We will see in the section 3.4.4 that, in our case, it is almost 100%.
Finally, the global detection efficiency of the MCP is obviously a determinant factor. This last point is in our case the most limiting factor as the detection efficiency of the MCP is not very well known. Our group use similar MCP for a long time and by experience, we know that their efficiency is $30 \pm 10\%$. The method to calibrate the MCP in an absolute way necessitates a precise imaging of the cloud that we do not have implemented in our setup. The principle is to photoionize a fraction of the MOT and to compare the number of atoms lost with the number of detected ions.
Nevertheless, if this uncertainty limits quite strongly the absolute determination of the ions number arriving on the MCP, it does not reduce the accuracy of the relative measurements that we can do.

3.4.2 TOF of the charged particles

In this section we describe the path, from the Rydberg excitation region to the MCP, of the ions or electrons resulting from the ionization of the Rydberg atoms. We call this step the "time of flight" (TOF).

The TOF of the charged particles can be "visualized" on the fig 3.3. We see that, in addition to the two main grids used to apply an electric field during the laser excitation and field ionize the Rydberg atoms, we have added in our chamber a third grids, identi-

cal and parallel to the first ones. This grid is placed at 1.5 cm from the closest grids. The purpose of this grid is to offer an additional way to control the TOF.
The TOF of the charged particles is determined in our setup by 4 potentials corresponding to 3 regions where the electric field is uniform (at least in first approximation). This configuration is the famous one highlighted by Wiley and McLaren [Wiley and McLaren, 1955], except that, in their case, the last region is a free field region.
It has been shown that in function of the values of the electric fields present in the three regions, very interesting features can be obtained in regards to the arrival characteristics of the particles on the detector. Namely, there is a condition of time focusing, position mapping or velocity mapping.
In the frame of this thesis, we do not have really study those features since they could be mainly useful for the imaging of the Rydberg atoms. In the current state of our experimental setup, we have just started to do such an imaging (see section 3.4.4) and the use of the features offered by the Wiley-McLaren configuration should be the subject of further experiments.

3.4.3 State selective detection

In this section, we present the way to perform the detection of the Rydberg atoms allowing to determine in which Rydberg states they was excited.
To achieve such a so-called state selective detection, we use a temporally shaped electric field pulse to ionize the Rydberg atoms. Since the different Rydberg states are not ionized at the same electric field, they are not ionized at the same time and then not detected at the same time by the MCP. In looking carefully at the MCP signal, we can distinguish between the ions or electrons generated by the ionization of atoms excited in different Rydberg states.

To create the desired temporal shape of the electric field pulse, we use a home made electronic box. As inputs to this box, we send a constant potential and a TTL which determines the beginning of the electric field pulse. The output of the box is a raising potential going from zero to the input potential with a given time constant. This time constant can be choose through the value of the capacitor present in the box. In the fig 3.7 we show a typical temporally shaped potential coming from the box.

One advantage of this shape is that, for a given range of Rydberg states that we want to detect, we can adjust the input potential of the box to be just slightly bigger than the potential at which the Rydberg state with the lowest energy is ionized. Doing this, the slope of the electric field is small in the region where the different Rydberg states are ionize. This allows to have a good temporal separation between the ionization of the

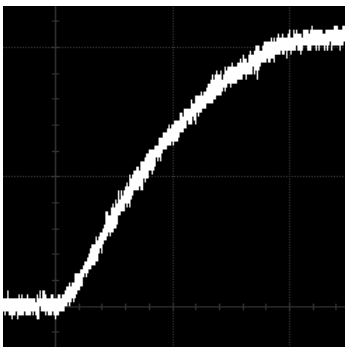

Figure 3.7: Typical electric field ramp for the state selective detection

different Rydberg states. While the final slope is small, the initial slope is high, allowing to have a total duration of the electric field pulse reasonably short in comparison to the Rydberg atoms lifetime.

To illustrate, a bit more in details, the signal obtained in the frame of the state selective detection. We present the data corresponding to the situation of the experiments presented in the section 3.6.
The different Rydberg states excited by the laser pulse have here a principal quantum number around 23. The electric field is raised in a total time of 4μs with a maximum value of 4.3 kV.cm^{-1}. The duration of the TOF is around 10 μs.
In the fig3.8 we show the signal recorded by the oscilloscope after a laser excitation of different Rydberg states. The laser excitation is done in presence of an electric field of 79 V.cm^{-1} where no Förster resonance appears. Also, at this quite low electric field, the Stark mixing of each states remains week and the excited states can be still labeled using the zero-field states basis without ambiguity.

We see in the fig3.8 that the different Rydberg states lead effectively to different detection signal allowing to differentiate them.
However, we see that the "selectivity" of the detection is not perfect as their is still some overlapping in the detection signal of the different Rydberg states. This is mainly due to the fact that, under the effect of the raising electric field, a zero-field Rydberg state "meets" an important number of crossing with other states (we can refer here to a Stark diagram for more of clarity). In the case of non-hydrogenic atoms those crossings are often avoided ones. Consequently, in function of the raising speed of the electric field, an initial zero-field Rydberg state is more or less mixed with other states when the ionization is reached. We say that there is several "paths of ionization" which lead to the observed spread of the detection signal of each Rydberg state. Another effect comes from the blackbody induced transitions between the Rydberg states. This effect

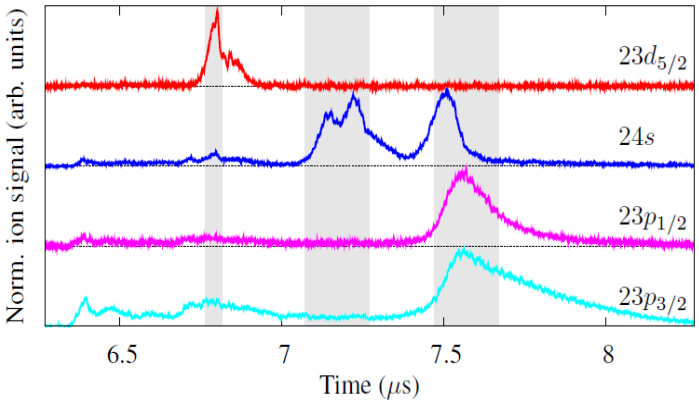

Figure 3.8: Averaging over 30 shot of the signal recorded by the oscilloscope after the excitation of different Rydberg states. The detection parameters are the same for all the states, the four traces have been vertically offset and normalyzed for clarity

is dependent of the time between the excitation and ionization pulses during which the Rydberg atoms are free to evolve. The best way to limit this effect is to reduce this time.

Despites this overlapping, in order to know precisely the number of Rydberg atoms excited in each of the different states when several Rydberg states are simultaneously excited in the experiment, we use the following procedure.
On the fig3.8, we have represented three gray areas corresponding to temporal gates in the detection signal. We first attribute, at each one of those gates, the detection of Rydberg atoms in different states. For instance, $23d_{5/2}$, 24s and $23p_{3/2}$+$23p_{1/2}$ from the first to the last temporal gate. We have then defined here the d, s and p-gate, other quantum numbers being forgotten for simplicity.
In looking at the signal of the fig3.8, it is possible to evaluate the crosstalk between the different gates.
In addition, the ionization efficiency is not 100% since the ionization field is just slightly higher than the ionization threshold. Moreover, it is different for the different Rydberg states. To take this in account, for each of the investigated Rydberg states, we have measure the ionization efficiency with the shaped electric field pulse used for the experiments in comparing it with the case of a complete ionization.
From this, we can define a crosstalk matrix which also takes in account ionization efficiency. This matrix allows to determine, from the MCP signal, the absolute number of atoms excited in the different Rydberg states.
For example, for the situation of the experiment presented in the section, we have

$$\begin{pmatrix} \mathrm{d} \\ \mathrm{s} \\ \mathrm{p} \end{pmatrix}_{\text{experiment}} = N_{det} \begin{pmatrix} 2.016 & -0.0644 & -0.082 \\ -0.100 & 4.645 & -0.275 \\ 0.083 & -3.147 & 4.149 \end{pmatrix} \begin{pmatrix} \mathrm{d} \\ \mathrm{s} \\ \mathrm{p} \end{pmatrix}_{\text{gate}} \tag{3.8}$$

Here, N_{det} is a coefficient exprimed in $(\mathrm{mV.ns})^{-1}$ which characterizes the average relation between the integrated gates signal and the number of Rydberg atoms present in the experiment. Its value depends of the potential applied on the external plate of the MCP. Due to the temporal dependence of the redistribution between the Rydberg state due to the blackbody induced transitions, this matrix is valid for a fixed delay between the excitation and ionization pulses. In our experiments, we take care to not change this delay unless we decide to define a new matrix.

For Rydberg states with n around 23, the relative uncertainty on the fraction of Rydberg atoms excited on the different state is of the order of 5%.
This uncertainty increases a lot when the principal quantum number n of the Rydberg states increases. Indeed, for larger n, the difference of electric field at which the neighboring Rydberg states are ionized is smaller. There is also more complex and mixed paths of ionization. Those effect leads to a less good separation of the different Rydberg states in the MCP signal. In this case, it is possible to improve the separation between the excited Rydberg states in applying a microwave field on the atoms just before the ionization pulse. The purpose is to transfer one of the excited Rydberg states toward another Rydberg states which is more separated from the other ones. We had tried this in our setup for Rydberg state with $n = 53$ and we succeeded to transfer around 50% of the excited $53\mathrm{p}_{1/2}$ Rydberg atoms in the $53\mathrm{d}_{3/2}$ state. This involved an absorption of a single photon of the micro-wave field with an energy difference of around 59 GHz.

In a general way, in the frame of the state selective detection, it is quite important to have a good control of the TOF of the particles.
The most important condition that we have to realize is a short TOF. Indeed, if the Rydberg states having the lowest energies are ionized the latest, the corresponding ions or electrons are also the most accelerated. They could arrive before the other ones if the TOF is not short enough.
To compensate this effect and to improve the separation between the Rydberg states, it could be very interesting to have temporally shaped electric fields in other spatial regions than the ionization one.

3.4.4 Imaging of the Rydberg atoms

In this section, we present the type of signal that we have obtained in using the phosphor screen present at the back of the MCP. In the frame of this thesis, we have used this 2-dimensional spatial detection in a very rudimentary way and the results presented here are far to be really useful for the imaging of the Rydberg distribution. Nevertheless, some general informations can be obtained from this spatial detection.

The anode of the MCP that we use in our setup is a luminescent phosphor screen (P43 from Hamamatzu). When a burst of electrons, generated inside the MCP from an incoming particle, arrives on the phosphor screen, this latter emits light. We have placed in our setup a camera, focused on this phosphor screen to acquired the corresponding 2-dimensional signal.
The spatial resolution that we get with this system is given by the size of the MCP channels. In our case, it is 12μm. The temporal resolution of the phosphor screen is very low, each spot having a "lifetime" of around 1 ms. Consequently, the images that we get from the phosphor screen are register after that all the ions created by the pulsed electric field have reached the MCP.

It is quite interesting to look at the images resulting from the excitation and the detection of few Rydberg atoms. In the fig3.9 we show one of the obtained image.

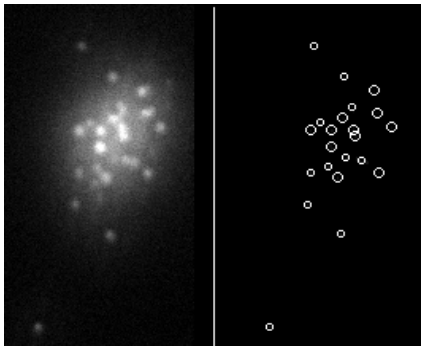

Figure 3.9: Image of the phosphor screen after the excitation of few Rydberg atoms. Left, image taken by the camera. Right, result of the image treatment.

We see on the fig3.9 that the ions resulting from the ionization of the Rydberg atoms are clearly identifiable on such an image. In our setup, we analyze the image coming from the camera with Labview. On the fig3.9, in regards to the image itself, we show the "image" obtained after a treatment realized with Labview. We see that we are able to numerically identify each ion spot, allowing to determine the number of detected ions

as well as their positions. Very useful informations about Rydberg atoms physic might be obtained from this type of image. However, up to know, we have looked to those images only for curiosity.

Another type of images that we have obtained correspond to the excitation of many Rydberg atoms, we show in the fig3.10 one of those images.

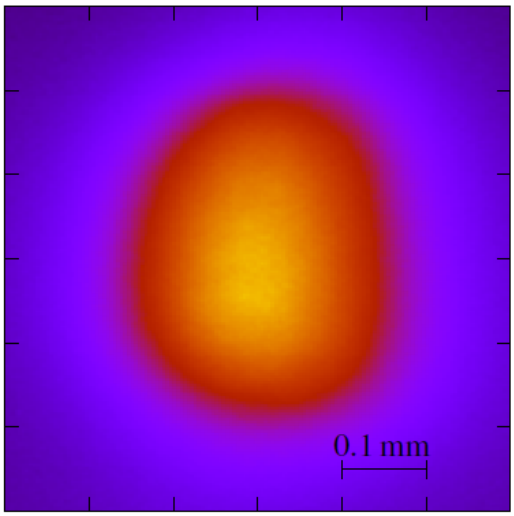

Figure 3.10: Image obtained by looking at the phosphor screen of the MCP after the excitation and the detection of many Rydberg atoms. The intensity of the light emitted by the phosphor screen is here translated in different colors with an arbitrary code.

The first information that we can get from this image is that almost all the ions created by the ionization electric field pulse reach the MCP. Indeed, on this image, we see that the size of the full ions distribution on the MCP is of the order of few hundreds of μm, which is smaller than the total size of the MCP (around 2cm).

Our knowledge of the TOF of the particles in our setup, does not allow us to have a precise information of the initial size of the Rydberg distribution. This is mainly due to the Coulomb repulsion during the TOF but also to the focusing effects on the MCP detector. Indeed, the finite size of the MCP induces curvatures of the electric field lines for off-axis position in the TOF region. The latter effect should be weaker than the Coulomb repulsion leading to an image larger than the initial Rydberg distribution.
Nevertheless, the size of the image, give an order of magnitude of the initial size of the Rydberg distribution. The image of the fig3.10 allows thus to determine the order of magnitude of the Rydberg density since the calibration of the MCP allows to know the number of excited Rydberg atoms. For the situation of the image of the fig3.10, corre-

sponding to the 3-photon excitation of the $23p_{3/2}$ Rydberg state, we had measured that the number of Rydberg atoms was around 10^5 and from the image, we can evaluate that the order of magnitude of the Rydberg atoms density is around 10^{10} at.cm^{-3}.

Interestingly, we use also such an imaging of the Rydberg distribution as a tool for our experimental setup. Indeed, we use it to superpose the excitation region of the two paths of laser excitation (2- or 3-photons excitation). To do this, we excite the atoms in a given Rydberg state, in presence of electric field, successively with one or the other of the excitation path. We are then able to check if, in both case, the ions arrive in the same position or not, this provides a 2-dimensional spatial information. Also in looking at the arrival time of the ions, we are able to check if, in both case, the ions arrive at the same time or not, this provides the information on the third spatial dimension.

We see with those few examples that the possibility to image the Rydberg atoms leads quickly to very interesting information. However, the results presented here correspond only to the first step toward a spatial imaging of the Rydberg distribution. In this frame, a precise study of different TOF configurations and of the Coulomb repulsion between the charged particles could offer nice perspectives.
One interesting possibility could be to study the spatial correlations in blockaded Rydberg ensemble.
In addition, as mention in the section 1.3.2, the possibility to image the Rydberg distribution, together with a state selective detection in an experiment where two different Rydberg states are excited, could offer the possibility to study the diffusion of a Rydberg excitation. Such a diffusion having possible analogy with exciton propagation or could be use to implement quantum walk (eventually random in presence of optical lattices).
I would like to mention here that, in comparison with in-situ optical imaging of the Rydberg atoms which are currently theoretically study or even realized in the case of small ensemble [Schauß et al., 2012], the Coulomb repulsion between the charged particles gives a big drawback to the field ionization method. Indeed, the strong interaction between charged particle can very quickly perturbs totally the initial distribution of Rydberg atoms.
Nevertheless, the Coulomb repulsion can be studied. For example, considering two identical particles of charge q and mass m distant of d_0 with a null relative velocity at $t = 0$, the distance d at a time t between the two particles is given by the following formula (with $C = \frac{2q^2}{m\pi\epsilon_0}$).

$$\sqrt{\frac{d}{d_0}(\frac{d}{d_0} - 1)} + \ln\left(\sqrt{\frac{d}{d_0}} + \sqrt{\frac{d}{d_0} - 1}\right) = \frac{\sqrt{C}}{d_0^{3/2}}t \tag{3.9}$$

This (non-invertible) formula is quite interesting to study the effects of the Coulomb interaction during a TOF. For example, it shows (and quantify) that after a certain time, two particles initially close from each other will be more separated than two particles initially more separated.
In the frame of blockaded Rydberg ensemble, we see that the blockade radius might be translated in term of a maximum distance at which two particles can be detected. This non-studied assumption is more an example to show that, despites the Coulomb repulsion, spatial imaging of Rydberg ensemble using a detection by field ionization could lead to interesting informations.
An already obtained result is the one reported in the reference [Schwarzkopf et al., 2011] (see the section 1.4.4 of the chapter 1).

3.5 temporal sequence of the experiments

In this section, we present the typical temporal sequence that we use for our experiments. On the fig 3.11, we show a schematic representation of this temporal sequence.

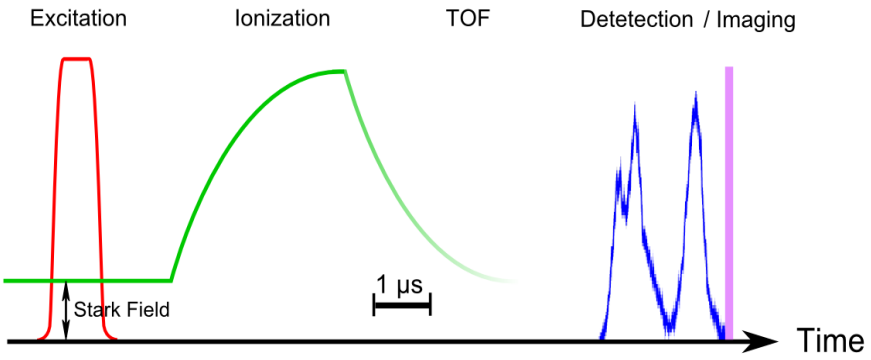

Figure 3.11: Typical experimental sequence performed in our setup.

The temporal control of all the elements involved in the experiment (lasers, electric fields, oscilloscope, camera) is done using a digital delay generator (DG 645 from Standford Research Systems). The sequence is repeated in our setup with a frequency of 10 Hz. The timescale of the experiment is 1 μs.
At this time scale, we have a full control over all the elements and they can be adjusted in function of what we want to study. We give here the values for the experiments which are presented in the section 3.6.
The Rydberg excitation pulse is 0.5μs long. After a delay of 1.5μs, we apply the electric field ramp to ionize the Rydberg atoms, the total duration of this pulse is 4 μs and the Rydberg atoms are ionize in the last part of the ramp. the created charged particles

are then accelerated toward the MCP, with a typical TOF of 7 μs, which is spread out of around 1 μs. The detection signal is recorded with the oscilloscope. Once all the particles detected, we take an image of the phosphor screen (we have 1ms to do it).

To achieve the presentation of the experimental setup, I would just mention a small trick that we use concerning the temporal control of the experiment. In our setup, some of the lasers used for the Rydberg excitation are stabilized using the simple absorption method which involves to modulate the laser frequency. If it is possible to not modulate the laser itself but only the part of the beam involved in the locking scheme using for example an AOM, in our setup, the frequency of the lasers is modulated through their current supply and the frequency modulation is present in the beam send to the atoms. In order to reach a better stability of the Rydberg excitation in regards to this modulation, we manage to modulate the frequency of the different laser at the same frequency (using "external modulation" option of the current supply) and to trig the full sequence (i.e. the standford box) according to this modulation. The implementation of this technique led to a clear improvement of the Rydberg excitation stability.

3.6 Observation of a 4-body process

In this section, we present the main result obtained with our experimental setup, it consists in the experimental observation of a coherent process involving the interaction between 4 Rydberg atoms.
This 4-body process can be described, in a general way, as the fact that two 4-body quantum states $|\Psi_1\rangle$ and $|\Psi_2\rangle$ describing 4 non-interacting Rydberg atoms are coupled together under the effect of the interactions between the Rydberg atoms.
In the situation that we have observed, the state $|\Psi_1\rangle$ corresponds to 4 Rydberg atoms in the state $23p_{3/2}$ and the state $|\Psi_2\rangle$ corresponds to 4 Rydberg atoms in the states $24s$, $24s$, $23p_{1/2}$ and $23d_{5/2}$. In setting the laser excitation to excite the atoms in the state $23p_{3/2}$, we did observe atoms in the state $23d_{5/2}$. This observation reveals, without ambiguity, the coupling between the two 4-body quantum states.

An interesting feature of this experimental observation is that those two 4-body quantum states are not coupled directly by the Rydberg interactions. Indeed the four atomic Rydberg states with which the two 4-body quantum states are composed are all different and the by essence the electrostatic interaction coupled only the Rydberg atoms 2 by 2. The origin of the coupling between those 4-body quantum states comes from the existence of two Förster resonances appearing at very close electric fields. Those two

Förster resonances can be described by the following equations

$$2 \times 23p_{3/2} \rightarrow 23s + 24s \tag{3.10}$$

$$2 \times 24s \rightarrow 23p_{1/2} + 23d_{5/2} \tag{3.11}$$

We have observed those two Förster resonances respectively at $\approx$ 79.9 V.cm^{-1} and $\approx$ 80.4 V.cm^{-1}.
It is the extreme vicinity in electric field of those two Förster resonances which allows us to observe the mentioned 4-body process which can be view as the reaction

$$4 \times 23p_{3/2} \rightarrow 2 \times 23s + 23p_{1/2} + 23d_{5/2} \tag{3.12}$$

We have observed this process for an electric field of $\approx$ 80.0 V.cm^{-1}.

Despites the presence of an electric field, we label in all this section the single-atom states as the zero-field Rydberg states. The fact is that, for the electric field involved in those processes, the mixing between the zero-field Rydberg states due to the electric field is quite small and the Rydberg states excited in the experiments are mainly composed by the zero-field states with which there are labeled. Nevertheless, this mixing is non-negligible as proved by the observation of the Förster resonance of the equation 3.11 which would be not existing otherwise (quadrupolar interactions are here very small).
In addition, all the Rydberg states involved in those processes have $|m_j| = \frac{1}{2}$. Due to the Stark effect, states with other $|m_j|$ are degenerated in energy, for example the Förster resonance of the equation 3.10 with 23p$_{3/2}$ ($|m_j| = 3/2$) instead of $1/2$ appears at an electric field of around 88 V.cm^{-1} which quite far away from the investigated Förster resonances.

3.6.1 Observation of the two Förster resonances

On the fig 3.12 we show the experimental measurements relative to the observation of the two 2-body Förster resonances of the equations 3.10 and 3.11.

On the fig 3.12, we clearly see the appearance of the two Förster resonances.
It is interesting to notice the fraction of excited 24s atoms ($\approx 33\%$) obtained in the case of the Förster resonance of the equation 3.10. This indicates that the 2-body Förster resonance is completely saturated. We get 33% because the Rydberg atoms in the 23s states are not detected, otherwise we would get 25% which is, at resonance, the real proportion of 24s atoms within all the Rydberg atoms.

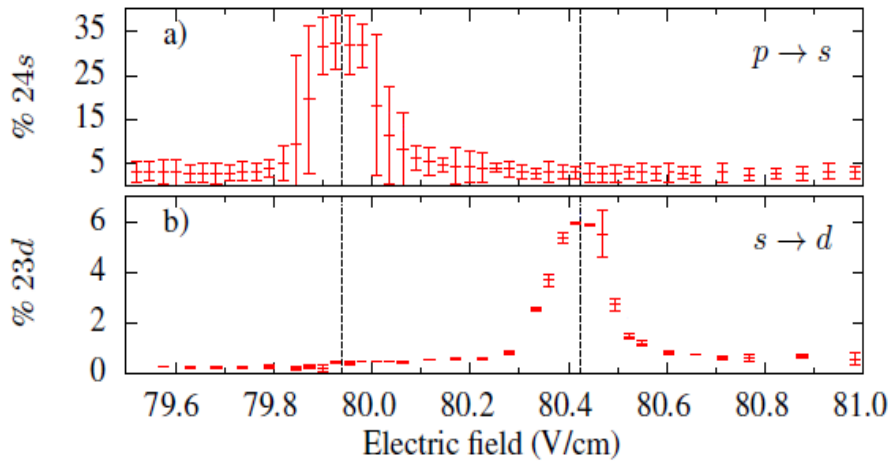

Figure 3.12: Experimental measurements of the Förster resonances. a) Measured fraction of 24s atoms within the total number of atoms in a detectable state in function of the applied electric field. Here, the laser excitation is set to excite the Stark shifted $23p_{3/2}$ state. b) Measured fraction of $23d_{5/2}$ atoms within the total number of Rydberg atoms in function of the applied electric field. Here, the laser excitation is set to excite Stark shifted 24s state. In both case, error bars take in account the uncertainty on the measured number of atoms as well as the electric field inhomogeneity affecting more the $23p_{3/2}$ than the 24s state

The quite low fraction of excited $23d_{5/2}$ obtained in the case of the Förster resonance of the equation 3.10 can be explained by the electric field inhomogeneity in our experimental setup the density of excited 24s Rydberg atoms in our experiment (see section 3.7.1).

3.6.2 Observation of the 4-body process

On the fig 3.13 we show the experimental measurement relative to the observation of the 4-body process describes by the equation 3.12.

Although, the obtained fraction of $23d_{5/2}$ atoms is quite small, we clearly see on the fig 3.13 the sharp resonance corresponding to the 4-body process.
We see on the fig 3.13 that the resonance line exhibits a small elbow structure on the left side. This feature has been carefully checked (as indicated by the small error bars of the corresponding points) and seems to be intrinsic to the observed process.

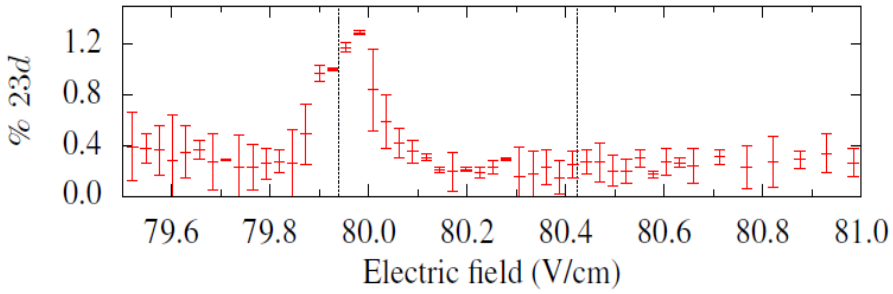

Figure 3.13: Experimental measurements relative to the 4-body process. Measured fraction of $23d_{5/2}$ atoms within the total number of atoms in function of the applied electric field. Here, the laser excitation is set to excite Stark shifted $23p_{3/2}$ state. Error bars take in account the uncertainty on the measured number of atoms as well as the electric field inhomogeneity. The position in electric field of the two Förster resonances is represented by the vertical black dashed lines

3.6.3 Density dependence

Since we are in presence of few-body processes, it is quite interesting to measure their density dependences. The relevant density is here the Rydberg atoms density and is directly linked to the efficiency of the Rydberg excitation. To vary the density of Rydberg atoms we have alterated the power of the excitation lasers using a set of neutral density. On the fig 3.14 we present the obtained results.

On the fig 3.14, we clearly see that the density dependence of the different few-body processes are the one that we can expect, i.e., a square dependence for the two Förster resonances and a fourth power dependence for the 4-body process.

3.6.4 4-body processes in a variable electric field

In this section, we present the results of the experiments that we have done in order to observe a better transfer from $23p_{3/2}$ to $23d_{5/2}$. The idea of those experiments is to change the applied electric field after the Rydberg excitation in a such a way that the electric field would be, in a first time, the resonant field for the first Förster resonance and, in a second time, the resonant field for the second Förster resonance. Doing this, both Förster resonances are successively resonant and the total transfer is enhanced in comparison to the case where the electric field is constant. In the fig 3.15, we have represented the number of atoms found in the state $23d_{5/2}$ in function of the total number of excited Rydberg atoms and the "Jump" of electric field. The initial electric field is 79.94 V.cm^{-1} and the laser excitation is set to excite the $23p_{3/2}$ Rydberg state.

On the fig 3.15, we see that for an electric field Jump corresponding to the difference

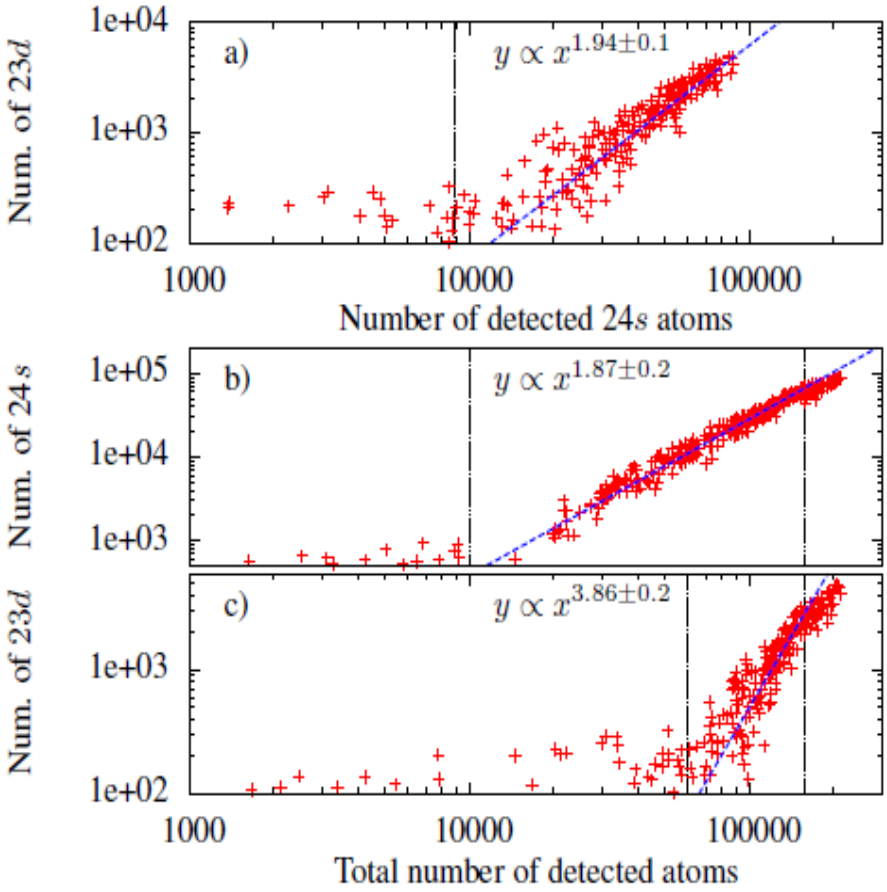

Figure 3.14: Experimental measurements of the density dependences of the different few-body processes. All the graph are plot in Log-Log scale. a) Measured number of excited $23d_{5/2}$ atoms in function of the measured number of excited 24s atoms. Here, the laser excitation is set to excite the Stark shifted 24s state. b) Measured number of excited 24s atoms in function of the measured number of all the detectable Rydberg atoms. c) Measured number of excited $23d_{5/2}$ atoms in function of the measured number of all the Rydberg atoms. In b) and c) the laser excitation is set to excite the Stark shifted $23p_{3/2}$ state. The best fit of those different data are shown by the blue dashed lines and their coefficients with relative error are written on the graphs. The region taken in account to calculate the fits are the ones demarcated by the vertical dotted-dashed black lines

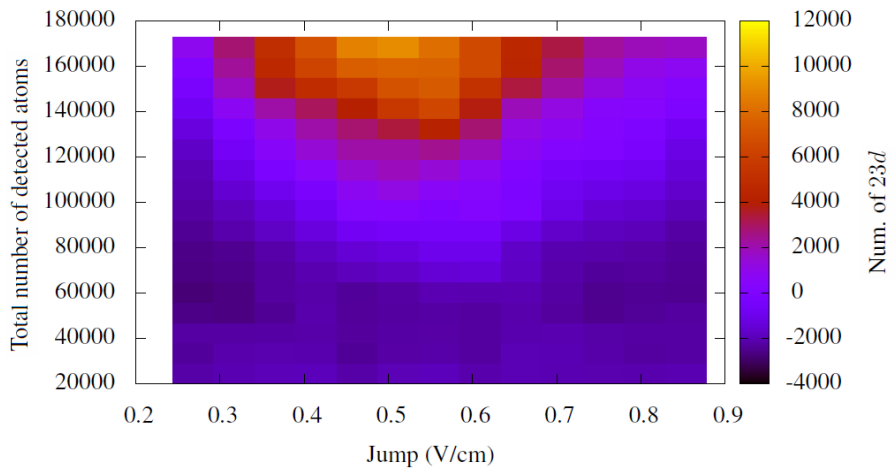

Figure 3.15: 4 body process in a variable electric field. The number of $23d_{5/2}$ atoms is represented with a color code in function of the total number of Rydberg atoms and the amplitude of the electric field Jump. Initially, $23p_{3/2}$ Rydberg atoms are excited and the electric field is 79.94 V.cm^{-1}.

between the resonant field of the 2 Förster resonances, we observe up to 5% of transfer from $23p_{3/2}$ to $23d_{5/2}$.

3.7 Modeling of the few-body processes

In this section, we give some theoretical insights to the few-body processes that we have observed in our experiments.

3.7.1 Förster resonance

The theoretical description of a Förster resonance has been already approach in the section 1.3.2 of the chapter 1 and are underlying to the calculation of the chapter 2. We have seen that the physical situation corresponds to an avoided crossing of two 2-body Rydberg states. This avoiding crossing appears if both states have the same (non-interacting) energy at a given electric field and if they are coupled together under the effect of the Rydberg-Rydberg interaction.
In this section, we will see that the knowledge of only few parameters allow to precisely characterize a Förster resonance. We give the value of the relevant parameters in the case of the two Förster resonances that we have observed experimentally.

As we can see, for example on the fig 3.12, a Förster resonance is a quite sharp resonance in electric field. Consequently, it is sufficient to consider only a small range of electric field around the resonant field to fully describe a Förster resonance. This has two very useful consequences for the theoretical modeling of a Förster resonance. First we can consider that the energy of the two 2-body non-interacting Rydberg states varies linearly with the electric field. Secondly, we can consider that the coupling between those two states is constant within the relevant range of electric field, in a sense, we consider here that the decomposition of the Stark shifted Rydberg states on the zero-field basis states do not change within the relevant range of electric field.
Under those approximations, a Förster resonance, in addition to its resonant field, can be fully characterized by three quantities, the slope in electric field of each 2-body non-interacting Rydberg states and the coupling between those states. Each of those quantities are taken at the resonant field of the Förster resonance. They can be easily obtained theoretically using, for example, the calculations presented in the chapter 2 of this manuscript.
The coupling due to the dipole-dipole interaction between the two 2-body Rydberg states depends of the distance between the two atoms. However, this distance can be view as a parameter since the total coupling is the product of two atomic dipole moment divided by the cube of the interatomic distance.

With the knowledge of those parameters, a Förster resonance can be fully characterized. For a given interatomic distance, we can plot a diagram such as the one presented on the fig3.16.

In the case of the Förster resonance of the equation 3.10, we have

$$\frac{dE_{2\times 23p_{3/2}}}{dF} \approx -400\text{MHz.(V.cm}^{-1})^{-1} \tag{3.13}$$

$$\frac{dE_{23s+24s}}{dF} \approx -30\text{MHz.(V.cm}^{-1})^{-1} \tag{3.14}$$

$$V_1 \approx \frac{67.5}{R^3_{/\mu m}}\text{MHz} \tag{3.15}$$

In the case of the Förster resonance of the equation 3.11, we have

$$\frac{dE_{2\times 24s}}{dF} \approx -40\text{MHz.(V.cm}^{-1})^{-1} \tag{3.16}$$

$$\frac{dE_{23p_{1/2}+23d_{5/2}}}{dF} \approx 65\text{MHz.(V.cm}^{-1})^{-1} \tag{3.17}$$

$$V_2 \approx \frac{18.5}{R^3_{/\mu m}}\text{MHz} \tag{3.18}$$

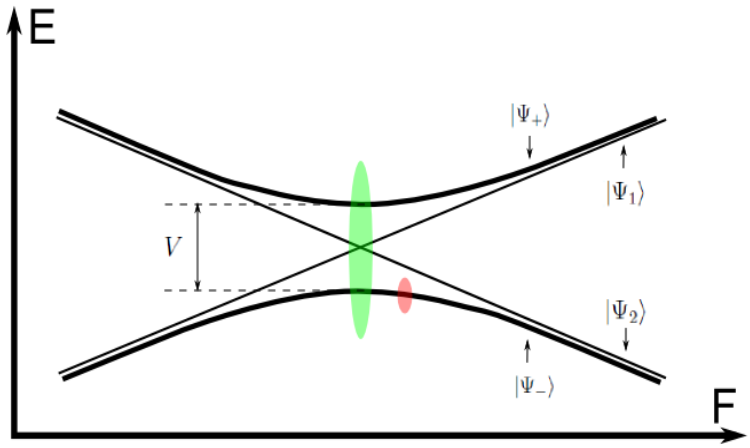

Figure 3.16: Schematic representation of a Förster resonance. The green and red spots represent laser excitations which are mentioned in the text

The energy and the decomposition on the non-interacting basis $\{|\Psi_1\rangle, |\Psi_2\rangle\}$ of the two eigenstates of the interacting system $|\Psi_+\rangle$ and $|\Psi_-\rangle$ can be obtained, at a given electric field F, by the diagonalization of the following matrix

$$\begin{pmatrix} E_1(F) & V \\ V & E_2(F) \end{pmatrix} \tag{3.19}$$

In the case where the electric field is exactly resonant, the two eigenstates are the symmetric and antisymmetric superposition of the non-interacting states, i.e., $|\Psi_\pm\rangle = 1/\sqrt{2}(|\Psi_1\rangle \pm |\Psi_2\rangle)$. Their difference in energy is exactly the coupling V between the two non-interacting states.

It is very interesting to study the state which is populated by a laser excitation of such a system. Indeed, in function of the ratio between the laser coupling, given by its Rabi frequency Ω, and the difference of energy between the two eigenstates $\widetilde{\Delta E}$, the populated state, and its temporal evolution once the laser excitation is turned off, are very

different. We present here two limit cases.

In the regime where $\Omega \ll \widetilde{\Delta E}$, the populated state is purely one eigenstate of the system. In this case, their is no temporal evolution when the laser excitation is turned off. This case is represented by the red point on the fig3.16.

In the regime where $\Omega \geq \widetilde{\Delta E}$, the populated state is a coherent superposition of the two eigenstates. The temporal evolution of the system, when the laser is turned off, exhibits a coherent dynamics. A very interesting case is found when the electric field is exactly at resonance and when the superposition is equally weighted at the end of the laser excitation. This case is represented by the green point on the fig3.16. In this case, the coherent evolution of the system corresponds to a Rabi oscillation between the two non-interacting states and the frequency of the oscillation is given by the coupling between the states. This can be easily seen in writing formally the populated quantum state.
If at $t = 0$, when the laser is turned off, we have

$$|\Psi(t=0)\rangle = \frac{1}{\sqrt{2}}(|\Psi_+\rangle + |\Psi_-\rangle) = \frac{1}{\sqrt{2}}(\frac{1}{\sqrt{2}}(|\Psi_1\rangle + |\Psi_2\rangle) + \frac{1}{\sqrt{2}}(|\Psi_1\rangle - |\Psi_2\rangle)) = |\Psi_1\rangle \tag{3.20}$$

At a time t, with the appropriated choice of phase, we have

$$|\Psi(t)\rangle = \frac{1}{\sqrt{2}}(|\Psi_+\rangle + \mathrm{e}^{-iVt}\,|\Psi_-\rangle) \tag{3.21}$$

We see here that the evolution of the quantum state corresponds effectively to a Rabi oscillation between the non-interacting quantum states, for example, at a time $t = \pi/V$, the system is in the state $|\Psi_2\rangle$.

Those two limit cases show that the ratio $\Omega/\widetilde{\Delta E}$ plays a determinant role in the dynamics of the system. However, for a real laser excitation, several effects comes on top of this very simple description. The quantum dynamics has to be consider from the beginning of the laser excitation. The incoherent broadening induces statistical distribution of the laser excitation field. We have also to consider the state which is coupled by the laser field to this system and the possible blockade effects, unless we consider a direct two photons absorption from both atoms in the ground state.

We see here that the determination of the Förster resonance diagram as the one shown of the fig 3.16 together with a study of the quantum dynamics during and after the laser

excitation could allow to model quite precisely a system of two atoms excited by a given laser field toward a Rydberg state in which the atoms interact through a Förster resonance.
However, in our experiment, we are dealing with the excitation of an atomic cloud where many pairs of atoms interact in the same time. This make the modeling much more difficult since several relevant parameters are varying within the Rydberg excitation region. Namely, in function of the position of the atoms, the Rabi frequency of the laser excitation is different, the electric field is different due to the electric field inhomogeneity and the density of Rydberg atoms is different. Even in the case of an uniform density, the distance between the closest atoms is randomly distributed. Since the dipole-dipole coupling between two atoms depends of the cube of their relative distance, the distribution of the interatomic distances has a very strong impact on the coupling strengths. In addition, we have also to consider the incoherent broadening of the laser excitation.
Due to all those effects, we have not try in the frame of this thesis to model precisely the experimental results for the two observed Förster resonances. Nevertheless, we can give qualitative explanation for the observed fraction of the "product" state for both Förster resonances.

In the case of the Förster resonance of the equation 3.10, the laser excitation is set to excite the $23p_{3/2}$ Rydberg state. Due to the electric field inhomogeneity and the quite important slope of the Stark shifted $23p_{3/2}$ state energy in function of the electric field ($\approx$ 200 MHz.(V.cm^{-1})$^{-1}$), the volume in which we really excite Rydberg atoms is reduced in comparison to the full Rydberg excitation volume. We have evaluated that this volume is a sphere with a radius of around 100 μm. Within this volume, the absolute inhomogeneity of the electric field is around 0.05 V.cm^{-1} for a mean value of 80 V.cm^{-1}. The evaluated number of excited Rydberg atoms is around 10^5 giving an average Rydberg density of around 2 10^{10} at.cm^{-3}. The most probable interatomic distances between two neighbor atoms is around 2 μm. The typical coupling between a pairs of atoms is then of the order of 10 MHz.
Considering all those values, we see that, in our experiments, the excitation of the pairs of atoms interacting through the Förster resonance of the equation 3.10 is done, for a resonant mean electric field, in the very central region of the Förster resonance. This is schematically represented in the fig 3.17

On the fig 3.17, we see that the eigenstates of the different pairs of atoms are always close to be a superposition with equal weights of the two non-interacting states. The Förter resonance is then "saturated" over the full Rydberg cloud. This leads to the observed fraction of Rydberg atoms in the state 24s which have been observed.

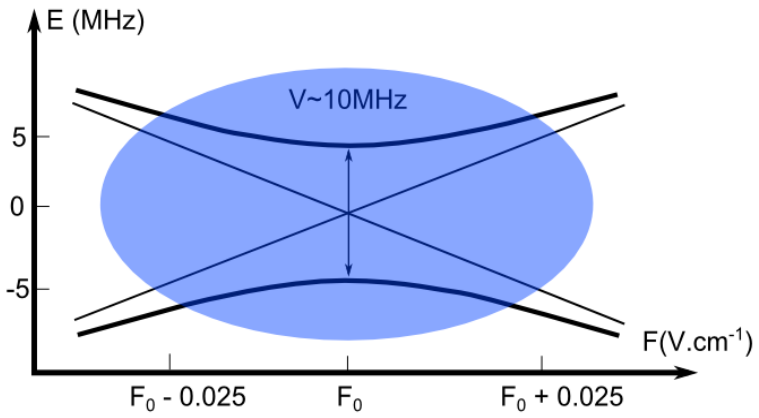

Figure 3.17: Schematic representation of the excitation of the Förster resonance of the equation 3.10 in our experiments

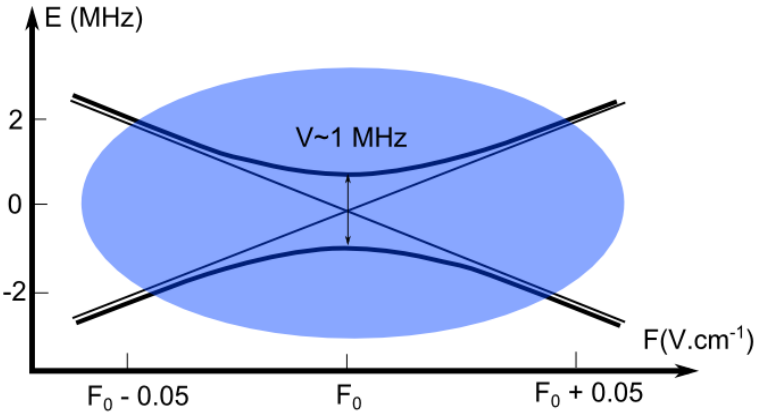

Figure 3.18: Schematic representation of the excitation of the Förster resonance of the equation 3.11 in our experiments

In the case of the Förster resonance of the equation 3.11, the laser excitation is set to excite the 24s Rydberg state. Due to the electric field inhomogeneity and the quite small slope of the Stark shifted 24s state energy in function of the electric field ($\approx$ 20 MHz.(V.cm^{-1})$^{-1}$) the volume in which we excite Rydberg atoms is the full Rydberg excitation volume which is around 0.02 mm^3. Within this volume, the absolute inhomogeneity of the electric field is around 0.1 V.cm^{-1} for a mean value of 80 V.cm^{-1}. The evaluated number of excited Rydberg atoms is around 10^5 which leads to an average Rydberg density of around 5 10^9 at.cm^{-3}. The most probable interatomic distances between two neighbor atoms is around 3 μm. The typical coupling between a pairs of atoms is of the order of 1 MHz.
Considering all those values, it appears that, in our experiments, the excitation of the

pairs of atoms interacting through the Förster resonance of the equation 3.11 is done, for a resonant mean electric field, in a quite spread region of the Förster resonance. This is schematically represented in the fig 3.18.

We see on the fig 3.18, that the eigenstates of a lot of pairs of atoms are just the non-interacting eigenstates, i.e., that a lot of pairs are not interacting through the Förster resonance. This leads to the small observed fraction (6%) of Rydberg atoms in the state $23\mathrm{d}_{5/2}$ which have been observed.

3.7.2 Modeling of the 4-body process

In order to model the 4-body process observed in our experiment, we have developed a quite minimal model to describe a system of four interacting Rydberg atoms.

We aim to describe a system where the four atoms are all equidistant from each other (in a tetrahedron configuration).
In this model, we have putted together the two Förster resonances which lead to the 4-body process. We consider four 4-body (non-interacting) quantum states labeled by $|pppp\rangle$, $|ss'pp\rangle$, $|ss'ss'\rangle$ and $|p's'ds'\rangle$. Here, s, s′, p, p′ and d correspond respectively to the 24s, 23s, $23\mathrm{p}_{3/2}$, $23\mathrm{p}_{1/2}$ and $23\mathrm{d}_{5/2}$ Rydberg states and we consider that the 4-body states are the superposition of all the possible combination relative to the exchange of atoms. Since the atoms are all equidistant, those different combinations have all the same characteristics and are all identically populated.
We can write the Hamiltonian of the system $H_{\text{4-body}}$ as

$$H_{\text{4-body}} = \begin{pmatrix} \mathrm{E}_{|pppp\rangle}(F) & \mathrm{V}_1 & 0 & 0 \\ \mathrm{V}_1 & \mathrm{E}_{|ss'pp\rangle}(F) & \mathrm{V}_1 & 0 \\ 0 & \mathrm{V}_1 & \mathrm{E}_{|ss'ss'\rangle}(F) & \mathrm{V}_2 \\ 0 & 0 & \mathrm{V}_2 & \mathrm{E}_{|p's'ds'\rangle}(F) \end{pmatrix} \tag{3.22}$$

To express the different quantities of this Hamiltonian, we can use the fact that the range of investigated electric field F is small, as it is done in the modeling of the Förster resonances.
The coupling terms V_1 and V_2 are considered to be constant and correspond to the ones involved in the two Förster resonances presented in the section 3.7.1.
The energy of each 4-body states are considered to vary linearly with the electric field and we define them by the slope of the corresponding 4-body Rydberg states at the electric field of 80 V.cm^{-1} and by the resonant conditions corresponding to the experimental

observation of the two Förster resonances.
The different slopes of the states in function of the electric field can be evaluated with the calculation presented in the chapter 2 of this manuscript.
To visualize those informations, on the fig 3.19, we have represented the energy diagram of the different 4-body (non-interacting) Rydberg states that we model.

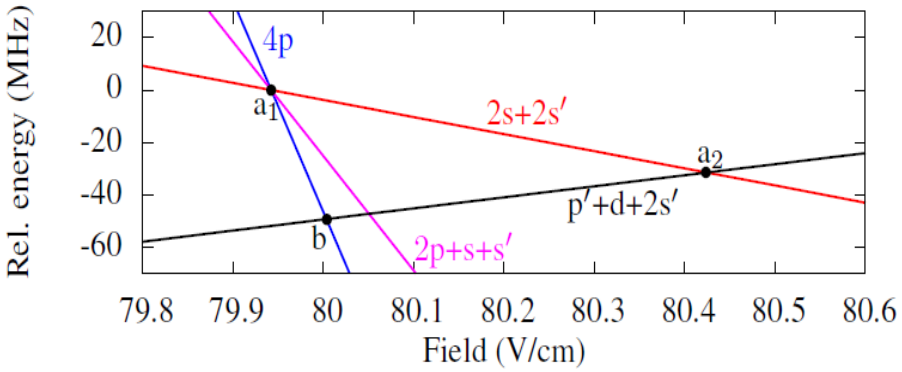

Figure 3.19: Energy diagram of different 4-body (non-interacting) states in function of the electric field. The slopes of the lines corresponds to the calculated ones, their position is set in function of the experimentally observed positions of the two Förster resonances. The two Förster resonances are highlighted by the points lebeled respectively a1, a2. The point labeled b corresponds to the position where the 4-body process should appear.

Our modeling of the 4-body process consists in solving the equation of evolution of the density matrix of the system $\hat{\sigma}$ for different electric fields and interatomic distances. We set the system to be at $t = 0$ in the state $|pppp\rangle$. The time of evolution is set to be 1.5μs, which is the time between the end of the laser pulse and the beginning of field ionization pulse in the experiment.
For each electric field and each interatomic distance, we can extract the fraction of atoms excited in the $23d_{5/2}$ Rydberg state at the end of the modeled process. It corresponds to the quarter of the population of the state $|p's'ds'\rangle$.
In our model we then do two averages of the obtained results. A first average is done according to the electric field to take in account the electric field inhomogeneity. A second one is done according to the distance between the atoms. For this latter, we assume that the possible values are given by the cubic Erlang distribution corresponding to the evaluated density of Rydberg atoms excited in our experiment.
The Erlang distribution $f(r,k)$ gives, in an uniform gas of density d, the probability $4^2 f(r,k)$ to find one atom and its k^{th} neighbor at a distance r. This distribution is given here, with $R_d = (\frac{4\pi}{3}d)^{-\frac{1}{3}}$

$$f(r,k) = \frac{3}{4\pi k!}\frac{(r^3)^{k-1}}{(R_d^3)^k}\exp^{-(\frac{r}{R_d})^3} \tag{3.23}$$

In the fig 3.20, we have plotted the results of our model together with the experimental data already presented on the fig 3.13.
We see on the fig 3.20 that the simple model that we have implemented exhibits a relatively good agreement with the experimental data. In addition to the fraction of $23d_{5/2}$ atoms, the model exhibits also the elbow structure of the resonance line observed experimentally.
This agreement seems to indicate that, as we expected, the 4-body process that we have observed is effectively linked to the existence of two Förster resonances very close in electric field.

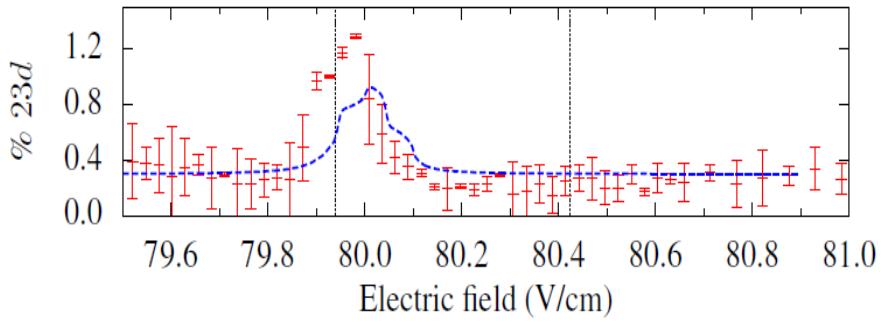

Figure 3.20: Comparison between the model and the experimental data. Fraction of $23d_{5/2}$ atoms within the total number of Rydberg atoms in function of the applied electric field. The data (red markers) corresponds to the ones presented on the fig3.13. The blue dashed line corresponds to the result of the model with a constant offset which corresponds to the background of the experimental $23d_{5/2}$ signal. The position in electric field of the two Förster resonances is represented by the vertical black dashed lines

3.8 Conclusion and outlooks

The experimental observation of the 4-body process that we have presented in this chapter represents an important step toward the study of coherent mechanisms involving few-body quantum states.
The experiments that we have performed open the way to the characterization and the control of the interactions between few Rydberg atoms from which we can expect very prolific behavior. A very interesting point is the relatively low density (MOT density) at which it has been possible to observe the 4-body process.

Working for example with magnetically trapped sample, the observation of 6-, 8-body processes should be reasonably approachable.

Staying in a MOT, the purpose of future experiments will be to studied more "isolated" 4-body processes. The one that we have observed being a bit slot in the middle of two 2-body Förster resonances. The use of two colours excitation should also allow to access a much larger variety of 3 or 4 processes.

In our experiments, we have shown that the application of variable dc electric fields can be an efficient way to controle the interacting Rydberg atoms. This comes in addition to laser excitation itself. In addition to an enhancement of the interactions for particular values of the electric field, the possibility to manipulate few-body Rydberg states through adiabatic/diabatic transition could offer very nice perspectives. Stark driven Landau-Zener transitions has been already studied for interacting pairs [Saquet et al., 2010].

As we have seen in the chapter 1 and 2, the interaction between two Rydberg atoms already leads to very rich features. This concerns the eigen energies but also there dynamics. For example, a very beautiful experiments reported in [Nipper et al., 2012b], have shown the coherence of the Förster resonance interactions by using a pair state interferometer.
Using such methods in cold atoms gases or working with sample composed by single few-body systems should allow to access the full "time-resolved" quantum states dynamics of interacting few-body systems. Such study fall in a very modern and deep field of research related to quantum chemistry or molecular biology.

Chapter 4

Many-body experiments

In this chapter, we present the experiments done in the "Dipartimento di Fisica" of the University of Pisa in the frame of this thesis.
The main purpose of those experiments is to study the excitation of a cold atomic cloud toward Rydberg states in the regime of strong interactions. In this regime, the interactions between the Rydberg atoms are such that the many-body quantum correlations determine the general behavior of the laser excitation.

The way to investigate the system in our experiment is the counting statistics of the number of detected Rydberg atoms. The main result obtained in the frame of this thesis is the observation of a highly subpoissonian statistics of the number of detected Rydberg atoms in an atomic cloud excited in the blockade regime. This observation, reported in [Viteau et al., 2012], is a strong signature of the collective behavior of the Rydberg atoms in the regime of blockade. The quasi deterministic number of Rydberg excitations that we have observed is a confirmation that the blockaded Rydberg gases offer very nice perspectives for the generation of non classical states.
This result came just after the first realization of a coherent Rydberg excitation in a 1-dimensional optical lattice [Viteau et al., 2011] which is also presented in this manuscript.

The experimental setup used for those experiments is a more than ten years old setup having already provided many beautiful results (and undergoes a fire in 2005). This setup allows a fantastic control of an atomic cloud of rubidium 87 atoms. Ultra low temperature are achieved allowing the formation of Bose-Einstein Condensates (BEC). The use of optical lattices allows a further control of the trapped matter-wave. Namely, a dynamical control of the tunneling has been realized [Lignier et al., 2007] through the shaking of the lattice, and many interesting effects arising from BEC trapped in periodic

potential have been observed [Sias et al., 2008; Eckardt et al., 2009; Lignier et al., 2009; Zenesini et al., 2010]. BEC in optical lattice have been also used in this setup to study driven two-level systems [Tayebirad et al., 2010] and a high fidelity quantum driving through a super-adiabatic protocol has been achieved [Bason et al., 2012]. The possibility to excite the atoms toward Rydberg states has finally open the way to the study of interacting quantum systems which is the subject of this thesis. Since this experimental setup has been largely depicted in the references that we just mentioned, in this manuscript, we present it quite briefly and we mainly focus on the points interesting for the Rydberg experiments.

4.1 Cold atomic samples in various density and geometry

The modularity of the atomic sample created in our experimental setup offers very nice possibilities for the study of interacting Rydberg gases. First, the ground state atomic density that we can obtain ranges from 10^{10} at.cm^{-3} to more than 10^{13} at.cm^{-3} with at least 10^5 atoms for all those densities. Also, in regards to the typical order of magnitude of the Rydberg blockade radius (10μm), the geometry can be either 3-dimensional, 1-dimensional or even "zero-dimensional". Finally, using the optical lattice, the atomic sample can be view as an ensemble of zero-dimensional packets.
In this section we present the different configurations in which we prepare the atomic sample before the excite the atoms toward a Rydberg state.

4.1.1 MOT

The first type of cold atomic cloud that we can create consists in a Magneto-Optical Trap (MOT). In our experimental setup, the Rubidium 87 atoms are first loaded in a so-called 2D-MOT in the "collection" part of the vacuum chamber. The trapped atoms are then pushed toward a classical MOT situated in the "science" part of the vacuum chamber. There, the pressure is of the order of 10^{-11} mbar.
In the frame of the Rydberg experiments, because we want to, we work with quite small MOT. The typical number of atoms is 10^4 for a typical mean density of few 10^{10} at.cm^{-3}. The temperature is of the order of 200 μK.
The realization of such a small MOT is not obvious. To work in this regime, we have to limit quite a lot the size of the cooling beams and a lot of attention have thus to be payed to the alignment of those beams.
The atoms trapped in the MOT provide us a 3-dimensional cold atomic sample whom

the typical dimension is few 100 μm.

4.1.2 BEC in a cross dipole trap

It is possible in our setup to reach the Bose-Einstein condensation of the atomic cloud. To do this, the atoms trapped in the MOT are transfered, after an optical molasses sequence, in a Time-average Orbital Potential (TOP) magnetic trap. First step of evaporation are done in the TOP trap, then, the atoms are loaded in a cross dipole trap where evaporative cooling is done until the condensation.
The laser use for the dipole trap is a 1030 nm Yb:YAG laser with an output cw power of 3 W. The laser is separated in 2 beams focused on the atoms with a waist of around 70 μm.
With this method, the created BEC are composed of typically 10^5 atoms with a density of few 10^{13} At.cm^{-3}. The temperature is of the order of few nK.
The BEC trap in the cross dipole trap provide us an ultra-cold atomic sample which can be view as an almost "zero-dimensional" sample with typical dimensions of the order of few μm. In the fig 4.1, we show an image of the BEC taken after a time of flight.

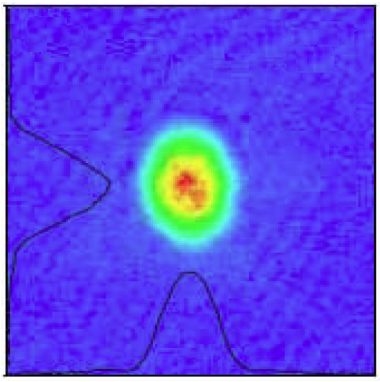

Figure 4.1: Image of the BEC.

4.1.3 1-dimensional BEC

In order to create an atomic sample having a 1-dimensional shape, we turn off one arm of the cross dipole trap. We can then let expand the BEC in the remaining dipole trap beam and the BEC acquires a so-called cigar-shape (see fig 4.2). By varying the time of expansion of the BEC before the Rydberg excitation, the longitudinal size of the atomic cloud ranges from few μm (initial size) until up to 1mm. On the other hand, the radial

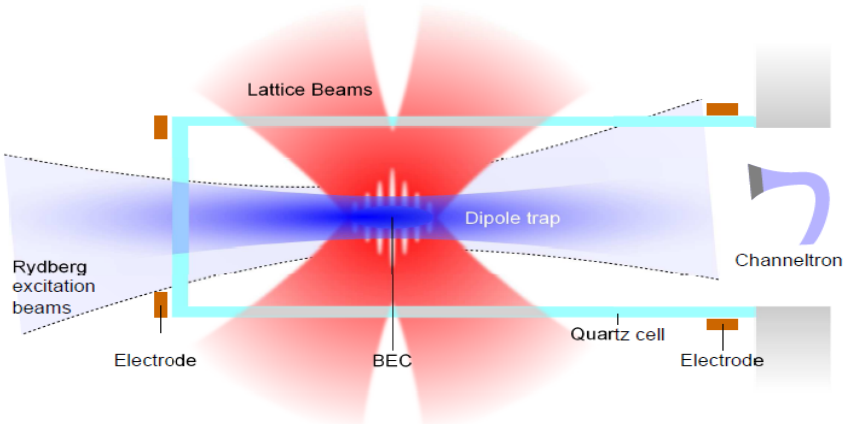

Figure 4.2: Schematic drawing of the "post-BEC" experimental setup, the different elements are mentioned in the text.

dimension stays roughly at its initial value of few μm.
On the fig 4.3, we show images of expanded BEC for two different times of expansion

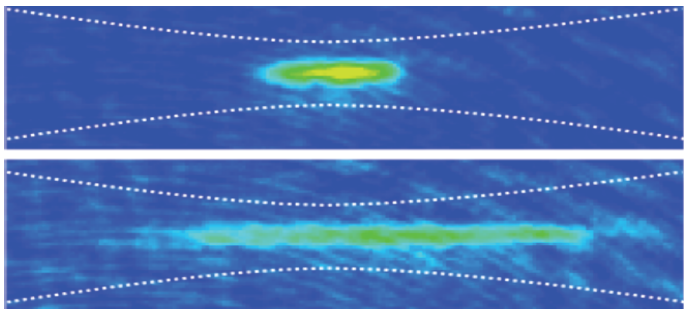

Figure 4.3: Images of the BEC for two different times of expansion in the 1D dipole trap, respectively 10 and 50ms for the upper and the lower image. The dipole trap envelope is schematically represented by the dashed white curves. Since those pictures are taken after a TOF, the size of the image is not relevant, however, the TOF is the same for both picture showing the effective expansion of the BEC

4.1.4 BEC in optical lattices

The last geometrical configuration that we can obtain in our setup involves the use of optical lattices. In our setup, we have implemented the possibility to create 1-dimentionnal optical lattices using two "counterpropating" laser beams (see fig 4.2).
Both beams comes from a MOPA TA100 of Toptica with an output power of around 750 mW for a wavelength $\lambda \approx 849$ nm.

Once the elongated BEC is created, we can ramp up the lattice beam (adiabatically for the Rydberg study) and then cutting in slices the 1-dimensional BEC. The rang of power of the lattice beams allows a large control on the axial potential seen by the atoms. Very strong confinement can be obtain, the size of on-site wave function can easily by made 10 times smaller than the lattice spacing.
In order to get different lattice spacings, we can manage to cross the two lattices beams with different angle θ (defined to be the angle between the direction of propagation of one beam and the direction perpendicular of the propagation direction of the other beam).
The lattice spacing d_L is then given by

$$d_L = \frac{\lambda}{2\sin\left(\frac{\theta}{2}\right)} \tag{4.1}$$

Since we have to change physically the beam directions to change the angle θ, the lattices spacing can not be changed "instantaneously". This is more a general parameter which is at most weekly changing.
The optical access in our setup allows to vary the lattice spacing from $\approx 0.5\mu$m to $\approx 25\mu$m. In comparison to the typical manageable blockade radii (10μm), we see here that the lattice spacing can be either larger or smaller. This allows to have a single Rydberg excitation either "localized" on one lattice site or "delocalized" over several lattice sites.
On the fig 4.4, we show an in-situ imaging of the atomic sample in presence of optical lattice with a lattice spacing of around 25μm. This very large lattice spacing has been achieved only recently in our setup and Rydberg experiments have not been preformed with this configuration yet.

Figure 4.4: In-situ imaging of the atomic cloud in presence of optical lattice. The lattice spacing is around 25μm

4.1.5 Characterization the atomic cloud

For all the sample created in our setup, we characterize the atomic cloud using an absorption imaging technique. It consists in sending a laser beam resonant with the cooling transition through the atomic sample and look to the intensity profile of the beam with a camera. In measuring the absorption of the beam, proportional to the atomic density, we can then reconstruct a 2-dimensional density profiles of the atomic cloud integrated on the third direction.
The CCD camera that we use is from DTA, taking in account a beam size magnification of 2 using an objective placed in front of the CCD, the spatial resolution of the system is around 2.2μm.
We associate, in our setup, this imaging with a precise time of flight. During this time of flight, the atomic cloud is in free fall. The density profile can be measured for different time of free expansion of the sample and we have then access to its initial dynamics. Here, both the temperature and the trap frequencies play a role and can be investigated. To image the BEC, we need to have a time of flight where the cloud expands (typically of the order of 10 ms) in order to get a reasonable spatial precision. However, for the MOT or for expanded BEC with or without lattices, we do also "in-situ" imaging.
The precision reaches in our setup on the density and the number of atoms resulting from the absorption measurements has been evaluated to be better than 20%.

4.2 Rydberg excitation

In this section, we present briefly the laser system that we use to excite the atoms toward Rydberg states. We present also the main characteristics of the laser excitation.

4.2.1 General scheme

The laser excitation system implemented in our setup is a coherent two-photons excitation. From the ground state atoms, we can excite atoms in Rydberg states nl with n ranging from 30 to 120 and l is either s or d. As discuss in the section 1.4.4 of the chapter 1, the coherence of the excitation is ensure by the fact that the excitation is detuned from the intermediate state, in our case the typical detuning is 1 GHz. In the fig4.5 we have represented a schematic energy diagram of the Rydberg excitation corresponding to our experiments.

The detuning of the excitation from the intermediate state allows a coherent excitation of the Rydberg states from the ground state but it also prevents from an undesirable photoionization of the atoms. Indeed, the 420 nm laser can directly ionize the atoms ex-

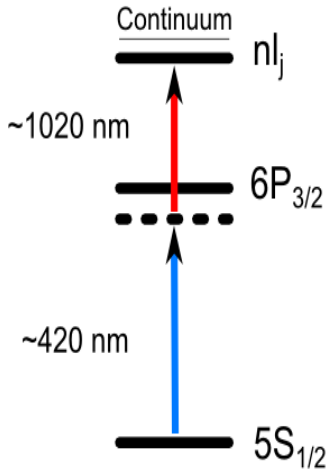

Figure 4.5: Energy diagram of the coherent 2-photons Rydberg excitation

cited in the state $6p_{3/2}$ and the associated oscillator strength is quite high (much higher than the one associated to ionization of the Rydberg states). It is then essential to avoid completely the population of this state, i.e., work with a large detuning. Nevertheless, in our experimental procedure, the photoionization of the $6p_{3/2}$ provide us with a very useful way (by detecting the created ions) to set the 420 nm laser on the transition $5s \rightarrow 6p_{3/2}$ and then to detune it afterward in a controllable way.
The photoionization is also used to calibrate the Rydberg atoms detection.

4.2.2 Excitation lasers

To realize the first step of the Rydberg excitation $5s \rightarrow 6p_{3/2}$, we use a 840 nm MOPA laser TA 100 from Toptica which is sent in a doubling cavity SGH 1004 from Toptica. The output power at 420nm is around 50mW.
The laser beam is sent toward the atomic cloud where it is focused with a typical waist of 100 μm and a typical power of 20 mW.

For the second step of the Rydberg excitation $6p_{3/2} \rightarrow nl$, we use a DL 100 diode laser from Toptica with a lasing range from 1000 to 1030 nm which allows the excitation of Rydberg states with n ranging from 30 to 120. In fact this laser allows also to reach the continuum but for $n > 120$ it is quite difficult to have a precise control on the Rydberg state that we excite. This laser is injected in a TIGER laser from Sacher whom the grating have been replaced by a mirror, for an output power of around 400mW.
The laser beam is focused on the atoms with a typical waist of 100 μm and a typical power of 150 mW.

In our setup, both Rydberg excitation laser are almost collinear and also almost collinear to the dipole trap laser beam in which the BEC is expanded (see fig4.2). The goal is here to have the longest Rydberg excitation region.
Both Rydberg excitation laser passes through an AOM before to reach the atoms allowing to perform pulsed excitation. The raising time of the AOMs is around 80 ns.

4.2.3 Stabilization of the lasers frequency

In order to stabilize the frequency of the Rydberg excitation lasers, we use in our setup a Fabry-Perot cavity (FP). Both Rydberg excitation lasers are send in the FP, with also a reference laser locked in an atomic transition (for instance a part of the cooling laser of the MOT). Using the FP, a Labview program has been developed in order to stabilize the Rydberg excitation laser. Interestingly, we can also scan them in a controllable way using the program.

To do this, the length of the FP cavity is continuously modulated over its full free spectral range with a frequency of around 200 Hz. On the transmission signal of the FP, the program identifies transmission pics corresponding to each of the Rydberg excitation laser and two pics corresponding to the reference laser. The two pics of the reference laser allow to determine a well defined relative frequency scale for the position at which other pics appear. So, from the FP transmission signal, the program can generate error signals allowing to stabilize each Rydberg excitation laser. For instance, to generate the error signal, for one laser, the program measures the relative position of the transmission pics corresponding to this laser and the reference laser and compares it to a reference position. This error signal is finally send, in our case, to a PID 110 Toptica module acting on the Rydberg excitation laser (for both laser).
With this technique, in addition to stabilize the lasers, we can also scan them in a controllable way by changing the reference positions used to generate the error signals. In the Labview program, we enter the wavelength values of the three lasers allowing to have an interfaced reading and setting of the relative motion of the laser frequency directly in MHz. The possible range of scan (overlooking undesirable laser mode jump) is of the order of 1 GHz.

Due to the quite low modulation frequency of the FP, which is limited by the Labview program calculations speed, this technique allows mainly to compensate the temperature drift and only slightly the mechanical noise. Nevertheless, we measure that, on the

ms time scale, the combined frequency variation of the Rydberg excitation lasers is of the order of 1 MHz. In the following, this quantity is called the jitter of the Rydberg excitation.

Concerning the linewidth of the Rydberg excitation (on the μs time scale), which is then determine by the intrinsic quality of the Rydberg excitation lasers and the overall mechanical stability of the setup, we have evaluated that the combined value for both Rydberg excitation lasers is around 300 kHz.

4.2.4 Characteristics of the coherent excitation

Since we perform a coherent excitation of the Rydberg states from the ground state by detuning the Rydberg excitation from the intermediate state, we can determine the total Rabi frequency of the Rydberg excitation.
The total Rabi frequency Ω_R can be expressed in function of the Rabi frequency of both excitation steps Ω_1 and Ω_2 and the detuning from the intermediate state Δ

$$\Omega_R = \frac{\Omega_1 \Omega_2}{2\Delta} \tag{4.2}$$

In our setup, we typically work with $\Delta = 1$ GHz.

The Rabi frequency of each step is calculating using the knowledge of the dipole moment of the associated transition and the experimental measurement of the laser power and the laser waist at the position of the atoms.
In our setup, the waist and the Rayleigh length of the two excitation laser beams is much larger than the atomic sample, the intensity of the beams is then the same for all the atoms.
The Rabi frequency of the Rydberg excitation of a given Rydberg state $nl_j(m_j)$ can be determined with a precision of the order of 10%. In the experiments presented here we have excited l =d Rydberg state, due to the polarization of the lasers, we excite in the same time several magnetic sublevels of a given Rydberg state nd_j. Since the transition dipole moment is different for each magnetic sublevels, they experiment also different Rabi frequencies and we have to make the proper average over the different accessible magnetic sublevels to determine the effective Rabi frequency. Given different states $|r_i\rangle$ with Rabi frequencies Ω_i a superposition $\frac{1}{\Omega}\sum_i \Omega_i |r_i\rangle$ of the different states is excited with a total Rabi frequency Ω given by

$$\Omega = \sqrt{\sum_i \Omega_i^2} \tag{4.3}$$

Although it depends of the Rydberg states that we excite and of the daily measured excitation lasers power, the Rabi frequency of the Rydberg excitation are typically of the order of few tens of kHz.

Concerning the total detuning of the Rydberg excitation (which is the sum of the detuning of each step), we can determine and control it with a precision of the order of 1 MHz (limited by the jitter of the laser excitation).

In our setup, a general source of imprecision for the Rydberg excitation comes from the presence of undesirable electric field. Our science chamber is made in quartz and can suffer from charging effects. If we mainly excite Rydberg atoms in zero field, the use of field ionization detection (see section 4.3.1) involves the exposure of the cell to high voltages and charging effects have been seen.
As a first precaution, we reduce as most as possible the duration of the high voltages pulses. Secondly, by checking regularly the position of the Rydberg line and if needed wait that the cell becomes free of charge, we manage to perform the Rydberg excitation in presence of a non controlled electric field smaller than 5 mV.cm^{-1}. In regard to the determination of the Rydberg excitation characteristics, this value corresponds to negligible effects.

4.3 Rydberg atoms detection and counting statistics

In our setup, the detection of the Rydberg atoms is done using the field ionization method. The created ions are accelerated toward a detector. From the detector signal, we measure the number of ions which have been detected. In the frame of our experiments, we are interested to investigate the interacting Rydberg gases using the Rydberg excitations counting statistics. In this section, we present in which experimental conditions we obtain such statistical informations.

4.3.1 Rydberg detection and measurements

After the Rydberg excitation pulse, we apply at the position of the atoms an electric field pulse to ionize the Rydberg atoms. To do this we use two pairs of electrodes as represented in the fig4.6. The maximum difference of potential applied between those two

pairs of electrodes during the pulse is around 5 kV. Due to the quartz cell, a screening effect reduces the field seen by the atoms. Using this system, we can not ionize Rydberg states with a principal quantum number lower than 52 for d states and 54 for s states, to be safe 53d and 55s are then the lowest Rydberg levels that we can investigated. The typical duration of the ionization pulse is few μs with a measured very short rise time (few ns). The use of short ionization pulses ensures a short exposure of the quartz cell to high voltages and avoids charging effects.

To detect the created ions, we use in our setup a Channel Electron Multiplier (CEM) KKBL510 CEM, called the channeltron. The channeltron has an internal gain determined by a potential, we set it to the maximum (-2.4 kV) as we want to detect single ions. The output signal of the channeltron resulting from the detection of one ion is amplified using a fast timing amplifier and finally acquired by an oscilloscope, a WaveRunner from LeCroy.

The channeltron is situated at around 15 cm from the Rydberg excitation region. However, its position is not right on the axis determined by the atomic cloud position and the direction of the electric field of the ionization pulse. Although the ions are attracted by the channeltron as the closest pairs of electrodes have a potential of -1 kV, we placed an intermediate grid along the ions path to "help" them to reach the channeltron. This grid is situated at 10 cm from the atomic cloud and we applied on it a potential of around -1.5 kV.

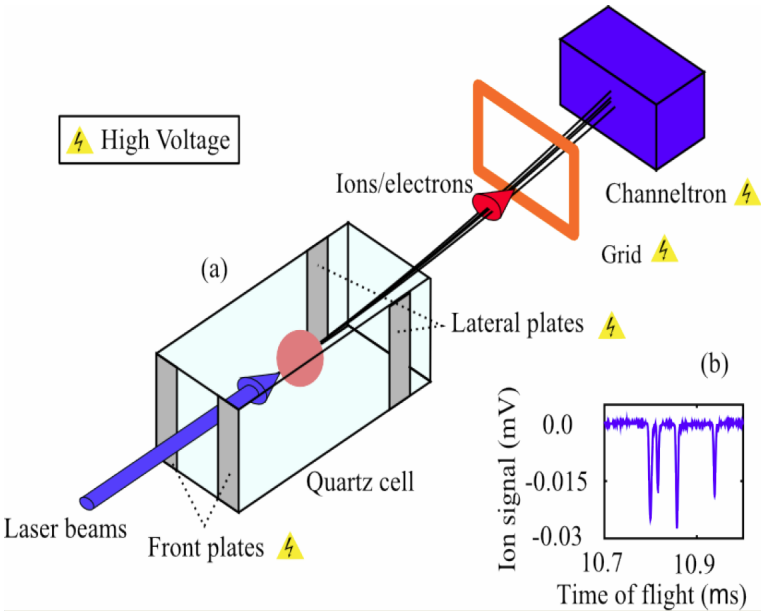

Figure 4.6: Schematic representation of the experimental detection setup.

On the fig 4.6, we see a typical detection signal acquired by the oscilloscope. We

see that the number of detected ions can be precisely determined from this signal. In our experiments, we do it with a Labview program and the number of detected ions is determined with an accuracy better than 5%. This number is the physical quantity that we record to investigate the laser excitation of an interacting Rydberg gas.

4.3.2 Detection efficiency

In our experiments, we want to know precisely the number of Rydberg atoms created by the excitation pulse. If those Rydberg atoms are all ionized by the electric field pulse and if we can almost absolutely determine the number of detected ions, all the created ions are not detected. It is very important to know the efficiency of detection of our system. Two effects play a role in the detection efficiency, the proportion of ions reaching the detector and the detector efficiency.
It has been evaluated that the detection efficiency η of our system is $\eta = 35\% \pm 10\%$.
The method used for such determination have been reported in details in [Viteau et al., 2010]. The determination of the detection efficiency consists in comparing, during a photoionization process, the number of detected ions with an evaluation of the atomic loss from the cloud. In order to get a determination of the detection efficiency as accurate as possible, the photoionization of the atomic sample is performed for different atomic density (MOT and BEC) and laser power.
For the detection efficiency determination as well as in the frame of our experiments, we want to avoid completely saturation effects of the detector. We have evaluated that for a number of detected ions below 50, we do not saturate the detector, consequently we always work in this regime in our experiments.
In all the treatment of our experimental results, we consider that the processes involved in the detection efficiency follows a poissonian statistics (is a random process). This is very important as it plays a role in the determination of the Rydberg excitations statistics from the detected ions statistics.

4.3.3 Experimental sequences and "Shots per run"

In this section, we present the experimental sequence of our experiments. We do not deal with the details of the atomic sample preparation (the beginning of the experimental sequence). It is obviously very different in the case of a MOT or of a BEC.
For a given experimental situation, we want to measure the counting statistics of the number of Rydberg atoms excited by the Rydberg excitation pulse. By essence, we have to repeat several time the same experimental situation.

The experimental conditions are in principle reproducible. However, in practice, the number of parameters involves in the experiment makes that the experimental situation is never exactly the same. This is especially true for the BECs which are always slightly different (in the good days) from one run to another.
In order to get reliable statistics, we perform within the same experimental run, several cycles of Rydberg excitation/detection (several shots). For our experimental conditions, the number of Rydberg atoms excited in one shot is small in comparison to the total number of atoms and we can reasonably assume that the experimental situation is the same for all the shots performed in the same run excepted in regards to the laser jitter. All the shots done in one run represent a units of statistical measurements, there number corresponds to the accuracy of the statistical quantities determination.

In our experiment, the MOT works in a permanent regime, also the experimental sequence is quite simple and fast. We first turn off the MOT beams, then we apply several shots of Rydberg excitation/detection. We then turn on the MOT beams to reload the MOT and start a new sequence. For the data presented in this manuscript, the number of shots done in one MOT is 100.

In the case of BEC, the experimental sequence to obtain a BEC is around 2 minutes long. This is mostly due to the TOP trap sequence and the time need to load of a sufficient number of atoms in the MOT to obtain a BEC. Once the BEC is formed, we apply the several shots of Rydberg excitation/detection. Finally, we performed an imaging of the BEC in order to measure the number of atoms and the atomic density associated to the measurements that we just took. For the data presented in this manuscript, the number of shots done in a BEC is 15.
Interestingly, using the optical lattice, it has been possible to study the effect of those shots on the phase coherence of the condensate. On the fig 4.7, we show the measurements of the interference pattern resulting from the interference of the different fraction of the BEC coming from several lattice site during a TOF. This measurement is done with and without the application of Rydberg excitation/detection shots.

We clearly see on the fig 4.7 that the presence of the Rydberg shots does not perturb significantly the interference pattern of the splitted BEC. This is in fact quite impressive since the Rydberg shots involve laser excitation, application of high voltages and creation of charged particle inside the BEC. Anyway, the measurement presented in the fig 4.7 ensure us that the effect of the Rydberg shots consists only in removing a small number of atoms from the BEC.

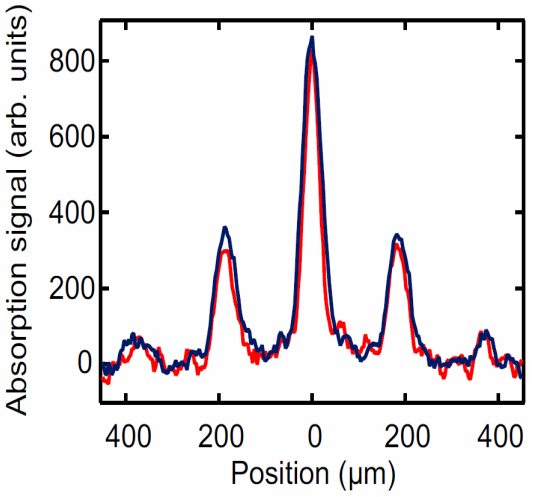

Figure 4.7: Interference pattern resulting from the BEC trapped in the optical lattice. The blue curve is taken without having performed Rydberg excitation/detection shots. The red curve is taken having performed 10 shots of Rydberg excitation/detection.

4.3.4 Mean number of Rydberg excitations

From the ensemble of detected ions numbers associated to the different shots, the first quantity that we calculate is simply the mean number of Rydberg excitations.

From a mean number of detected ions N_d, the mean number of Rydberg excitations N_R is given by the detection efficiency η.

$$N_R = \frac{N_d}{\eta} \tag{4.4}$$

In the frame of our measurements, the uncertainty on the mean number of Rydberg excitations comes from the uncertainty on the detection efficiency (10%).

4.3.5 Mandel Q factor

The second statistical quantity that we have look at is the Mandel Q factor [Mandel, 1979]. This is a quantity related to the variance of the statistical distribution. For a given statistical distribution with a mean n and a variance σ^2, the Mandel Q factor is defined by

$$Q = \frac{\sigma^2}{n} - 1 \tag{4.5}$$

The same quantity without the "-1" is called the Fano factor [Fano, 1947].

A poissonian statistics, which characterizes random or uncorrelated processes, has a Q factor equal to 0. The so-called sub- and super-poissonian statistics have respectively a negative and a positive Q factor. The absolute minimum for the Q factor of a statistical distribution is -1, this case corresponds to a statistical distribution with a null width or in other terms to a process which gives always the same result.

For a process resulting from the measurement of a quantum system, the Q factor is linked to the so-called quantum projection noise. The value of the Q factor is linked to the distribution of the quantum system wave function over the different eigenstates of the measurement.
The "meaning" of the Q factor in the frame of the interacting Rydberg gas is presented on the section 4.7. In this section we just present the determination and the uncertainty on the Rydberg excitation Q factor in our experiments.

In the case of a poissonian detection, the Q factor of the Rydberg excitations Q_R is linked to the Q factor of the detected ions Q_d through the detection efficiency η, exactly like for the mean.

$$Q_R = \frac{Q_d}{\eta} \tag{4.6}$$

The uncertainty on the Q factor of the Rydberg excitation is first given by the uncertainty of the detection efficiency. We have also to consider that the detection process is not necessary poissonian and that the equation 4.6 is not necessary true. Eventual deviations from this law are not easy to measure. Nevertheless, in our setup, in looking at the detected Q factor resulting from uncorrelated processes like the photoionization or the Rydberg excitation in an almost non-interacting case, we have found that our detection system is very close to be poissonian. At most, we could attribute an uncertainty on the Q factor of the Rydberg excitation of 20% due to this effect.
Finally, it is also interesting to study the effect of the finite number of shots used to calculate the detected Q factor. We present here the result of a numerical study of this question.
We have simulated several realizations of a process, having set the statistical distribution of the process to be a Gaussian with different mean and Q factor. For one obtained sample, it is then possible to calculate its Q factor. For a given number of realizations (number of shots), we have study the statistical distribution of the Q factor in function of the mean and the Q factor of the process. A quite interesting result is that the statistical distribution of the Q factor seems to do not depend of the mean of the process. Although

it might possible to demonstrated it mathematically, it is in fact quite intuitive as the Q factor is a quantity normalized by the mean. On the fig 4.8, we have represented the spraid of the calculated Q factor in function of the number of shots, for initial Q factors of 0 and -0.4.

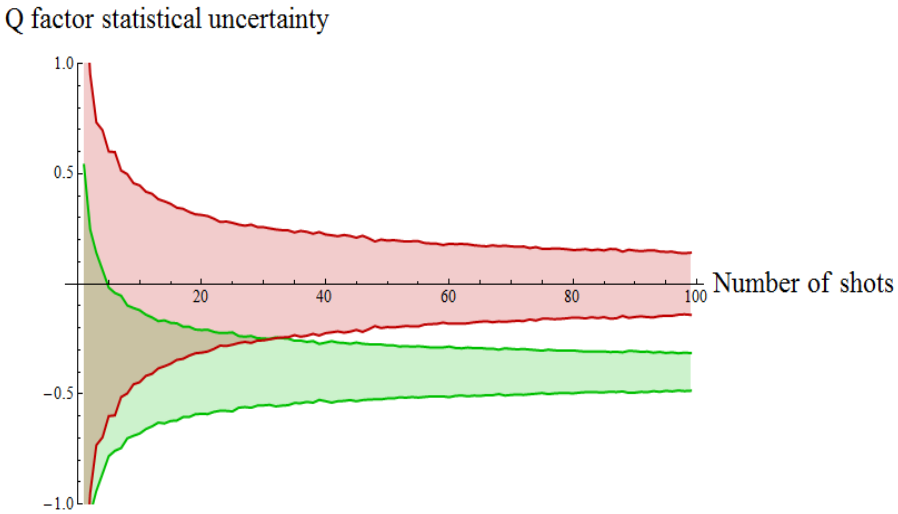

Figure 4.8: Dispersion of the Q factor measurements in function of the number of shots. The red area corresponds to a "real" Q factor of 0, the green one to -0.4. In both cases, the decreasing solid line represent the variance calculated for 500 realisations with an offset equal to the real Q factor.

From the fig 4.8 and similar one for other values of the Q factors, we can evaluate the uncertainty on the detected Q factor associated to the finite number of shots used to obtain it. The error bars on the Q factor experimental measurements presented in the following are evaluated by this method. Also it allows to determine the number of shot needed to clearly identify a given sub-poissonian process. Obviously, without such considerations, several measurements of the Q factor taken in similar situation allow also to say if an observed value of the Q factor is reproducible or not.

4.4 Summary of the experimental setup

In this section, as a summary of the precedent sections, we present the type of experiments that we can performed in our setup to study strongly interacting Rydberg gases.

We have seen in the section 4.1 that we can first prepare the atomic sample in various conditions of density and geometry. Thanks to the accuracy of the cold atoms

techniques, this is done in a very controllable way.
We have seen in the section 4.2 that we can then perform a coherent excitation of the ground state atoms toward a given Rydberg states. Several parameters of the excitation can be changed in a controllable way, namely, the detuning and the duration of the excitation can be varied. We can control of course the Rydberg state that we excite, this allow to change the strength of the Rydberg-Rydberg interactions. All the experiments presented in this manuscript correspond to an excitation in zero field and the Rydberg-Rydberg interaction is then of the Van-der-Waals type.
Finally, as presented in the section 4.3, for a given experimental situation, we can measure the mean and the Q factor of the Rydberg excitations number distribution in a reliable way.

4.5 Rydberg excitation in 1-dimensional lattice

In this section we report experiments done using 1-dimensional optical lattice. The use of optical lattice allows to obtain atomic samples composed by several packets of atoms. In comparison to a continuous sample, we expect to see stronger effects of the coherent collective dynamics of the Rydberg excitation.
The Rydberg excitation in 1-dimensional lattice is largely studied theoretically (see section 1.4.3 of the chapter 1). It is shown that, in this geometry, the collective Rydberg excitations should lead to very interesting many-body behaviors. The experimental realization of such systems should allow to access them.
The results presented here, reported in [Viteau et al., 2011], represent the first experimental demonstration of the coherent excitation of Rydberg atoms in 1-dimensional optical lattices.

4.5.1 Experimental procedure

The experimental procedure used for the experiments with optical lattice consists in letting expand the BEC in the 1-dimensional dipole trap (see section 4.3). Then, adiabatically ramping up the lattice beams power. Finally, ramping down and up again the dipole trap power. The purpose of this last step is to keep only the atoms which are inside the lattice. Here, the radial dipole force created by the two lattice beams plays a role. We manage to ramp down the power of the dipole trap until the point where only the cumulated light field of the dipole trap and the lattice beams is able to maintain the atoms again the gravity. The atoms outside the lattice field fall and thus leave the investigated atomic sample.

This experimental procedure allows to create a well define atomic configuration before the Rydberg excitation. The atomic sample is composed by a 1-dimensional chain of "zero-dimensional" packets. Whereas the "volume" of this sample is constant, the total number of atoms can be changed by letting expand the BEC in the dipole trap for different time before to ramp up the lattice power.

In the experiments reported here, the lattice spacing has been set to be $d_l = 2.27\mu$m. The two lattice beams cross thus each other with a quite large angle (see fig 4.2). The region where the lattice is present, which define the total length of the atomic sample, is composed by around 100 lattice sites for a total length of around 0.23 mm.
Looking at one packet, its radial size results from the confinement created by the dipole trap, it is of the order of 2μm. On the other hand, the axial size is determined by the lattice depth, we typically set it to be around 0.2μm.
On the fig 4.9 we have represented schematically this configuration

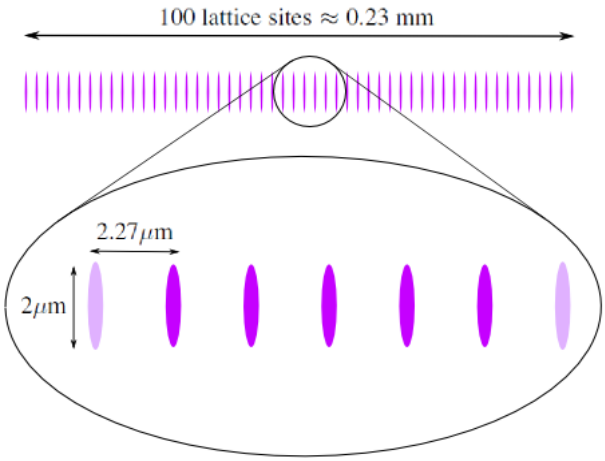

Figure 4.9: Schematic representation of the atomic cloud trapped in the 1-dimensionnal optical lattice.

4.5.2 Comparison with the continuous case

As a preliminary experiment, we have performed the Rydberg excitation with and without the presence of the optical lattice. In this experiment, the time of expansion of the BEC in the 1-dimensional dipole trap is such that the total length is smaller than the region where the lattice is present. Consequently, the presence of the lattice leads only to the formation of atomic packets and do not modify the total length of the atomic cloud.

On the fig4.10, we show the detected number of Rydberg excitations after the excitation of the $53d_{5/2}$ state in function of the laser pulse duration. This with and without the presence of the lattice beams. For this experiment, the lattice beams have been alternatively hidden or not to the atoms from one experimental run to another, thus, the two curves have been acquired "in the same time".

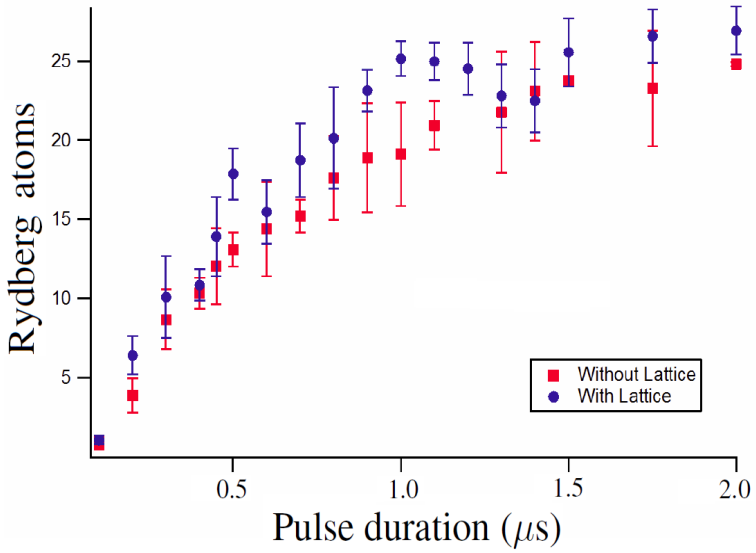

Figure 4.10: Detected number of $53d_{5/2}$ Rydberg atoms in function of the pulse duration. The number of Rydberg atoms have been evaluated from the number of detected ions and the detection efficiency. Red squares correspond to the continuous case (without lattice). Blue circles correspond to the case with lattice.

On the fig4.10, we see that the presence of the lattice does not lead to a big modification of the Rydberg excitation dynamics in comparison to the continuous case. Nevertheless, in presence of the lattice, we observe small oscillations on top of the general dynamics. Those oscillations are clearly due to the fact that the different strengths of the Rydberg-Rydberg interactions are regrouped in different classes due to the discontinuity of the atomic sample. However, this effect remains quite small since the separation between two adjacent packets (2.27μm) is in fact comparable to the radial expansion of each packet (2μm).

4.5.3 Collective dynamics

On the fig4.11 we have represented, for three different time of expansion of the BEC, the number of Rydberg atoms obtained for different pulse durations. The three different

times of expansion corresponds to different total numbers of atoms in the sample or again to different numbers of atoms inside each lattice site. We give here the average number of atoms contained in each lattice sites $\langle N_i \rangle$, the three set of data presented on the fig 4.11 corresponds to $\langle N_i \rangle$ ≈500, 200 and 50.
The investigated state is the $53d_{5/2}$ Rydberg state, the Rabi frequency of the coherent excitation has been evaluated to be around $2\pi\times$ 30 kHz.

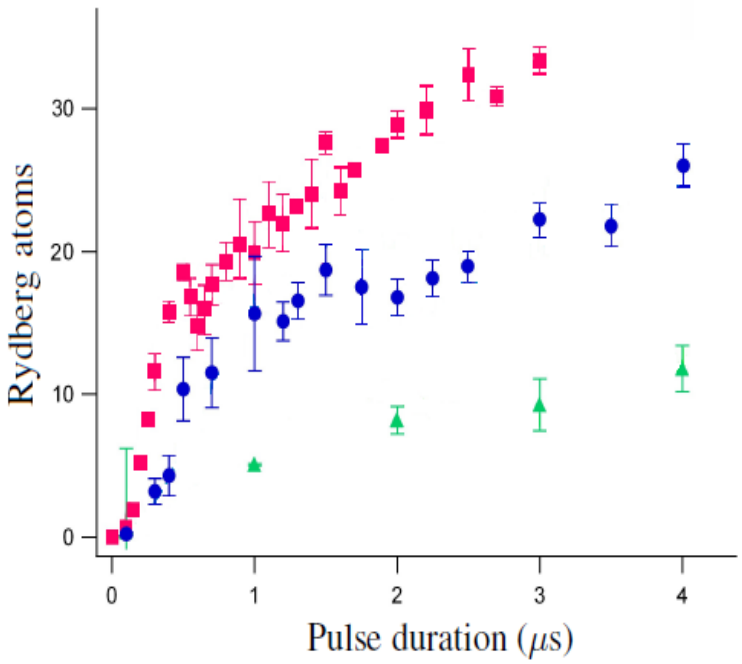

Figure 4.11: Detected number of $53d_{5/2}$ Rydberg atoms in function of the pulse duration. The number of Rydberg atoms have been evaluated from the number of detected ions and the detection efficiency. The three set of data correspond to an average number of atoms per lattice site of around 500 (red squares), 200 (blue circles) and 50 (green triangles)

On the fig4.11, we see the general scaling of the Rydberg excitation dynamics in function of the number of atoms. Bigger the number of atoms is, faster is the dynamics. A relative scaling of the different curves with $\sqrt{N}$ is compatible with the measurements of the fig 4.11 and their experimental uncertainties. This confirms the expected collective dynamics of the Rydberg excitation in the blockade regime.

We have seen with the comparison with the continuous case that, for the lattice spacing set for those experiments, the lattice does not lead to big modifications. This even for the

$53d_{5/2}$ state which is the less interacting Rydberg state that we can excite in our setup. Consequently, it has been quite natural after those results to modify the optical access in the setup in order to reach larger lattice spacing. If a lattice spacing of around 25 μm is now reachable in our setup, the 1-dimensional lattice experiments have not restart wet.

In any case, this demonstration of a coherent Rydberg excitation in a 1-dimensional optical lattice paves the way toward the investigation of very interesting many-body behaviors.

4.6 Observation of a highly sub-poissonian statistics

In this section, we report experimental measurements of the Q factor associated to the Rydberg excitation of a blockaded ensemble. We have observed, for a resonant excitation, highly sub-poissonian statistics of the Rydberg excitation. The Mandel Q factor of the Rydberg excitation has been found in several experimental situations, to be close to -1, which correspond to an almost deterministic number of Rydberg atoms.

The experiments presented here concerns the Rydberg excitation in a tiny MOT. Similar experiments have been also performed in BEC, i.e. at much larger densities, with comparable results. Nevertheless, for reasons of reliability of the underlying statistical quantities due to the limited number of shots, we present here the results corresponding to the MOT where larger statistical samples are used.

4.6.1 Excitation dynamics

We report here the investigation of both the mean and the Q factor of the Rydberg excitation in function of the duration of the laser excitation for a resonant excitation.

The atomic sample consists in a MOT of around 8000 atoms with a 3D-gaussian atomic density with a mean density around 1.5 10^{10} at.cm^{-3}.
The laser excitation is resonant with the transition between the ground state and the $71d_{5/2}$ Rydberg state, the 2-photon Rabi frequency has been evaluated to be $2\pi\times40$ kHz.
On the fig 4.12 we report the measurements concerning the ions detected after the laser excitation.

On the fig 4.12, we see that in the same time that the number of excitations increases, the Q factor takes negative values. Quite quickly, the Q factor reaches a very

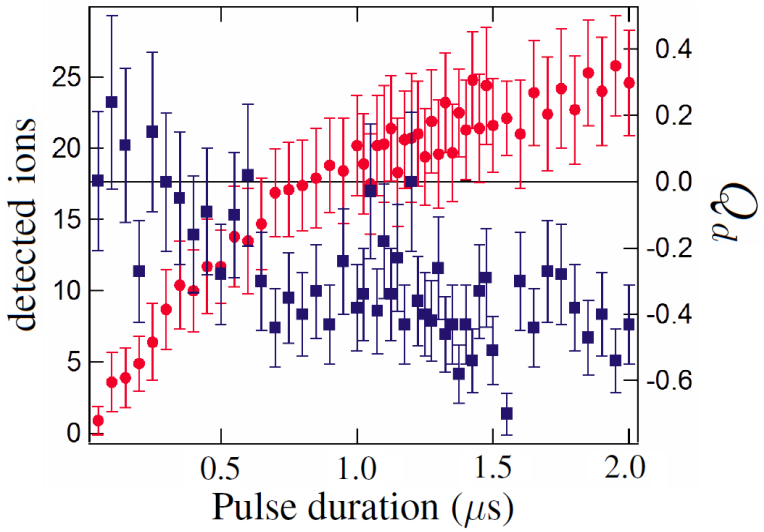

Figure 4.12: Excitation of $71d_{5/2}$ Rydberg atoms, number of detected ions and associated Q factor in function of the pulse duration. Red circles represent the number of detected ions, blue squares represent the detected Q factor

low value and remains constant afterward. This value, concerning the detected ions, is $Q_d = -0.4 \pm 0.1$. Taking in account the detection efficiency $35 \pm 10\%$, we see that the Q factor relative to the number of Rydberg excitations Q_R is found to be very close to be -1. Both the uncertainty on the detection efficiency and the fact that the detection is not necessary poissonian have to be taken into account to evaluate the uncertainty on the Rydberg excitations Q factor. This gives $Q_R < -0.6$.

Also it is not the main purpose of this experiment, we can quickly look at the number of Rydberg excitations obtained in the saturation regime.
Although it is not so clear on the number of ions (the Q factor exibits a much clearer saturation) we can estimate that we are in the saturation regime for a pulse duration of 1μs. The number of Rydberg excitations is in this case around 60 in taking into account the detection efficiency. The size of the MOT is in this experiment of the order of 5 $10^5 \mu m^3$. This correspond to an average volume per Rydberg excitation of around 8 $10^3 \mu m^3$ or in the blockade sphere picture a blockade radius of around 12 μm. For an excitation of 1 μs the Fourier broadening determine the effective linewidth which is thus $2\pi \times 1$ MHz. The most interacting C_6 coefficient within the $d_{5/2}$+$d_{5/2}$ channel is around $2\pi \times 2.5$ 10^3 GHz.μm^6 leading to a blockade radius of around 11.5 μm.
We see here that the effective C_6 coefficient resulting from the rich Zeeman structure of the $d_{5/2}$+$d_{5/2}$ channel seems to be mostly determined by the most interacting configurations.

Concerning the collective dynamics, in keeping a number of Rydberg excitation of 60, the number of atoms per excitation is around 150 leading in the Super Atom picture to a collective Rabi frequancy of around $2\pi\times$ 0.5 MHz. This is in good agreement with the timescale of the fig 4.12.

The most important observation of the fig 4.12 concerns the Q factor of the Rydberg excitation in the saturation regime: $-1 < Q_R < -0.6$.

4.6.2 Scan of the Rydberg line

In addition to the dynamics of the Rydberg excitation at resonance, we have also investigated the counting statistics behavior for off resonance excitation.
On the fig 4.13, we show the measurement of both the mean and the Q factor of the numbers of detected ions for different laser excitation frequencies. Here, the number of atoms is around 5 10^4 with a mean density around 4 10^{10} At.cm^{-3}.
The laser excitation is resonant with the transition between the ground state and the $71_d5/2$ Rydberg state, the 2-photon Rabi frequency is around $2\pi\times$40 kHz. The pulse duration is 0.3μs.

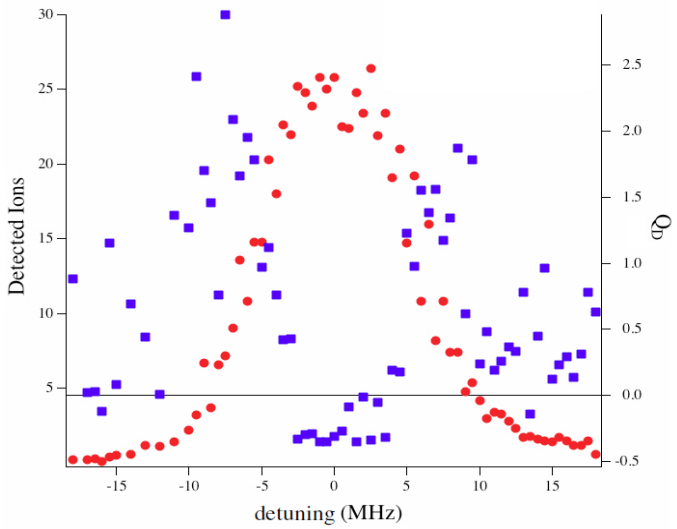

Figure 4.13: Excitation of $71d_{5/2}$ Rydberg atoms, number of detected ions and associated Q factor in function of the detuning of the laser. The pulse dureation is 0.3 μs. Red circles represent the number of detected ions, blue squares represent the detected Q factor. To not charge to much the figure, error bars have been omitted but they are of the same order than the ones of the fig 4.12.

On the fig 4.13, looking at the mean number of detected ions, we clearly see the scan of the Rydberg line, this latter having a width of around $2\pi\times$ 5 MHz. Looking now at the Q factor, we see that, if it takes negative value at resonance, we found positive values on the edges of the Rydberg line. For the Rydberg excitations Q factor, the maximum value are around 3. Those positive values could correspond to interesting physical behavior for off resonant excitation. However, the jitter of the laser excitation (of the order of 1 MHz) induces for sure positive value of the Q factor on the edge of the line. Indeed, here, a small variation of the laser frequency induces a big change of the number of Rydberg excitations and thus a super-poissonian statistics. This is briefly study in the appendix B.

4.7 Q factor and quantum projection noise

In this section, we discuss the physical meaning of the Q factor (or identically the variance) related to a given measurement. We examine especially the meaning of the highly negative Q factor that we have observed experimentally.
The Q factor is intrinsically linked to the so-called quantum projection noise induces by the measurement which is performed. The quantum basis associated to the measurement (the projection basis) is here very important since the Q factor will be determined by the "distribution" of the wave-function on the different states of this basis. Moreover, the measurement value associated to each states of the projection basis plays a crucial role. For example, the wave-function of the system can be a superposition of many projection basis states, but if all of those states are associated to the same measurement value, the Q factor will be -1.

Formally, the measurement (projection + measurement value) of a system can be written as an operator $\hat{m}$. In the projection basis $\{|i\rangle\}_i$, $\hat{m}$ is diagonal and its eigenvalues m_i are the measurement values of the states $|i\rangle$.
The mean value of the physical measurement is the operator $\hat{m}$ and the Q factor can be formally written as the operator $\hat{Q} = \frac{\hat{m^2}-(\hat{m})^2}{\hat{m}} - 1$ where $\hat{m^2} = \hat{m}.\hat{m}$. In the projection basis, $\hat{m^2}$ is diagonal and its eigenvalues are the squares of the measurements values of the projection basis states. In the expression of $\hat{Q}$ the evaluation of the operators has to be done before the arithmetic operations.

4.7.1 Two-levels system

In this section, we consider the case of a two-levels system.
We first consider that the two levels correspond to measurement values of 0 and 1. We

label the levels respectively $|g\rangle$ and $|r\rangle$ since this corresponds to the case of one of our atom. Indeed, during the detection process in our experiments, an atom is either projected in the Rydberg state, is ionized and leads to 1 count on the detector or is projected in the ground state leading to 0 count in the detector. This do not take into account the detection efficiency.

In the basis $\{|g\rangle, |r\rangle\}$ the measurement operator is written

$$\hat{m} = \begin{pmatrix} 0 & 0 \\ 0 & 1 \end{pmatrix} \tag{4.7}$$

In this particular case, we have $\hat{m^2} = \hat{m}$ and $\hat{Q} = -\hat{m}$.

If P_r is the probability to find the system in the state $|r\rangle$, the system is in the state $|\Psi\rangle = \sqrt{1-P_r}|g\rangle + \sqrt{P_r}|r\rangle$. In this case, the mean value of the measurement $\langle\Psi|\hat{m}|\psi\rangle$ is P_r and the Q factor $\langle\Psi|\hat{Q}|\psi\rangle$ of the measurement is $-P_r$.

For a single atoms doing Rabi oscillation between the ground state and the Rydberg state, the Q factor associated to its measurement is also doing "Rabi oscillation" between 0 and -1.

We have also studied the case were the two levels do not corresponds to measurement values of 0 and 1. For example, when those values are 1 and 2 or again 0 and 2, we can see on the fig 4.14 that the results are very different.

We see on the fig 4.14 that the Q factor takes always highly negative value if the amplitude between the different measurement values is small in comparison to their mean. On the other hand, the Q factor can take positive values if the amplitude between the different measurement values is large in comparison to their mean. Although the system investigates here is a two-levels system, the latter rules concerns also multi-levels systems.

4.7.2 Assembly of uncorrelated two-levels systems

In this section, we discuss the fact that the observation of highly negative Q factor is due to the atomic correlation induces by the blockade effect. This can be shown by doing a comparison with the case of uncorrelated atoms.

The measurement of an assembly of N uncorrelated two-levels systems follows a sim-

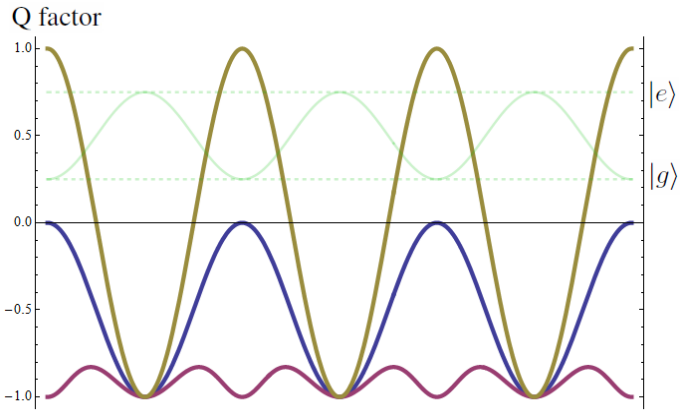

Figure 4.14: Relation between the Q factor of a two-level system and its internal dynamics. The dynamics of the system is shown by the light green curve, the system is doing Rabi oscillation between the ground state $|g\rangle$ and an excited state $|e\rangle$. The three thick curves corresponds to three systems having different measurement values in their ground and excited states. For the blue curve it is 0 and 1, for the red it is 1 and 2 and for the yellow it is 0 and 2

ple rule, both the mean value and the variance of the total measurement are the sum of the individual mean value and variance. In statistics, we say that the realization are independent and our situation corresponds to a so-called Bernoulli process.
Considering an assembly of N atoms, identical and uncorrelated. Defining $\hat{m}_i$ as the measurement operator of each atoms, the total mean value operator is given by $\hat{m} = \sum_i \hat{m}_i$ and the total Q factor [1] by $\hat{Q} = -\frac{\sum_i (\hat{m}_i)^2}{\sum_i \hat{m}_i}$.
We consider a sample of 1000 atoms with slightly different Rabi frequencies $\Omega_i = \Omega(1+\alpha_i)$, the α_i being regularly distributed within $]-\frac{1}{10}, \frac{1}{10}]$. On the fig 4.15, we have represented the evolution of the total mean value and Q factor in function of the time starting with all the atoms in the ground state at $t = 0$. We have limited the plot at short time, where the number of excitation stays quite small.

The fig 4.15 illustrates the fact that when the mean value of the Rydberg excitation is small in comparison to the total number of atoms, we can not find a highly negative value of the Q factor in such a system of uncorrelated atoms.
The measurement of both small mean value and highly negative Q factor can not be explained without atomic correlations and can thus be used as a test of the blockade regime.

[1] This is true for two-levels system when levels are 0 and 1, if not we have $\hat{Q} = \frac{\sum_i (\hat{m_i^2} - (\hat{m}_i)^2)}{\sum_i \hat{m}_i} - 1$

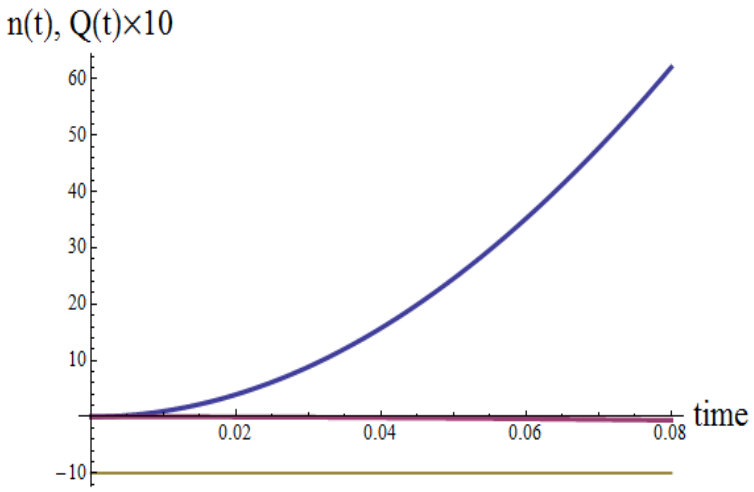

Figure 4.15: Evolution of the Q factor of an ensemble of identical and uncorrelated two-levels systems doing Rabi oscillations. The total number of excitation is represented by the blue curve, the Q factor by the red curve with a magnification of 10.

It is quite interesting to look at the long term regime of such a system since the Q factor takes a non so intuitive value. This is represented on the fig 4.16

On the fig 4.16, we see that, as expected, the mean value of the Rydberg excitation is in the long term regime the half of the total number of atoms. However the Q factor is in this case -0.75.
This can be understood by the fact that the dynamics in Sin^2 of the Rabi oscillations leads to the fact that the atoms are more often close to one level or the other rather than in the middle.

4.7.3 Fully blockaded ensemble

In this section, we present the Q factor asociate to a fully blockaded ensemble. A fully blockaded ensemble of N atoms is such that the Rydberg-Rydberg interactions prevent from the simultaneous excitation of two Rydberg atoms in the sample. As mentioned in the section 1.4.1 of the chapter 1, in presence of a laser field resonant with the transition ground state $\rightarrow$ Rydberg state, the system is doing Rabi oscillation between the collective ground state and the collective state with one Rydberg excitation.
Considering that the projection states of the measurement corresponds to those collective states. A fully blockaded ensemble behaves thus like a single atom concerning its measurement and its Q factor is equal to $-P_R$ if P_R is its probability to be in the collective state with one excitation. It corresponds to the blue curve on the fig 4.14.

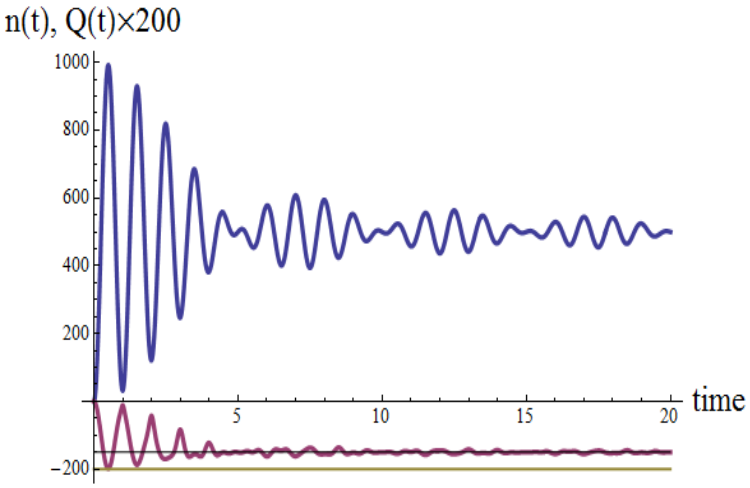

Figure 4.16: Evolution of the Q factor of an ensemble of identical uncorrelated two-levels systems doing Rabi oscillation. The total number of excitation is represented by the blue curve, the Q factor by the red curve with a magnification of 200.

4.7.4 Q factor and collective basis

To describe the Rydberg excitation of an ensemble of atoms we can use a collective basis. In such a basis, we can define for each quantum state the total number of Rydberg excitations that it contains.
In considering that the projection states of the Rydberg excitation measurement correspond to the collective states, the measurement values are integer numbers ranging from 0 to the total number of atoms of the sample.
The Q factor of such a system is given by the distribution of the wave function on the different subsets of states containing the same number of Rydberg excitations.

Considering a collective basis, highly negative Q factors appear quite naturally. This will occur if the wave function is distributed over quantum states whom the range of measurements values is smaller than their mean.

The Super Atom picture can be associated to a "semi-collective" basis since an assembly of Super-Atoms is an ensemble of (almost) independent collective particles. In the Super Atom picture, the different Super-Atoms are doing Rabi oscillations with different frequencies. In the saturation regime, the value that the Q factor of such a system would takes is the same than the one presented in the section where we treat the case of an assembly of independent two-levels systems. The Q factor of the Rydberg excitation in the Super-Atom picture takes then a value of $Q \approx -0.75$ in the saturation regime. This

result is quite interesting, because it fixes the minimum value that the Q factor can take in considering that the atomic correlation are associated to collective single excitations.

In the chapter 5 of this manuscript, we present a cooperative model where the system is describes using the so-called Dicke collective states. Although this model contains non trivial approximations, highly negative Q factor ($Q \approx -0.8$) are found and the quantitative agreement with experimental results is quite good.

In the theoretical study of 1-dimensional ring lattice with the prefect blockade approximation, the Q factor is calculated from the distribution of the system wave function over each subset of states with the same number of Rydberg excitations. In the reference [Olmos et al., 2010], once the steady state of the system is reached, the Q factor of the Rydberg excitation is found to be $Q = -0.676$.

We see here that highly negative Q factors are strongly linked to the existence of collective excitation in the system.
The experimental observation of the Q factor presented in the section 4.6 indicates clearly that the experiments are done in a regime of strong interactions and that the measurements which is performed is associated to the projection of the system onto collective states.
If the precise values that the Q factor takes in function of the excitation parameters could allow to obtain very interesting informations on the studied system, the experimental uncertainty in our system does not allow to check very precisely the prediction of the theoretical models. Nevertheless, from the observed values, we can say without ambiguity that the wave function of the system is quite strongly restricted to a range of collective states which contain a similar number of Rydberg excitations.

4.8 Conclusion and outlooks

The experiments presented in this chapter represent important progresses for the experimental investigation of interacting Rydberg gases.

The demonstration of the coherent Rydberg excitation of a BEC confined in a 1-dimensional optical lattice pave the way toward the study of very interesting collective behaviors.

The experiments presented here have been done with a relatively small lattice spacing in regards to the typical blockade radius. Recent development in our experimental

setup allow to reach much larger lattice spacings (25 μm). As illustrated in the fig 4.17, this offer the possibility to investigate the regimes where a single Rydberg excitation is either localized on only one lattice site, nor delocalized over several ones.

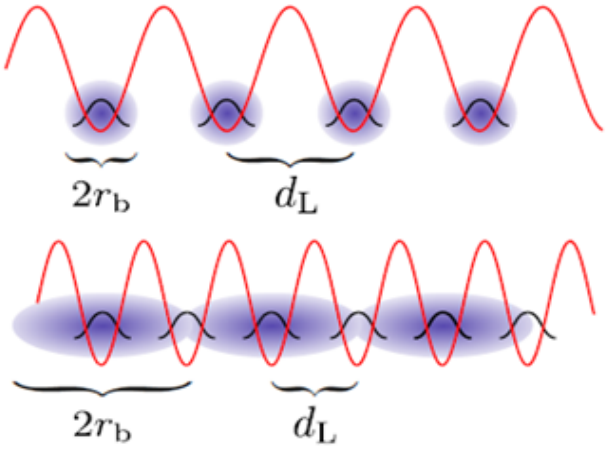

Figure 4.17: Schematic representation of the Rydberg excitation of a 1-dimensional lattice. We see have highlighted the possibility to vary the ratio between lattice spacing and blockade radius.

As it is depicted by several theoretical works, the implementation of such systems should lead to the observation of genuine collective behavior. Namely with the formation of many-body states having very interesting photon emission properties.

The other important result obtained in the frame this thesis is the observation of a highly sub-poissonian statistics of the Rydberg number distribution in the regime of strong interactions.
Within the accuracy of our measurements we can clearly affirm that those observations arise from the creation of collective excitations in the system.
Very interestingly, the observations that we made seems to indicates that the Rydberg excitation is restricted to a very small range of values. The measured Q factors have been found to be very close to -1 (experimental uncertainties give $Q < -0.6$). Similar values have also been reported in [Hofmann et al., 2012] in the frame of an EIT process involving strong Rydberg interactions.
If precised, those observations point out a quite spectacular behavior of strongly interacting Rydberg gases. In the saturation regime, a quasi-deterministic number of Rydberg excitations is present at every time of a coherent excitation and does not suffer from quantum projection noise.

In further experiments, the Rydberg excitation in 1-dimensional lattice with variable parameters together with a measurements of the statistical distribution will be for sure investigated.
For the time being, one topic is currently attracting our attention, the realization of a fully blockaded ensemble containing (at least) a mesoscopic number of atoms. This is an essential step toward the control of strongly interacting Rydberg gases and its use in the frame of quantum engineering. However, it appears that the required conditions are not easy to reach and perform such an experiments would represent a big step for the dipole blockade Physics.

Chapter 5

Many-body modeling, cooperative model

In this chapter, we report the theoretical investigations done in the frame of this thesis concerning the coherent excitation of strongly interacting Rydberg gases.
As mentioned in the section 1.4.3 of the chapter 1, the modeling of a Rydberg gas in the regime of strong interaction is a very challenging task. Because the full quantum resolution of the system is limited to very small numbers of atoms, several theoretical approaches are currently investigated to model larger systems.
In the frame of this thesis, we have study the problem using the Dicke basis, introduced in [Dicke, 1954]. The so-called Dicke collective states possesses a very useful property : they are defined in function of their symmetry relative to the electromagnetic field. The symmetry mentioned here lies in the fact that the atoms are undiscernable in regards to the electromagnetic field. The Dicke collective states can be defined such that the laser excitation only coupled the states with the same symmetry providing great simplification in the treatment of the problem.
The Dicke states appears to be a nice theoretical tool to study the coupling of an ensemble of identical atoms with the electromagnetic field. It has been mainly used in the frame of the Superradiance phenomenon, review in [Gross and Haroche, 1982] and very recently in [Lin and Yelin, 2012] due to recent developments in this field. In those references, the electromagnetic field is quantified, the collective spontaneous emission is investigated as well as all kinds of tricky quantum effects. Those treatments use quantum electrodynamics calculations which overpass largely the formalism use in this thesis.
In this manuscript, we stay with a semi-classical description of the light-matter interaction. We report the development of a theoretical model to describe the coherent laser excitation of an atomic ensemble in presence of interactions between the excited atoms

(Rydberg atoms). The model is based on the fact that in one hand the laser excitation coupled states with the same symmetry and in the other hand the Rydberg-Rydberg interaction coupled Dicke states of different symmetries. This coupling leads to a strong modification of the excitation dynamics in comparison to the non interacting case.
The model presented here is far to describe completely the Rydberg excitation of an atomic gas in the regime of strong interaction. However, several features observed experimentally are well reproduce by the model, like the highly negative values of the Q factor or the non-shifted position of the Rydberg line.
From the model and the collective states mechanisms, it has been possible to extract some physical concepts which seems to be well adapted to the laser excitation of a strongly interacting Rydberg gaz. In this manuscript, we present those concepts and we make some links with other theoretical developments.

5.1 Dicke basis

In this section, we present the formal definition of the Dicke collective states. Since we want to look at the excitation of the atomic ensemble by a given laser field, we define the Dicke states in function of this laser field. This is a small modification compare to the original case of [Dicke, 1954]. By using the Dicke collective state, we treat the case of non-interacting atoms. Although the use of a many-body basis is here not required, this simple example shows clearly that the Dicke states are well adapted to deal with collective excitations.

5.1.1 Collective operator and Dicke states

We consider an ensemble of N identical two-levels atoms. The levels of each atoms are the ground state $|g\rangle$ and a Rydberg state $|r\rangle$. The position of an atom i is $\vec{R}_i$. We consider a monochromatic laser field defined by its wave vector $\vec{k}$.

From the transition and projection operators $\hat{\sigma}^i_{\alpha\beta} = |\alpha_i\rangle \langle\beta_i| \, (\alpha, \beta = g, r)$ of each atom i, we define a set of three collective operators

$$\hat{R}^{+}_{\vec{k}} = \sum_{i=1}^{N} \hat{\sigma}^{i}_{rg} \mathrm{e}^{i\vec{k}.\vec{R}_i} \tag{5.1}$$

$$\hat{R}^{-}_{\vec{k}} = \sum_{i=1}^{N} \hat{\sigma}^{i}_{gr} \mathrm{e}^{-i\vec{k}.\vec{R}_i} \tag{5.2}$$

$$\hat{R}^{(3)}_{\vec{k}} = \frac{1}{2} \sum_{i=1}^{N} \hat{\sigma}^{i}_{rr} - \hat{\sigma}^{i}_{gg} \tag{5.3}$$

In the most general case, there is no phase factors in the definition of the collective operators. However, since we want to treat the laser excitation of the atomic ensemble, we include from the beginning the spatial characteristics of the excitation laser field through its wave vector $\vec{k}$ in the definition of the Dicke states. This is in fact essential to make the symmetry properties of the Dicke states rigorously true. Without phase factors, the symmetry properties hold only in the case where the expansion of the atomic ensemble is much smaller than the wavelenght of the electromagnetic field. We see that with the phase factor, the symmetry properties are rigorously defined for only one particular mode of the electromagnetic field. This is well adapted when the atomic system is driven by a laser field. However, for the treatment of the spontaneous emission, it is preferable to not include any phase factors and the "Dicke dynamics" is more complex (see for example [Das et al., 2008]).

The collective operators commute as

$$\left[\hat{R}^{+}_{\vec{k}}, \hat{R}^{-}_{\vec{k}}\right] = 2\hat{R}^{(3)}_{\vec{k}} \tag{5.4}$$

$$\left[\hat{R}^{+}_{\vec{k}}, \hat{R}^{(3)}_{\vec{k}}\right] = 2\hat{R}^{+}_{\vec{k}} \tag{5.5}$$

We finally define the collective operator $\hat{R}^{2}_{\vec{k}}$ as

$$\hat{R}^{2}_{\vec{k}} = \hat{R}^{(3)2}_{\vec{k}} + \frac{1}{2}(\hat{R}^{+}_{\vec{k}}\hat{R}^{-}_{\vec{k}} + \hat{R}^{-}_{\vec{k}}\hat{R}^{+}_{\vec{k}}) \tag{5.6}$$

The Dicke states are defined to be the common eigenstates of $\hat{R}^{2}_{\vec{k}}$ and $\hat{R}^{(3)}_{\vec{k}}$. We note here the strong analogy with angular momentum operators. A Dicke state can be labeled by its eigenvalues related to those operators. The Dicke states $|c, m\rangle$ verify

$$\hat{R}^{(3)}_{\vec{k}}|c,m\rangle = m|c,m\rangle \tag{5.7}$$

$$\hat{R}^{2}_{\vec{k}}|c,m\rangle = c(c+1)|c,m\rangle \tag{5.8}$$

Here, the quantum number c, called the cooperative number, denotes the symmetry of the state relatively with the laser excitation and m corresponds physically to the inversion of population of the Dicke state (number of atoms in $|r\rangle$ - number of atoms in $|g\rangle$). We have $c \in [\![0; N/2]\!]$ and $m \in [\![-c; c]\!]$.

In the following, we will labeled the Dicke states as $|j, c\rangle$ where $j = N/2 - m$ corresponds to the number of atoms in the Rydberg state, c remain the same. We can rewrite the range of values that j and c can take as $j \in [\![0; N]\!]$ and $c \in [\![|\frac{N}{2} - j|, \frac{N}{2}]\!]$.

Due to the symmetry of the laser excitation. Only the states with the same cooperative number c are coupled together by the laser field.

5.1.2 Dicke basis

The quantum wave function of a system of N two-levels atoms evolves in a Hilbert space of dimension 2^N. We can form a quantum basis of the system using 2^N linearly independent Dicke states. For this we choose $N_c = \binom{N}{N/2-c} - \binom{N}{N/2-(c+1)}$ states having the same j and c. N_c is called the degeneracy of the Dicke states.

A Dicke basis of an ensemble of N identical non interacting two-levels atoms can be represented by the diagram shown in the fig5.1

Due to the symmetry of the laser excitation. Only the states with the same cooperative number are coupled by the laser field. Obviously, those states will be effectively coupled if the transition $|g\rangle \rightarrow |r\rangle$ has a non null dipole moment and if the laser is resonant with this transition.

Within a Dicke basis, the states with the maximum cooperative number $c = N/2$ have an important role. Those states are called the fully symmetrical Dicke states. There is only one fully symmetrical Dicke state per level of excitation and only one way to define them.
For a given number of excitation j, the dimension of the associated subset, noted $M^{(j)}$, is the number of possibility to choose j excited atoms within the N atoms, $M^{(j)} = \binom{N}{j}$. We note $|j, q\rangle$ the state where j excitations are localized on the atoms specified by q

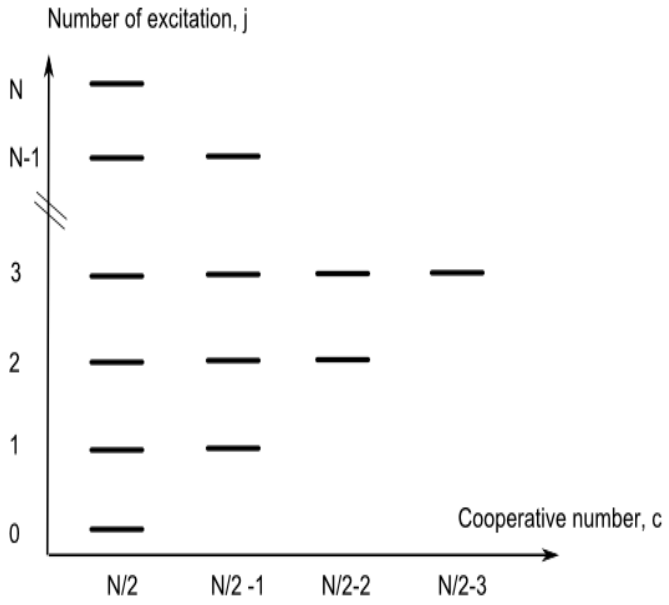

Figure 5.1: Schematic representation of a Dicke basis in the non interacting case. The degeneracy of each level is given in the text.

which is then a set of j numbers. We call atomic state or configuration this kind of state, for example

$$|j = 2, q = \{3, 5\}\rangle = |g, g, r, g, r, g, ..., g\rangle \tag{5.9}$$

The fully symmetrical Dicke collective state with j excitations, noted $|j, s\rangle$ is defined as the symmetrical superposition of states $|j, q\rangle$, $q \in [\![1; M^{(j)}]\!]$.

$$|j, c = N/2\rangle = |j, s\rangle = \frac{1}{\sqrt{M^{(j)}}} \sum_{q=1}^{M^{(j)}} \mathrm{e}^{-i\phi_q} |j, q\rangle \tag{5.10}$$

The phase factor $\mathrm{e}^{-i\phi_q}$ arises from the definition of the collective operators. For $q = \{3, 5\}$ we have $\phi_q = \vec{k}.\vec{R}_3 + \vec{k}.\vec{R}_5$. This example shows how determining the phase factors $\mathrm{e}^{-i\phi_q}$.

The fully symmetrical Dicke state with one Rydberg excitation corresponds to the Rydberg state populated in the case of a fully blockaded ensemble or again, it corresponds to the excited state of a Super Atom.

The other states of the basis can be found by using the so-called Young tables and there is several way to define an orthogonal basis composed by Dicke states.

As illustrative examples, we present in the table 5.1 and 5.2, the Dicke basis in the case of two atoms (for two atoms there is only one possible Dicke basis) and a Dicke basis for three atoms. In both cases we do the comparison with the natural basis of the atomic ensemble, called in the following the atomic basis. We have skip out the phase factors.

Number of Rydberg excitations	Atomic basis	Dicke basis
0	$\|g,g\rangle$	$\|g,g\rangle$
1	$\|r,g\rangle$	$\frac{1}{\sqrt{2}}(\|r,g\rangle + \|g,r\rangle)$
	$\|g,r\rangle$	$\frac{1}{\sqrt{2}}(\|r,g\rangle - \|g,r\rangle)$
2	$\|r,r\rangle$	$\|r,r\rangle$

Table 5.1: Atomic and Dicke basis for 2 atoms

Nb of Rydberg excitations	Atomic basis	Dicke basis
0	$\|g,g,g\rangle$	$\|g,g,g\rangle$
1	$\|r,g,g\rangle$	$\frac{1}{\sqrt{3}}(\|r,g,g\rangle + \|g,r,g\rangle + \|g,g,r\rangle)$
	$\|g,r,g\rangle$	$\frac{1}{\sqrt{6}}(\|r,g,g\rangle + \|g,r,g\rangle - 2\|g,g,r\rangle)$
	$\|g,g,r\rangle$	$\frac{1}{\sqrt{2}}(\|r,g,g\rangle - \|g,r,g\rangle)$
2	$\|g,r,r\rangle$	$\frac{1}{\sqrt{3}}(\|g,r,r\rangle + \|r,g,r\rangle + \|r,r,g\rangle)$
	$\|r,g,r\rangle$	$\frac{1}{\sqrt{6}}(\|g,r,r\rangle + \|r,g,r\rangle - 2\|r,r,g\rangle)$
	$\|r,r,g\rangle$	$\frac{1}{\sqrt{2}}(\|g,r,r\rangle - \|r,g,r\rangle)$
3	$\|r,r,r\rangle$	$\|r,r,r\rangle$

Table 5.2: Atomic and one Dicke basis for 3 atoms

In the dicke basis of the table 5.2, a particular role have been given to the atom placed in third position. Obviously similar basis can be formed via the exchange the position of the atoms. We see here that there is several possibility to define a Dicke basis.
On the table 5.1 and 5.2 we do not have specified the symmetry of the Dicke states. The first state of each lign are fully symmetric Dicke states $c = N/2$, the other ones have all a cooperative number $c = N/2 - 1$.

5.1.3 Laser excitation in the non interacting case

In this section, we treat the laser excitation of an ensemble of N identical two-levels atoms in the case where there is no interaction between the atoms in the excited state (we still label the excited state by $|r\rangle$).
This situation is very simple since the atoms behaves identically and independently. The

problem could be treated in the one atom basis, the full system being just a superposition of identical, idependent (uncorrelated) atoms. In this situation, we know that all the atoms of the system do in-phase Rabi oscillations at the single atom Rabi frequency Ω. However, we treat here the problem using the collective Dicke states. We show that the collective description, although useless in this particular case, leads to the correct results.

In the frozen gas approximation, neglecting all incoherent process, the Hamiltonian of the system can be written as (see section 1.4.1 of the chapter 1)

$$H = -\hbar\delta\sum_{i=1}^{N}\hat{\sigma}_{rr}^{i} + \frac{\hbar\Omega}{2}\sum_{i=1}^{N}\left[\hat{\sigma}_{gr}^{i}\mathrm{e}^{i\vec{k}.\vec{R}_i} + \hat{\sigma}_{rg}^{i}\mathrm{e}^{-i\vec{k}.\vec{R}_i}\right] \tag{5.11}$$

This Hamiltonian differs from the one of the equation 1.42 by the fact that there is no more interaction terms. We have also add the relative phase of the laser at the position of the atoms which is the correct form for the laser excitation.

Using the Dicke collective states, since the collective ground state of the system is fully symmetrical, starting from the ground state a $t = 0$, only the fully symmetrical Dicke states $|j, s\rangle$ will be populated during the excitation process.

The wave function of the system can be written in the Dicke basis as

$$|\Psi(t)\rangle = \sum_{j=0}^{N} a_j(t)\,|j, s\rangle \tag{5.12}$$

The coupling between the adjacent states $|j, s\rangle$ induces by the laser exitation $\hat{H}_L = \frac{\Omega}{2}\sum_{i=1}^{N}\left[\hat{\sigma}_{gr}^{i}\mathrm{e}^{i\vec{k}.\vec{R}_i} + \hat{\sigma}_{rg}^{i}\mathrm{e}^{-i\vec{k}.\vec{R}_i}\right]$ is given by

$$\langle j, s|\,\hat{H}_L\,|j+1, s\rangle = \frac{\Omega}{2}\sqrt{(N-j)(j+1)} \tag{5.13}$$

A practical way to determine the "collective" factor $\sqrt{(N-j)(j+1)}$ present in the equation 5.13 is to think in terms of atomic states. The state $|j, s\rangle$ is composed by $M^{(j)}$ atomic states having all the weight $1/\sqrt{M^{(j)}}$. Each of those state are coupled with $N - j$ atomic states with $j + 1$ excitations. In the state $|j+1, s\rangle$ those latter atomic states have all a weight $1/\sqrt{M^{(j+1)}}$. The collective enhancement of the Rabi frequency can be determined by the following formula with $M^{(j)} = \binom{N}{j}$.

$$M^{(j)}\frac{1}{\sqrt{M^{(j)}}}(N-j)\frac{1}{\sqrt{M^{(j+1)}}}=\sqrt{(N-j)(j+1)} \tag{5.14}$$

Knowing the laser coupling between the states $|j,s\rangle$, the Shrödinger equation associated to the evolution of the system is given by the following set of $N+1$ coupled differential equations

$$i\frac{da_j}{dt}=-\delta j a_j+\sqrt{(N-j)\,(j+1)}\frac{\Omega}{2}a_{j+1}+\sqrt{(N-j+1)\,j}\frac{\Omega}{2}a_{j-1} \tag{5.15}$$

We see that, although we treat the problem with the full quantum basis of the N two-levels atoms, the Dicke basis allows to extract $N+1$ states which will be effectively populated. The evolution of the system is then describes by only $N+1$ differential equation and can be solved for quite large N.
The number of excitations $n(t)$ present in the system is given by

$$n(t)=\sum_{j=0}^{N} j\,|a_j(t)|^2 \tag{5.16}$$

On the fig5.2 we have represented the evolution of $n(t)$ in function of the time. For the calculations, we took $N=100$ and $\Omega=2\pi$, this for two detuning $\delta=0$ and $\delta=\Omega$.

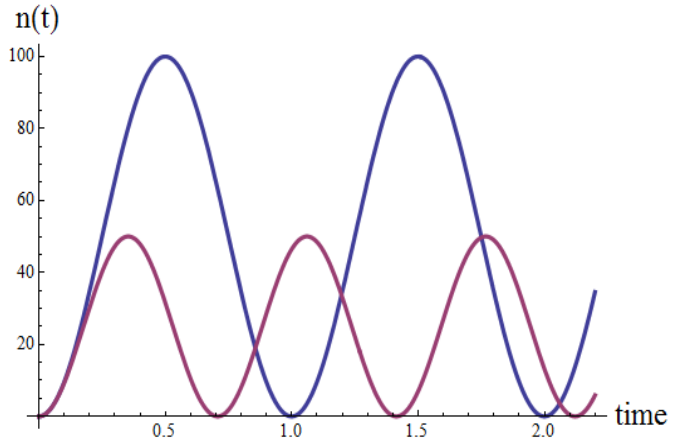

Figure 5.2: Evolution in function of the time of the total number of excitations in an ensemble of 100 identical non interacting atoms. This evolution is given by calculations in the Dicke basis. The time is given in unit of Rabi frequency.

We see on the fig5.2 that the evolution of the system calculated in the Dicke basis correspond to the one that we expect for the laser excitation of an assembly of identical

and uncorrelated atoms. All the atoms are doing Rabi oscillations in phase between the ground state and the excited state. The excitation carried by the atoms are summed leading to this "macroscopic" Rabi oscillation.
We can also from the equation calculate the corresponding Q factor (as well as the full statistics). We found it to be the one expected for an assembly of independent two-levels systems doing in-phase Rabi oscillations.
Those simple calculations illustrate the fact that the Dicke basis is a nice tool to deal with many-body systems.

5.2 Cooperative model

In this section we present the model that we have developed in order to study the laser excitation of an assembly of atoms toward an interacting Rydberg state using the Dicke collective states.
The Rydberg-Rydberg interactions have two effects on the Dicke collective states. First, the states with the same number of excitations are no more degenerated in energy. Secondly, their are coupled together independently of their cooperative numbers.
On the fig 5.3 we have qualitatively represented an "interacting Dicke basis" underlining those two effects.

Due to the coupling between the Dicke states of different symmetry, the many-wave function is no more restricted to the fully symmetrical Dicke states as it was the case in the section 5.1.3. Consequently, the Dicke states which are populated during the excitation/interaction process are a-priori very numerous. In our model, to derive computable equations, we made approximation leading to consider only few states per level of excitations.

The equations of our cooperative model are derived in three steps. We first treat the laser excitation of the fully-symmetrical Dicke states. Then, for each level of excitations, we calculate the coupling between the fully symmetrical Dicke state and the states with other symmetry. Finally we treat perturbatively the excitation of the non-symmetrical Dicke states.

Whereas the Dicke basis is well adapted to deal with the laser excitation due to its properties of symmetry it is not well adapted to deal with the Rydberg-Rydberg interactions. On the other hand, the atomic basis is very well adapted to deal with the Rydberg-Rydberg interaction since the interaction Hamiltonian is diagonal in the atomic basis.

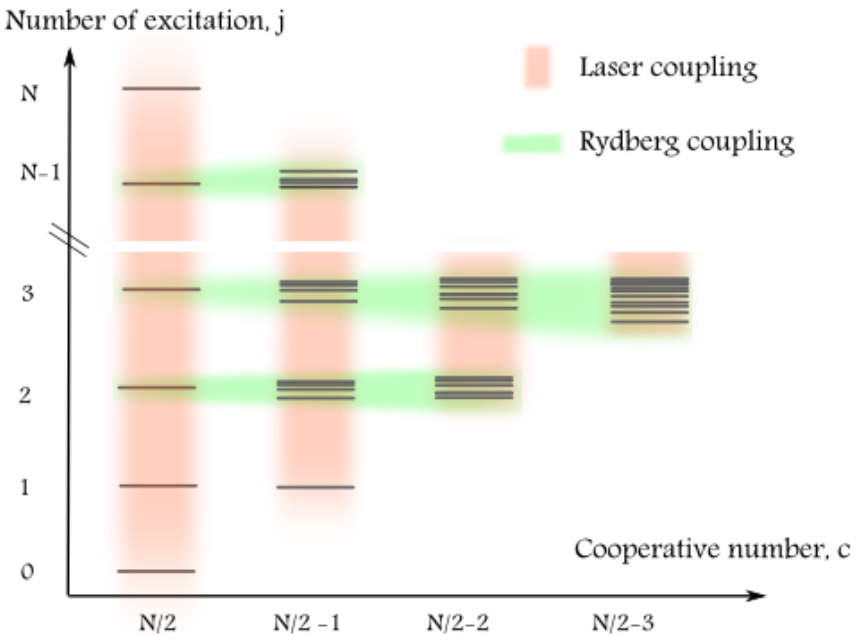

Figure 5.3: Dicke states in the case of interacting particles. An electromagnetic field acts independently in each subset of states with the same symmetry (vertically), the Rydberg-Rydberg interaction coupled the states with the same number of excitation (horizontally). States with same j and c are no more degenerated in energy due to the Rydberg-Rydberg interactions.

Consequently, in our model, to calculate the coupling between the fully symmetrical states and the states with other symmetry, we work with a special basis which contain, for each level of excitation, the symmetrical Dicke state and slightly modified atomic states. The fact to switch back and for from the Dicke basis to this modified atomic basis makes the derivation of the equations not very easy to follow. Nevertheless, the calculations done in the modified atomic basis are very interesting in the frame of the modeling of interacting gases and constitute a central point of our collective model.

The derived equation are not linked to a particular atomic sample (where we define the position of each atoms) but corresponds to an average case. The calculations presented here are done in a case of a 3-dimensional sample with a uniform density, neglecting edges effects and with isotropic Van-der-Waals interactions. Nevertheless, it is possible to model samples with different geometries and interaction potentials with the same treatment.
The equations of the model are reasonably computable for $j < 100$ and there is no restriction on the total number of atoms except $N \gg j$.

5.2.1 Hamiltonian and interaction parameter

The Hamiltonian of the system that we model is the one given in the equation 1.42

$$H = -\hbar\delta\sum_{i=1}^{N}\hat{\sigma}_{rr}^{i} + \frac{\hbar\Omega}{2}\sum_{i=1}^{N}\left[\hat{\sigma}_{gr}^{i} + \hat{\sigma}_{rg}^{i}\right] + \sum_{i=1,j<i}^{N} V_{ij}\hat{\sigma}_{rr}^{i}\hat{\sigma}_{rr}^{j}$$

The conditions of validity of this Hamiltonian have been discussed in the section 1.4.1 of the chapter 1.
In this Hamiltonian, the relative phase of the laser at the position of the atoms is skip out. For reason of simplicity, we stay with this description. Consequently, we should also remove the phase factor from the definition of the collective Dicke states.

In the derivation of the model, the Rydberg-Rydberg interactions will appears in the equation through only one parameter η.
Physically, η is the interaction energy between one atom in the Rydberg state and all the other atoms taken one by one in the Rydberg state. The calculation of η is discussed in the appendix C.1, we take

$$\eta = \sum_{q=1}^{N-1} V(R_q) \tag{5.17}$$

Where R_q is the most probable distance between one atom and its q^{th} neighbor given by the Erlang distribution. $V(R) = C_6/R^6$ is the Rydberg-Rydberg interaction potential. η depends then of the C_6 coefficient and the density of the gas.

5.2.2 Laser excitation of the fully symmetrical Dicke states

In this section, as a first step toward the resolution of the problem, we derive an equation for the laser excitation of the fully symmetrical Dicke states.
This situation is similar to the one presented in the section 5.1.3 except that we take in account the interaction energy of the symmetrical Dicke states. However, we neglect for now the coupling due to the Rydberg-Rydberg interactions between the states with the same number of excitations.
Since the symmetry of the states is conserved by the laser excitation, starting from the ground state which is fully symmetric, only the fully symmetrical states $|j, s\rangle$ are populated. The wave function of the system is then written as

$$|\Psi(t)\rangle = \sum_{j=0}^{N} a_j(t)\,|j,s\rangle \tag{5.18}$$

Under this approximation, the only effect of Rydberg-Rydberg interaction $\hat{V} = \sum_{i=1,j<i}^{N} V_{ij}\hat{\sigma}_{RR}^{i}\hat{\sigma}_{RR}^{j}$ is to shift the energy levels of the fully symmetrical states. We note $W^{(j)} = \langle j,s|\,\hat{V}\,|j,s\rangle$ the interaction energy of states $|j,s\rangle$. As shown in the appendix C.1, we can take

$$\langle j,s|\,\hat{V}\,|j,s\rangle = W^{(j)} = \frac{j(j-1)}{2(N-1)}\eta \tag{5.19}$$

As explain in the section 5.1.3, the laser coupling $\hat{H}_L = \frac{\Omega}{2}\sum_{i=1}^{N}\left[\hat{\sigma}_{gR}^{i} + \hat{\sigma}_{Rg}^{i}\right]$ between two adjacent fully symmetrical states is given by

$$\langle j,s|\,\hat{H}_L\,|j+1,s\rangle = \frac{\Omega}{2}\sqrt{(N-j)(j+1)} \tag{5.20}$$

From this, the equation of evolution of $|\Psi(t)\rangle$ with respect to the Hamiltonian of the equation 5.17 can be written as a system of coupled equations given by

$$\begin{aligned} i\frac{da_j}{dt} &= -\delta j a_j + W^{(j)} a_j \\ &\quad + \sqrt{(N-j)(j+1)}\frac{\Omega}{2}a_{j+1} \\ &\quad + \sqrt{(N-j+1)\,j}\frac{\Omega}{2}a_{j-1} \end{aligned} \tag{5.21}$$

5.2.3 Inclusion of the Van-der-Waals coupling

We will now consider the coupling due to the Rydberg-Rydberg interactions between a fully symmetrical state and other states having the same number of excitation.
Whereas the Dicke collective states are very useful for the treatment of the laser excitation due to the conservation of the symmetry, they are not very convenient to treat the Rydberg-Rydberg interaction, by contrast, atomic states $|j,q\rangle$ are them very well adapted because they diagonalize the Rydberg-Rydberg interaction. In our model, we built a special basis, idea being to use atomic states while keeping the fully symmetrical Dicke state.
The construction of this basis is given in the appendix C.2, the basis contains the state $|j,s\rangle$ and

$M^{(j)}-1$ states noted $|j,\widetilde{q}\rangle$ which are quasi identical to the atomic states $|j,q\rangle$.
Using this basis, the wave function of the system is written as

$$|\Psi(t)\rangle=\sum_{j=0}^{N}\left(a_j(t)|j,s\rangle+\sum_{q=1}^{M^{(j)}-1}b_{j\widetilde{q}}(t)|j,\widetilde{q}\rangle\right) \tag{5.22}$$

The Hilbert space in which evolves this wave function is the full space of the many-body system.
By neglecting the laser excitation of the non fully symmetrical Dicke states, the equation of evolution of $|\Psi(t)\rangle$ according to the Hamiltonian of the equation 5.17 is written as the following system of coupled equations

$$\begin{aligned} i\frac{da_j}{dt} &= -\delta j a_j+W^{(j)}a_j \\ &\quad+\sqrt{(N-j)(j+1)}\frac{\Omega}{2}a_{j+1} \\ &\quad+\sqrt{(N-j+1)j}\frac{\Omega}{2}a_{j-1} \\ &\quad+\sum_{\widetilde{q}=1}^{M^{(j)}-1}W^{(j)}_{s\widetilde{q}}b_{j\widetilde{q}} \end{aligned} \tag{5.23}$$

$$i\frac{db_{j\widetilde{q}}}{dt}=\left(-\delta j+W^{(j)}_{qq}\right)b_{j\widetilde{q}}+W^{(j)}_{s\widetilde{q}}a_j \tag{5.24}$$

Where $W^{(j)}_{qq}$ is the interaction energy of the atomic state $|j,q\rangle$ associated to $\left|j,\widetilde{q}\right\rangle$ and $W^{(j)}_{s\widetilde{q}}=\langle j,s|V|j,\widetilde{q}\rangle=\frac{1}{\sqrt{M^{(j)}}}\left[W^{(j)}_{qq}-W^{(j)}\right]$ (see ()).
Since the true atomic states $|j,q\rangle$ will no more appear and that the link between $|j,\widetilde{q}\rangle$ and $|j,q\rangle$ is well specified, we replace in the following $\widetilde{q}$ by q to simplify the notation.
The above system of equation can be formally transformed in a system of integrodifferential equations as derived in the appendix C.3.

$$i\quad\frac{da_j}{dt}=-\delta j a_j+W^{(j)}a_j \tag{5.25}$$

$$+\sqrt{(N-i)(i+1)}\frac{\Omega}{2}a_{j+1}+\sqrt{(N-j+1)j}\frac{\Omega}{2}a_{j-1} \tag{5.26}$$

$$+\int_0^t f^{(j)}(\tau)\exp(i\delta j\tau)a_j(t-\tau)\,d\tau$$

Where we define the correlation function $f^{(j)}$ as

$$f^{(j)}(\tau) = \sum_q \frac{1}{M^{(j)}} \left[\left[W_{qq}^{(j)2} - 2W_{qq}^{(j)} W^{(j)} + W^{(j)2} \right] \exp\left(-iW_{qq}^{(j)}\tau\right) \right] \tag{5.27}$$

This transformation is, up to now, exact. We show in the appendix C.4 that, under approximations based on time-scales considerations, valid for $j \ll N$, the correlation functions can be written in a very simple manner as the sum of a constant term and a Dirac term.

$$f^{(j)}(\tau) \approx W^{(j)2} - iW^{(j)}\delta(\tau) \tag{5.28}$$

Using this expression, the integrodifferential equations system becomes

$$\begin{aligned} i\frac{da_j}{dt} &= -\delta j a_j \\ &\quad + \sqrt{(N-i)(i+1)}\frac{\Omega}{2} a_{j+1} \\ &\quad + \sqrt{(N-j+1)j}\frac{\Omega}{2} a_{j-1} \\ &\quad - iW^{(j)2} \int_0^t \exp(i\delta j\tau)\, a_j(t-\tau)\, d\tau \end{aligned} \tag{5.29}$$

Doing the inverse transformation which is presented in the appendix C.3, we can rewrite this system by introducing for each level of excitation a state $|j, ns\rangle$. This single state describes the ensemble of non-fully symmetrical states with j excitations.
The equation of evolution becomes

$$\begin{aligned} i\frac{da_j}{dt} &= -\delta j a_j \\ &\quad + \sqrt{(N-j)(j+1)}\frac{\Omega}{2} a_{j+1} \\ &\quad + \sqrt{(N-j+1)j}\frac{\Omega}{2} a_{j-1} \\ &\quad + W^{(j)} c_j \\ i\frac{dc_j}{dt} &= -\delta j c_j + W^{(j)} a_j \end{aligned} \tag{5.30}$$

The wave function takes the form

$$|\Psi(t)\rangle = \sum_{j=0}^{N} \left(a_j(t)\,|j,s\rangle + c_j(t)\,|j,ns\rangle\right) \tag{5.31}$$

In considering the effect of Rydberg-Rydberg interactions, we see that for each level of excitation, a superposition of the fully symmetrical state $|j,s\rangle$ and states with other symmetry described by $|j,ns\rangle$ is excited. A remarkable point is that the interaction energy $W^{(j)}$ of the state $|j,s\rangle$ present in the equation 5.21 is now totally compensated and is replaced by a coupling with $|j,ns\rangle$. This leads to a symmetric line shape of the Rydberg excitation as we can observe experimentally [Singer et al., 2004; Pritchard et al., 2010; Viteau et al., 2012].
The physical interpretation is that the states which are populated in the system are, for each level of excitation, the fully symmetrical state at which is subtracted strongly interacting atomic states. Those states are indeed not or only very slightly "Rydberg shifted".

5.2.4 Laser excitation of the non-fully symmetrical states

The equation equation 5.30 describes the situation were laser excitations of non-fully symmetrical states is totally neglected. The last part of our theoretical development is to include such excitations.
In the equation 5.30, non-fully symmetrical states are described by one state $|j,ns\rangle$. In our model, we assume that this state is essentially a superposition of Dicke states with the minimum degree of symmetry. In the Dicke formalism, it corresponds to states with a cooperative number c equal to $\left(\frac{N}{2}-j\right)$. This is justified by the fact that those states are much more numerous than states with other symmetry. Indeed, among the $M^{(j)} = \binom{N}{j}$ states with j excitations, the number of states with cooperative number not equal to $\left(\frac{N}{2}-j\right)$ is $\binom{N}{j-1}$, it is a very small proportion as long as we have $j \ll \frac{N+1}{2}$ which is true in the case of hardly blockaded ensemble.
The states with a minimum degree of symmetry have a very interesting property with respect to the laser excitation. They are coupled with states having j+1 excitations but are not coupled with states having j-1 excitations since this subset does not contain states with the right symmetry.
Therefore, the states $|j,ns\rangle$ assumed to be states with the minimum degree of symmetry noted in the Dicke formalism $\left|j, c=\frac{N}{2}-j\right\rangle$ are, under the effect of the laser, only coupled toward the states of the form $\left|j+1, c=\frac{N}{2}-j\right\rangle$. The Rydberg-Rydberg interactions will then essentially coupled those states with the states of the form $\left|j+1, c=\frac{N}{2}-(j+1)\right\rangle$ which are, again, the most numerous in the $j+1$ excitations subset.

In our model, we describe this two steps process (excitation + coupling) by one perturbative laser excitation, we define for that a new kind of state, noted $|j, NS\rangle$, which are also a superposition of states with the minimum degree of symmetry. We consider that the population of the state $|j, ns\rangle$ is perturbativelly transfered to the state $|j+1, NS\rangle$ and we consider that once a state $|j, NS\rangle$ is populated, its population is transfered to the state $|j+1, NS\rangle$. For simplicity, for those two transfers, we take the same rate $\Gamma^{(j)}$

$$\Gamma^{(j)} = \frac{\Omega^2 (N-2j)}{4} \times \left[\frac{\frac{\Delta\omega}{2}}{\frac{\Delta\omega^2}{4} + \left(\delta - j\frac{\eta}{N-1}\right)^2} + \frac{\frac{\Delta\omega}{2}}{\frac{\Delta\omega^2}{4} + \left(\delta + j\frac{\eta}{N-1}\right)^2} \right] \tag{5.32}$$

Here, the perturbative laser excitation is temporally limited by the linewidth of the laser $\Delta\omega$. We consider that the Rabi frequency associated to this excitation is the one of the excitation of the states with minimum cooperative number given by $\Omega\sqrt{N-2j}$ [Dicke, 1954] and we consider that the additional detuning between level j and $(j+1)$ due to Rydberg-Rydberg interactions is $j\frac{\eta}{N-1}$ which is the energy difference between $|j, s\rangle$ and $|j+1, s\rangle$. In the equation 5.32, the rate is symmetrized. We use this rate in order to keep the symmetry of the system in relation to the laser detuning which is present in the equations until this last step. Nevertheless, we have also solved the equations of our model in using a non-symmetrized rate, written in this case

$$\Gamma^{(j)} = \frac{\Omega^2 (N-2j)}{4} \times \left[\frac{\frac{\Delta\omega}{2}}{\frac{\Delta\omega^2}{4} + \left(-\delta + j\frac{\eta}{N-1}\right)^2} \right] \tag{5.33}$$

According to this treatment of the laser excitation of the non-symmetrical states, the wave function of the system takes the form

$$|\Psi(t)\rangle = \sum_{j=0}^{N} \left(a_j(t) |j, s\rangle + c_j(t) |j, ns\rangle + d_j(t) |j, NS\rangle \right) \tag{5.34}$$

We can express the equation of evolution of the system by adding the perturbative laser excitation to the equation 5.30. We use population equations for the states $|j, NS\rangle$, for that we define $\rho_j = |d_j|^2$.

$$
\begin{aligned}
i\frac{da_j}{dt} &= -\delta j a_j \\
&\quad +\sqrt{(N-j)\,(j+1)}\frac{\Omega}{2}a_{j+1} \\
&\quad +\sqrt{(N-j+1)\,j}\frac{\Omega}{2}a_{j-1} \\
&\quad +W^{(j)}c_j \\
i\frac{dc_j}{dt} &= -\delta j c_j + W^{(j)}a_j - i\frac{\Gamma_j}{2}c_j \\
\frac{d\rho_j}{dt} &= \Gamma_{j-1}\left|c_{j-1}\right|^2 + \Gamma_{j-1}\rho_{j-1} - \Gamma_j\rho_j
\end{aligned}
\tag{5.35}
$$

We present in the fig 5.4 a schematic description of this equations.

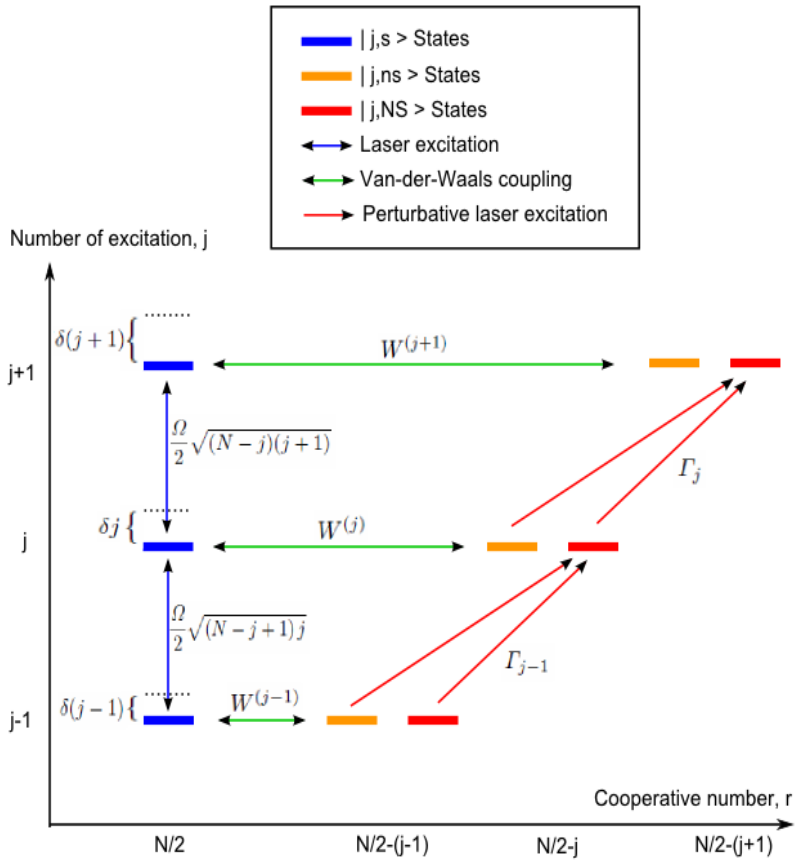

Figure 5.4: Schematic description of the cooperative model equations

The equations 5.35 are the final equations of our cooperative model. As the system is

describes by 3 states per level of excitation, those equations consist in a system of $3N_{max}$ coupled differential equations where N_{max} is the maximum number of excitations which can be present in the system. This system is then very reasonably computable.

5.2.5 Results of our cooperative model

In this section we present the results of our cooperative model. Once the equations 5.35 solved, we calculate two quantities, the mean number of Rydberg excitations present in the system, $n(t)$, and the Mandel Q factor, $Q(t)$.

$$n(t) = \sum_j \left[j \left(|a_j(t)|^2 + |c_j(t)|^2 + \rho_j(t) \right) \right] \tag{5.36}$$

$$Q(t) = \frac{\sum_j \left[j^2 \left(|a_j(t)|^2 + |c_j(t)|^2 + \rho_j(t) \right) \right] - n(t)^2}{n(t)} - 1 \tag{5.37}$$

Time dependence

In fig 5.5, we plot the results of the cooperative model for the temporal evolution of $n(t)$ and $Q(t)$. We consider a resonant excitation ($\delta = 0$). The parameters correspond to the experimental situation presented in the section 4.6.1 of the chapter 4, i.e, the number of atoms is 8000, $\Omega = 2\pi \times 40$ kHz and η is evaluated from an atomic density d =1.5 10^{10}cm^{-3} and $C_6 = -2\pi \times 7$ GHz.μm^6 which is the minimum interaction value for the $71_d 5/2$ Rydberg state.

We see in the fig 5.5 that the number of excitations present in the system exhibits a fast growing before to reach a regime where the dynamics is slow down. Concerning the Q factor, we see a quite sharp drop, Q factor going from 0 to around -0.8.
In the fig 5.6 we plot in function of the time the populations of the different states of the system. We see that the symmetrical states $|j, ns\rangle$ are first populated, there is then a transition where the excitations begin to be non-fully symmetric and $|j, ns\rangle$ populated. The steady growing regime is reached when excitations are present trough the $|j, NS\rangle$ states.

Scan of the Rydberg line

In fig 5.7 we have represented a scan of the Rydberg line. The parameters are the ones of the experimental situation presented in the section 4.6.2 of the chapter 4, i.e. the number of atoms is now 5 10^4 and the atomic density d =4 10^{10}cm^{-3}. The laser pulse duration is 300 ns.

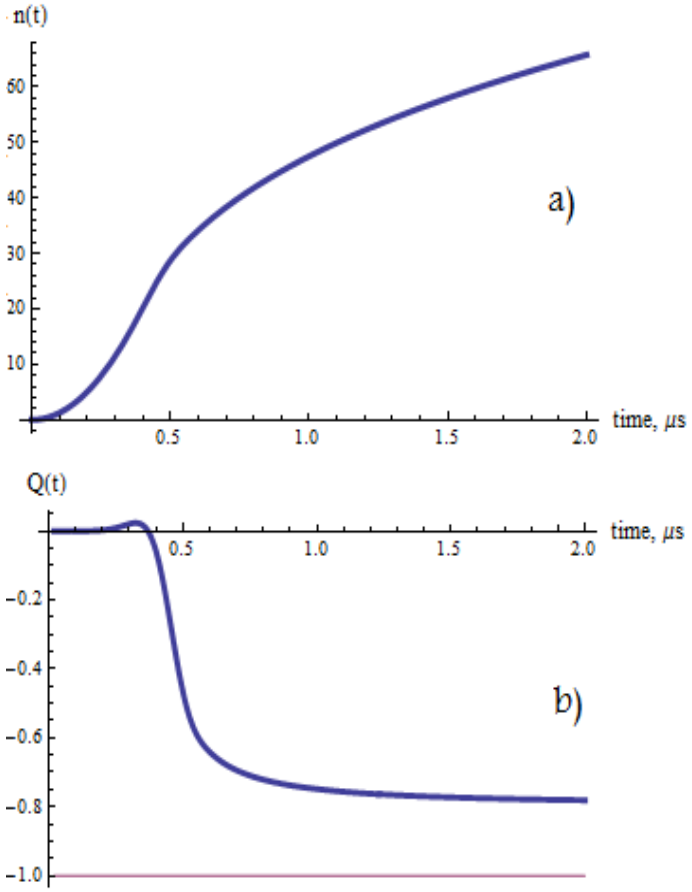

Figure 5.5: a) evolution in function of the time of n.
b) evolution in function of the time of Q, the red line $Q(t) = -1$ represents the minimum value than the Mandel Q factor can take.

The evolution of the Q factor in function of the laser detuning shows a quite interesting behavior. We first recognize the negative value of the Q factor for a laser at resonance, on the edges of the line, we see that the model predicts positive values of the Q factor. We see finally that the Q factor takes huge positive values when the number of excitation goes to zero.

We have finally performed the calculations using the perturbative excitation rate of the equation 5.33.
Results are shown in the fig 5.8. We see that the Rydberg line is now slightly asymmetric. The effects on the Q factor is much stronger. We observe the suppression of the positive values on the side corresponding to the Rydberg-Rydberg interaction sign.

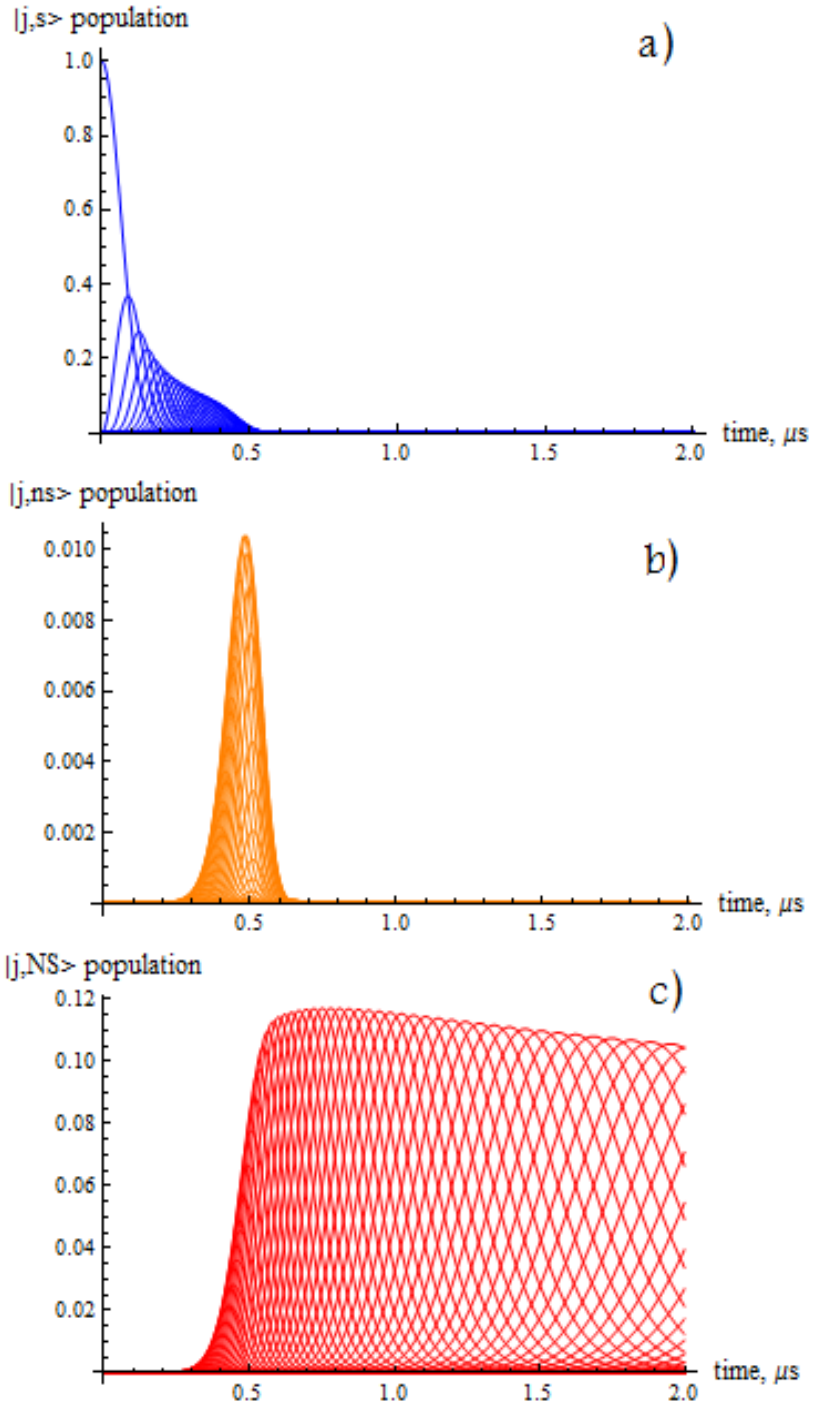

Figure 5.6: Evolution in function of the time of the $|j, s\rangle$ states populations (a); the $|j, ns\rangle$ states (b) and the $|j, NS\rangle$ states (c).

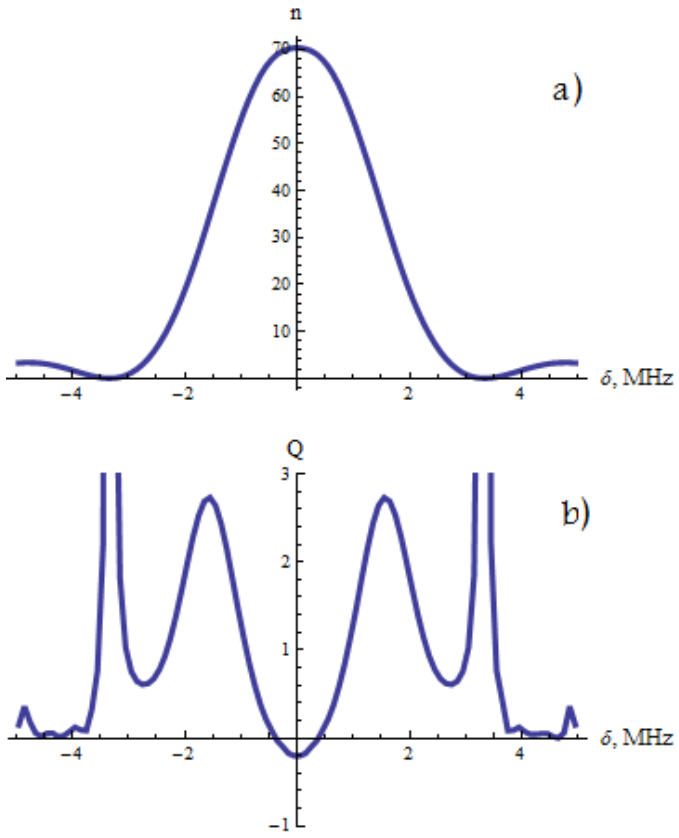

Figure 5.7: a) evolution in function of the detuning of n.
b) evolution in function of the detuning of Q. Those results are obtained using symmetrized rates for the perturbative excitations

5.2.6 Comparison with experimental data

In fig 5.9 we compare the results of the model with the experimental data presented in the chapter 4. We find on the fig 5.9 a good quantitative agreement between the model and the experiments.

A so good agreement between the model and the experiments is in fact quite surprising since we know that the model does not match perfectly the physical system. As a main limitation, the way to deal with the laser excitation of non symmetrical states is not fully rigorous and we show in the section 5.2.7 that it enhanced the blockade effect. On the other hand, the Zeeman structure associated to the l =d state investigated experimentally is not present in the model. The C_6 coefficient taken into account corresponds to the one of the less interacting potential curve whereas it seems that it is the biggest one which determine the experimental results. The very good agreement found in the

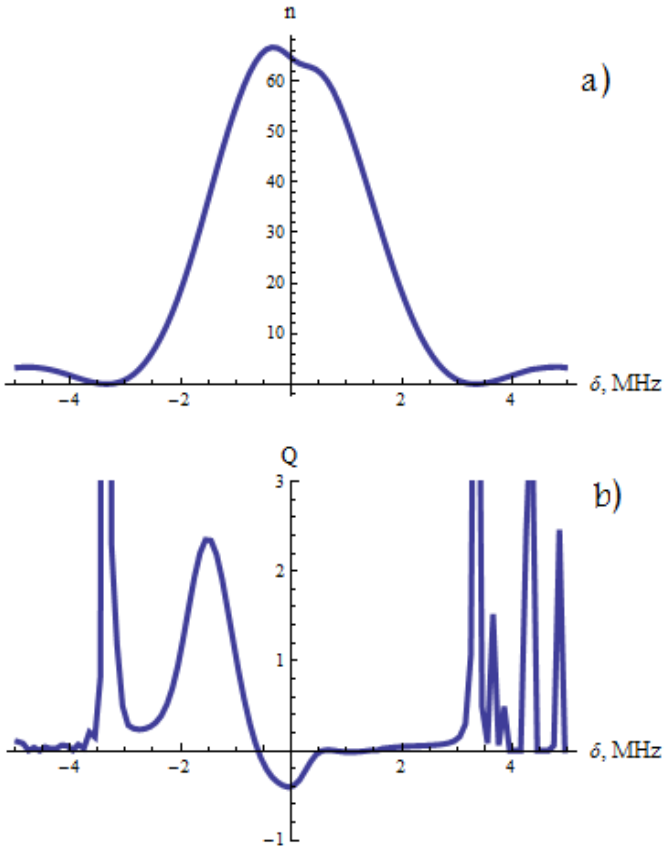

Figure 5.8: a) evolution in function of the detuning of n.
b) evolution in function of the detuning of Q. Those results are obtained using non-symmetrized rates for the perturbative excitations

fig 5.9 should be linked to a compensation of those two effects in this particular case.
Another enhancement of the agreement is related to the laser jitter which should be responsible of positive Q factor on the sides of the Rydberg line where the model already predict positive Q factor. The effect of the laser jitter on the Q factor is presented in the appendix B.
Nevertheless, the comparison of the model results with the experimental data is very promyzing. Namely concerning the general dynamics, the highly negative Q factors and the non-shifted position and the symmetry of the line.

Concerning the difference between the experimental and the modeled linewidth, it should be explained by several obvious effects which are not taken into account in the model. As a non exhaustive list, we can cite Doppler effect, Fourier broadening, presence of small electric field and laser jitter.

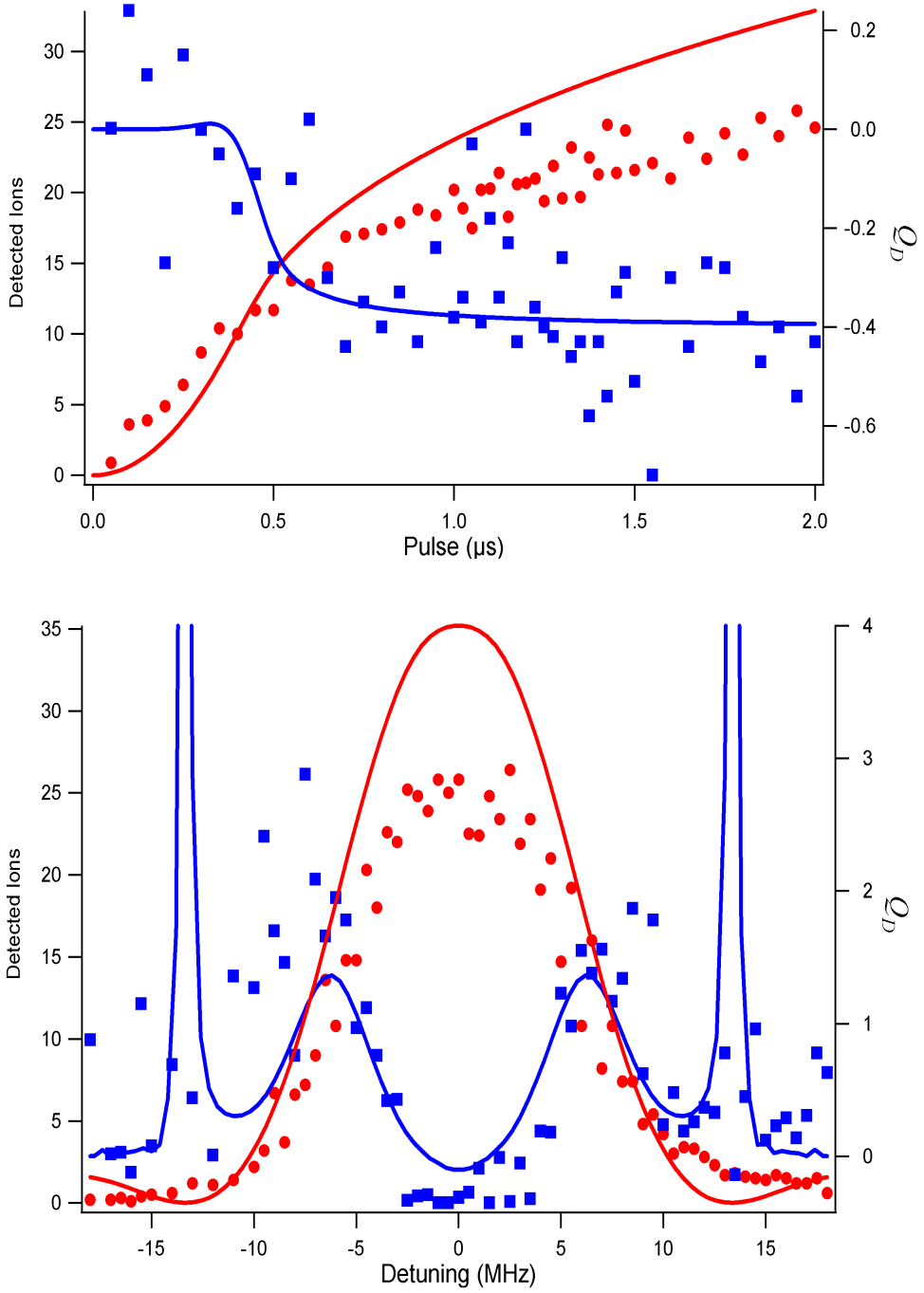

Figure 5.9: Comparison of experimental data and theoretical results for the time dependence and the scan of the line, theoretical number of Rydberg excitations and Q factor are multiplied by 0.5 to take in account the efficiency of detection of the experimental setup. We have multiplied the width of the theoretical results in the scan by a factor 4 to highlight the quantitative agreement, several explanations for this difference between theoretical and experimental widths are given in the text. On both graph, red squares are the detected ions number, blue circles are the detected Q factor.

5.2.7 Discussion and possible improvements

In this section, we come back on the approximations of the model and we discuss the physical interpretation of the results. We highlight also the important novelty that the model brings for our understanding of the interacting Rydberg gases.

The first approximation of the model comes from the treatment of the correlation functions. As mentioned in the appendix C.4, the treatment presented here corresponds to an averaged case valid for $N \gg 1$ and $j \ll N$ and it could be very interesting to look more in the details of the correlation functions.

The main approximation of the model is the treatment of the non-symmetrical states excitation. If the characteristics of the symmetrical states (collective Rabi frequencies, interaction energies and coupling with the other states) are well established, those concerning the non-symmetrical states involved in the perturbative excitation are more approximative. The fact is that the determination of those quantities is quite tricky because we use only one effective state to describe the very numerous non-symmetrical states.
However, the laser excitation of the non-symmetrical states should be highly determinant for the dynamics of the system. This is what is shown by the two first steps of the model where the Rydberg-Rydberg interactions induces a fast evolution of the system toward those states.
It seems that, in the present state of the model, the choice of the pertubative laser excitation rate leads to non enough efficient excitations of the non-symmetrical states.
To check this, we can look at the number of excitations in the saturation regime that we can expect from the simple blockade sphere picture. The physical parameters set in the model ($C_6 = 2\pi \times -7$ GHz.μm^6, $\Delta_\omega = 2\pi \times 300$kHz, N =8000 and d =1.5 10^{10} cm^{-3}) correspond to a blockade radius of around 6μm for a total volume of around 5 $10^5 \mu$m^3. This gives room to at least 300 Rydberg excitations. The results of the model exhibits clearly a lower number of Rydberg excitations (< 100 for reasonable time scale).
This could be explained by the fact that the pertubative rate is calculated for a strongly shifted transition (the shift corresponds to the difference in energy between the fully symmetrical Dicke states of the concerning levels) whereas, as in the case of the fully symmetrical states, the existence of non strongly interacting configurations in the upper level should allow non strongly shifted transitions (until a complete blockade).

Despites those approximations, the orders of magnitude of the number of Rydberg excitations, the dynamics and the Q factor predicted by the model for resonant and off-resonant excitation are quite relevent. The non-shifted position of the Rydberg line is

also a very nice feature of the model.

The model brings also a quite new insight for the modeling of interacting Rydberg gases. From the model, we can propose a physical, qualitative description of the excitation dynamics of an atomic gas toward interacting Rydberg states. This description is schematized using the Dicke basis in the fig 5.10.

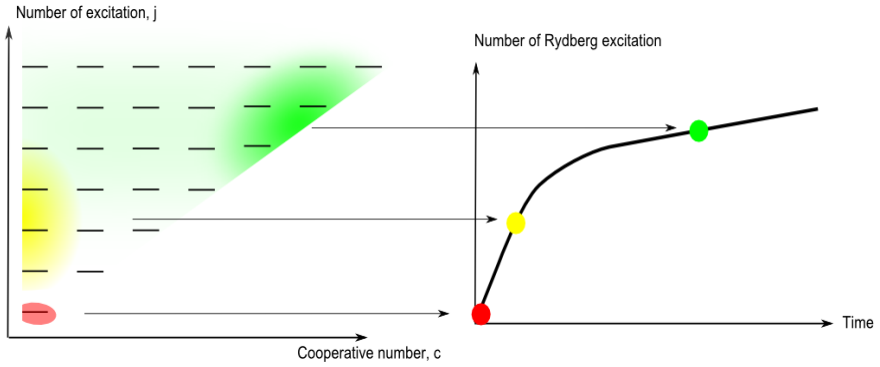

Figure 5.10: Schematic vision of the collective excitation. The colored areas give an idea of the Dicke states population at different time.

A quite intuitive physical interpretation for the laser excitation of an atomic ensemble toward Rydberg states is that the populated states, for each level of excitation, are superpositions of the atomic states which are non-blockaded. This have been already mentioned for example in [Lesanovsky, 2011] and is in fact implicites in the methods which involve a truncation of the Hilbert space according to the blockade radius.
In the Dicke basis of the whole system, the populated states are superpositions of the fully symmetrical Dicke state and states with other symmetries.

When only few Rydberg excitations are present in the system, the interaction energies corresponding to the different configurations are basically small. The coupling toward the non-symmetrical Dicke states is then weak and the Rydberg excitation is mainly present through the fully-symmetrical Dicke states. Also, in this regime, the laser excitation is more favorable at resonance since the largest part of the configuration are almost non-shifted (for one excitation they are all exactly non shifted). This last point explains the non-shifted position of the Rydberg line observed experimentally.
On the other hand, when the number of Rydberg excitation becomes important, the interaction energies corresponding to the different configuration are also important. consequently, the coupling toward the non-symmetrical Dicke states is strong and the Rydberg excitation should be mainly present trough non-symmetrical Dicke states.

The fact that the Dicke states with the minimum of symmetry are first the most numerous and secondly non coupled to states containing less excitations should then have a strong effect on the excitation dynamics, namely with the appearance of highly negative Q factor. Indeed, as soon as the raising of the excitation would be slow down, due to the population of non-symmetrical Dicke states and the associated restricted deexcitation, the wave function of the system would be (at least partially) accumulated in the corresponding levels.

In our model, the reduction of the excitation raising speed and the highly negative values of the Q factor come together with the pertubative laser excitation. Even if the associated parameters set in the presented equations are found to anticipate the blockade effect, this behavior should appears in any case when the blockade would be effective. Nevertheless, it is clear that in the present state of the model, this effect is enhanced in assuming that the symmetrical Dicke states are coupled only to states having the minimum degree of symmetry. Although this is strongly indicated when looking at the number of states having the minimum cooperative number, the real wave function has for sure non null components relative to the other states leading to a more complex dynamics.

The only way to access properly the full dynamics would be to write down more precisely the states which are populated. In the methods using the perfect blockade approximation, this is done using an enumeration of the configurations which are blockaded (or not blockaded).
This is briefly discussed in the section 5.3 in the frame of the Dicke collective states.

In comparison to those methods, a very interesting point of the cooperative model is that "ab-initio" evaluation of quantities like the blockade radius or the number of blockaded configuration is not involved. The collective Rabi frequencies present in the model come from the total number of atoms and the number of Rydberg excitations, also the blockade effect is present through a dynamical coupling between the symmetrical states and states with other symmetries. This feature of the cooperative model comes from the use of the master integrodifferential equation and the treatment of the correlation functions.
In future work, we should compare the model predictions with other experimental situations in particular with l =s states to determine in which conditions this treatment is valid and until which point can we extract reliable results from it.

5.3 "Blockaded" Dicke basis

In this section, we study, using the Dicke collective states, some mechanisms linked to the excitation of an interacting Rydberg ensemble. Some simple situations are investigated. The purpose of this section is to point out that the Dicke collective states can be use as a quite general formalism to deal with interacting Rydberg gases. We also make some links with other theoretical developments.

5.3.1 Step of excitation

In this section we study the situation corresponding to one step of laser excitation of a fully symmetrical Dicke state in a simplified case. We treat the problem in the Dicke basis and we show that it can be well understood in another basis that we call the blockaded Dicke basis. We make also a link with the equations of our cooperative model.

We consider that initially the system is in the fully symmetrical Dicke state with j-1 excitations $|j-1,s\rangle$. We study the laser excitation of $|j-1,s\rangle$ toward the fully symmetrical Dicke state with j excitations $|j,s\rangle$. We note $\langle j-1,s|\hat{H}_L|j,s\rangle = \Omega_c$ the laser coupling between those two states.
Looking at the states containing j excitations, we consider that there is in total M configurations (atomic states). We consider that B configurations have an interaction energy equal to W, we call those configurations the blockaded configurations and we note them $|a_{bi}\rangle$, $i \in [\![1;B]\!]$. We consider that the $M-B$ other configurations have an interaction energy equal to 0, we call them the non-blockaded configurations and we note them $|a_i\rangle$, $i \in [\![1;M-B]\!]$.
Formally, defining an interaction Hamiltonian, $\hat{H}_{int}$ (diagonal in the atomic basis) the latter considerations can be written as $\langle a_{bi}|\hat{H}_{int}|a_{bi}\rangle = W$ and $\langle a_i|\hat{H}_{int}|a_i\rangle = 0$.

The fully symmetrical Dicke state with j excitation $|j,s\rangle$ is by definition

$$|j,s\rangle = \frac{1}{\sqrt{M}}\left(\sum_{i=1}^{M-B}|a_i\rangle + \sum_{i=1}^{B}|a_{bi}\rangle\right) \tag{5.38}$$

We define the non-fully symmetrical collective state $|j,ns\rangle$ as

$$|j,ns\rangle = \frac{1}{\sqrt{M\beta(1-\beta)}}\left(\beta\sum_{i=1}^{M-B}|a_i\rangle - (1-\beta)\sum_{i=1}^{B}|a_{bi}\rangle\right) \tag{5.39}$$

Where $\beta = \frac{B}{M}$ is the fraction of blockaded configurations.

The state $|j, ns\rangle$ is normalized and orthogonal with $|j, s\rangle$. Since we are dealing with Dicke state we have $\langle j-1, s|\hat{H}_L|j, ns\rangle = 0$. We can show that it exists no other states orthogonal to $|j, s\rangle$ and $|j, ns\rangle$ coupled to them by $\hat{H}_{int}$.
We have

$$\begin{aligned}
\langle j, s|\hat{H}_{int}|j, s\rangle &= \beta W && (5.40)\\
\langle j, ns|\hat{H}_{int}|j, ns\rangle &= (1-\beta)W && (5.41)\\
\langle j, s|\hat{H}_{int}|j, ns\rangle &= -\sqrt{\beta(1-\beta)}W && (5.42)\\
& && (5.43)
\end{aligned}$$

The interaction Hamiltonian $\hat{H}_{int}$ in the basis $\{|j, s\rangle, |j, ns\rangle\}$ is then written as

$$\hat{H}_{int} = \begin{pmatrix} \beta W & \text{-}\sqrt{\beta(1-\beta)}W \\ \text{-}\sqrt{\beta(1-\beta)}W & \text{(1-}\beta\text{)}W \end{pmatrix} \tag{5.44}$$

We can diagonalize this Hamiltonian. The eigenstates are two collective states (which are not Dicke states) that we note $|A\rangle$ and $|A_b\rangle$ written as

$$|A\rangle = \frac{1}{\sqrt{M-B}} \sum_{i=1}^{M-B} |a_i\rangle \tag{5.45}$$

$$|A_b\rangle = \frac{1}{\sqrt{B}} \sum_{i=1}^{B} |a_{bi}\rangle \tag{5.46}$$

Those two states are respectively the symmetrical superposition of all the non-blockaded configurations and of all the blockaded configurations. There energies are respectively 0 and W and we have $|A\rangle = \sqrt{1-\beta}|j, s\rangle + \sqrt{\beta}|j, ns\rangle$ and $|A_b\rangle = \sqrt{\beta}|j, s\rangle - \sqrt{1-\beta}|j, ns\rangle$.

The total Hamiltonian of the system $\hat{H} = \hat{H}_L + \hat{H}_{int}$ is written in the basis $\{|j-1, s\rangle, |j, s\rangle, |j, ns\rangle\}$ as

$$\hat{H} = \begin{pmatrix} 0 & \Omega_c & 0 \\ \Omega_c & \beta W & \text{-}\sqrt{\beta(1-\beta)}W \\ 0 & \text{-}\sqrt{\beta(1-\beta)}W & \text{(1-}\beta\text{)}W \end{pmatrix} \tag{5.47}$$

In the basis $\{|j-1, s\rangle, |A\rangle, |A_b\rangle\}$, $\hat{H}$ as

$$\hat{H} = \begin{pmatrix} 0 & \sqrt{1-\beta}\Omega_c & \sqrt{\beta}\Omega_c \\ \sqrt{1-\beta}\Omega_c & 0 & 0 \\ \sqrt{\beta}\Omega_c & 0 & \mathrm{W} \end{pmatrix} \tag{5.48}$$

Those formal calculations show how from a fully symmetrical Dicke state $|j-1,s\rangle$ the laser excites, if it exists, a non-interacting (non-shifted) superposition of the upper fully symmetrical Dicke state $|j,s\rangle$ and a state with another symmetry $|j,ns\rangle$. In this example the excited state is simply the symmetrical superposition of the non-blockaded configurations $|A\rangle$, it can be view as the "non-shifted part" of the fully symmetrical Dicke states. $|A_b\rangle$ is the "shifted part" of the fully symmetrical Dicke state, if the interaction energy of the blockaded configurations is sufficiently large ($W \gg \Omega_c$) it is not populated.

Formally, we can define the state $|A\rangle$ as the fully symmetrical Dicke state of a "blockaded" Dicke basis. In this blockaded Dicke basis, we have remove all the blockaded configuration (it is then equivalent to the basis formed in the methods which involves a truncation of the Hilbert space according to the blockade radius).
The laser coupling between two adjacent fully symmetrical Dicke states of the blockaded Dicke basis is reduced in comparison to the full Dicke basis by a quantity relative to the number of blockaded configurations.
In the blockaded Dicke basis, a fully symmetrical state is coupled in the upper level only with the fully symmetrical state but is not necessary coupled in the lower level only with the fully symmetrical state.

On the fig 5.11, we have schematically represented the system with the two basis used in this section

It is quite interesting to look at the treatment done in our cooperative model corresponding to the situation that we have described.
In identifying $\sqrt{(N-j)(j+1)}\Omega$ to Ω_c, we can formally translate the equation 5.30 of the model into an Hamiltonian $\hat{H}_{cm}$ written in the basis $\{|j-1,s\rangle, |j,s\rangle, |j,ns\rangle\}$

$$\hat{H}_{Cm} = \begin{pmatrix} 0 & \Omega_c & 0 \\ \Omega_c & 0 & \beta W \\ 0 & \beta W & 0 \end{pmatrix} \tag{5.49}$$

The Hamiltonians $\hat{H}_{cm}$ and $\hat{H}$ are not equivalent. Nevertheless, starting at $t = 0$ in the state $|j-1,s\rangle$, it appears that both Hamiltonian give the same results at short time. In the fig 5.12 we have represented the population of the three states of the system

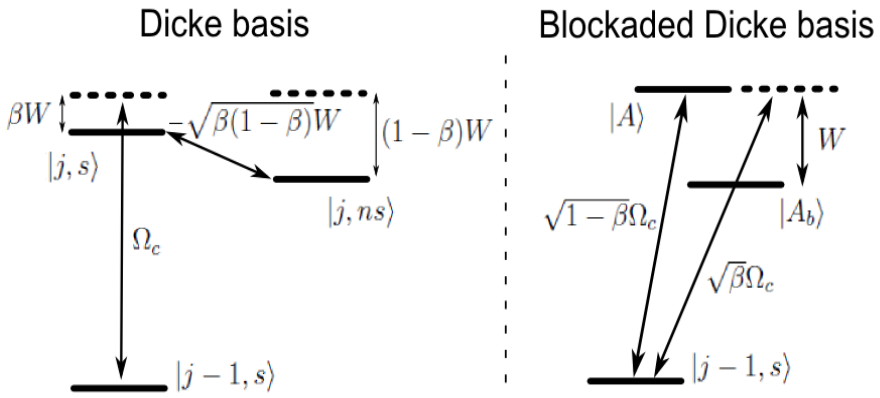

Figure 5.11: Schematic representation of the system in the two basis mentioned in the text.

in function of the time, for both Hamiltonians. The calculation are done with $\beta = \frac{3}{5}$, $\Omega_c = 2\pi \times 10^6$ and $W = 2\pi \times 10^7$. Those values of Ω_c and W corresponds to reasonable experimental values of collective Rabi frequency and interaction between Rydberg atoms.

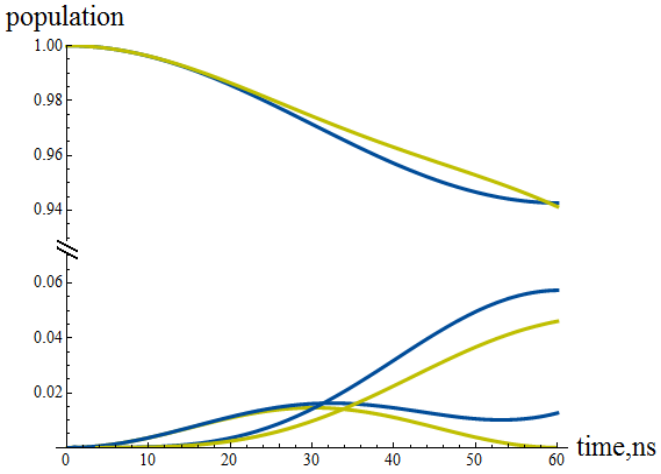

Figure 5.12: Population of the three states of the system in function of the time starting in $|j-1,s\rangle$ at $t = 0$. The cooperative model Hamiltonian $\hat{H}_{cm}$ gives the blue curves. The Hamiltonian $\hat{H}$ gives the yellow curves.

The calculations presented in the fig 5.12 corresponds to one step of excitation taken as a close three-levels system. We see that the equations of the cooperative model describes correctly the system at short time (in this example for $t \leq 25$ ns). Nevertheless,

bigger is the interaction energy, shorter is the time at which the results start to be different.
In this example, it has been possible to determine explicitely the populated Dicke states. In the case where the interaction energies are "randomly" distributed, it would not have been so simple. We see here the powerful treatment applied in the cooperative model which allows to consider this "non-shifted" step of laser excitation in a general case (in fact a continuous case, see appendix C.4).

5.3.2 "Perfect blockade" of a single lattice site, Super Atom picture

In this section, we study a quite simple situation. We consider that the atomic sample is composed by several atomic packets in condition of single packet perfect blockade. This corresponds concretely to a lattice with very large lattice spacing and very strong confinement of each packets or more generally to small atomic packets well separated from each other (compare to the blockade radius). We consider an ensemble of N_s packets composed by N_0 atoms. In this situation, we know that each packets should behave like a Super Atom and do in-phase Rabi oscillations at the collective Rabi frequency $\sqrt{N_0}\Omega$.
Nevertheless, we treat the problem in the blockaded Dicke basis. Here, the "symmetry" of the system is such that within each level of excitation, all the non-blockaded configurations are completely equivalent. This leads to the fact that only the fully symmetrical states of the blockaded Dicke basis will be populated if the system is initially in the ground state. We note $|j, sb\rangle$ the fully symmetrical states of the blockaded Dicke basis.

By an enumeration of the non-blockaded configuration (no more than 1 excitation whithin the same packet) we can calculate the number of configurations $M_b^{(j)}$ that each state $|j, sb\rangle$ contains

$$M_b^{(j)} = \frac{1}{j(j-1)} \prod_{i=1}^{j} N_0(N_s - j + 1) \tag{5.50}$$

As it is done in the section 5.1.3 we can determine the "collective" Rabi frequency associated to the laser coupling $\hat{H}_L = \frac{\Omega}{2} \sum_{i=1}^{N} \left[\hat{\sigma}_{gr}^i \mathrm{e}^{i\vec{k}.\vec{R}_i} + \hat{\sigma}_{rg}^i \mathrm{e}^{-i\vec{k}.\vec{R}_i} \right]$ between two adjacent states $|j, sb\rangle$ as following.
The state $|j, sb\rangle$ is composed by $M_b^{(j)}$ atomic states having all the weight $1/\sqrt{M_b^{(j)}}$. Each of those state are coupled with $(N_s - j)N_0$ atomic states with $j+1$ excitations. In the state $|j+1, s\rangle$ those latter atomic states have all a weight $1/\sqrt{M^{(j+1)}}$. This gives

$$\langle j, sb| \hat{H}_L |j+1, sb\rangle = \frac{\Omega}{2}\sqrt{N_0}\sqrt{(N_s - j)(j+1)} \tag{5.51}$$

As expected, the equation of evolution of the wave function in the blockaded Dicke basis is formally the same than the one of a non interacting system of N_s atoms with a single atom Rabi frequency of $\sqrt{N_0}\Omega$, i.e., an assembly of non-interacting Super Atoms. Like in the situation of the section 5.1.3, the treatment of the system in the blockaded Dicke basis gives the expected dynamics as shown in the fig 5.13

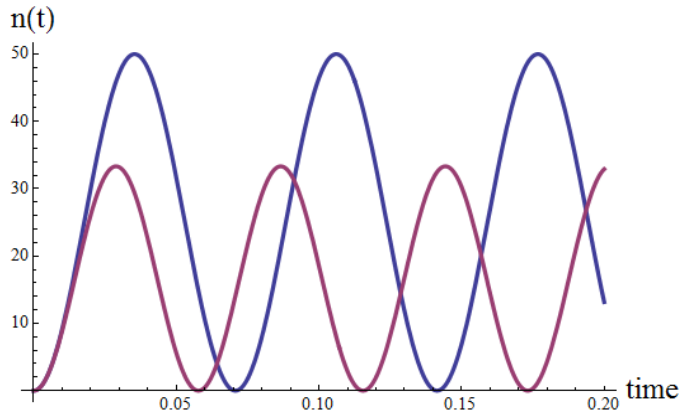

Figure 5.13: Evolution in function of the time of the total number of excitations in an ensemble of 50 identical blockaded atomic packets, each one containing 200 atoms. This evolution is given by calculations in the blockaded Dicke basis. The time is given in unit of single atom Rabi frequency Ω. The blue curve correspond to $\delta = 0$, the red curve to $\delta = 10\Omega$

In the fig 5.13, for $\delta = 0$, we see a "macroscopic" Rabi oscillation at the frequency $\sqrt{N_0}\Omega$ resulting from the in-phase Rabi oscillation of each atomic packet. Interestingly, the excitation of this system of Super Atoms is much more robust again the detuning of the laser than in the non interacting case. Since the Rabi frequency associated to the excitation of each Super-Atoms is enhanced by a factor $\sqrt{N_0}$, in comparison to the non interacting case, to get an equivalent effect of the detuning, this latter has also to be enhanced by $\sqrt{N_0}$. On the fig 5.13, we see that a detuning $\delta = 10\Omega$ leads to an excitation still greater than the half of its absolute maximum.
Concerning the Q factor, we found it to be the one expected for an assembly of independent two-levels systems doing in-phase Rabi oscillations.

5.3.3 Modeling of more complex situations

The situations of the section 5.3.1 and 5.3.2 correspond to ideal cases and we have shown that the Dicke basis allows to treat the problem completely in a quite simple way. However, for more complex situations (more realistic one), the description of the system becomes quickly very tedious without further approximations. In this section, we present in a qualitative way the modeling of interacting Rydberg gases using the blockaded Dicke basis.

We can look first at an atomic sample confined in 1-dimensional lattice in the situation of blockade between nearest neighbor. The treatment with the Dicke collective states is already hardly complexified. This holds in the fact that the non-blockaded configurations containing the same number of excitations are not all equivalent. For example, we have represented on the fig 5.14, two particular configurations containing two excitations.

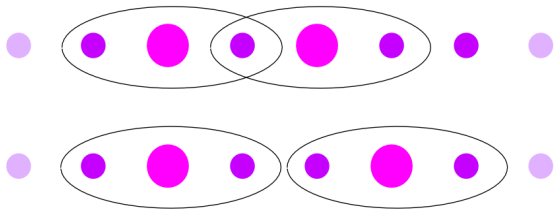

Figure 5.14: Schematic representation of an atomic ensemble in presence of lattice. A single Rydberg excitation is represented by a pink circle, an ensemble of ground state atoms by a purple circle. We have represented two configurations containing two Rydberg excitations.

The two configurations of the fig5.14 are not equivalent since they are not coupled to the same number of configurations with three excitations. In the frame of the collective states mechanisms, this leads to the fact that those two configurations will take part of two different Dicke states corresponding to the same level of excitation but having different coupling with the other states.
In the case of a ring lattice, all the configurations with one excitation are equivalent and the fully symmetrical state with one excitation is the only state of this level which would be populated. However, for a linear lattice, even the configurations with one excitation are not all equivalent. Due to the edge effects, we have to deal with the population of several Dicke states even for one excitation.

We see here that to treat correctly the problem we have to define several collective

states per level of excitations.

The treatment of 1 or 2-dimensional lattices has been largely investigated by the methods of "perfect blockade" (see section 1.4.3 of the chapter 1).
It might be possible and quite interesting to translate in the frame of the blockaded Dicke basis the techniques of configuration enumeration used in those methods. This would allow to define the proper set of Dicke collective states allowing to describe lattice systems.
For example, in those methods the treatment of the Rydberg excitations in term of quantum hard-object allows to describe the system as a so-called Tonk's gas for which the number of microcanonical states (non blockaded configurations) have been calculated (see for example [Ates and Lesanovsky, 2012]).
An other technique developed in the frame of the perfect blockade is to look at the coupling between the different configurations using graph representations (see for example [Olmos et al., 2009a]). Interestingly, in such graphs, the equivalent configurations have been already regrouped and the "translation" in terms of Dicke state should be quite easy.
The coherent thermalization of the system described by the perfect blockade models could be understood in the frame of the blockaded Dicke basis by the complex dynamics resulting from the population of several Dicke states per level of excitations.

In the following, we briefly present how the deviation from the perfect blockade approximation could be treated in the blockaded Dicke basis.
The perfect blockade approximation consists in setting to 0 the interaction energy of a non blockaded configuration, in other words, the tail of the long-range Rydberg-Rydberg interaction is neglected.
On the fig 5.15, we have drawn the situation corresponding to the experimental one presented in the section 4.5 of the chapter 4. Two particular configurations are represented.

In considering an isotropic Van-der-Waals interaction, we can calculate the ratio between the interaction energies E_{int} of the two configurations labeled $|a_1\rangle$ and $|a_2\rangle$ of the fig 5.15.

$$\frac{E_{int,|a_1\rangle}}{E_{int,|a_2\rangle}} \approx 1.7 \tag{5.52}$$

By taking $C_6 = 1$ GHz.μm^6 and 50 populated lattice sites (experimentally there is 100 lattice sites in total), the interaction energies of the two configurations are respectively around 6 and 10 MHz.
This means that those two configurations will experience a relative dephasing with a

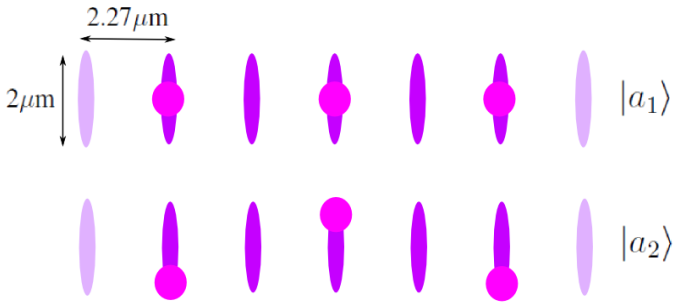

Figure 5.15: Schematic representation of the experimental atomic ensemble in presence of lattice. The Rydberg excitations are represented by the pink circles. $|a_1\rangle$ and $|a_2\rangle$ are two equivalent configurations within the perfect blockade approximation.

rate of 4 MHz. In the frame of the Dicke collective states restricted to those two configurations, this rate corresponds to the coupling between the symmetrical and the non-symmetrical states.

We see here that the collective excitations which are a-priori equivalent can experience a quite fast dephasing due to the Rydberg-Rydberg interactions.
Interestingly, we can define the upper limit for the dephasing rate τ_j between the different configurations containing j excitations. It is linked to the effective linewidth of the laser Δ_ω.

$$\tau_j = j \times \Delta_\omega \tag{5.53}$$

In the fig 5.16, we have drawn a blockaded Dicke basis where, in a completely qualitative way, we have represented the two features mentioned in this section.

The fig 5.16 represents schematically the theoretical treatment which could be operated using the blockaded Dicke basis.
In this frame, the effect of the Rydberg-Rydberg interactions is split into two effects. A pure blockade effect, taken in account through the basis itself, and a relative dephasing of the non-blockaded configurations.
In the cooperative model, those two effects are treated together. In keeping the spirit of the cooperative model for the "dephasing part" of the problem, the use of the blockaded Dicke basis could allow to write down more precisely the Dicke states which are populated.

The notion of blockaded Dicke basis seems to be quite well adapted to the interacting Rydberg gases.
We can note that by essence, a blockaded Dicke basis is equivalent to the basis used in

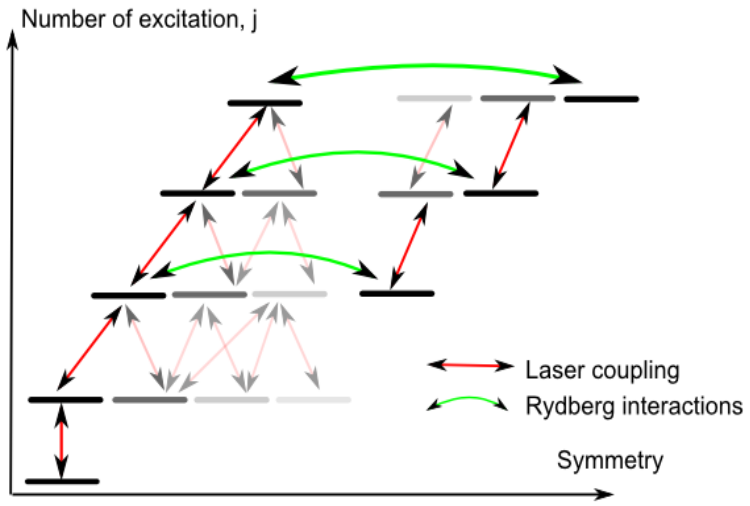

Figure 5.16: Schematic representation of the system in the frame of the blockaded Dicke Basis. We have underlined the complex dynamics resulting from the laser coupling between the basis states as well as the dynamical coupling toward poorly symmetrical states due to the Rydberg-Rydberg interactions.

the methods aiming to solve exactly the many-body Hamiltonian using a truncation of the Hilbert space according to the blockaded configurations.
Also, since it has a quite strong link with the methods of perfect blockade, it should be possible to use the expertize acquired in this frame.

A very interesting feature of the Dicke states is that several effects can be included in their definition. We have seen that the spatial phase of the excitation laser can be directly included in the Dicke states definition. In a blockaded Dicke basis, we remove the configurations which would be for sure non excited. As another illustrative example, the fully symmetrical Dicke states can be defined to take into account the laser intensity inhomogeneity. We give here the case of one excitation

$$|1,s\rangle = \frac{1}{\sqrt{\sum_{i=1}^{N}\Omega_i^2}}\frac{1}{\sqrt{N}}\sum_{i=1}^{N}\Omega_i \mathrm{e}^{-i\vec{k}.\vec{r}_i}\,|r_i\rangle \tag{5.54}$$

Where Ω_i is the Rabi frequency associated to each atom i of the sample. This state is effectively the one which is populated by the laser excitation starting from the collective ground state. For a fully blockaded ensemble, this state form a close two-level system together with the collective ground state.
Defining such a state could be useful to deal with quasi-fully blockaded ensembles.

The Dicke collective states appears also to be a quite relevant theoretical frame to deal with dephasing mechanisms. They appears in the Dicke basis as a coupling between the states with different symmetries.
The dephasing between different configurations is for example proposed in [Bariani et al., 2012] as a protocol for entanglement generation.
Interestingly, if the dephasing between the configurations is first associated to Rydberg-Rydberg interactions. It can be also related to other decoherence effects. For example, in [Bienaimé et al., 2012], authors study the possibility to find a system composed by a large number of 2-levels atoms in subradiant states (less symmetrical Dicke states) due to various decoherence effect like the Doppler effect.
In [Honer et al., 2011], the dephasing between the configurations containing 1 excitations (i.e. not due to the interactions) is involved for the implementation of photon counting devices. Authors propose for example a dephasing induced by a spatial and temporal inhomogeneity of a laser field intensity (Speckle).

In general terms, the spirit of a "Dicke treatment" for the excitation of many-body interacting systems is to define, within the many-body states, which one are naturally excited by the laser in given conditions of interactions and how much additional effects will dephase them. By calculating the relevant quantities, this treatment could be an alternative method to rate equations to obtain reliable quantitative predictions for the dipole blockade Physics.

5.4 Conclusion and outlooks

The calculations presented in this chapter put a quite new view on the strongly interacting Rydberg gases.

We have seen in this chapter that the Dicke basis allows to describe efficiently the dynamics of interacting ensembles in simple cases with the advantage to be by essence a many-body basis. We have seen for example that a fully collective description give naturally the Super Atoms picture when the sample is composed by several atomic packets.

The cooperative model that we have developed point out a new mechanism which could be quite determinant for the dynamics of strongly interacting Rydberg gases. The idea is the following, if the Rydberg-Rydberg interactions reduce the Rydberg excitation of the gas due to the blockade effect, they can also reduce its deexcitation due to symmetry

effects.
To give a "classical" equivalent to this effect we can think that once the system is close to saturation, the Rydberg excitations are almost localized in a cristal-type arrangement (in fact a superposition of them), then when one Rydberg atoms is deexcited, there is more than one ground state atoms which can be excited to refine a complete filling of the volume. The Rydberg excitations number being thus maintained to high values.
In this frame, the highly negative Q factors that have been observed experimentally can be well understood, whatever their values could be once more finely precised.

The non-shifted position of the Rydberg line in the case of strong interactions find also a good theoretical explanation in the frame of collective excitations. It is the numerical domination of the non-interacting collective states for the few first excitations which provides the best efficiency to a resonant laser excitation.

Finally we have seen that further theoretical development in the frame of the Dicke collective states could allow to describe in a quite reliable and simple way interesting behaviors of interacting Rydberg gases. Namely with the description of interactions or decoherence induced dephasing in terms of coupling between states with different symmetries.

If the theoretical developments presented in this chapter merit to be reinforced in order to reach reliable, predictive capacities, they show that the Dicke collective states should have a nice role to play in the fantastic task which is to describe the behavior of strongly interacting Rydberg gases.

General conclusion

In the frame of this thesis, a quite large range of physical situations related to Rydberg atoms and interacting Rydberg gases have been studied, both experimentally and theoretically. This diversity shows that Rydberg atoms Physics encompasses a large panel of physical effects ranging from very technical to very fundamental ones. In both cases, the wonderful properties of Rydberg atoms make them fascinating objects to study and allow for promising technological applications.

Since the different chapters of this manuscript are quite independent and have been separately concluded, we focus on this general conclusion on the main results that have been presented.

Numerical calculations allowing to access the quantum states of a pair of interacting Rydberg atoms in presence of static, uniform, external electric and magnetic field have been implemented.
The results of those calculations do not exhibit important unknown features but they allow to access the interacting pair states for very small interatomic distances what can not be done without numerical calculations. At such interatomic distances the interactions are so huge that the eigenenergies are completely disorganized. The precise knowledge of the so-called spaghetti curves in this region is important since such close pairs of atoms are present in ultra-cold atomic samples.
Various 2-body resonances can be determined as well as dipole-dipole coupling values including magnetic degeneracy or non-degeneracy.
In a general way those numerical calculations are a useful tool to get a systematical evaluation of experimental parameters.

A coherent 4-body interaction process between Rydberg atoms have been observed experimentally. This process can be formally described by the following reaction

$$4 \times 23p_{3/2} \rightarrow 2 \times 23s + 23p_{3/2} + 23d_{5/2} \tag{5.55}$$

The dipole-dipole coupling between the two 4-body quantum states is a second order coupling and comes from the coherent combination of the two reactions

$$2 \times 23p_{3/2} \rightarrow 23s + 24s \tag{5.56}$$

$$2 \times 24s \rightarrow 23p_{1/2} + 23d_{5/2} \tag{5.57}$$

This interpretation is confirmed by a quite simple model dealing with 4-body states which allows to describe successfully the process. A further confirmation comes from the enhancement of the process for a variable electric field allowing to bring successively at resonance the two 2-body processes. This latter experimental manipulation shows the possibility to control such few-body processes through the applied electric field.
This observation has been done at a quite small atomic density and shows the possibility to study phenomena involving more partners.

The first demonstration of a coherent excitation of Rydberg atoms in a 1-dimensional optical lattice has been realized. This in the blockade regime. This first experiment has not been done in the best condition to investigate precisely the underlying many-body dynamics. This holds namely with the excitation of a $l = d$ Rydberg state and a non so large lattice spacing. Nevertheless, this experiments is a proof of principle that it is possible with current experimental techniques to investigate the genuine many-body behaviors expected for such a geometrical configuration.

A highly sub-poissonian statistics of the Rydberg excitation in the regime of blockade have been observed in a 3-dimensional MOT. The measured values of the Q factor range in $-1 < Q < -0.6$ with a quite strong appetency for -1. Those observations reveal without ambiguity the collective nature of the Rydberg excitation in the regime of strong interactions.
By studying the link between Q factor and quantum projection noise, the interest to measure such a quantity to characterize many-body systems have been shown. Namely, we found that a Q factor less than -0.75 would demonstrate that atomic correlations are present at a deeper level than single collective excitations.

Finally, the excitation dynamics of interacting Rydberg gases has been investigated theoretically using the Dicke collective states. In this frame, a cooperative model has been developed. The model shows that the interactions between the atoms induce the excitation of collective states having a different symmetry than the ones naturally excited by

the laser. A mechanism of accumulation of the many-body wave function on the states with the minimum degree of symmetry has been proposed from the simple but strong argument that those states are much more numerous than the other ones. Together with the blockade itself this mechanism could strongly determine the dynamics of the system leading to natural crystal-type arrangements of the Rydberg excitations or deterministic numbers of Rydberg excitations.

Appendix A

Numerov method

In this section, we give the way to calculate the Rydberg states radial wave functions with the Numerov method. We give also more accurate form than the Coulomb potential for the radial potential.

A.1 Numerov method with variable step

The Numerov method is an iterative technique to calculate second order differential equation of the form

$$\left[\frac{d^2}{dr^2} + f(r)\right] u(r) = 0 \tag{A.1}$$

The radial Schrödinger equation is usually put on the form

$$\left[\frac{d^2}{dr^2} - \frac{l(l+1)}{r^2} + \frac{2\mu_e}{\hbar^2}(E_{nlj} - V_{eff}(r))\right] u(r) = 0 \tag{A.2}$$

Where $u(r) = rR(r)$ and $R(r)$ is the radial wave function associated to the eigenenergy E_{nlj}. $V_{eff}(r)$ is the effective potential seen by the Rydberg electron.

This equation can be solved with the classical Numerov method which gives a way to found the function $u(r)$ at different radius r_i with a constant step between two adjacent r_i.
Interestingly the use of a variable step between the r_i simplifies a lot the resolution and allows to find directly the solution of the radial wave function $R(r)$ it-self.
In all the following, the quantity are written in atomic units and we consider a Coulomb potential $V_{eff}(r) = -\frac{1}{r}$.

The set of radius r_i at which $R(r)$ is calculating is given by

$$r_i = r_0 \mathrm{e}^{-h.i} \tag{A.3}$$

Where r_0 is the larger radius at which $R(r)$ will be calculated and h a "linear" increment. We take usually

$$h = 0.01 \tag{A.4}$$
$$r_0 = 2n(n+15) \tag{A.5}$$

Where n is the principal quantum number of the Rydberg state in question.

Defining the quantity

$$g(i) = \frac{1}{r_i^2}(\frac{-1}{r_i} - E_{nlj})(l+\frac{1}{2})^2 \tag{A.6}$$

Where l is the orbital quantum number of the Rydberg state in question and E_{nlj} its energy.

We can show that the values of $R(r_i)$ are given by the recursive equation

$$R(r_i) = R(r_{i-2})(g(i-2) - \frac{12}{h^2}) + R(r_{i-1})\left(\frac{10g(i-1)+\frac{24}{h^2}}{\frac{12}{h^2}-g(i)}\right) \tag{A.7}$$

To initiate the calculation we use the fact that any Rydberg wave function has an exponential decrease at large distance. We do not care for now to the absolute value of the wave function since it will be normalized at the end of the calculations. We set thus

$$R(r_0) = 1.10^{-10} \tag{A.8}$$
$$R(r_1) = 2.10^{-10} \tag{A.9}$$

The radial wave function $R(r)$ is then calculated from $r = r_0$ to r_{min}. Since E_{nlj} is not an eigenenergy of the potential V_{eff}, the calculated radial wave function $R(r)$ start to diverges at small r. We numerically check this divergence and stop the calculations (we set r_{min}) slightly before it. We have always r_{min} of the order of 1 (the Bohr radius a_0 in atomic units) meaning that the calculations are done accurately for a very large range of distances (since the Rydberg radial wave functions have a huge spatial expansion).

The obtained radial wave function $R(r)$ is finally normalized and can be used for the

calculation of the radial matrix elements.

A.2 Other forms of the radial potential

The Coulomb potential is the most simple form for the potential seen by the Rydberg electron. Since the radial expansion of the Rydberg electron is huge, it is in fact quite accurate to use it for the calculations. Nevertheless, we can add to the Coulomb potential some terms having a well defined physical meaning.

The most important term that we can taken into account into the radial potential is the so-called core polarization term. It induces a correction V_P in the radial potential of the form

$$V_P = \frac{-\alpha_d}{2}\frac{1}{r^4} + \frac{-\alpha_q}{2}\frac{1}{r^6} + ... \tag{A.10}$$

Where α_d and α_q are the dipole and quadrupole polarizabilities of the ionic core. There values for lithium, sodium and cesium are for example given in [Gallagher, 1994].

Another term that we can taken into account in the radial potential comes from the Spin-Orbit coupling. If this latter is mostly determinant for the angular wave function, it induces also a small modification to the radial potential. In atomic units, the Hamiltonian of the Spin-Orbit coupling H_{SO} is written as

$$H_{SO} = \frac{\alpha^2}{2}\left(\frac{1}{r}\frac{dV_{eff}(r)}{dr}\right)\vec{L}.\vec{S} \tag{A.11}$$

Where α is the fine structure constant. The additional term in the radial potential due to the Spin-Orbit coupling is then for a Rydberg state nl_j

$$V_{SO}(r) = \frac{\alpha^2}{2}\frac{1}{r^3}(j(j+1) - l(l+1) - \frac{3}{4}) \tag{A.12}$$

Taken into account those two terms would lead to a more accurate expression of the effective potential. However, in [Zimmerman et al., 1979] it is shown that they leads to very small correction in the final result of the radial matrix elements and that the Coulomb potential can be comfortably used for the calculations.

A method have been proposed in [Klapisch, 1971] to determine radial potentials V_{eff} in such a way that the eigenenergies of those potential reproduce directly the experimental values of the Rydberg states energy. According to this very interesting method, the quantum defect values are used to adjust the potentials but the Rydberg states energy

are found in solving the eigenvalues equation of the corresponding potentials.
The radial potential determined by this method are of the form

$$V_{eff}(r) = -\frac{1 + (Z-1)\mathrm{e}^{-\alpha_1 r} - r(\alpha_3 + \alpha_4 r)\mathrm{e}^{-\alpha_2 r}}{r} - \frac{\alpha_d}{2r^4}(1 - \mathrm{e}^{-\left(\frac{r}{r_c}\right)^6}) \qquad \text{(A.13)}$$

Where Z is the atomic number of the considered atom. The different coefficients, depending thus of the quantum defect values, can be found in [Marinescu et al., 1994]. In the expression A.13 we refine the presence of the core polarization and overall that at large distance the potential is equivalent to the Coulomb potential.

Appendix B

Laser jitter effect on the Q factor, numerical study

In this section, we present a numerical study of the effect of the excitation laser jitter on the Q factor.
The principle of this study is, for given a Rydberg line and an assumed statistical distribution, to simulate a sample of shots taken at slightly different laser frequency (according to the jitter) and calculate the Q factor of this sample.

An important point is that we have done all the study with the data concerning the detected ions. Nevertheless, we have check that the results obtained directly with the ions distribution are the same than the ones which would have been obtained by, first divide the experimental data by the detection efficiency (to translate in Rydberg), do the study and translate back in terms of ions numbers.

B.1 Simulation of the experimental Q factor

Taken a set of experimental data like the one of the fig B.1 we first do a fit of the Rydberg line.

The fit obtained on the fig B.1 allows to define the Rydberg line "numerically".
Such a line corresponds to the mean number of the Rydberg excitation in function of the detuning. We have then to define the full statistical distribution associated to this mean number for each detuning.
Concerning the Q factor, we take for a resonant excitation, the experimental Q factor, i.e. -0.4. Then we assume that the "Q factor line" is proportional to the Rydberg line

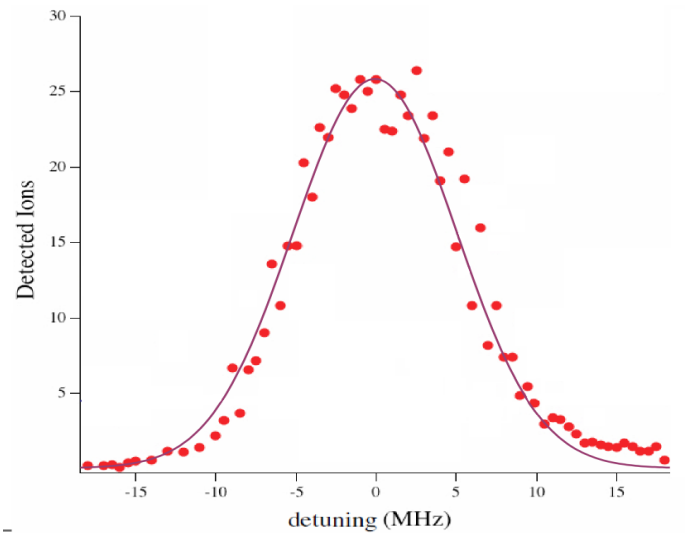

Figure B.1: Experimental data Rydberg line and its Lorentzian fit.

as represented on the fig B.2

The values of the Q factor assumed here is obviously associated to a quite strong physical assumption.
As mentioned in the section 4.7.4 of the chapter 4, in the case of an assemble of identical and uncorrelated two-levels systems (with measurements values, 0 and 1), if P_r is the probability of each system to be in the excited state, the Q factor of the whole system is $-P_r$. From this consideration we have set the Q factor being proportional to the mean number of Rydberg excitation.

Once the mean number and the Q factor determined for each detuning, we make another assumption to determine the full distribution. We consider a Gaussian distribution having those mean value and Q factor.

Looking now at the laser jitter, we consider that for a mean detuning δ and a jitter σ_L the detuning of the laser δ_i for a given shot is chosen according to the following gaussian distribution

$$\mathrm{e}^{-\frac{(\delta_i-\delta)^2}{2\sigma_L^2}} \tag{B.1}$$

This distribution is exactly the one used in the Rydberg excitation laser stabilization program (see section 4.2.3 of the chapter 4) from which the experimental value of the jitter is evaluated. In the program, the laser frequency is measured in real time and the jitter is obtained by fitting the obtained (running) distribution by this formula. Although

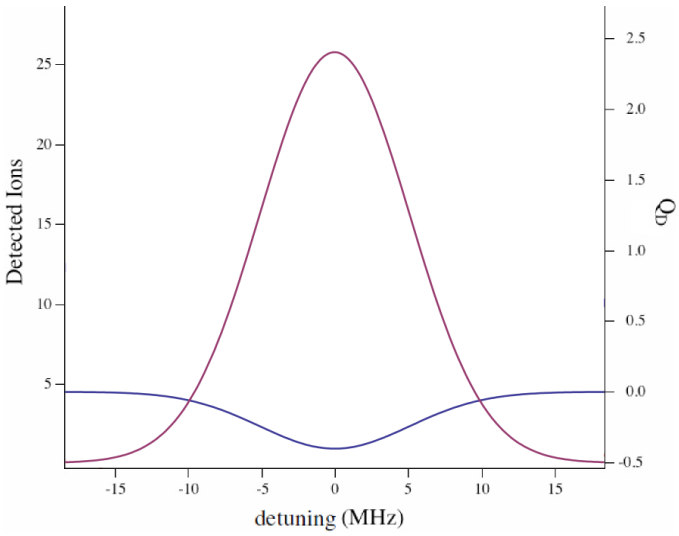

Figure B.2: Rydberg line and its corresponding Q factor assuming a proportionality between the mean number and the Q factor of the Rydberg excitation.

it varies (interestingly it is quite stable within one day), a typical evaluated value is 1.5 MHz.

Knowing the full distribution of the ions number for each detuning and the laser characteristics, we can properly simulate a sample of ions number as we get in the experiment.
For a detuning δ, we take 100 shots. For each shot i, we first "choose" the laser detuning δ_i according to the distribution B.1 and then we "choose" an ions number N_i according to the ions number distribution at the detuning δ_i.
We can finally calculate the Q factor Q_d of the sample $\{N_i\}$.

For a jitter of 1 MHz, we plot on the fig B.3 the obtained results together with the experimental data

On the fig B.3, we clearly see that, starting with negative values of the Q factor all along the line, the laser jitter leads to positive values of the Q factor on the edges of the the Rydberg lines. The correspondence with experimental data is in addition quite demonstrative.
Nevertheless, the evaluation of the jitter is not perfect since, for example, the locking cavity instability is included in the laser jitter. Also the physical assumptions used to define the ions number distribution for the simulation could play a non negligible role.
To conclude, if it is not really possible to say if the positive Q factors observed on the sides of the Rydberg lines is totally due to the laser jitter, we can affirm that it is responsible of a big part.

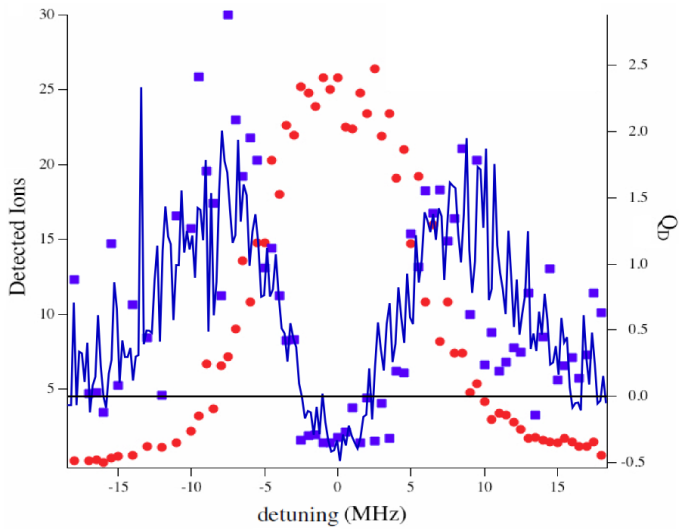

Figure B.3: Experimental Rydberg line with the measured Q factor (blue squares), the blue solid line corresponds to the results of the numerical simulation for a laser jitter of 1.5 MHz.

B.2 Evolution of the Q factor with the jitter

On the fig B.4 we have represented the results of the simulated Q factor for different values of the laser jitter. To get slightly less noisy curves the simulated samples are composed for those calculations of 250 shots.

We see on the fig B.4 the quite dramatic effect of the laser jitter on the Q factor. The locking setup of the Rydberg excitation laser is not the best that we can do. To this regards, performed a similar experiment with nice locking scheme (500 kHz) could allow to be totally free of the jitter effect. In our setup we are currently working on the implementation of a new locking scheme described for example in [Rohde et al., 2010] which should allow to reduce significantly the jitter of the Rydberg excitation.

B.3 Laser jitter effect on positive Q factor

In this section, we present very briefly the effect of the laser jitter on the results of the Q factor obtained with the cooperative model.
This study is only qualitative for two reasons. First it has been done at a time where the equations of the model was not the ones presented in the section 5.2 of the chapter 5. The equations used to obtain the graph of the fig B.5 are in fact the one presented in the reference [Viteau et al., 2012]. Also since the linewidths obtained by the model are smaller than the experimental ones, the use of real value of the jitter is not relevant.

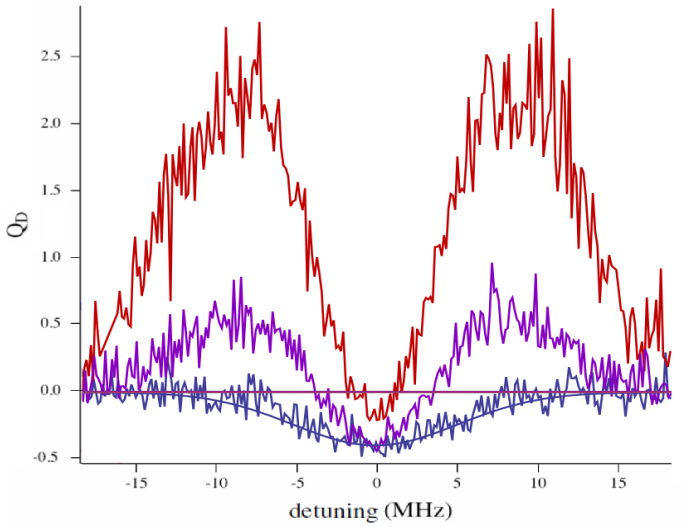

Figure B.4: Q factor obtained with numerical simulations for different values of the laser jitter. The smooth solid line is the initial Q factor, the other lines correspond respectively from the lower to the higher one to laser jitters of 0.3, 1 and 2 MHz.

The interest of the fig B.5 is only to look at the effect of the laser jitter on the Q factor when positive values are intrinsically present.

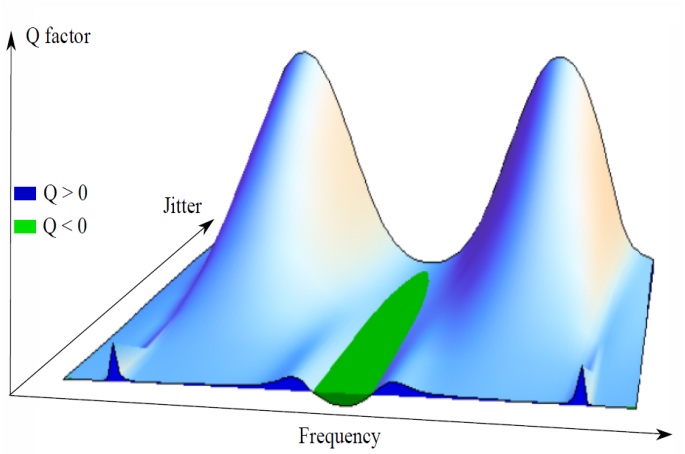

Figure B.5: Evolution of the Q factor in function of the laser jitter.

On the fig B.5, we see that the positive Q factor present intrinsically in the Rydberg distribution are progressively hidden by the jitter effect. For sufficiently large jitter, the positive Q factor are only due to the effect of the laser jitter on the edges of the Rydberg

line. Interestingly, we see that the negative Q factor on the center of the line is a bit more robust to the laser jitter than positive Q. Finally, the very sharp spikes initially present in the Q factor are quickly erased by the jitter effect.

Appendix C

Complement to the cooperative model

In this section, we give the different informations relative to the equations of the cooperative model presented in the section 5.2 of the chapter 5 which are not given there.

C.1 Interaction parameter

To calculate the interaction energies of the fully symmetrical Dicke state, we need to give explicit values to all the interactions terms $W_{qq}^{(j)}$.
We first consider the case of 2 excitations ($j = 2$). The $M^{(j)} = \frac{N(N-1)}{2}$ interaction terms $W_{qq}^{(2)}$ correspond to the interaction energy of all possible pair of atoms.

$$\left\{W_{qq}^{(2)}\right\} = \{V_{ij}\}_{j\neq i} \tag{C.1}$$

Looking at one particular atom, $i = 1$, it can form $(N-1)$ pairs leading to $(N-1)$ interaction terms $\{V_{ij}\}_{j\neq i} = \{V(R_{ij})\}_{j\neq i}$.
Assuming a uniform density, the Erlang distribution [Torquato et al., 1990] allows to determine the most probable distances between one atom and its q^{th} neighbors

$$R_q = \frac{q\left(\frac{3}{\pi}\right)^{\frac{1}{3}}\Gamma\left[\frac{1}{3}+q\right]}{2^{\frac{2}{3}}d^{\frac{1}{3}}q!} \tag{C.2}$$

We use this distances to explicit the interaction terms between the atom 1 and all the other atoms

$$\{V_{1j}\}_{j\neq 1} = \{V(R_q)\}_{q\in[\![1;N-1]\!]} \tag{C.3}$$

Assuming that all the atoms have the same environment and neglecting edge effects. The interaction terms for the other atoms are the same than for the particular atoms 1

$$\{V_{ij}\}_{i\neq j} = \{V(R_q)\}_{q\in[\![1;N-1]\!]}\ \forall i \in [\![1;N]\!] \tag{C.4}$$

We can then write the ensemble $\left\{W_{qq}^{(2)}\right\}$ as a repetition of the ensemble $\{V(R_q)\}$

$$\left\{W_{qq}^{(2)}\right\}_{q\in[\![1;\frac{N(N-1)}{2}]\!]} = \frac{N}{2} \otimes \{V(R_q)\}_{q\in[\![1;N-1]\!]} \tag{C.5}$$

We use here the simplified notation $\otimes$ for the repetition of an ensemble. The factor $\frac{1}{2}$ come from the fact that the pairs appear 2 times when we look separately at all the N atoms.

For the other levels of excitation ($j > 2$), we will use the same kind of treatment. We first remark that any interaction term $W_{qq}^{(j)}$ corresponding to j excitations is a sum of $\frac{j(j-1)}{2}$ pair interaction as there is $\frac{j(j-1)}{2}$ different pairs in an assembly of j particles. We then consider that each term $W_{qq}^{(j)}$ have to be choose within the ensemble $\left\{\frac{j(j-1)}{2}V(R_q)\right\}_{q\in[\![1;N-1]\!]}$ and we express the ensemble $\left\{W_{qq}^{(j)}\right\}$ as the repetition of the ensemble $\left\{\frac{j(j-1)}{2}V(R_q)\right\}_{q\in[\![1;N-1]\!]}$, number of repetition being simply $\frac{M^{(j)}}{N-1}$.

$$\left\{W_{qq}^{(j)}\right\} = \left(M^{(j)}\frac{1}{N-1}\right) \otimes \left\{\frac{j\,(j-1)}{2}V(R_q)\right\} \tag{C.6}$$

The explicit expressions of the η parameter and interaction energies of fully symetrical states $W^{(j)}$ are

$$\eta = \sum_{q=1}^{N-1} V(R_q) \tag{C.7}$$

$$W^{(j)} = \frac{1}{M^{(j)}}\sum_{q=1}^{M^{(j)}} W_{qq}^{(j)} = \frac{j\,(j-1)}{2}\frac{\eta}{N-1} \tag{C.8}$$

The equation C.8 allow to link all the $W^{(j)}$ to η which is then the only parameter to calculate in order to implement the equations of the model.

C.2 Construction of the modified atomic basis

In each subset of j excitation, we take the fully symmetrical Dicke state $|j,s\rangle$ and the $M^{(j)}$ atomic states $|j,q\rangle$. We have to remove one state to get the right dimension, we remove the atomic state that we call $|j,M\rangle$ such as

$$\langle j, M| \hat{V} |j, M\rangle \approx \langle j, s| \hat{V} |j, s\rangle \tag{C.9}$$

We assume in the following a perfect equality, which is an reasonable hypothesis if the number of atoms is large.
Then we modify slightly states $|j, q\rangle$

$$|j, q'\rangle = |j, q\rangle + \alpha |j, M\rangle \tag{C.10}$$

Finally we remove in all states $|j, q'\rangle$ the symmetrical part following the idea of the Gram-Schmidt process.

$$\left|j, \widetilde{q}\right\rangle = |j, q'\rangle - \langle j, s \mid j, q'\rangle |j, s\rangle \tag{C.11}$$

Tacking $\alpha = \frac{1}{\sqrt{M^{(j)}-1}}$, the ensemble formed by the state $|j, s\rangle$ and the $M^{(j)} - 1$ states $\left|j, \widetilde{q}\right\rangle$ is an orthonormal basis of the subset of j excitations.
The matrix elements of the Rydberg-Rydberg interaction for this basis are given by :

$$\langle j, s| \hat{V} |j, s\rangle = W^{(j)} \tag{C.12}$$

$$\langle j, s| \hat{V} |j, \widetilde{q}\rangle = \frac{1}{\sqrt{M^{(j)}}} \left[W_{qq}^{(j)} - W^{(j)}\right] \doteq W_{s\widetilde{q}}^{(j)} \tag{C.13}$$

$$\left\langle j, \widetilde{q}\right| \hat{V} \left|j, \widetilde{q}\right\rangle = W_{qq}^{(j)} \tag{C.14}$$

$$\left\langle j, \widetilde{q}\right| \hat{V} \left|j, \widetilde{p}\right\rangle = 0 \tag{C.15}$$

Where $W_{qq}^{(j)}$ is the interaction energy of the atomic state $|j, q\rangle$ associated to $\left|j, \widetilde{q}\right\rangle$ ($W_{qq}^{(j)} = \langle j, q| \hat{V} |j, q\rangle$).
We see here that the advantage of this basis is that the Rydberg interaction is diagonal in the restriction of the space to the non fully symmetrical Dicke states.

C.3 Master integrodifferential equation derivation

We start from the following system of equation

$$
\begin{aligned}
i\frac{da_j}{dt} &= -\delta j a_j + W^{(j)} a_j \\
&+\sqrt{(N-j)\,(j+1)}\frac{\Omega}{2} a_{j+1} \\
&+\sqrt{(N-j+1)\,j}\frac{\Omega}{2} a_{j-1} \\
&+\sum_{q=1}^{M^{(j)}-1} W_{sq}^{(j)} b_{jq}
\end{aligned}
\tag{C.16}
$$

$$
i\frac{db_{jq}}{dt} = \left(-\delta j + W_{qq}^{(j)}\right) b_{jq} + W_{sq}^{(j)} a_j \tag{C.17}
$$

We define γ_{jq} as following

$$
b_{jq}(t) = \gamma_{jq}(t) \exp\left(-i\left(-\delta j + W_{qq}^{(j)}\right) t\right) \tag{C.18}
$$

the equation C.17 can be write as

$$
i\frac{d\gamma_{jq}}{dt} = W_{qs}^{(j)} a_i \exp\left(i\left(-\delta j + W_{qq}^{(j)}\right) t\right) \tag{C.19}
$$

We formally integrate this equation and write the equation C.16 as

$$
i\frac{da_j}{dt} = -\delta j a_j + W^{(j)} a_j \tag{C.20}
$$

$$
+\sqrt{(N-j)\,(j+1)}\frac{\Omega}{2} a_{j+1} + \sqrt{(N-j+1)\,j}\frac{\Omega}{2} a_{j-1} \tag{C.21}
$$

$$
+i\sum_q \int_0^t \left(W_{sq}^{(j)}\right)^2 a_i(t-\tau) \exp\left(-i\left(-\delta j + W_{qq}^{(j)}\right)(\tau)\right) d\tau \tag{C.22}
$$

Using

$$
\left(W_{sq}^{(j)}\right)^2 = \frac{1}{M^{(j)}}\left[W_{qq}^{(j)2} - 2W_{qq}^{(j)} W^{(j)} + W^{(j)2}\right] \tag{C.23}
$$

We finally get

$$i \quad \frac{da_j}{dt} = -\delta j a_j + W^{(j)} a_j \tag{C.24}$$

$$+\sqrt{(N-i)\,(i+1)}\frac{\Omega}{2}a_{j+1} + \sqrt{(N-j+1)\,j}\frac{\Omega}{2}a_{j-1} \tag{C.25}$$

$$+\int_0^t f^{(j)}\left(\tau\right)\exp\left(i\delta j\tau\right)a_j\left(t-\tau\right)d\tau \tag{C.26}$$

Where we define the correlation function $f^{(j)}$ as

$$f^{(j)}(\tau) = \sum_q \frac{1}{M^{(j)}}\left[\left[W_{qq}^{(j)2} - 2W_{qq}^{(j)}W^{(j)} + W^{(j)2}\right]\exp\left(-iW_{qq}^{(j)}\tau\right)\right] \tag{C.27}$$

C.4 Simplification of the correlation functions

We want to calculate the correlation functions $f^{(j)}$.
We will first consider the correlation function $f^{(2)}\left(\tau\right)$, indeed, using the expression C.6 we can show that all the correlation functions $f^{(j)}$

$$\sum_q \frac{1}{M^{(j)}}\left[\left[W_{qq}^{(j)2} - 2W_{qq}^{(j)}W^{(j)} + W^{(j)2}\right]\exp\left(-iW_{qq}^{(j)}\tau\right)\right] \tag{C.28}$$

are related to $f^{(2)}$ by the simple relation

$$f^{(j)}\left(\tau\right) = \left(\frac{j\left(j-1\right)}{2}\right)^2 f^{(2)}\left(\frac{j\left(j-1\right)}{2}\tau\right) \tag{C.29}$$

Consequently, calculation of $f^{(2)}$ will allow us to calculate all the correlation functions $f^{(j)}$

$f^{(2)}$ can be decomposed in 3 parts :

$$f^{(2)} = f_1^{(2)} + f_2^{(2)} + f_3^{(2)} \tag{C.30}$$

$$f_1^{(2)}\left(\tau\right) = \frac{1}{N-1}\sum_{q=1}^{N-1}\left[V(R_q)^2\exp\left(-iV(R_q)\tau\right)\right] \tag{C.31}$$

$$f_2^{(2)}\left(\tau\right) = \frac{1}{N-1}\sum_{q=1}^{N-1}\left[-2V(R_q)W^{(2)}\exp\left(-iV(R_q)\tau\right)\right] \tag{C.32}$$

$$f_3^{(2)}(\tau) = \frac{1}{N-1}\sum_{q=1}^{N-1}\left[W^{(2)2}\exp\left(-iV(R_q)\tau\right)\right] \tag{C.33}$$

Each part can be calculated, for that we use the continuous approximation, for example, in the case of $f_1^{(2)}$

$$f_1^{(2)}(\tau) = \frac{1}{N-1}\int_1^{N-1}\left(V(R_q)\right)^2\exp\left(-iV(R_q)\,\tau dq\right. \tag{C.34}$$

On the fig C.1, real and imaginary part of the 3 functions are plotted. We can see that strong simplifications can be made when we look at the time scale of the evolution of this functions in comparison to the time scale of evolution of the $a_2(t)$ coefficient which is of the order of $\frac{1}{W^{(2)}}$.
Time scale of evolution of $f_3^{(2)}$ is of the order of $\frac{1}{W_{min}^{(2)}}$ where $W_{min}^{(2)}$ is the weakest interaction among the ensemble $\left\{W_{qq}^{(2)}\right\}$. $f_3^{(2)}$ is then a long time scale function that we can consider as constant during the evolution time of $a_2(t)$.

$$f_3^{(2)}(\tau) \approx f_3^{(2)}(0) = W^{(2)2} \tag{C.35}$$

Concerning $f_2^{(2)}$ and $f_1^{(2)}$, we first see that $f_2^{(2)}$ can be neglect because its amplitude is 1000 times less than the one of $f_1^{(2)}$. Time scale of $f_1^{(2)}$ is of the order of $\frac{1}{W_{max}^{(2)}}$ where $W_{max}^{(2)}$ is the strongest interaction among the ensemble $\left\{W_{qq}^{(2)}\right\}$. $f_1^{(2)}$ is then a short time scale function and we can consider that $f_1^{(2)}$ is a Dirac's delta function

$$f_1^{(2)}(\tau) \approx \int_0^{\infty} f_1^{(2)}(t)\,dt \times \delta(\tau) = -iW^{(2)}\delta(\tau) \tag{C.36}$$

Doing this approximations, we can then write $f^{(2)}$ as a sum of a constant term and a Dirac term

$$f^{(2)}(\tau) \approx W^{(2)2} - iW^{(2)}\delta(\tau) \tag{C.37}$$

Using the equation C.29, we can show that this simplification can be made for all correlation functions and we have

$$f^{(j)}(\tau) \approx W^{(j)2} - iW^{(j)}\delta(\tau) \tag{C.38}$$

This is the form used for the correlation functions in the equations of the cooperative model.

The equation C.29 is, in a general way, true and a similar result is found in the reference [Stanojevic et al., 2012] (equation 8). However, with our treatment of the correlation functions, the maximum and the minimum interaction terms of each subset of j excitations play a central role as they determine the time scale of the different parts of the correlation functions. In the expression C.6 the maximum (minimum) interaction term for j excitations is a multiple of the maximum (minimum) pair interaction. Although this is a reasonable approximation as long as we have $j \ll N$, it is not true and we should find an appropriate correction to those terms. This would gives a restriction on the number of excitation j for which the approximation (function=dirac+constant term) is valid. In fact, as j increases, the time scale considerations that we use become less and less true and the exact structure of the correlation functions should play a role in the dynamics of the system. However we expect that for $j \ll N$, this has only a small effect.

In addition, an approximation in the treatment of the correlation functions comes from the continuous approximation. Indeed, the discretization of the interaction terms may have an effect on the correlation functions with namely a particular role of the strongest interactions terms. However, continuous approximation seems very reasonable for $N \gg 1$.

In the present state of the model, the treatment of the correlation functions corresponds in a sense to an averaged case valid for $N \gg 1$ and $j \ll N$.

It should be very interesting to study more in detail the correlation functions as they contains a lot of physical meaning. For example, as the correlation functions give the distribution of states coupled to the symmetrical Dicke states, the Fourier transform of the correlation functions should be linked to the spatial distribution of the excited Rydberg atom (we can indeed make the correspondence between the interaction energy and the distance between Rydberg atoms). It could be also very interesting to define the correlation functions involved in the couplings from a non-symetrical Dicke state.

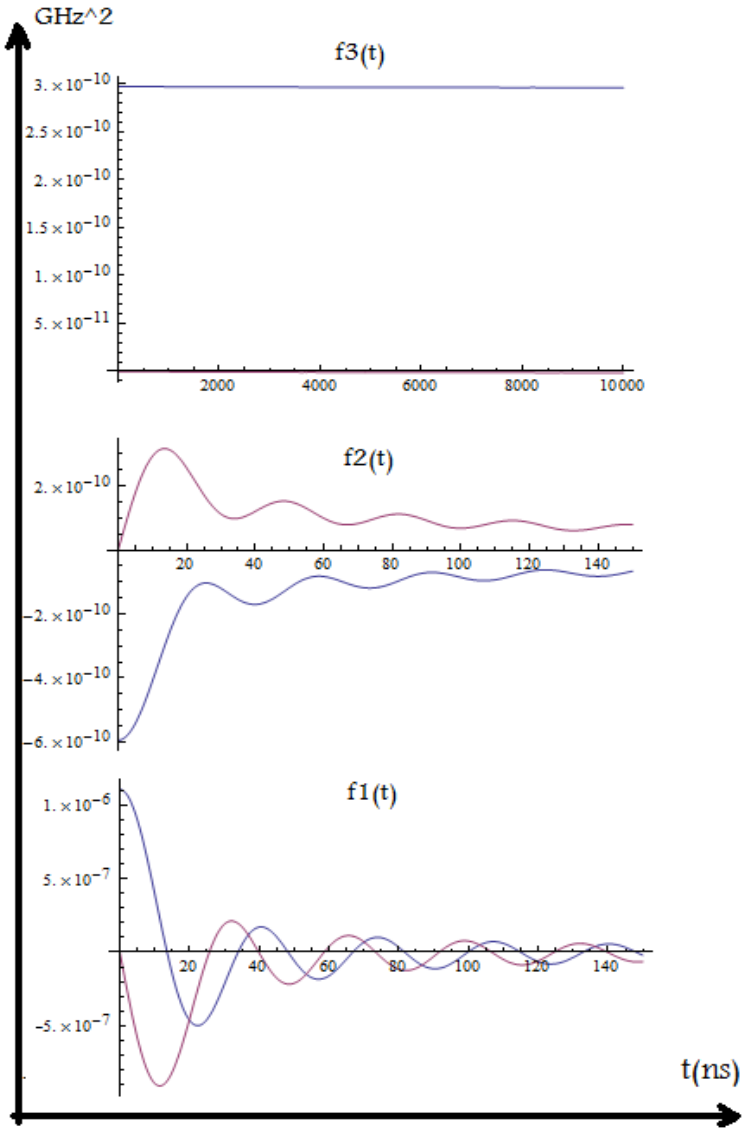

Figure C.1: We plot in function of the time, the values of real (blue lines) and imaginary part (red lines) of the three components of the correlation function $f^{(2)}$. $f_3^{(2)}$ is plotted on a much longer time scale $(10\mu s)$ than $f_1^{(2)}$ and $f_2^{(2)}$ $(150ns)$

Appendix D

Basic Mean-Field model

In this section we present some calculations done with a Mean-Field treatment. We use the Mean-Field theory in its simplest form, i.e. we neglect all the atomic correlations. The results presented here are not equivalent to the one presented for example in [Tong et al., 2004; Weimer et al., 2008]. In those references, the evaluation of the 2-body correlation function is taken into account.
We have done such calculations since the Mean-Field equations are very simple and leads to a kind of blockade anyway, the possibility to include effects like the laser line-width, Doppler effect or density variation in a very simple manner is quite interesting. If the full many-body equations would behave differently in regards to those effects, the results presented here give an idea of what we could expect from them.

D.1 Equation of the Mean-Field model

We consider the Hamiltonian of the dipole blockade H as presented in the chapter 1

$$H = -\hbar\delta\sum_{i=1}^{N}\hat{\sigma}_{rr}^{i} + \frac{\hbar\Omega}{2}\sum_{i=1}^{N}\left[\hat{\sigma}_{gr}^{i} + \hat{\sigma}_{rg}^{i}\right] + \sum_{i=1,j<i}^{N} V_{ij}\hat{\sigma}_{rr}^{i}\hat{\sigma}_{rr}^{j}$$

For the numerical values of the parameters, we keep the case modeled with the cooperative model as presented in the section 5.2 of the chapter 5. Thus, $|r\rangle = 71\mathrm{d}_{5/2}$, $V_{ij} = \frac{C_6}{R_{ij}^6}$ with $C_6 = -2\pi \times 7$ GHz.μm^6, $N = 8000$, $\Omega = 2\pi \times 40$ kHz and the sample is considered to uniform density d =1.5 $10^{10} at.cm^3$. We consider $\delta = 0$ if no other values are explicitly mentioned.

According to the Mean-Field hypothesis we assume,

$$\hat{\sigma}^{j} = \hat{\sigma}^{i}, \forall j \neq i \tag{D.1}$$

Where $\hat{\sigma}^i$ is the density matrix operator of the atom i. The equation of evolution of the density matrix, $\hat{\sigma}^1(t)$, of the atom 1, which will be our witness atom, is obtained by tracing the equation of evolution of the total density matrix, $\hat{\sigma}(t)$, over all the other atoms

$$i\hbar\frac{d}{dt}\left[\hat{\sigma}^1(t)\right] = \underset{j\neq 1}{Tr}\left[H, \hat{\sigma}(t)\right] \tag{D.2}$$

It is by making the trace that atomic correlation are "vanished" of the equations.
We transform this equation using the Bloch vector formalism to get the following system of equation

$$\begin{cases} \dot{n}_R(t) &= \frac{\Omega}{2}v(t) \\ \dot{v}(t) &= -\delta u(t) + \Omega(1-2n_R(t)) + \eta n_R(t)u(t) \\ \dot{u}(t) &= \delta v(t) - \eta n_R(t)v(t) \end{cases} \tag{D.3}$$

with

$$\eta = \sum_{q=1}^{N-1} V(R_q) \tag{D.4}$$

η is the same quantity than in the cooperative model and its expression has been discussed in the section C.1.
We recognize here the system of equation of a two levels atom in interaction with a laser field. There is an additional term, $\eta n_R(t)$ which correspond to the Rydberg-Rydberg interactions. This term acts like a detuning, indicating that the Rydberg-Rydberg interactions shift the energy level of the Rydberg state.

This treatment corresponds to the most basic Mean-Field model that we can derive, here quantum correlations are totally neglect. In the improved Mean-Field model of [Tong et al., 2004; Weimer et al., 2008], the fact that 2 atoms separated by less than a certain distance can not be excited simultaneously in the Rydberg state is take in account. This distance is the blockade radius, R_b, and can be evaluated in function of the parameters of the system (here we would have $R_b = (C_6/\hbar\Omega)^{1/6}$). Taking in account the 2-body correlations corresponds to define η as

$$\eta = \sum_{q=q_0, R_{q_0}\geq R_b}^{N-1} V(R_q) \tag{D.5}$$

Although the equation are formally identical, we stay in this manuscript with the basic Mean-Field model.

D.2 First results of the Mean-Field model

We show in the in the fig D.1 the result of the numerical resolution of the Mean-Field equations.

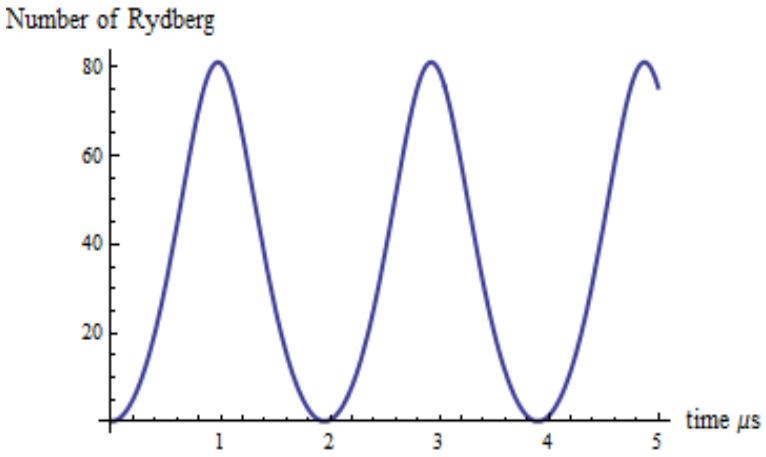

Figure D.1: Time evolution with the Mean-Field model

We see in the figD.1 a coherent evolution of the system exhibiting a Rabi oscillation. The maximum number of Rydberg is 100 times less than the number of atoms, so in a sens, there is a blockade effect. Looking at the time scale, we see that the frequency of oscillation is 12.5 times bigger than the Rabi frequency Ω.

D.3 Effect of the laser linewidth

Up to now, the laser was considered to be perfectly monochromatic. However, the laser linewidth, $\Delta\omega$, can be easily introduced in the Mean-Field equations, as it is the case for a two-levels atom, considering an average of the atomic quantities over the phase fluctuations of the laser [Blushs and Auzinsh, 2004].

$$\begin{cases} \dot{n}_R(t) &= \frac{\Omega}{2}v(t) \\ \dot{v}(t) &= -\delta u(t) + \Omega(1-2n_R(t)) + \eta n_R(t)u(t) - \Delta\omega v(t) \\ \dot{u}(t) &= \delta v(t) - \eta n_R(t)v(t) - \Delta\omega u(t) \end{cases} \tag{D.6}$$

We solve this new equation with same parameters as before and $\Delta\omega = 2\pi\times$ 300 kHz.

Results presented in the fig D.2 show a not surprising damping of the oscillations due to the decoherence engendered by the laser linewidth. However, there is also now a

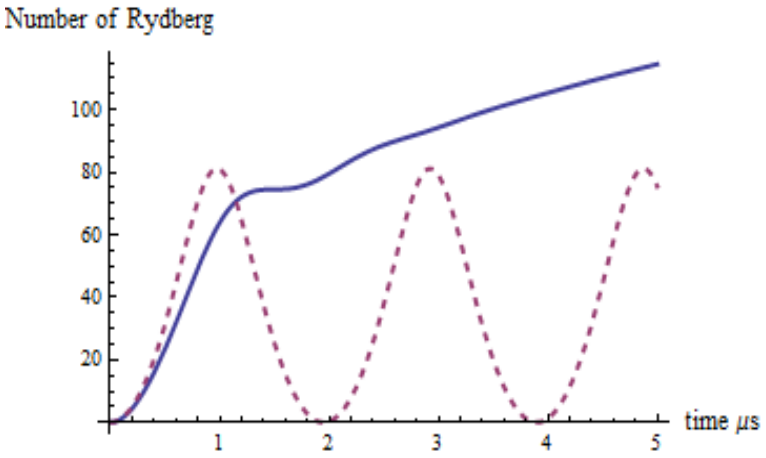

Figure D.2: Time evolution with the Mean-Field model including a laser linewidth $\Delta\omega$ (solid line), dashed line is the result of calculations without laser linewidth of the figD.1.

steady growing of the number of Rydberg. This can be interpreted by the fact that, again due to the decoherence engendered by the laser line width, the system tends to reach the state of equal superposition between ground and Rydberg state. Finite Rydberg lifetime would compensate this evolution but only after a certain time.

D.4 Doppler effect

Doppler effect can also be introduced in the Mean-Field model. We consider that the atomic sample is divided in many classes of velocity indexed by k. Calling v_k the velocity along the laser direction of the atoms of the class k. For this atoms, the laser detuning is $\delta_k = \delta - \frac{2\pi}{\lambda_{gr}} v_k$ where λ_{gr} =300 nm. Their number N_k is given by the Maxwell-Boltzmann distribution.

$$N_k = N\sqrt{\frac{m}{2\pi k_b T}} \int_{\frac{v_{k-1}+v_k}{2}}^{\frac{v_k+v_{k+1}}{2}} \exp\left(-\frac{1}{2}\frac{m}{k_b T}v^2\right) dv \tag{D.7}$$

Where m is the atomic mass and T the temperature.
For each class of speed k, we can write the equation of the Mean-Field model with the associated detuning δ_k. All the equations are coupled together via the interaction term which have to be summed over all the classes with the normalized weight $\frac{N_k}{N}$.

$$\begin{cases} \dot{n}_R^{(k)}(t) &= \frac{\Omega}{2} v^{(k)}(t) \\ \dot{v}^{(k)}(t) &= -\delta_k u^{(k)}(t) + \Omega(1 - 2n_R^{(k)}(t)) \\ &+ \eta \sum_k \frac{N_k}{N} n_R^{(k)}(t) u^{(k)}(t) \\ \dot{u}^{(k)}(t) &= \delta_k v^{(k)}(t) - \eta \sum_k \frac{N_k}{N} n_R^{(k)}(t) v^{(k)}(t) \end{cases} \tag{D.8}$$

The total Rydberg excitation value is obtained by summing the Rydberg population times the atom number for all the classes $\sum_k N_k n_R^{(k)}(t)$.

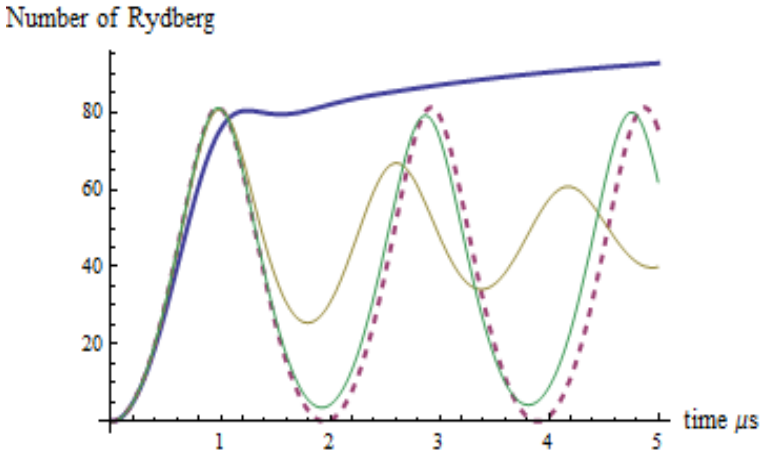

Figure D.3: Time evolution with the Mean-Field model including the Doppler effect for a temperature of $100\mu K$ (solid line). Dashed line is the result of calculations without Doppler effect of the figD.1. Thin solid lines are the results including the Doppler effect for a temperature of $10\mu K$ (yellow) and $1\mu K$ (green). Calculations with Doppler effect are made in the three cases with 25 velocity classes.

On the fig D.3, we plot the result obtained, without laser linewidth for three different temperature (100, 10 and 1 μK). It is interesting to notice that, even without decoherence processes, the sole Doppler effect hides the coherent oscillations for a temperature of $100\mu K$. On the other hand, for a temperature of $1\mu K$ we see that the Doppler effect has almost no effect on the first oscillations. This seems to indicate that, due to the Doppler effect, the range of temperature of a MOT is quite critical for the observation of coherent oscillation and can even prevent it. This problem is avoided with colder atomic samples.

D.5 Effect of Gaussian density

The atomic cloud (as well as the laser intensity) was up to now considered to be uniform over the whole volume. However, in number of experiment, the density of the cloud

is non uniform. Because the excitation dynamics in the regime of blockade is strongly density dependent this should have an influence on the system. In this section we present calculations assuming a Gaussian atomic density.
We used the Mean-Field equation without laser linewidth neither Doppler effect and solve it for different densities. We then sum the results together with a relative weight corresponding to a Gaussian density.

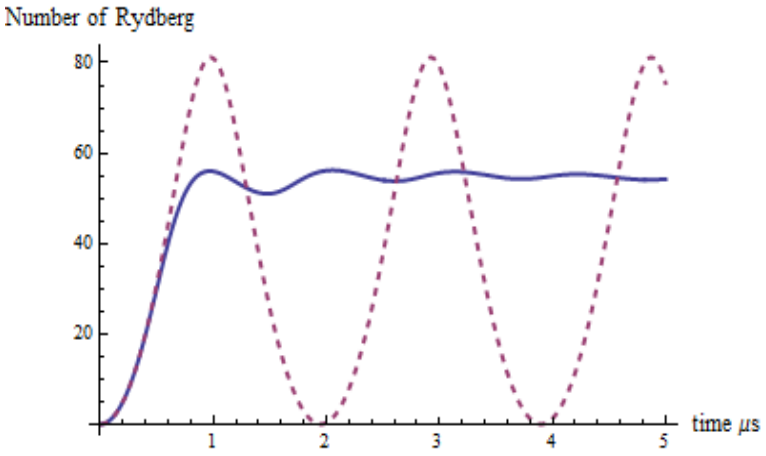

Figure D.4: Time evolution with the Mean-Field model assuming a Gaussian density of the cloud (solid line), dashed line is the result of calculations with a uniform density. For the Gaussian case, we used 99 different densities for the calculations.

As expected, we see in the fig D.4 that the main effect of a non uniform density is to damp the oscillations, the different classes of density having different oscillation frequencies.

D.6 Scan of the Rydberg line

In this section, we present the results of the Mean-Field model for the scan of the Rydberg line. We made calculation varying the detuning for different pulse duration, calculations include the laser linewidth $\Delta\omega = 2\pi\times$ 300 kHz.

We clearly see in the fig D.5 that the Rydberg line predicted by the Mean-Field model is shifted from resonance and asymmetric. As it was already depicted in reference [Schempp et al., 2010] that it is in contradiction with experimental results which show that in the regime of blockade, the line is symmetric and not shifted [Singer et al., 2004; Pritchard et al., 2010; Viteau et al., 2012]. This contradiction will be even clearer in the following section.

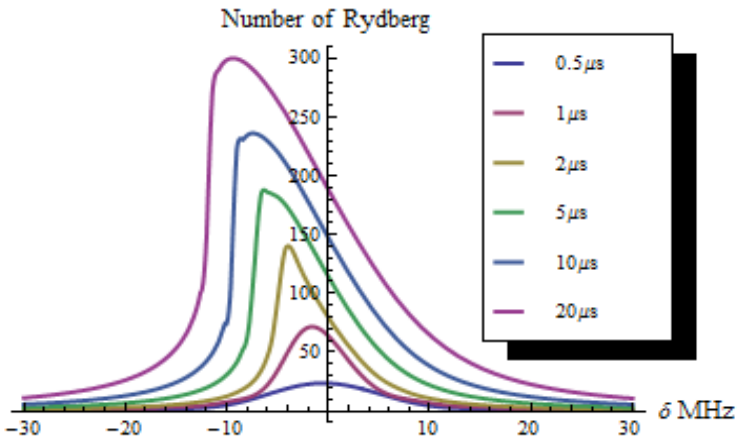

Figure D.5: Scan of the Rydberg line with the Mean-Field model

D.7 Effect of the Zeeman degeneracy

As mentioned in the section 2.5, in the case of Rydberg states with $l \neq 0$, the Zeeman degeneracy leads to different Rydberg-Rydberg interaction curves.
In this section, we study in the frame of the Mean-Field model the effect of this degeneracy. Since the treatment of Rydberg-Rydberg interaction is made using two-atoms basis and that the Mean-Field model, in essence, deals with one atom basis, a rigorous treatment is almost impossible. Also the interest of this is more qualitative and we will use several approximations.
The computation of the Rydberg-Rydberg interaction is done in the molecular referential witch is different from the excitation referential. We then decide to neglect all angular dependences to avoid consequent complications.
Keeping the case of $71d_{\frac{5}{2}}$ there is 6 different Rydberg states $|r_i\rangle$ corresponding to magnetic sub-levels. There is then 21 interaction potentials $\{V^{ij}(R)\}_{j\geq i}$ where $V^{ij}(R)$ is the interaction energy between an atom in state $|r_i\rangle$ and an atom in state $|r_j\rangle$ separated by a distance R. Although eigenvectors associated to the different interaction potential curves do not correspond to states of the form $|r_i, r_j\rangle$, we assign to each $V^{ij}(R)$ one of the calculated potentials. Doing this, we use the real values of the Rydberg-Rydberg interaction.
We finally consider that all the states have the same Rabi frequency $\Omega_i = \frac{\Omega}{\sqrt{6}}$.
We have developed the Mean-Field equations with the density matrix formalism using Lindblad operator [Lindblad, 1976] in order to include effect of the laser linewidth .

The effect of the Zeeman degeneracy appears very clearly on the fig D.6 as a wing on the red size of the line. The result obtained here is quite interesting. Indeed, the

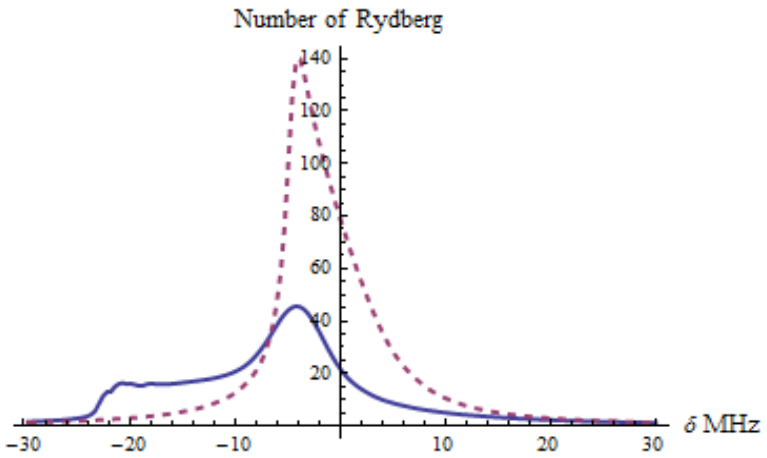

Figure D.6: Scan of the Rydberg line including Zeeman degeneracy (solid line). The dashed line correspond to the case of the section D.6. For both curves, the laser pulse duration is $2\mu s$

Mean-Field model predicts a shift of the Rydberg line proportional to the Rydberg-Rydberg interactions strength. For this particular case of a $d_{5/2}$ state, due to the strong Zeeman degeneracy, such a shift leads to the shape of the solid line of the fig D.6, highly asymmetric. So, the symmetry of the Rydberg line in the case of l =d states that we have observed in our experiments clearly infirms Mean-Field and similar models predicting this shift.

D.8 Role of atomic correlations

This section aims to discuss with a very simple example the role of atomic correlations in the blockaded Rydberg ensembles. For that, we compare Mean-Field calculations and exact calculations in the case of two interacting atoms. Exact calculation consist in the resolution of the equation of evolution of the density matrix with the Hamiltonian of the equation D.1 for two atoms. For the Mean-Field model, the parameter η becomes simply the interaction energy between the two atoms in the Rydberg state.
In both case, we obtain a time evolution which exhibit Rabi oscillation. We look only at the maximum value of the Rydberg excitation, in the fig D.7, we plot it in function of the interatomic distance.

For large interatomic distance, the Rydberg-Rydberg interaction is negligible and the two atoms can be excited in the same time in the Rydberg state, this leads to an excitation value of 2 as it appears in the both approaches. However, at small distance, we see a big difference between the two models. Whereas exact calculations predict that

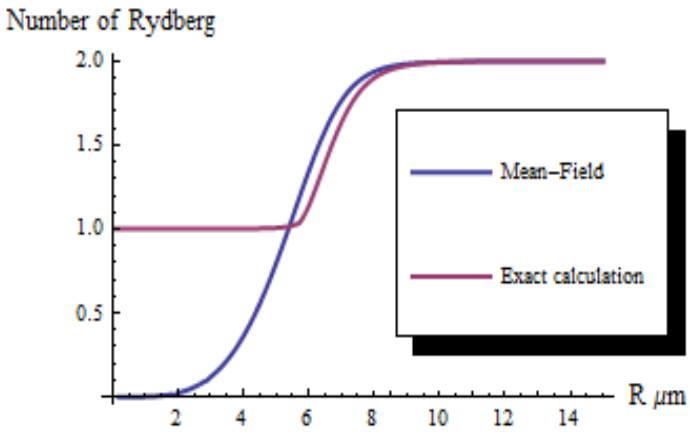

Figure D.7: Two atoms calculations. For those calculations, the C_6 coefficent is 25 GHz.μm^6

always one Rydberg excitation can be find in the system, the Mean-Field model gives a very small probability to find an excitation. The Mean-Field model underestimates the number of Rydberg excitation. This can be explained as following.
As atomic correlations are neglected in the Mean Field model, the two atoms state is necessarily separable and can be only in the form $(\alpha_g |g,\ g\rangle + \alpha_r |r,\ r\rangle)$. At small interatomic distances, the excitation value stays at a very low level because $|r,\ r\rangle$ is strongly shifted and its excitation is very unlikely.
In the exact treatment, the system can be in the state $\frac{1}{\sqrt{2}}(|g,\ r\rangle + |r,\ g\rangle)$. This state being not shifted it will be efficiently populated and the excitation value is at least one for all interatomic distances.
The state $\frac{1}{\sqrt{2}}(|g,\ r\rangle + |r,\ g\rangle)$ is the fully symmetrical Dicke states with one excitation within 2 atoms.
We understand with this simple example why we have to use collective states to describe the strongly interacting Rydberg gases.

Bibliography

[Abel et al., 2011] Abel, R. P., Carr, C., Krohn, U., and Adams, C. S. (2011). Electrometry near a dielectric surface using rydberg electromagnetically induced transparency. *Phys. Rev. A*, 84:023408.

[Abel et al., 2009] Abel, R. P., Mohapatra, A. K., Bason, M. G., Pritchard, J. D., Weatherill, K. J., Raitzsch, U., and Adams, C. S. (2009). Laser frequency stabilization to excited state transitions using electromagnetically induced transparency in a cascade system. *Applied Physics Letters*, 94(7):071107.

[Adams, 1997] Adams, C. (1997). Laser cooling and trapping of neutral atoms. *Progress in Quantum Electronics*, 21:1–79.

[Afrousheh et al., 2004] Afrousheh, K., Bohlouli-Zanjani, P., Vagale, D., Mugford, A., Fedorov, M., and Martin, J. D. (2004). Spectroscopic observation of resonant electric dipole-dipole interactions between cold rydberg atoms. *Physical Review Letters*, 93(23):233001–+.

[Amthor et al., 2009] Amthor, T., Denskat, J., Giese, C., Bezuglov, N. N., Ekers, A., Cederbaum, L. S., and Weidemüller, M. (2009). Autoionization of an ultracold rydberg gas through resonant dipole coupling. *European Physical Journal D*, 53:329–335.

[Amthor et al., 2010] Amthor, T., Giese, C., Hofmann, C. S., and Weidemüller, M. (2010). Evidence of Antiblockade in an Ultracold Rydberg Gas. *Physical Review Letters*, 104(1):013001–+.

[Amthor et al., 2007a] Amthor, T., Reetz-Lamour, M., Giese, C., and Weidemüller, M. (2007a). Modeling many-particle mechanical effects of an interacting rydberg gas. , 76(5):054702–+.

[Amthor et al., 2007b] Amthor, T., Reetz-Lamour, M., Westermann, S., Denskat, J., and Weidemüller, M. (2007b). Mechanical effect of van der waals interactions

observed in real time in an ultracold rydberg gas. *Physical Review Letters*, 98(2):023004–+.

[Anderson et al., 1998] Anderson, W. R., Veale, J. R., and Gallagher, T. F. (1998). Resonant dipole-dipole energy transfer in a nearly frozen rydberg gas. *Phys. Rev. Lett.*, 80:249.

[Ates et al., 2012] Ates, C., Garrahan, J. P., and Lesanovsky, I. (2012). Thermalization of a Strongly Interacting Closed Spin System: From Coherent Many-Body Dynamics to a Fokker-Planck Equation. *Physical Review Letters*, 108(11):110603.

[Ates and Lesanovsky, 2012] Ates, C. and Lesanovsky, I. (2012). Entropic enhancement of spatial correlations in a laser-driven Rydberg gas. , 86(1):013408.

[Ates et al., 2006] Ates, C., Pohl, T., Pattard, T., and Rost, J. M. (2006). LETTER TO THE EDITOR: Strong interaction effects on the atom counting statistics of ultracold Rydberg gases. *Journal of Physics B Atomic Molecular Physics*, 39:L233–L239.

[Ates et al., 2007a] Ates, C., Pohl, T., Pattard, T., and Rost, J. M. (2007a). Antiblockade in rydberg excitation of an ultracold lattice gas. *Physical Review Letters*, 98(2):023002–+.

[Ates et al., 2007b] Ates, C., Pohl, T., Pattard, T., and Rost, J. M. (2007b). Many-body theory of excitation dynamics in an ultracold rydberg gas. , 76(1):013413–+.

[Ates et al., 2011] Ates, C., Sevinçli, S., and Pohl, T. (2011). Electromagnetically induced transparency in strongly interacting rydberg gases. *Phys. Rev. A*, 83:041802.

[Bariani et al., 2012] Bariani, F., Dudin, Y. O., Kennedy, T. A. B., and Kuzmich, A. (2012). Dephasing of Multiparticle Rydberg Excitations for Fast Entanglement Generation. *Physical Review Letters*, 108(3):030501.

[Bason et al., 2008] Bason, M. G., Mohapatra, A. K., Weatherill, K. J., and Adams, C. S. (2008). Electro-optic control of atom-light interactions using rydberg dark-state polaritons. *Phys. Rev. A*, 77:032305.

[Bason et al., 2012] Bason, M. G., Viteau, M., Malossi, N., Huillery, P., Arimondo, E., Ciampini, D., Fazio, R., Giovannetti, V., Mannella, R., and Morsch, O. (2012). High-fidelity quantum driving. *Nature Physics*, 8:147–152.

[Bates and Damgaard, 1949] Bates, D. R. and Damgaard, A. (1949). The calculation of the absolute strengths of spectral lines. *Phil. Trans. R. Soc. London*, 242:101–??

[Bendkowsky et al., 2009] Bendkowsky, V., Butscher, B., Nipper, J., Shaffer, J. P., Löw, R., and Pfau, T. (2009). Observation of ultralong-range rydberg molecules. , 458:1005–1008.

[Beterov et al., 2012] Beterov, I. I., Mansell, C. W., Yakshina, E. A., Ryabtsev, I. I., Tretyakov, D. B., Entin, V. M., MacCormick, C., Piotrowicz, M. J., Kowalczyk, A., and Bergamini, S. (2012). Cooper minima in the transitions from low-excited and Rydberg states of alkali-metal atoms. *ArXiv e-prints*.

[Beterov et al., 2009] Beterov, I. I., Ryabtsev, I. I., Tretyakov, D. B., and Entin, V. M. (2009). Quasiclassical calculations of blackbody-radiation-induced depopulation rates and effective lifetimes of rydberg ns , np , and nd alkali-metal atoms with n<80. , 79(5):052504–+.

[Beterov et al., 2007] Beterov, I. I., Tretyakov, D. B., Ryabtsev, I. I., Ekers, A., and Bezuglov, N. N. (2007). Ionization of sodium and rubidium ns, np, and nd rydberg atoms by blackbody radiation. *Phys. Rev. A*, 75:052720.

[Bethe and Salpeter, 1957] Bethe, H. A. and Salpeter, E. E. (1957). *Quantum Mechanics of One- and Two-Electron Atoms*.

[Bienaimé et al., 2012] Bienaimé, T., Piovella, N., and Kaiser, R. (2012). Controlled Dicke Subradiance from a Large Cloud of Two-Level Systems. *Physical Review Letters*, 108(12):123602.

[Bloch et al., 2008] Bloch, I., Dalibard, J., and Zwerger, W. (2008). Many-body physics with ultracold gases. *Reviews of Modern Physics*, 80:885–964.

[Blushs and Auzinsh, 2004] Blushs, K. and Auzinsh, M. (2004). Validity of rate equations for Zeeman coherences for analysis of nonlinear interaction of atoms with broadband laser radiation. , 69(6):063806.

[Bohlouli-Zanjani et al., 2007] Bohlouli-Zanjani, P., Petrus, J. A., and Martin, J. D. D. (2007). Enhancement of rydberg atom interactions using ac stark shifts. *Physical Review Letters*, 98(20):203005–+.

[Boisseau et al., 2002] Boisseau, C., Simbotin, I., and Côté, R. (2002). Macrodimers: Ultralong range rydberg molecules. *Physical Review Letters*, 88(13):133004–+.

[Boller et al., 1991] Boller, K.-J., Imamolu, A., and Harris, S. E. (1991). Observation of electromagnetically induced transparency. *Phys. Rev. Lett.*, 66:2593–2596.

[Bouloufa et al., 1992] Bouloufa, N., Cacciani, P., Delande, D., Delsart, C., Gay, J. C., Luc-Koenig, E., and Pinard, J. (1992). From regularity to chaos: a direct experimental test using atoms in magnetic field. *Journal de Physique II*, 2:671–681.

[Brion et al., 2007] Brion, E., Pedersen, L. H., and Mølmer, K. (2007). Adiabatic elimination in a lambda system. *Journal of Physics A Mathematical General*, 40:1033–1043.

[Cano and Fortágh, 2012] Cano, D. and Fortágh, J. (2012). Nonadditive potentials between three Rydberg atoms. , 86(4):043422.

[Carr et al., 2009] Carr, L., DeMille, D., Krems, R., and Ye, J. (2009). Cold and ultracold molecules: science, technology and applications. *New Journal of Physics*, 11(055049):055049.

[Carroll et al., 2004] Carroll, T. J., Claringbould, K., Goodsell, A., Lim, M. J., and Noel, M. W. (2004). Angular dependence of the dipole-dipole interaction in a nearly one-dimensional sample of rydberg atoms. *Physical Review Letters*, 93(15):153001–+.

[Castellani and Cavagna, 2005] Castellani, T. and Cavagna, A. (2005). Spin-glass theory for pedestrians. *J. Stat. Mech*, 5012:52.

[Chambers et al., 1998] Chambers, A., Fitch, R., and Halliday, B. (1998). *Basic Vacuum Technology, 2nd Edition*. Inst. of Physics Publ.

[Chotia et al., 2008] Chotia, A., Viteau, M., Vogt, T., Comparat, D., and Pillet, P. (2008). Kinetic monte carlo modeling of dipole blockade in rydberg excitation experiment. *New Journal of Physics*, 10:5031–+.

[Cohen-Tannoudji, 1992] Cohen-Tannoudji, C. (1992). Laser cooling and trapping of neutral atoms: theory. , 219:153–164.

[Cohen-Tannoudji et al., 1986] Cohen-Tannoudji, C., Diu, B., and Laloe, F. (1986). *Quantum Mechanics, Volume 1*.

[Comparat and Pillet, 2010] Comparat, D. and Pillet, P. (2010). Dipole blockade in a cold Rydberg atomic sample [Invited]. *Journal of the Optical Society of America B Optical Physics*, 27:208–+.

[Comparat et al., 2005] Comparat, D., Vogt, T., Zahzam, N., Mudrich, M., and Pillet, P. (2005). Star cluster dynamics in a laboratory: electrons in an ultracold plasma. , 361:1227–1242.

[Côté et al., 2006] Côté, R., Russell, A., Eyler, E., and Gould, P. (2006). Quantum random walk with rydberg atoms in an optical lattice. *New Journal of Physics*, 8:156.

[Cubel et al., 2005] Cubel, T., Teo, B. K., Malinovsky, V. S., Guest, J. R., Reinhard, A., Knuffman, B., Berman, P. R., and Raithel, G. (2005). Coherent population transfer of ground-state atoms into rydberg states. , 72(2):023405–+.

[Dalibard and Cohen-Tannoudji, 1989] Dalibard, J. and Cohen-Tannoudji, C. (1989). Laser cooling below the Doppler limit by polarization gradients: Simple theoretical models. *Journal of the Optical Society of America B Optical Physics*, 6:2023–2045.

[Das et al., 2008] Das, S., Agarwal, G. S., and Scully, M. O. (2008). Quantum Interferences in Cooperative Dicke Emission from Spatial Variation of the Laser Phase. *Physical Review Letters*, 101(15):153601.

[Debernardi et al., 2012] Debernardi, N., van Vliembergen, R. W. L., Engelen, W. J., Hermans, K. H. M., Reijnders, M. P., van der Geer, S. B., Mutsaers, P. H. A., Luiten, O. J., and Vredenbregt, E. J. D. (2012). Optimization of the current extracted from an ultracold ion source. *New Journal of Physics*, 14(8):083011.

[Dicke, 1954] Dicke, R. H. (1954). Coherence in Spontaneous Radiation Processes. *Physical Review*, 93:99–110.

[Divincenzo, 1998] Divincenzo, D. P. (1998). The Physical Implementation of Quantum Computation. *Fortschritte der Physik*, 48:771–783.

[Dudin et al., 2012] Dudin, Y. O., Li, L., Bariani, F., and Kuzmich, A. (2012). Observation of coherent many-body Rabi oscillations. *ArXiv e-prints*.

[Dulieu and Gabbanini, 2009] Dulieu, O. and Gabbanini, C. (2009). The formation and interactions of cold and ultracold molecules: new challenges for interdisciplinary physics. *Reports on Progress in Physics*, 72(8):086401–+.

[D'yachkov and Pankratov, 1994] D'yachkov, L. G. and Pankratov, P. M. (1994). On the use of the semiclassical approximation for the calculation of oscillator strengths and photoionization cross sections. *Journal of Physics B Atomic Molecular Physics*, 27:461–472.

[Eckardt et al., 2009] Eckardt, A., Holthaus, M., Lignier, H., Zenesini, A., Ciampini, D., Morsch, O., and Arimondo, E. (2009). Exploring dynamic localization with a Bose-Einstein condensate. , 79(1):013611.

[Efimov, 1970] Efimov, V. (1970). Energy levels arising from resonant two-body forces in a three-body system. *Physics Letters B*, 33:563–564.

[Fabre et al., 1975] Fabre, C., Gross, M., and Haroche, S. (1975). Determination by quantum beat spectroscopy of fine-structure intervals in a series of highly excited sodium D states. *Optics Communications*, 13:393–397.

[Fabre and Haroche, 1983] Fabre, C. and Haroche, S. (1983). *Spectroscopy of one- and two-electron Rydberg atoms*, page 117.

[Fano, 1947] Fano, U. (1947). Ionization Yield of Radiations. II. The Fluctuations of the Number of Ions. *Physical Review*, 72:26–29.

[Farley et al., 1977] Farley, J., Tsekeris, P., and Gupta, R. (1977). Hyperfine-structure measurements in the Rydberg S and P states of rubidium and cesium. , 15:1530–1536.

[Farley and Wing, 1981] Farley, J. W. and Wing, W. H. (1981). Accurate calculation of dynamic stark shifts and depopulation rates of rydberg energy levels induced by blackbody radiation. hydrogen, helium, and alkali-metal atoms. , 23:2397–2424.

[Farooqi et al., 2003] Farooqi, S. M., Tong, D., Krishnan, S., Stanojevic, J., Zhang, Y. P., Ensher, J. R., Estrin, A. S., Boisseau, C., Côté, R., Eyler, E. E., and Gould, P. L. (2003). Long-range molecular resonances in a cold rydberg gas. *Physical Review Letters*, 91(18):183002–+.

[Förtser, 1948] Förtser, T. (1948). Intermolecular energy migration and fluorescence. *Annalen der Physik*, 2:55–75.

[Freinkman et al., 2003] Freinkman, B. G., Eletskii, A. V., and Zaitsev, S. I. (2003). Laser ion beam formation for nanotechnologies. *Soviet Journal of Experimental and Theoretical Physics Letters*, 78:255–258.

[Friedrich, 1998] Friedrich, H. (1998). *Theoretical Atomic Physics*. Springer.

[Gaëtan et al., 2009] Gaëtan, A., Miroshnychenko, Y., Wilk, T., Chotia, A., Viteau, M., Comparat, D., Pillet, P., Browaeys, A., and Grangier, P. (2009). Observation of collective excitation of two individual atoms in the rydberg blockade regime. *Nature Physics*, 5:115–118.

[Gallagher and Pillet, 2008] Gallagher, T. and Pillet, P. (2008). Dipole - dipole interactions of rydberg atoms. *Advances in Atomic, Molecular, and Optical Physics*, 56:161.

[Gallagher, 1994] Gallagher, T. F. (1994). *Rydberg Atoms*. Cambridge University Press, Cambridge.

[Goy et al., 1982] Goy, P., Raimond, J. M., Vitrant, G., and Haroche, S. (1982). Millimeter-wave spectroscopy in cesium Rydberg states. Quantum defects, fine- and hyperfine-structure measurements. , 26:2733–2742.

[Greene et al., 2000] Greene, C. H., Dickinson, A. S., and Sadeghpour, H. R. (2000). Creation of polar and nonpolar ultra-long-range rydberg molecules. *Physical Review Letters*, 85:2458–2461.

[Grego et al., 1996] Grego, S., Colla, M., Fioretti, A., Müller, J. H., Verkerk, P., and Arimondo, E. (1996). A cesium magneto-optical trap for cold collisions studies. *Optics Communications*, 132:519–526.

[Greiner et al., 2002] Greiner, M., Mandel, O., Esslinger, T., Hansch, T., and Bloch, I. (2002). Quantum phase transition from a superfluid to a mott insulator in a gas of ultracold atoms. *NATURE*, 415(6867):39–44.

[Gross and Haroche, 1982] Gross, M. and Haroche, S. (1982). Superradiance: An essay on the theory of collective spontaneous emission. , 93:301–396.

[Günter et al., 2012] Günter, G., Robert-de Saint-Vincent, M., Schempp, H., Hofmann, C. S., Whitlock, S., and Weidemüller, M. (2012). Interaction enhanced imaging of individual rydberg atoms in dense gases. *Phys. Rev. Lett.*, 108:013002.

[Gurian et al., 2012] Gurian, J. H., Cheinet, P., Huillery, P., Fioretti, A., Zhao, J., Gould, P. L., Comparat, D., and Pillet, P. (2012). Observation of a resonant four-body interaction in cold cesium rydberg atoms. *Phys. Rev. Lett.*, 108:023005.

[Han, 2010] Han, J. (2010). Direct evidence of three-body interactions in a cold $^{85}\mathrm{Rb}$ rydberg gas. *Phys. Rev. A*, 82:052501.

[Han et al., 2006] Han, J., Jamil, Y., Norum, D. V. L., Tanner, P. J., and Gallagher, T. F. (2006). Rb nf quantum defects from millimeter-wave spectroscopy of cold Rb85 Rydberg atoms. , 74(5):054502.

[Hanssen et al., 2008] Hanssen, J. L., Hill, S. B., Orloff, J., and McClelland, J. J. (2008). Magneto-Optical-Trap-Based, High Brightness Ion Source for Use as a Nanoscale Probe. *Nano Letters*, 8:2844–2850.

[Harvey and Stoicheff, 1977] Harvey, K. C. and Stoicheff, B. P. (1977). Fine structure of the n^2d series in rubidium near the ionization limit. *Phys. Rev. Lett.*, 38:537–540.

[Heidemann et al., 2008] Heidemann, R., Raitzsch, U., Bendkowsky, V., Butscher, B., Löw, R., and Pfau, T. (2008). Rydberg excitation of bose-einstein condensates. *Physical Review Letters*, 100(3):033601–+.

[Heidemann et al., 2007] Heidemann, R., Raitzsch, U., Bendkowsky, V., Butscher, B., Löw, R., Santos, L., and Pfau, T. (2007). Evidence for coherent collective rydberg excitation in the strong blockade regime. *Physical Review Letters*, 99(16):163601–+.

[Henkel et al., 2010] Henkel, N., Nath, R., and Pohl, T. (2010). 3D Roton-Excitations and Supersolid formation in Rydberg-excited BECs. page 1035.

[Hernández and Robicheaux, 2006] Hernández, J. V. and Robicheaux, F. (2006). Coherence conditions for groups of Rydberg atoms. *Journal of Physics B Atomic Molecular Physics*, 39:4883–4893.

[Hernández and Robicheaux, 2008a] Hernández, J. V. and Robicheaux, F. (2008a). Simulation of a strong van der waals blockade in a dense ultracold gas. *Journal of Physics B Atomic Molecular Physics*, 41:5301–+.

[Hernández and Robicheaux, 2008b] Hernández, J. V. and Robicheaux, F. (2008b). Simulations using echo sequences to observe coherence in a cold rydberg gas. *Journal of Physics B Atomic Molecular Physics*, 41(19):195301–+.

[Hofmann et al., 2012] Hofmann, C. S., Günter, G., Schempp, H., Robert-de-Saint-Vincent, M., Gärttner, M., Evers, J., Whitlock, S., and Weidemüller, M. (2012). Sub-Poissonian statistics of Rydberg-interacting dark-state polaritons. *ArXiv e-prints*.

[Honer et al., 2011] Honer, J., Löw, R., Weimer, H., Pfau, T., and Büchler, H. P. (2011). Artificial Atoms Can Do More Than Atoms: Deterministic Single Photon Subtraction from Arbitrary Light Fields. *Physical Review Letters*, 107(9):093601.

[Honer et al., 2010] Honer, J., Weimer, H., Pfau, T., and Büchler, H. P. (2010). Collective many-body interaction in rydberg dressed atoms. *Phys. Rev. Lett.*, 105:160404.

[Horbatsch et al., 2005] Horbatsch, M. W., Horbatsch, M., and Hessels, E. A. (2005). A universal formula for the accurate calculation of hydrogenic lifetimes. *Journal of Physics B Atomic Molecular Physics*, 38:1765–1771.

[Huang, 1963] Huang, K. (1963). *Statistical Mechanics*.

[Isenhower et al., 2010] Isenhower, L., Urban, E., Zhang, X. L., Gill, A. T., Henage, T., Johnson, T. A., Walker, T. G., and Saffman, M. (2010). Demonstration of a Neutral Atom Controlled-NOT Quantum Gate. *Physical Review Letters*, 104(1):010503–+.

[Jaksch et al., 2000] Jaksch, D., Cirac, J. I., Zoller, P., Rolston, S. L., Côté, R., and Lukin, M. D. (2000). Fast quantum gates for neutral atoms. *Physical Review Letters*, 85:2208–2211.

[Ji and Lesanovsky, 2011] Ji, S. andAtes, C. and Lesanovsky, I. (2011). Two-dimensional Rydberg Gases and the Quantum Hard-Squares Model. *Physical Review Letters*, 107(6):060406.

[Johnson et al., 2008] Johnson, T. A., Urban, E., Henage, T., Isenhower, L., Yavuz, D. D., Walker, T. G., and Saffman, M. (2008). Rabi Oscillations between Ground and Rydberg States with Dipole-Dipole Atomic Interactions. *Physical Review Letters*, 100(11):113003.

[Kempe, 2003] Kempe, J. (2003). Quantum random walks: an introductory overview. *Contemporary Physics*, 44:307–327.

[Killian et al., 2003] Killian, T. C., Ashoka, V. S., Gupta, P., Laha, S., Nagel, S. B., Simien, C. E., Kulin, S., Rolston, S. L., and Bergeson, S. D. (2003). Ultracold neutral plasmas: recent experiments and new prospects. *Journal of Physics A Mathematical General*, 36:6077–6085.

[Killian et al., 2007] Killian, T. C., Pattard, T., Pohl, T., and Rost, J. M. (2007). Ultracold neutral plasmas. *Physics Reports*, 449:77–130.

[Klapisch, 1971] Klapisch, M. (1971). A program for atomic wavefunction computations by the parametric potential method. *Computer Physics Communications*, 2:239–260.

[Klarsfeld, 1989] Klarsfeld, S. (1989). Alternative forms of the Coulomb approximation for bound-bound multipole transitions. , 39:2324–2332.

[Koch et al., 2008] Koch, T., Lahaye, T., Metz, J., Fröhlich, B., Griesmaier, A., and Pfau, T. (2008). Stabilization of a purely dipolar quantum gas against collapse. *Nature Physics*, 4:218–222.

[Kraemer et al., 2006] Kraemer, T., Mark, M., Waldburger, P., Danzl, J. G., Chin, C., Engeser, B., Lange, A. D., Pilch, K., Jaakkola, A., Naegerl, H. C., and Grimm, R. (2006). Evidence for efimov quantum states in an ultracold gas of cesium atoms. *Nature*, 440:315.

[Kritsun et al., 2004] Kritsun, O., Boiko, O., and Metcalf, H. (2004). Excitation of metastable helium atoms to rydberg states by stirap. *APS Meeting Abstracts*, pages D1026+.

[Kübler et al., 2010] Kübler, H., Shaffer, J. P., Baluktsian, T., Löw, R., and Pfau, T. (2010). Coherent excitation of Rydberg atoms in micrometre-sized atomic vapour cells. *Nature Photonics*, 4:112–116.

[Lahaye et al., 2009] Lahaye, T., Menotti, C., Santos, L., Lewenstein, M., and Pfau, T. (2009). The physics of dipolar bosonic quantum gases. *Rep. Prog. Phys.*, 72:126401.

[Laycock et al., 2011] Laycock, T., Olmos, B., and Lesanovsky, I. (2011). Creation of collective many-body states and single photons from two-dimensional Rydberg lattice gases. *Journal of Physics B Atomic Molecular Physics*, 44(18):184017.

[Lee et al., 1978] Lee, S. A., Helmcke, J., Hall, J. L., and Stoicheff, B. P. (1978). Doppler-free two-photon transitions to Rydberg levels: convenient, useful, and precise reference wavelengths for dye lasers. *Optics Letters*, 3:141–143.

[Lesanovsky, 2011] Lesanovsky, I. (2011). Many-Body Spin Interactions and the Ground State of a Dense Rydberg Lattice Gas. *Physical Review Letters*, 106(2):025301.

[Li et al., 2003] Li, W., Mourachko, I., Noel, M. W., and Gallagher, T. F. (2003). Millimeter-wave spectroscopy of cold Rb Rydberg atoms in a magneto-optical trap: Quantum defects of the ns, np, and nd series. , 67(5):052502.

[Li et al., 2004] Li, W., M.W. Noel, a. R., Tanner, P., Gallagher, T., Comparat, D., Laburthe-Tolra, B., Vanhaecke, N., Vogt, T., Zahzam, N., Pillet, P., and Tate, D. A. (2004). Evolution dynamics of a dense, frozen rydberg gas to plasma. *Phys. Rev. A*, 70:042713.

[Li et al., 2005] Li, W., Tanner, P. J., and Gallagher, T. F. (2005). Dipole-dipole excitation and ionization in an ultracold gas of rydberg atoms. *Physical Review Letters*, 94(17):173001–+.

[Li et al., 2006] Li, W., Tanner, P. J., Jamil, Y., and Gallagher, T. F. (2006). Ionization and plasma formation in high n cold rydberg samples. *European Physical Journal D*, 40:27–35.

[Liebisch et al., 2005] Liebisch, T. C., Reinhard, A., Berman, P. R., and Raithel, G. (2005). Atom counting statistics in ensembles of interacting rydberg atoms. *Physical Review Letters*, 95(25):253002–+.

[Liebisch et al., 2007] Liebisch, T. C., Reinhard, A., Berman, P. R., and Raithel, G. (2007). Erratum: Atom counting statistics in ensembles of interacting rydberg atoms [phys. rev. lett. 95, 253002 (2005)]. *Physical Review Letters*, 98(10):109903–+.

[Lignier et al., 2007] Lignier, H., Sias, C., Ciampini, D., Singh, Y., Zenesini, A., Morsch, O., and Arimondo, E. (2007). Dynamical Control of Matter-Wave Tunneling in Periodic Potentials. *Physical Review Letters*, 99(22):220403.

[Lignier et al., 2009] Lignier, H., Zenesini, A., Ciampini, D., Morsch, O., Arimondo, E., Montangero, S., Pupillo, G., and Fazio, R. (2009). Trap-modulation spectroscopy of the Mott-insulator transition in optical lattices. , 79(4):041601.

[Lin and Yelin, 2012] Lin, G. and Yelin, S. (2012). Superradiance: An integrated approach to cooperative effects in various systems. *Adv. At. Mol. Phys*, 61:295.

[Lindblad, 1976] Lindblad, G. (1976). On the generators of quantum dynamical semigroups. *Communications in Mathematical Physics*, 48:119–130.

[Löw et al., 2009] Löw, R., Weimer, H., Krohn, U., Heidemann, R., Bendkowsky, V., Butscher, B., Büchler, H. P., and Pfau, T. (2009). Universal scaling in a strongly interacting rydberg gas. , 80(3):033422–+.

[Löw et al., 2012] Löw, R., Weimer, H., Nipper, J., Balewski, J. B., Butscher, B., Büchler, H. P., and Pfau, T. (2012). An experimental and theoretical guide to strongly interacting Rydberg gases. *Journal of Physics B Atomic Molecular Physics*, 45(11):113001.

[Lukin et al., 2001] Lukin, M. D., Fleischhauer, M., Cote, R., Duan, L. M., Jaksch, D., Cirac, J. I., and Zoller, P. (2001). Dipole blockade and quantum information processing in mesoscopic atomic ensembles. *Physical Review Letters*, 87(3):037901–+.

[Mandel, 1979] Mandel, L. (1979). Sub-Poissonian photon statistics in resonance fluorescence. *Optics Letters*, 4:205–207.

[Marinescu et al., 1994] Marinescu, M., Sadeghpour, H. R., and Dalgarno, A. (1994). Dispersion coefficients for alkali-metal dimers. *Phys. Rev. A*, 49:982–988.

[Marques et al., 2006] Marques, M., Ullrich, C., Nogueira, F., Rubio, A., Burke, K., and Gross, E. (2006). *Time-dependent density functional theory*. Springer, Berlin.

[Martín-López et al., 2012] Martín-López, E., Laing, A., Lawson, T., Alvarez, R., Zhou, X.-Q., and O'Brien, J. L. (2012). Experimental realization of Shor's quantum factoring algorithm using qubit recycling. *Nature Photonics*, 6:773–776.

[Mayle et al., 2009] Mayle, M., Lesanovsky, I., and Schmelcher, P. (2009). Exploiting the composite character of Rydberg atoms for cold-atom trapping. , 79(4):041403.

[Messiah, 1962] Messiah, A. (1962). *Quantum mechanics*.

[Metcalf and van der Straten, 1994] Metcalf, H. and van der Straten, P. (1994). Cooling and trapping of neutral atoms. , 244:203–286.

[Metcalf and van der Straten, 1999] Metcalf, H. and van der Straten, P. (1999). *Laser Cooling and Trapping*. Springer.

[Miroshnychenko et al., 2012] Miroshnychenko, Y., Poulsen, U. V., and Mølmer, K. (2012). Directional emission of single photons from small atomic samples. *ArXiv e-prints*.

[Mohapatra et al., 2008] Mohapatra, A., Bason, M., Butscher, B., Weatherill, K., and Adams, C. (2008). A giant electro-optic effect using polarizable dark states. *Nature physics.*, 4(11):890–894.

[Mohapatra et al., 2007] Mohapatra, A. K., Jackson, T. R., and Adams, C. S. (2007). Coherent optical detection of highly excited rydberg states using electromagnetically induced transparency. *Phys. Rev. Lett.*, 98:113003.

[Mourachko et al., 1998] Mourachko, I., Comparat, D., de Tomasi, F., Fioretti, A., Nosbaum, P., Akulin, V. M., and Pillet, P. (1998). Many-body effects in a frozen rydberg gas. *Phys. Rev. Lett.*, 80:253.

[Mourachko et al., 2004] Mourachko, I., Li, W., and Gallagher, T. F. (2004). Controlled many-body interactions in a frozen rydberg gas. , 70(3):031401–+.

[Mülken et al., 2007] Mülken, O., Blumen, A., Amthor, T., Giese, C., Reetz-Lamour, M., and Weidemüller, M. (2007). Survival Probabilities in Coherent Exciton Transfer with Trapping. *Physical Review Letters*, 99(9):090601.

[Nipper et al., 2012a] Nipper, J., Balewski, J. B., Krupp, A. T., Butscher, B., Löw, R., and Pfau, T. (2012a). Highly Resolved Measurements of Stark-Tuned Förster Resonances between Rydberg Atoms. *Physical Review Letters*, 108(11):113001.

[Nipper et al., 2012b] Nipper, J., Balewski, J. B., Krupp, A. T., Hofferberth, S., Löw, R., and Pfau, T. (2012b). F\"orster interaction induced phase shift in a pair state interferometer. *ArXiv e-prints*.

[Numerov, 1924] Numerov, B. V. (1924). A method of extrapolation of perturbations. , 84:592–592.

[Olmos et al., 2009a] Olmos, B., González-Férez, R., and Lesanovsky, I. (2009a). Collective rydberg excitations of an atomic gas confined in a ring lattice. , 79(4):043419–+.

[Olmos et al., 2009b] Olmos, B., González-Férez, R., and Lesanovsky, I. (2009b). Fermionic collective excitations in a lattice gas of rydberg atoms. *Physical Review Letters*, 103(18):185302–+.

[Olmos et al., 2010] Olmos, B., González-Férez, R., and Lesanovsky, I. (2010). Creating collective many-body states with highly excited atoms. *Phys. Rev. A*, 81:023604.

[Olmos and Lesanovsky, 2010] Olmos, B. and Lesanovsky, I. (2010). Collective photon emission from symmetric states created with Rydberg atoms on a ring lattice. , 82(6):063404.

[Olmos and Lesanovsky, 2011] Olmos, B. and Lesanovsky, I. (2011). Rydberg rings. *Physical Chemistry Chemical Physics (Incorporating Faraday Transactions)*, 13:4208.

[Olmos et al., 2010] Olmos, B., Müller, M., and Lesanovsky, I. (2010). Thermalization of a strongly interacting 1D Rydberg lattice gas. *New Journal of Physics*, 12(1):013024.

[Oomori et al., 1987] Oomori, T., Ono, K., Fujita, S., and Murai, Y. (1987). Ion beam generation by field ionization of laser-excited Rydberg atoms. *Applied Physics Letters*, 50:71–73.

[Osterwalder and Merkt, 1999] Osterwalder, A. and Merkt, F. (1999). Using high rydberg states as electric field sensors. *Physical Review Letters*, 82:1831–1834.

[Overstreet et al., 2009] Overstreet, K. R., Schwettmann, A., Tallant, J., Booth, D., and Shaffer, J. P. (2009). Observation of electric-field-induced cs rydberg atom macrodimers. *Nature Physics*, 5:581–585.

[Petrosyan et al., 2011] Petrosyan, D., Otterbach, J., and Fleischhauer, M. (2011). Electromagnetically induced transparency with rydberg atoms. *Phys. Rev. Lett.*, 107:213601.

[Phillips et al., 1985] Phillips, W. D., Prodan, J. V., and Metcalf, H. J. (1985). Laser cooling and electromagnetic trapping of neutral atoms. *Journal of the Optical Society of America B Optical Physics*, 2:1751–1767.

[Piotrowicz et al., 2011] Piotrowicz, M. J., MacCormick, C., Kowalczyk, A., Bergamini, S., Beterov, I. I., and Yakshina, E. A. (2011). Measurement of the electric dipole moments for transitions to rubidium Rydberg states via Autler-Townes splitting. *New Journal of Physics*, 13(9):093012.

[Pohl et al., 2010] Pohl, R., Antognini, A., Nez, F., Amaro, F. D., Biraben, F., Cardoso, J. M. R., Covita, D. S., Dax, A., Dhawan, S., Fernandes, L. M. P., Giesen, A., Graf, T., Hänsch, T. W., Indelicato, P., Julien, L., Kao, C.-Y., Knowles, P., Le Bigot, E.-O., Liu, Y.-W., Lopes, J. A. M., Ludhova, L., Monteiro, C. M. B., Mulhauser, F., Nebel, T., Rabinowitz, P., Dos Santos, J. M. F., Schaller, L. A., Schuhmann, K., Schwob, C., Taqqu, D., Veloso, J. F. C. A., and Kottmann, F. (2010). The size of the proton. , 466:213–216.

[Pohl and Berman, 2009] Pohl, T. and Berman, P. R. (2009). Breaking the dipole blockade: Nearly resonant dipole interactions in few-atom systems. *Physical Review Letters*, 102(1):013004–+.

[Pohl et al., 2009] Pohl, T., Demler, E., and Lukin, M. D. (2009). Dynamical crystallization in the dipole blockade of ultracold atoms. *ArXiv e-prints*.

[Pohl et al., 2004a] Pohl, T., Pattard, T., and Rost, J. M. (2004a). Coulomb crystallization in expanding laser-cooled neutral plasmas. *Physical Review Letters*, 92(15):155003–+.

[Pohl et al., 2004b] Pohl, T., Pattard, T., and Rost, J. M. (2004b). Letter to the editor: On the possibility of 'correlation cooling' of ultracold neutral plasmas. *Journal of Physics B Atomic Molecular Physics*, 37:L183–L191.

[Porras and Cirac, 2008] Porras, D. and Cirac, J. I. (2008). Collective generation of quantum states of light by entangled atoms. , 78(5):053816.

[Pritchard et al., 2010] Pritchard, J. D., Maxwell, D., Gauguet, A., Weatherill, K. J., Jones, M. P. A., and Adams, C. S. (2010). Cooperative Atom-Light Interaction in a Blockaded Rydberg Ensemble. *Physical Review Letters*, 105(19):193603.

[Pritchard et al., 2012] Pritchard, J. D., Weatherill, K. J., and Adams, C. S. (2012). Non-linear optics using cold Rydberg atoms. *ArXiv e-prints*.

[Pupillo et al., 2010] Pupillo, G., Micheli, A., Boninsegni, M., Lesanovsky, I., and Zoller, P. (2010). Strongly correlated gases of rydberg-dressed atoms: Quantum and classical dynamics. *Phys. Rev. Lett.*, 104:223002.

[Pupillo et al., 2008] Pupillo, G., Micheli, A., Büchler, H. P., and Zoller, P. (2008). Condensed matter physics with cold polar molecules. *ArXiv e-prints*, 805.

[Raitzsch et al., 2008] Raitzsch, U., Bendkowsky, V., Heidemann, R., Butscher, B., Löw, R., and Pfau, T. (2008). Echo experiments in a strongly interacting rydberg gas. *Physical Review Letters*, 100(1):013002–+.

[Raitzsch et al., 2009] Raitzsch, U., Heidemann, R., Weimer, H., Butscher, B., Kollmann, P., Löw, R., Büchler, H. P., and Pfau, T. (2009). Investigation of dephasing rates in an interacting rydberg gas. *New Journal of Physics*, 11(5):055014–+.

[Reetz-Lamour et al., 2008] Reetz-Lamour, M., Amthor, T., Deiglmayr, J., and Weidemüller, M. (2008). Rabi oscillations and excitation trapping in the coherent excitation of a mesoscopic frozen rydberg gas. *Phys. Rev. Lett.*, 100:253001.

[Reinhard et al., 2008] Reinhard, A., Younge, K. C., Liebisch, T. C., Knuffman, B., Berman, P. R., and Raithel, G. (2008). Double-resonance spectroscopy of interacting rydberg-atom systems. *Physical Review Letters*, 100(23):233201–+.

[Reinhard et al., 2008] Reinhard, A., Younge, K. C., and Raithel, G. (2008). Effect of förster resonances on the excitation statistics of many-body rydberg systems. *Phys. Rev. A*, 78:060702.

[Robicheaux, 2005] Robicheaux, F. (2005). Ionization due to the interaction between two rydberg atoms. *Journal of Physics B Atomic Molecular Physics*, 38:333–+.

[Robicheaux and Hernández, 2005] Robicheaux, F. and Hernández, J. V. (2005). Many-body wave function in a dipole blockade configuration. *Phys. Rev. A*, 72(6):063403.

[Rohde et al., 2010] Rohde, F., Almendros, M., Schuck, C., Huwer, J., Hennrich, M., and Eschner, J. (2010). A diode laser stabilization scheme for $^{40}Ca^{+}$ single-ion spectroscopy. *Journal of Physics B Atomic Molecular Physics*, 43(11):115401.

[Runge and Gross, 1984] Runge, E. and Gross, E. K. U. (1984). Density-Functional Theory for Time-Dependent Systems. *Physical Review Letters*, 52:997–1000.

[Ryabtsev et al., 2011] Ryabtsev, I. I., Beterov, I. I., Tretyakov, D. B., Entin, V. M., and Yakshina, E. A. (2011). Doppler- and recoil-free laser excitation of rydberg states via three-photon transitions. *Phys. Rev. A*, 84:053409.

[Ryabtsev et al., 2007a] Ryabtsev, I. I., Tretyakov, D. B., Beterov, I. I., and Entin, V. M. (2007a). Effect of finite detection efficiency on the observation of the dipole-dipole interaction of a few rydberg atoms. , 76(1):012722–+.

[Ryabtsev et al., 2007b] Ryabtsev, I. I., Tretyakov, D. B., Beterov, I. I., and Entin, V. M. (2007b). Erratum: Effect of finite detection efficiency on the observation of the dipole-dipole interaction of a few rydberg atoms [phys. rev. a 76, 012722 (2007)]. , 76(4):049902–+.

[Ryabtsev et al., 2010] Ryabtsev, I. I., Tretyakov, D. B., Beterov, I. I., and Entin, V. M. (2010). Observation of the Stark-Tuned Förster Resonance between Two Rydberg Atoms. *Physical Review Letters*, 104(7):073003–+.

[Saffman and Walker, 2002] Saffman, M. and Walker, T. G. (2002). Creating single-atom and single-photon sources from entangled atomic ensembles. *Phys. Rev. A*, 66:065403.

[Saffman et al., 2010] Saffman, M., Walker, T. G., and Mølmer, K. (2010). Quantum information with rydberg atoms. *Rev. Mod. Phys.*, 82:2313–2363.

[Saquet et al., 2010] Saquet, N., Cournol, A., Beugnon, J., Robert, J., Pillet, P., and Vanhaecke, N. (2010). Landau-Zener Transitions in Frozen Pairs of Rydberg Atoms. *Physical Review Letters*, 104(13):133003.

[Schauß et al., 2012] Schauß, P., Cheneau, M., Endres, M., Fukuhara, T., Hild, S., Omran, A., Pohl, T., Gross, C., Kuhr, S., and Bloch, I. (2012). Observation of mesoscopic crystalline structures in a two-dimensional Rydberg gas. *Nature*, 491:87–91.

[Schempp et al., 2010] Schempp, H., Günter, G., Hofmann, C. S., Giese, C., Saliba, S. D., DePaola, B. D., Amthor, T., Weidemüller, M., Sevinçli, S., and Pohl, T. (2010). Coherent population trapping with controlled interparticle interactions. *Phys. Rev. Lett.*, 104:173602.

[Schwarzkopf et al., 2011] Schwarzkopf, A., Sapiro, R. E., and Raithel, G. (2011). Imaging spatial correlations of rydberg excitations in cold atom clouds. *Phys. Rev. Lett.*, 107:103001.

[Seaton, 1983] Seaton, M. J. (1983). REVIEW ARTICLE: Quantum defect theory. *Reports on Progress in Physics*, 46:167–257.

[Sedlacek et al., 2012] Sedlacek, J. A., Schwettmann, A., Kübler, H., Löw, R., Pfau, T., and Shaffer, J. P. (2012). Microwave electrometry with Rydberg atoms in a vapour cell using bright atomic resonances. *Nature Physics*, 8:819–824.

[Sias et al., 2008] Sias, C., Lignier, H., Singh, Y. P., Zenesini, A., Ciampini, D., Morsch, O., and Arimondo, E. (2008). Observation of Photon-Assisted Tunneling in Optical Lattices. *Physical Review Letters*, 100(4):040404.

[Silverstone, 1978] Silverstone, H. J. (1978). Perturbation theory of the Stark effect in hydrogen to arbitrarily high order. , 18:1853–1864.

[Singer et al., 2004] Singer, K., Reetz-Lamour, M., Amthor, T., Marcassa, L. G., and Weidemüller, M. (2004). Suppression of excitation and spectral broadening induced by interactions in a cold gas of rydberg atoms. *Physical Review Letters*, 93(16):163001–+.

[Singer et al., 2005] Singer, K., Stanojevic, J., Weidemüller, M., and Côté, R. (2005). Long-range interactions between alkali rydberg atom pairs correlated to the ns ns, np np and nd nd asymptotes. *Journal of Physics B Atomic Molecular Physics*, 38:295–+.

[Stanojevic and Côté, 2009] Stanojevic, J. and Côté, R. (2009). Many-body rabi oscillations of rydberg excitation in small mesoscopic samples. , 80(3):033418–+.

[Stanojevic et al., 2012] Stanojevic, J., Parigi, V., Bimbard, E., Ourjoumtsev, A., Pillet, P., and Grangier, P. (2012). Generating non-gaussian states using collisions between rydberg polaritons. *Phys. Rev. A*, 86:021403.

[Steck, 2003] Steck, D. (2003). Cesium d line data. http://steck.us/alkalidata.

[Stuhler et al., 2005] Stuhler, J., Griesmaier, A., Koch, T., Fattori, M., Pfau, T., Giovanazzi, S., Pedri, P., and Santos, L. (2005). Observation of dipole-dipole interaction in a degenerate quantum gas. *Physical Review Letters*, 95(15):150406–+.

[Sun and Robicheaux, 2008a] Sun, B. and Robicheaux, F. (2008a). Numerical study of two-body correlation in a 1D lattice with perfect blockade. *New Journal of Physics*, 10(4):045032.

[Sun and Robicheaux, 2008b] Sun, B. and Robicheaux, F. (2008b). Numerical study of two-body correlation in a 1D lattice with perfect blockade. In *APS Division of Atomic, Molecular and Optical Physics Meeting Abstracts*, page L2143.

[Tanner et al., 2008] Tanner, P. J., Han, J., Shuman, E. S., and Gallagher, T. F. (2008). Many-body ionization in a frozen rydberg gas. *Physical Review Letters*, 100(4):043002–+.

[Tauschinsky et al., 2010] Tauschinsky, A., Thijssen, R. M. T., Whitlock, S., van Linden van den Heuvell, H. B., and Spreeuw, R. J. C. (2010). Spatially resolved excitation of rydberg atoms and surface effects on an atom chip. *Phys. Rev. A*, 81:063411.

[Tauschinsky et al., 2008] Tauschinsky, A., van Ditzhuijzen, C. S. E., Noordam, L. D., and van den Heuvell, H. B. V. L. (2008). Radio-frequency-driven dipole-dipole interactions in spatially separated volumes. , 78(6):063409–+.

[Tayebirad et al., 2010] Tayebirad, G., Zenesini, A., Ciampini, D., Mannella, R., Morsch, O., Arimondo, E., Lörch, N., and Wimberger, S. (2010). Time-resolved measurement of Landau-Zener tunneling in different bases. , 82(1):013633.

[Thoumany et al., 2009a] Thoumany, P., Germann, T., Hansch, T., Stania, G., Urbonas, L., and Becker, T. (2009a). Spectroscopy of rubidium Rydberg states with three diode lasers. *Journal of Modern Optics*, 56:2055–2060.

[Thoumany et al., 2009b] Thoumany, P., Hänsch, T., Stania, G., Urbonas, L., and Becker, T. (2009b). Optical spectroscopy of rubidium Rydberg atoms with a 297 nm frequency-doubled dye laser. *Optics Letters*, 34:1621.

[Tinkham, 1964] Tinkham, M. (1964). *Group Theory and Quantum Mechanics*. Internationale series in pure and applied Physics. McGraw-Hil Book Co.

[Tokihiro et al., 1995] Tokihiro, T., Manabe, Y., and Hanamura, E. (1995). Superradiance of frenkel excitons with any degree of excitation prepared by a short-pulse laser. *Phys. Rev. B*, 51(12):7655–7668.

[Tong et al., 2004] Tong, D., Farooqi, S. M., Stanojevic, J., Krishnan, S., Zhang, Y. P., Côté, R., Eyler, E. E., and Gould, P. L. (2004). Local blockade of rydberg excitation in an ultracold gas. *Physical Review Letters*, 93(6):063001–+.

[Torquato et al., 1990] Torquato, S., Lu, B., and Rubinstein, J. (1990). Nearest-neighbor distribution functions in many-body systems. *Phys. Rev. A*, 41:2059–2075.

[Urban et al., 2009] Urban, E., Johnson, T. A., Henage, T., Isenhower, L., Yavuz, D. D., Walker, T. G., and Saffman, M. (2009). Observation of rydberg blockade between two atoms. *Nature Physics*, 5:110–114.

[van Ditzhuijzen et al., 2008] van Ditzhuijzen, C. S. E., Koenderink, A. F., Hernández, J. V., Robicheaux, F., Noordam, L. D., and van den Heuvell, H. B. V. L. (2008). Spatially resolved observation of dipole-dipole interaction between rydberg atoms. *Physical Review Letters*, 100(24):243201–+.

[Varshalovich et al., 1987] Varshalovich, D., Moskalev, A., and Khersonskii, V. (1987). *Quantum theory of angular momentum*. World Scientific Pub. Co., Teaneck, NJ.

[Viteau et al., 2011] Viteau, M., Bason, M. G., Radogostowicz, J., Malossi, N., Ciampini, D., Morsch, O., and Arimondo, E. (2011). Rydberg atoms in one-dimensional optical lattices. *ArXiv e-prints*.

[Viteau et al., 2011] Viteau, M., Bason, M. G., Radogostowicz, J., Malossi, N., Ciampini, D., Morsch, O., and Arimondo, E. (2011). Rydberg excitations in bose-einstein condensates in quasi-one-dimensional potentials and optical lattices. *Phys. Rev. Lett.*, 107:060402.

[Viteau et al., 2008] Viteau, M., Chotia, A., Comparat, D., Tate, D. A., Gallagher, T. F., and Pillet, P. (2008). Melting a frozen rydberg gas with an attractive potential. , 78(4):040704–+.

[Viteau et al., 2012] Viteau, M., Huillery, P., Bason, M. G., Malossi, N., Ciampini, D., Morsch, O., Arimondo, E., Comparat, D., and Pillet, P. (2012). Cooperative Excitation and Many-Body Interactions in a Cold Rydberg Gas. *Physical Review Letters*, 109(5):053002.

[Viteau et al., 2010] Viteau, M., Radogostowicz, J., Chotia, A., Bason, M. G., Malossi, N., Fuso, F., Ciampini, D., Morsch, O., Ryabtsev, I. I., and Arimondo, E. (2010). Ion detection in the photoionization of a Rb Bose-Einstein condensate. *Journal of Physics B Atomic Molecular Physics*, 43(15):155301.

[Vogt et al., 2007] Vogt, T., Viteau, M., Chotia, A., Zhao, J., Comparat, D., and Pillet, P. (2007). Electric-field induced dipole blockade with rydberg atoms. *Phys. Rev. Lett.*, 99:073002.

[Vogt et al., 2006] Vogt, T., Viteau, M., Zhao, J., Chotia, A., Comparat, D., and Pillet, P. (2006). Dipole blockade at förster resonances in high resolution laser excitation of rydberg states of cesium atoms. *Physical Review Letters*, 97(8):083003–+.

[Walker and Saffman, 2005] Walker, T. G. and Saffman, M. (2005). Zeros of rydberg rydberg föster interactions. *Journal of Physics B Atomic Molecular Physics*, 38:309–+.

[Walker and Saffman, 2008] Walker, T. G. and Saffman, M. (2008). Consequences of zeeman degeneracy for the van der waals blockade between rydberg atoms. , 77(3):032723–+.

[Walker and Saffman, 2012] Walker, T. G. and Saffman, M. (2012). Entanglement of Two Atoms Using Rydberg Blockade. *Advances in Atomic Molecular and Optical Physics*, 61:81–115.

[Walz-Flannigan et al., 2004] Walz-Flannigan, A., Guest, J. R., Choi, J.-H., and Raithel, G. (2004). Cold-rydberg-gas dynamics. *Phys. Rev. A*, 69:063405.

[Weatherill et al., 2008] Weatherill, K. J., Pritchard, J. D., Abel, R. P., Bason, M. G., Mohapatra, A. K., and Adams, C. S. (2008). FAST TRACK COMMUNICATION: Electromagnetically induced transparency of an interacting cold Rydberg ensemble. *Journal of Physics B Atomic Molecular Physics*, 41(20):201002.

[Weber and Sansonetti, 1987] Weber, K.-H. and Sansonetti, C. J. (1987). Accurate energies of nS , nP , nD , nF , and nG levels of neutral cesium. *Phys. Rev. A*, 35:4650–4660.

[Weimer et al., 2008] Weimer, H., Löw, R., Pfau, T., and Büchler, H. P. (2008). Quantum critical behavior in strongly interacting rydberg gases. *Physical Review Letters*, 101(25):250601–+.

[Weimer et al., 2011] Weimer, H., Müller, M., Büchler, H. P., and Lesanovsky, I. (2011). Digital Quantum Simulation with Rydberg Atoms. *ArXiv e-prints*.

[Weimer et al., 2010] Weimer, H., Müller, M., Lesanovsky, I., Zoller, P., and Büchler, H. P. (2010). A Rydberg quantum simulator. *Nature Physics*, 6:382–388.

[White, 1934] White, H. E. (1934). *Introduction to atomic spectra*.

[Wigner and Griffin, 1959] Wigner, E. and Griffin, J. (1959). *Group Theory and Its Application to the Quantum Mechanics of Atomic Spectra*. Pure and applied Physics. Academic Press.

[Wiley and McLaren, 1955] Wiley, W. C. and McLaren, I. H. (1955). Time-of-Flight Mass Spectrometer with Improved Resolution. *Review of Scientific Instruments*, 26:1150–1157.

[Wüster et al., 2011] Wüster, S., Ates, C., Eisfeld, A., and Rost, J. M. (2011). Excitation transport through Rydberg dressing. *New Journal of Physics*, 13(7):073044.

[Wüster et al., 2010] Wüster, S., Stanojevic, J., Ates, C., Pohl, T., Deuar, P., Corney, J. F., and Rost, J. M. (2010). Correlations of Rydberg excitations in an ultracold gas after an echo sequence. , 81(2):023406–+.

[Younge and Raithel, 2009] Younge, K. C. and Raithel, G. (2009). Rotary echo tests of coherence in rydberg-atom excitation. *New Journal of Physics*, 11(4):043006–+.

[Younge et al., 2009] Younge, K. C., Reinhard, A., Pohl, T., Berman, P. R., and Raithel, G. (2009). Mesoscopic rydberg ensembles: Beyond the pairwise-interaction approximation. , 79(4):043420–+.

[Zenesini et al., 2010] Zenesini, A., Ciampini, D., Morsch, O., and Arimondo, E. (2010). Observation of Stückelberg oscillations in accelerated optical lattices. , 82(6):065601.

[Zhao et al., 2009] Zhao, J., Zhu, X., Zhang, L., Feng, Z., Li, C., and Jia, S. (2009). High sensitivity spectroscopy of cesium Rydberg atoms using electromagnetically induced transparency. *Optics Express*, 17:15821.

[Zimmerman et al., 1979] Zimmerman, M. L., Littman, M. G., Kash, M. M., and Kleppner, D. (1979). Stark structure of the rydberg states of alkali-metal atoms. *Phys. Rev. A*, 20(6):2251–2275.

[Zuo et al., 2009] Zuo, Z., Fukusen, M., Tamaki, Y., Watanabe, T., Nakagawa, Y., and Nakagawa, K. (2009). Single atom Rydberg excitation in a small dipole trap. *Optics Express*, 17:22898.